To the Graduate Council:

I am submitting herewith a dissertation written by Neil Andrew Whittemore entitled "I. Conformational Studies of Monoacylated Anthocyanins: Factors That Affect Their Color Stability; II. Design and Synthesis of Electroactive Oligodeoxynucleotides. Probes for Nucleic Acid Hybridization." I have examined the final copy of this dissertation for form and content and recommend that it be accepted in partial fulfillment of the requirements for the degree of Doctor of Philosophy, with a major in Chemistry.

David C. Baker

David C. Baker

James Q Chambers

James Q. Chambers

Major Professors

We have read this dissertation
and recommend its acceptance:

Spiro D. Alexandratos

Donald K. Dougall

Engin H. Serpersu

Accepted for the Council:

Associate Vice Chancellor and
Dean of The Graduate School

I. CONFORMATIONAL STUDIES OF MONOACYLATED ANTHOCYANINS: FACTORS THAT AFFECT THEIR COLOR STABILITY

II. DESIGN AND SYNTHESIS OF ELECTROACTIVE OLIGODEOXYNUCLEOTIDES. PROBES FOR NUCLEIC ACID HYBRIDIZATION

A Dissertation

Presented for the

Doctor of Philosophy

Degree

The University of Tennessee, Knoxville

Neil Andrew Whittemore

May 1999

DEDICATION

This dissertation is dedicated to my family:

my dad, Brian Arthur Whittemore,

my mum, Gillian Ford Whittemore,

my gran, Constance Smith,

and my sister, Helen Louise Whittemore

for their considerable and unfailing support.

ACKNOWLEDGMENTS

I am deeply indebted to Profs. David C. Baker, James Q. Chambers, Donald K. Dougall, and Engin H. Serpersu for their help, support, and patience during my time at the University of Tennessee–Knoxville. I also thank the Department of Chemistry at UTK for funding and the opportunity to be a Science Alliance Student Operator on the Bruker AC 250 and AMX 400 spectrometers.

Without the words of encouragement of the many friends that I have met in my six-year stay, I would not be where I am today. In particular, Mindy Asbury, Jesse and Berri Cross, Mark Constantine, Stefan Deutscher, Dori Lewis, Mrs. Donna Lewis and family, Mrs. Betty Lebow—for being my surrogate grandma since 1993, Susan and Alan Spraggins, the Heck and Dozier families and their many relations, who accepted me as one of their "large" family at Thanksgiving and Christmas, and Michael Wiitkamp, are gratefully acknowledged.

In addition to the friends I have met outside of the Department, much of this work would not be possible without the superb support of staff members of the Department of Chemistry at UTK. In particular, I thank Gene French, Bill Gurley, and Johnny Jones of the electronics department; Tim Free, Johnnie Nelson, and Eddie Wilson in the machine shop, Elder Mellon and Art Pratt in the glassblowing shop; Susan Hartzog, Bobby and Darryl Lay, Sharon Marshall, and Marilyn Ownby of the stockroom. Whilst I was teaching, the help I received from

Dr. Al Hazari and Pat Martin was invaluable. Dr. Hongjun Pan is thanked for passing on much of his knowledge about acquiring NMR experiments in the brief time I have known him. All the past and present staff members of the Mass Spectrometry Center, UTK are acknowledged for their support.

This work would not have been possible without the past and present group members of Prof. David C. Baker's and James Q. Chambers' research groups. Without the outstanding collaborative efforts of Isis Pharmaceuticals Inc., Carlsbad, CA, the electroactive ODNs, which are a focal point of Part Two of this dissertation, would be mere pipe dreams. Especially helpful in securing these invaluable ODNs were Dr. P. Dan Cook, Mr. Gopal B. Inamati, and Dr. Muthiah Manoharan (project coordinator).

However, most important to me are my family: the Whittemore's and Connie at 110 Greythorn Drive, West Bridgford, who at her age can wear a purple hat anytime she likes—she has deserved this honor! As I have grown older, I have become aware that one has many traits that remind one of one's parents. In my adolescent years these were an annoyance to me as I attempted to become an individual; however, as I have grown older, I realize that I would take great pride in being half the person my parents are. Without their love and support for everything I have wanted to do in my life—which has meant the world to me—I would never have had the courage or confidence to do many of the things that I have done in my life.

ABSTRACT

Anthocyanins, which are the highly colored compounds responsible for most of the non-green colors in plants, are glycosides of benzopyrilium (flavylium) salts that are subject to hydration by water at the flavylium C-2 position, with loss of coloration at near-neutral pH. Biosynthetic acylation with supplied cinnamic or benzoic acids at the O-6 Glc terminus of a set of anthocyanins produces compounds with enhanced color stability that are of the structure, 6-*O*-acyl-β-D-Glc*p*-(1→6)-β-D-Gal*p*-(1→O^3)-cyanidin, with and without a β-D-Xyl*p* branch at the 2-*O*-Gal position. In order to investigate the conformational behavior of these compounds with the aim of probing the mechanism for their color stabilization, five compounds, four with the 2-*O*-β-Xyl branch, including the non-acylated compound and three compounds where acyl = 3,4,5-trimethoxybenzoyl, 4-fluorocinnamoyl, 3,4,5-trimethoxycinnamoyl, plus the latter compound lacking the 2-*O*-β-D-Xyl group, were subjected to quenched molecular dynamics (QMD) using a dielectric continuum of methanol, and the results of these calculations were correlated with NMR data to yield families of conformers. The result was the finding that these molecules were quite flexible, with discrete families of conformers that afforded differing degrees of protection from attack at C-2 by solvent. MOLCAD was further used to visualize these characteristics. Two mono-cinnamoylated anthocyanins have been subjected to similar QMD studies

in a continuum of water, with the aim of correlating conformational preferences with color stability in an aqueous environment. Structure–activity relationships that emerged are being used to design highly color-stabilized anthocyanins that have potential as food colorants.

The design and programmable synthesis of electroactive oligodeoxynucleotides (ODNs) that bear a covalently attached 9,10-anthraquinone (AQ) moiety via a hexylamino linker arm was achieved using a phosphoramidite derivative of a 2′-*O*-modified uridine. Prior to the successful synthesis of these ODNs, attempts were made to synthesize C-8-modified 2′-deoxyadenosine derivatives that could be similarly used in an automated ODN synthesizer; however, these were difficult to prepare and do not readily form duplexes. Electrochemical studies of the 2′-*O*-modified AQ–ODNs on a hanging drop mercury electrode (HMDE) suggest that these ODNs may be useful as probes for hybridization, but that the HMDE is an unsuitable electrode to study these processes.

TABLE OF CONTENTS

PART ONE:

Conformational Studies of Monoacylated Anthocyanins: Factors That Affect Their Color Stability

I. INTRODUCTION 2
A. Structure and Properties of Anthocyanins 2
1. Historical Perspective 2
B. The Food/Pharmaceutical, and Nutraceutical Industry and Anthocyanins 4
C. Stability of Anthocyanins 6

II. STATEMENT OF THE PROBLEM 11

III. RESULTS AND DISCUSSION 14
A. Semibiosynthesis, Isolation and Characterization of Anthocyanins 14
B. Determination of the Color Stability of Anthocyanins 15
C. ^{1}H NMR Studies in Methanol-d_4 17
1. General 17
2. Analysis of 1D ^{1}H NMR Data 17
3. 2D ^{1}H NMR Studies 21
4. Low-Temperature ^{1}H NMR Studies 29
D. Molecular Modeling Studies in Methanol 42
1. Quenched Molecular Dynamics (QMD) Studies 42
2. Conformational Families 45
a. Classification of conformations 45
3. Structural Features of the Conformational Families 69
a. FLAC conformational families 94
b. FLD conformational families 95
c. FRAC conformational families 95
d. FRB conformational families 96
e. FRD conformational families 97
f. FUAC conformational families 97
g. NLAC conformational families 98
h. NRAC conformational families 98
i. NRD conformational families 98
j. NUAC conformational families 99
k. FUACOP and NUACOP conformational families 99
l. Miscellaneous conformational families 99

m. Summary 101
4. Molecular Dynamics Simulations of These Conformational Families 102
5. Molecular Visualization of Conformational Families Using *Mol*ecular *C*omputer *A*ided *D*esign (MOLCAD) 109
E. Molecular Modeling Studies in Water 119
1. General 119
2. QMD Studies 119
3. Conformational Families 120
4. Structural Features of the Conformational Families 133
5. Molecular Dynamics Simulations of These Conformational Families 135
6. Molecular Visualization of the Dynamics of **4-FCIN** and **345-TCIN** Using MOLCAD 152
F. Correlating the Behavior of Monocinnamoylated Anthocyanins in Water to Their Color Stability Data 167
1. General 167
2. Ratio of "Flipped" to "Nonflipped" Conformers 167
3. Flexibility of the Monocinnamoylated Anthocyanins 168
4. Micro-environment Surrounding C-2 169

IV. EXPERIMENTAL 171
A. Materials and Methods 171
B. Biological Material 172
C. Culture Preparation 172
D. Isolation of Anthocyanins 173
E. ^{1}H NMR Data Acquisition 175
1. Sample Preparation 175
2. 2D ^{1}H NMR Studies 175
F. Molecular Modeling 176
1. General Procedures 176
2. Evaluation of the Conformers in Methanol 178
3. Classification System 178
4. Evaluation of the Conformers From the QMD Study in Water 181
G. Evaluation of Conformers with *Mol*ecular *C*omputer *A*ided *D*esign (MOLCAD) 181
H. Determination of Equilibrium Constants 182

V. CONCLUSIONS 183

VI. FURTHER WORK 189

REFERENCES AND NOTES 200

PART TWO:

Design and Synthesis of Electroactive Oligodeoxynucleotides. Probes for Nucleic Acid Hybridization.

I. INTRODUCTION 219
A. Nucleic Acids 219
1. General 219
2. Structure of Deoxyribonucleic Acid (DNA) 219
3. Synthesis of DNA 221
a. Polymerase chain reaction (PCR) 221
b. Phoshphoramidite methodology 224
4. Nucleic Acid Hybridization 227
B. Probes for Nucleic Acid Hybridization 228
1. General 228
2. Methods of Labeling and Detection 232
a. Radioactive labels 232
b. Nonradioactive labels 233
(i) Fluorescent reporter groups 234
(ii) Enzyme-linked ODNs 234
(iii) The ODN–biotin–avidin–XXX system 236
(iv) Electrochemical methods 237

II. STATEMENT OF THE PROBLEM 239

III. RESULTS AND DISCUSSION 241
A. Overall Strategy 241
B. Synthesis of C-8 Modified 2′-Deoxyadenosine (First-generation Electroactive Bioconjugates) 242
1. Review of the Literature 242
2. Retrosynthetic Analysis 244
3. Preparation of Monoprotected Diamines 246
4. Attachment of the Hexylamino Linker Arm 249
5. Synthesis of the Naphthoquinone–2′-Deoxyadenosine Conjugate **1** 253
6. Electrochemical Studies on the Novel Naphthoquinone–2′-Deoxyadenosine Conjugate **1** (First-generation Bioconjugate) 253

C. Synthesis of 2′-*O*-Modified Nucleosides (Second-generation Electroactive Bioconjugates) 255
1. General 255
2. Synthesis 1,4-Naphthoquinone–Thymidine (NQ–Thymidine) Bioconjugates 255
3. Synthesis of 9,10-Anthraquinone–Uridine (AQ–Uridine) Bioconjugates 259
a. General 259
b. Preparation of novel AQ–ODNs 260
D. Electrochemical Studies 263
E. Hybridization Studies 265

IV. EXPERIMENTAL 271
A. General Methods 271
B. Materials and Solvents 275
C. Synthesis of C-8 Modified Nucleosides (First-generation Electroactive Conjugates) 276
Preparation of 6-(*N*-Benzyloxycarbonylamino)hexanol (**7**) . . 276
Preparation of 6-(*N*-Benzyloxycarbonylamino)-1-*O*-(methylsulfonyl)hexanol (**8**) 277
Preparation of 1-Azido-6-(*N*-benzyloxycarbonylamino)-hexane (**9**) 278
Preparation of 6-(*N*-Benzyloxycarbonylamino)hexylamine (**10**) 278
Synthesis of 8-Bromo-3′,5′-*O*-(1,1,3,3-tetraisopropyl-disiloxane-1,3-diyl)-2′-deoxyadenosine (**18**) 279
Synthesis of 8-[6-(*N*-Benzyloxycarbonylamino)hexylamino]-3′,5′-*O*-(1,1,3,3-tetraisopropyldisiloxane-1,3-diyl)-2′-deoxyadenosine (**19**) 280
Attempted hydrogenolysis of compound **19** 281
a. Trimethylsilyl iodide 281
b. Catalytic hydrogenation using gaseous hydrogen 281
c. Catalytic hydrogenation using hydrogen-transfer . 282
Synthesis of 8-[6-(*N*-Benzyloxycarbonylamino)hexylamino]-2′-deoxyadenosine (**21**) 282
Preparation of *S*-(2-Methyl-1,4-naphthoquinon-3-yl)-β-mercaptopropionic Acid *N*-Hydroxysuccinimide (NHS) ester (**3**) 283
Hydrogenolysis of 8-[6-(*N*-Benzyloxycarbonylamino)hexyl-amino]-2′-deoxyadenosine (**21**) 283
Formation of the NQ–2′-Deoxyadenosine conjugate (**1**) 284
Preparation of 11-Aminoundecanol (**11**) 285

Preparation of 11-(*N*-Benzyloxycarbonylamino)undecanol (**12**) 286
Preparation of 11-(*N*-Benyloxycarbonylamino)-1(-*O*-methyl-sufonyl) undecanol (**13**) 287
Preparation of 1-Azido-11-(*N*-benzyloxycarbonylamino)-undecane (**14**) 288
Preparation of 11-(*N*-Benzyloxycarbonylamino)undecylamine (**15**) 288
D. Synthesis of 2′-*O*-Modified Nucleosides (Second-generation Electroactive Conjugates) 289
Preparation of *S*-(2-Methyl-1,4-naphthoquinon-3-yl)-β-mercaptopropionic Acid Pentafluorophenyl Ester (**23**) 289
2′-*O*-[6-[2-Oxo-*S*-(2-Methyl-1,4-naphthoquinon-3-yl)-β-mercaptopropionyl]hexyl]-5′-*O*-(4,4′-dimethoxytrityl)-thymidine (**25**) 290
2′-*O*-[6-[2-Oxo-*S*-(2-Methyl-1,4-naphthoquinonyl-3)-β-mercaptopropionyl]hexyl]thymidine (**26**) 291
Compatibility Testing of 2′-*O*-[6-[2-Oxo-*S*-(2-Methyl-1,4-naphthoquinon-3-yl)-β-mercaptopropionyl]hexyl]thymidine (**26**) with Solutions Used in an Automated ODN Synthesizer 292
9,10-Anthraquinone-2-carboxylic Acid Pentafluorophenyl Ester (**34**) 292
2′-*O*-[6-[2-Oxo-(9,10-anthraquinon-2-yl)amino]hexyl]-5′-*O*-(4,4′-dimethoxytrityl)uridine (**35**) 293
2′-*O*-[6-[2-Oxo-(9,10-anthraquinon-2-yl)amino]hexyl]-uridine (**31**) 294
2′-*O*-[6-[2-Oxo-(9,10-anthraquinone-2-yl)amino]hexyl]-5′-*O*-(4,4′-dimethoxytrityl)uridine 3′-[2-cyanoethylbis(1-methyl-ethyl)phosphoramidite] (**29**) 295
E. 2′-*O*-Modified AQ–ODNs **27a–c** and **28** 295
1. Synthesis and Characterization 296
5′-d(AU*G CAT TCT GCC CCC AAG AG)-3′ (**27a**) . . 296
5′-d(ATG CAT TCU* GCC CCC AAG AG)-3′ (**27b**) . . 296
5′-d(AU*G CAT TCU* GCC CCC AAG AG)-3′ (**27c**) . 297
5′-d(GAU*CT)-3′ (**28**) 297
2. Determination of the Concentration of the Novel ODNs **27a–c** and **28** 297
3. Electrochemical Studies 298
4. Hybridization Conditions 298
V. CONCLUSIONS 300

VI. FURTHER WORK 301

REFERENCES AND NOTES 303

APPENDICES 329
APPENDIX A. Miscellaneous Data that Pertains to the Conformational Studies of Monoacylated Anthocyanins 330
APPENDIX B. ^{1}H and ^{13}C NMR Spectra for Compounds Used to Synthesize C-8-Modified Electroactive Nucleosides 350
APPENDIX C. ^{1}H and ^{13}C NMR Spectra for Compounds Used to Synthesize 2′-*O*-Modified Electroactive Oligodeoxynucleotides . . . 373

VITA 395

LIST OF TABLES

PART ONE:

Conformational Studies of Monoacylated Anthocyanins: Factors That Affect Their Color Stability

Table 1. Rate and equilibrium constants involved in color loss in selected anthocyanins 16
Table 2. Effect of acylation on the chemical shifts of H-4 and H-8 18
Table 3. NMR-derived restraints for **CyanGXG** in methanol-d_4 23
Table 4. NMR-derived restraints for **345-TMBENZ** in methanol-d_4 24
Table 5. NMR-derived restraints for **4-FCIN** in methanol-d_4 25
Table 6. NMR-derived restraints for **345-TCIN–X** in methanol-d_4 26
Table 7. NMR-derived restraints for **345-TCIN** in methanol-d_4 27
Table 8. Results of the QMD studies in methanol 44
Table 9. Dihedral angles measured in **CyanGXG**—a study in methanol 49
Table 10. RMS deviation value for each conformational family of **CyanGXG** in methanol 50
Table 11. Dihedral angles measured in **345-TMBENZ**—a study in methanol 51
Table 12. RMS deviation values for each conformational family of **345-TMBENZ**—a study in methanol 52
Table 13. Dihedral angles measured in **4-FCIN**—a study in methanol . . 53
Table 14. RMS deviation values for each conformational family of **4-FCIN** in methanol 54
Table 15. Dihedral angles measured in **345-TCIN–X**—a study in methanol 55
Table 16. RMS deviation values for each conformational family of **345-TCIN–X** —a study in methanol 56
Table 17. Dihedral angles measured in **345-TCIN**—a study in methanol 57
Table 18. RMS deviation values for each conformational family of **345-TCIN** in methanol 58
Table 19. Dihedral angles measured in **4-FCIN** in water 129
Table 20. RMS deviation value for each conformational family of **4-FCIN** 130
Table 21. Dihedral angles measured in **345-TCIN** in water 131
Table 22. RMS deviation value for each conformational family of **345-TCIN** 132

LIST OF FIGURES

PART ONE:

Conformational Studies of Monoacylated Anthocyanins: Factors that Affect Color Stability

Fig. 1. The structure of common anthocyanins 3
Fig. 2. Mechanism for color loss in anthocyanins 8
Fig. 3. General structure of anthocyanins produced from tissue cultures of the Wild Carrot, *Daucus carota* 10
Fig. 4. Anthocyanins used in molecular modeling and ^{1}H NMR studies 12
Fig. 5. Network of long-range ROEs in **4-FCIN** 28
Fig. 6. Low-temperature ^{1}H NMR studies of **CyanGXG** in methanol . 31
Fig. 7. Low-temperature ^{1}H NMR studies of **345-TMBENZ** in methanol 33
Fig. 8. Low-temperature ^{1}H NMR studies of **4-FCIN** in methanol 35
Fig. 9. Low-temperature ^{1}H NMR studies of **345-TCIN** in methanol . . 37
Fig. 10. Low-temperature ^{1}H NMR studies of **345-TCIN–X** in methanol 39
Fig. 11. Dihedral angles of **4-FCIN** used in the classification system . 48
Fig. 12. A complete network of long-range ROEs satisfied in the conformational families of **CyanGXG** 59
Fig. 13. A complete network of long-range ROEs satisfied in the conformational families of **345-TMBENZ** 61
Fig. 14. A complete network of long-range ROEs satisfied in the conformational families of **4-FCIN** 63
Fig. 15. A complete network of long-range ROEs satisfied in the conformational families of **345-TCIN–X** 65
Fig. 16. A complete network of long-range ROEs satisfied in the conformational families of **345-TCIN** 67
Fig. 17. The FLAC conformational families in methanol 70
Fig. 18. The FLD conformational families in methanol 72
Fig. 19. The FRAC conformational families in methanol 74
Fig. 20. The FRB conformational families in methanol 76
Fig. 21. The FRD conformational families in methanol 78
Fig. 22. The FUAC conformational families in methanol 80
Fig. 23. The NLAC conformational families in methanol 82
Fig. 24. The NRAC conformational families in methanol 84

Fig. 25. The NRD conformational families in methanol 86
Fig. 26. The NUAC conformational families in methanol 88
Fig. 27. The OP conformational families in methanol 90
Fig. 28. Miscellaneous conformational families in methanol 92
Fig. 29. The dihedral angle ϕ_1 of **4-FCINNRD** as a function of time during a 5 ns molecular dynamics simulation at 400 K in a dielectric continuum of methanol 104
Fig. 30. Conformations in the "flipping" process of **4-FCINNRD** in methanol 107
Fig. 31. The "flipping" process of **4-FCINNRD** in methanol as visualized by Molecular Lipophilic Potential (MLP) 111
Fig. 32. The "flipping" process of **4-FCINNRD** in methanol as visualized by Molecular Local Curvature (MLC) 113
Fig. 33. The "flipping" process of **4-FCINNRD** in methanol as visualized by Molecular Electrostatic Potential (MEP) 115
Fig. 34. "Flipped" conformational families of **4-FCIN** in water 121
Fig. 35. "Flipped" conformational families of **345-TCIN** in water 123
Fig. 36. "Nonflipped" conformational families of **4-FCIN** in water 125
Fig. 37. "Nonflipped" conformational families of **345-TCIN** in water . 127
Fig. 38. The dihedral angle ϕ_1 of **4-FCINNRD1** as a function of time during a 5 ns molecular dynamics simulation at 400 K in a dielectric continuum of water 136
Fig. 39. The dihedral angle ϕ_1 of **4-FCINFRD1** as a function of time during a 5 ns molecular dynamics simulation at 400 K in a dielectric continuum of water 138
Fig. 40. The dihedral angle ϕ_1 of **4-FCINNRD2** as a function of time during a 5 ns molecular dynamics simulation at 400 K in a dielectric continuum of water 140
Fig. 41. The dihedral angle ϕ_1 of **345-TCINFRD1** as a function of time during a 5 ns molecular dynamics simulation at 400 K in a dielectric continuum of water 143
Fig. 42. The dihedral angle ϕ_1 of **345-TCINFRD2** as a function of time during a 5 ns molecular dynamics simulation at 400 K in a dielectric continuum of water 145
Fig. 43. Conformations in the "flipping" process of **4-FCINNRD** in water 147
Fig. 44. Conformations in the "flipping" process of **345-TCINFRD** in water 150
Fig. 45. The "flipping" process of **4-FCINFRD1** in water as visualized by Molecular Lipophilic Potential (MLP) 153
Fig. 46. The "flipping" process of **4-FCINFRD1** in water as visualized by Molecular Electrostatic Potential (MEP) 155

Fig. 47. The "flipping" process of **4-FCINFRD1** in water as visualized by Molecular Local Curvature (MLC) 157
Fig. 48. The "flipping" process of **345-TCINFRD1** in water as visualized by Molecular Lipophilic Potential (MLP) 160
Fig. 49. The "flipping" process of **345-TCINFRD1** in water as visualized by Molecular Electrostatic Potential (MEP) 162
Fig. 50. The "flipping" process of **345-TCINFRD1** in water as visualized by Molecular Local Curvature (MLC) 164
Fig. 51. Factors that impact color stability of cinnamoylated anthocyanins 188
Fig. 52. Carboxylic acids to be used in the rational design of a "super" color stable monoacylated anthocyanin 194

PART TWO:

Design and Synthesis of Electroactive Oligodeoxynucleotides. Probes for Nucleic Acid Hybridization

Fig. 1. Structures of the five major bases in nucleic acids 220
Fig. 2. Structures of the four 2′-deoxynucleosides 222
Fig. 3. Attachment of a 2′-deoxyribonucleotide to CPG 225
Fig. 4. Schematic of the solid-phase synthesis of oligodeoxynucleotides by the phosphoramidite method 226
Fig. 5. Watson-Crick base-pairing for C:G (left) and T:A (right) ... 229
Fig. 6. Strategy to synthesize electroactive oligodeoxynucleotides 240
Fig. 7. Electroactive AQ–ODN bioconjugates prepared using phosphoramidite methodology 261
Fig. 8. Building blocks in the synthesis of electroactive AQ–ODN conjugates 262
Fig. 9. Typical melting curve for 0.35 μM **27a** and **32** in pH 6.83 0.1 M phosphate buffer, with 0.1 M NaCl 266
Fig. 10. Cyclic voltammetry of **27a** plus complementary 20-mer **32** .. 268
Fig. 11. Cyclic voltammetry of **27a** plus noncomplementary 20-mer **33** 269

LIST OF SCHEMES

PART TWO:

Design and Synthesis of Electroactive Oligodeoxynucleotides. Probes for Nucleic Acid Hybridization

Scheme 1. Retrosynthetic analysis of the synthesis of electroactive bioconjugates 245
Scheme 2. Synthesis of monoprotected diamine **10** 247
Scheme 3. Synthesis of monoprotected diamine **15** 248
Scheme 4. Preparation of protected 8-Br-2′-deoxyadenosine **18** 251
Scheme 5. Attempted preparation of silyl compound **20** 252
Scheme 6. Synthesis of the first-generation electroactive naphthoquinone–2′-deoxyadenosine **1** 254
Scheme 7. Synthesis of the second-generation electroactive naphthoquinone–thymidine conjugates **25** and **26** . . . 256
Scheme 8. Can the NQ moiety survive the conditions experienced in the automated ODN synthesizer? 258
Scheme 9. Synthesis of electroactive AQ–ODN conjugates **27a–c** and **28** 264

PART ONE:

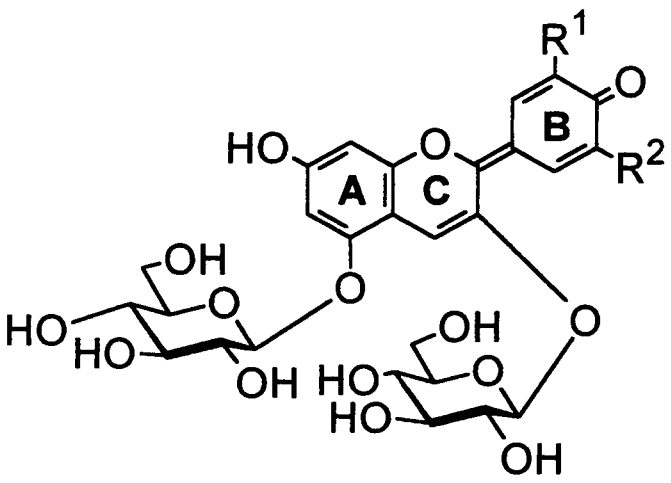
CONFORMATIONAL STUDIES OF MONOACYLATED ANTHOCYANINS: FACTORS THAT AFFECT THEIR COLOR STABILITY

I. INTRODUCTION[1]

A. Structure and Properties of Anthocyanins

1. Historical Perspective. Since the discovery by Willstätter in the early part of this century that the same pigment cyanin (Fig. 1.)—a member of the family of the highly colored compounds known as anthocyanins—was present in both the blue cornflower, *Centaurea cyanus*, and the red rose,[2] a considerable amount of research has been done to establish what phenomena are responsible for the beautiful colors of flowers observed in nature.[3] Structurally, anthocyanins have both aglycon (anthocyanidin) and glycone domains. It is the anthocyanidin nucleus that is responsible for the intense color observed when these compounds are dissolved in aqueous medium. Although not shown in Fig. 1., the vast majority of anthocyanins that occurs in nature is acylated along the glycosidic backbone, which can consist of saccharide sub-units other than β-D-glucopyranose. For example, an anthocyanin isolated from the potato, *Solanum tuberosum*, bears a 4-*O*-acylated α-L-rhamnospyranosyl moiety.[4]

In very early studies, researchers observed that anthocyanins have an orange-red color in strongly acidic medium, whereas in weakly acidic or near-neutral pH, a purple to blue color was evident. Therefore, the difference in color between the blue cornflower and the red rose could be explained by a difference



R^1	R^2	Anthocyanin	Aglycon
H	H	Pelargonin	Pelargonidin
OH	H	Cyanin	Cyanidin
OCH_3	H	Peonin	Peonidin
OH	OH	Delphin	Delphinidin
OCH_3	H	Petunin	Petunidin
OCH_3	OCH_3	Malvin	Malvidin

Fig. 1. The structure of common anthocyanins.

in the pH of the sap. However, other workers indicated that sap could not be alkaline and proposed that the distinct blue color resulted from a complexation of magnesium ions and this anthocyanin.[5] Further studies have revealed that this is a rather simplistic view of the phenomena that are observed in the blue cornflower.[3] Although it was not until very recently that the precise nature of the blue color development in the blue cornflower, *Centaurea cyanus*, was elucidated.[6] The color results from a ligand-to-metal charge transfer (LMCT) absorption band of the protocyanin pigment, which is composed of six molecules each of malonylflavone and succinylcyanin, complexed with both ferric and magnesium ions.

The search to explain the color development in flowers, such as the blue cornflower, has resulted in advances in how to study the behavior of anthocyanins in aqueous media.[3] Researchers have employed these methods to assess the potential of these natural and highly colored substances as colorants in the nutraceutical and pharmaceutical industries.[3,7,8]

B. The Food/Pharmaceutical, and Nutraceutical Industry and Anthocyanins

Colorants used in the food, pharmaceutical, and nutraceutical industries are, for the most part, synthetic dyestuffs that have come under increasing

scrutiny in recent years for their safety. There is a movement among these industries to find natural replacements for the synthetics, largely driven by the perception by the public that synthetics are less healthful than natural colors. Clearly there is a demand for stable, nontoxic colorants of natural origin, and the consumer is ready to pay a premium price for all-natural foods.

Among the possibilities for natural colorants are the anthocyanins, which are the compounds responsible for most of the non-green coloration in plants. Anthocyanins are responsible for the coloring of apples, strawberries, grapes, red cabbage, as well as for the reds, blues, and purples of flowers (for a general structure of anthocyanins, see Fig. 1). While reviews in the field indicate that industrial interest for anthocyanins is high,[9,10] there is only limited use of these compounds at the present time, mainly due to the fact that these compounds (a) are of limited availability and (b) many lose their color at or near-neutral pH, precluding their use in most foodstuffs. These issues have been discussed in the First International Symposium on Natural Colors for Foods, Nutraceuticals, Confectionerys, and Beverages (November 7–10, 1993, University of Massachusetts, Amherst, MA.) Anthocyanins derived from red cabbage, red fruit, and grape are commercially available at this time. As for color stability, most anthocyanins retain their color at low pH, i.e., at pH <2, but lose their color due to hydration by water at pH ~6 (for details, see the next section).

There is a recognized need for new, color-stable anthocyanins in the food

and related industries. Such products, which would easily sell for several hundred dollars per kilogram, are "value-added" products in the truest sense, as they can be derived from sugar sources available to the biotechnology industry.

C. Stability of Anthocyanins

Stable anthocyanins have been isolated, chemically characterized, and studied for two decades. Goto et al. reported[11] in 1982 a stable anthocyanin isolated from *Gentiana makino.* Subsequent reports of stable anthocyanins include those of Idaka et al.[12] (one from *Brassica oleracea)*; of Kondo et al.[13] (from *Lobelia erinus*); Kondo et al.[14] and Terahara et al.[15,16] (from *Clitora ternatea*); Yoshida et al.[17,18] (from *Dioscorea alata*); and Lu et al.[19,20] (from *Pharbitis nil*). Goto and Kondo[3] in their comprehensive review conclude that anthocyanins acylated with at least two molecules of cinnamic acid show increased stability and offer explanations for their increased stabilities. Additional acylated anthocyanins have been reported by Andersen et al.;[4] by Gläßgen et al.;[21-23] by Idaka et al.;[24] by Johansen et al.;[25] by Lu et al.;[26] by Odake et al;[27] and by Saito et al.[28] However, no color and/or compound stability data are provided, leaving stabilities of these compounds open to question.

The color stability of an anthocyanin is measured on solutions buffered at pH 6–7 by the change in absorbance with time at the λ_{max} in the visible portion

of the spectrum. While color stability is generally observed at pH ≤2, rapid absorbance changes are observed at pH 6–7. Dangles et al.[29,30] have attributed this to the rapid hydration of the highly colored flavylium portion of the anthocyanin at the C-2 position, giving rise to an uncharged, colorless hemiacetal (OH group at C-2). This reaction, a part of a dynamic equilibrium, is depicted in Fig. 2. While the hydration reaction is central to the process of color loss, other pH dependent processes such as the loss of a proton from the flavylium species to give a quinonoidal base, as well as ring-opening of the hemiacetal, all serve to remove the red-colored species from the equilibrium.

The rate constants and equilibrium constants for the hydration reaction of a series of five anthocyanins from *Pharbitis nil* have been measured by Brouillard and co-workers.[29,30] For this series, which has pelargonidin as a common aglycon with sugars attached at the 3- and 5-positions of the aglycon and a series of caffeic acid residues that number 0–4, the stabilities are shown to increase (hydration decreases) with increasing acylation. The decreases in the rate of hydration are believed to be due to the increased π-bond interactions between the acyl moiety and the $C=O^+$ bond of the flavylium species. Goto and Kondo,[3] and Yoshida et al.,[11,31] have evidence from NMR spectral data on anthocyanins from *Gentiana makinoi* and *Ipomoea tricolor* that, in acidic solution,

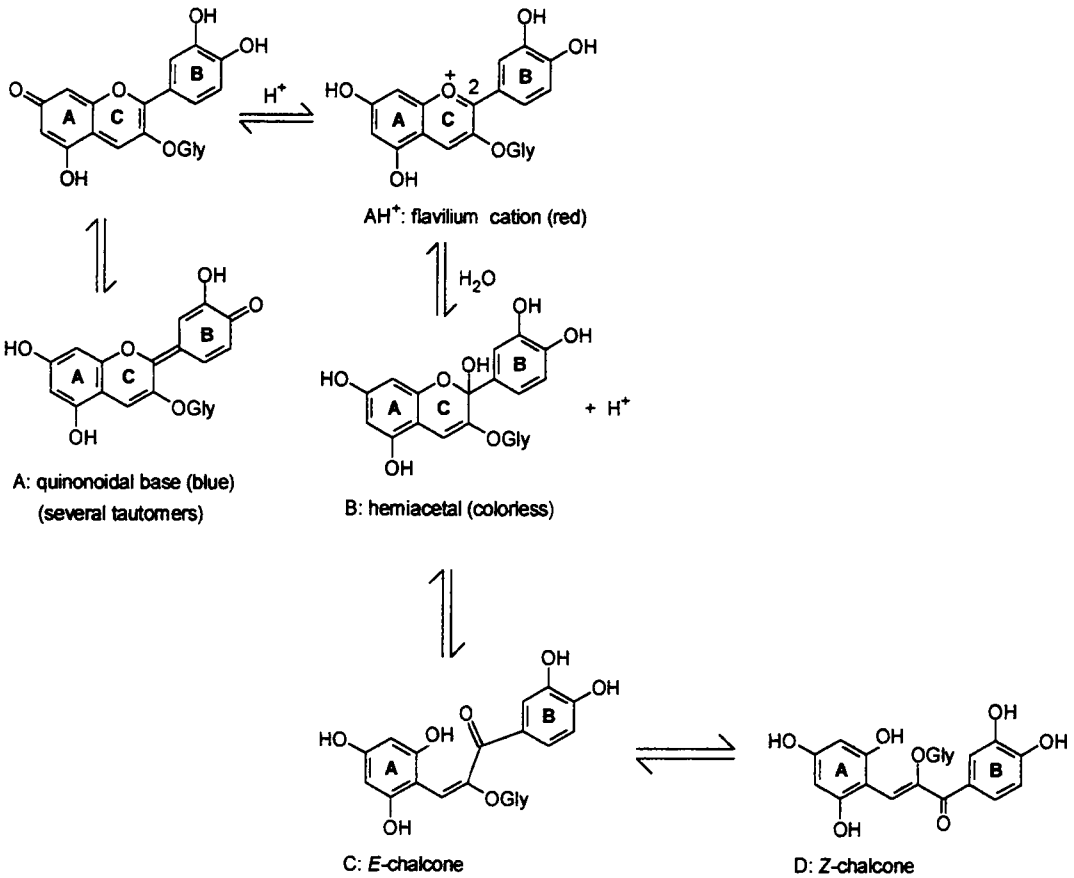


Fig. 2. Mechanisms for color loss in anthocyanins.

the conformations of the molecules are such that the flavylium moiety and the acyl groups are stacked with one another—termed intramolecular copigmentation or sandwich-type stacking. The models they have suggested, however, do not account for the observed decreases in hydration, as the site of hydration at C-2 is not protected from attack by water on both sides of the $C=O^+$ group. Furthermore, there have not been any studies to ascertain the effects of other substituted cinnamoyl groups on color stability.

Although Goto and Kondo[3] concluded that only anthocyanins having two or more cinnamoyl groups are stable, there were at least two examples, prior to our work, where anthocyanin color stability was associated with one acyl group. Yoshida et al.[17] showed that the mono-sinapoylated β-D-Glc6Sin-(1→6)-β-D-Glc-(1→O^3)-Cya (Sin = sinapoyl, 4-hydroxy-3,5-dimethoxycinnamoyl) from *Dioscorea alata* was much more stable at pH 6.0 than its non-acylated counterpart. In work carried out in these laboratories,[32] it was demonstrated that monosinapoylated β-D-Glc6Sin-(1→6)-[β-D-Xyl-(1→2)-]β-D-Gal-(1→O^3)-Cya (for the general structure of these anthocyanins, see Fig. 3) from wild carrot cell cultures enjoys increased color stability over its nonacylated counterpart. Thus monoacylated anthocyanins of this type were recognized as potential candidates for stabilized food coloring compounds. Furthermore, these compounds provide an opportunity to explore the role of the acyl group in increasing the color stability of the anthocyanin in solution.

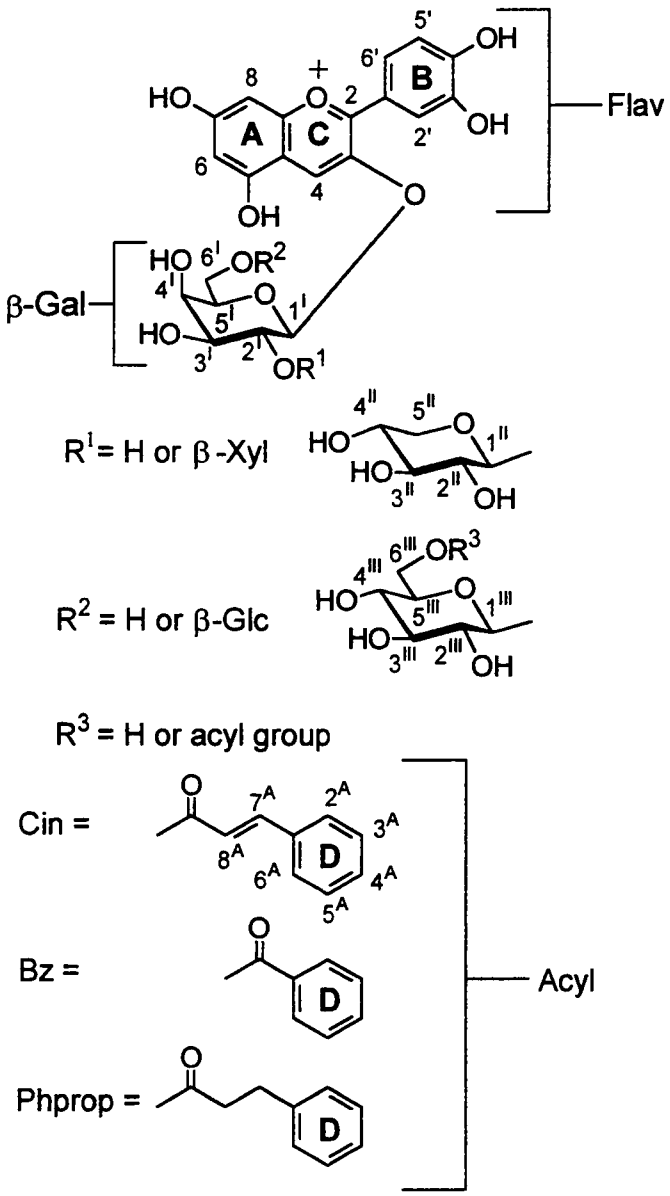


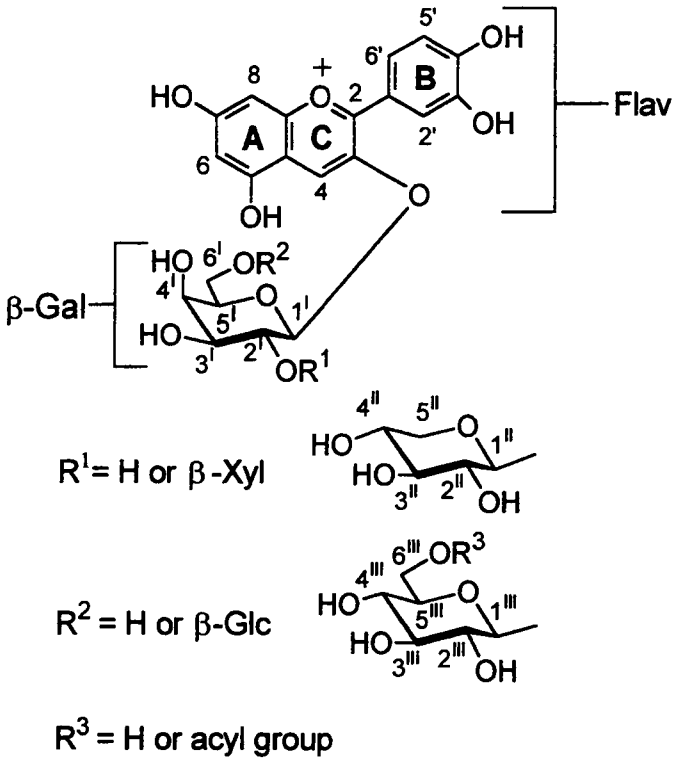
Fig. 3. General structures of anthocyanins produced from tissue cultures of the Wild Carrot, *Daucus carota.*

II. STATEMENT OF THE PROBLEM

Both 1D and 2D NMR studies of certain monoacylated anthocyanins (see Fig. 4) have revealed that the acyl moiety stacks with the **A–C** ring of the flavylium moiety within the same molecule—this phenomenon is known as copigmentation—thus impeding the attack of water; however, the precise nature of these intramolecular interactions is not well understood.[33-35]

In order to rigorously examine the nature of the intramolecular interactions in the series of semi-biosynthetically prepared anthocyanins,[34] a general molecular modeling protocol had to be developed that would permit the construction of reasonable models of monoacylated anthocyanins in either water or methanol. Moreover, the models thus generated should be validated by data acquired in 2D NMR studies. Knowledge of the low-energy conformations that these molecules adopt in water would permit a thorough examination of the processes that result in the increased color stability of monoacylated anthocyanins over their nonacylated counterparts.

If particular phenomena observed from the modeling protocol could be correlated to the observed color stability in aqueous solutions, researchers would have a potent weapon in their arsenal to predict the color stability of monoacylated anthocyanins. Ultimately, this could lead to rational design—analogous to the approach in the pharmaceutical industry—of a "super"



CyanGXG	R^1 = β-Xyl	R^2 = β-Glc	R^3 = H
345-TCIN	R^1 = β-Xyl	R^2 = β-Glc	R^3 = 3,4,5-$(OMe)_3$-Cin
345-TCIN–X	R^1 = H	R^2 = β-Glc	R^3 = 3,4,5-$(OMe)_3$-Cin
4-FCIN	R^1 = β-Xyl	R^2 = β-Glc	R^3 = 4-F-Cin
345-TMBENZ	R^1 = β-Xyl	R^2 = β-Glc	R^3 = 3,4,5-$(OMe)_3$-Bz

Fig. 4. Anthocyanins used in molecular modeling and ^{1}H NMR studies.

anthocyanin. This compound would exhibit greater color stability in neutral pH than any compounds produced so far in the laboratories of Dougall and Baker.[34]

III. RESULTS AND DISCUSSION

A. Semibiosynthesis, Isolation and Characterization of Anthocyanins

The semibiosynthetic method used to acylate the O-6 Glc terminus of anthocyanins of the general structure, β-D-glucopyranosyl-(1→6)-β-D-galactopyranosyl-(1→O^3)-cyanidin, with and without a β-D-xylopyranosyl branch at the 2-*O*-Gal position (see Fig. 3) using wild carrot, *Daucus carota*, has proven to be a robust and versatile method to incorporate various acyl moieties.[34] Of the 24 compounds that have been prepared, isolated and fully characterized by ^{1}H NMR and mass spectrometry using this method, **CyanGXG**, **345-TMBENZ**, **4-FCIN**, **345-TCIN, 345-TCIN–X** (see Fig. 4) were judiciously selected as candidates for rigorous conformational analysis, using a combination of NMR and molecular modeling techniques (For full spectral data on all 24 compounds, refer to pp 332–335 in Appendix A).

Once reasonable structures for each of the five compounds in solution are generated, the effects that certain functionalities of the acyl groups have on the conformation of these anthocyanins could be determined. For example, the comparison of the models for **345-TCIN** and **345-TMBENZ** would permit the effect on the structure of the exocyclic double bond to be studied. Comparison of the molecular models constructed for **345-TCIN–X** and **345-TCIN** would show

what influence the β-Xyl moiety exerts on the conformation of these anthocyanins in solution. The precise role of each of the acyl moieties in influencing the conformation of these anthocyanins in solution can be discerned by comparing the models derived from the monoacylated anthocyanins to the nonacylated **CyanGXG**. An added advantage is that the five compounds have differing color-stability data profiles, from the worst (**CyanGXG**) to one of the best (**345-TCIN** and **345-TCIN–X**) (discussed in the section entitled, "Determination of the Color Stability of Anthocyanins"). Thus, the conformational preferences of these molecules in solution could be correlated to their color-stability data.

B. Determination of the Color Stability of Anthocyanins

The rate constants in the key processes (see Fig. 2) involved in the loss of color of anthocyanins for the entire series of 24 compounds[34] were determined experimentally according the protocol used by Dangles and co-workers.[29] All the constants for the five compounds examined are shown in Table 1 (for all the data of the entire series of compounds, see Table 1 in recently submitted paper,[36] p 336 in Appendix A). The rate constant for the hydration reaction at C-2 of the flavylium nucleus (k_1), and the rate constant for the dehydration reaction at C-2 (k_2), lead directly to the calculation of the equilibrium constant for the hydration

reaction (K_h)—the key process that results in the loss of color in anthocyanins. Therefore K_h provides an excellent measure of the color stability of anthocyanins, and a means to compare the color stability of each of the anthocyanins under investigation. The larger the K_h for a particular anthocyanin, the less color stable the anthocyanin. Thus, **CyanGXG** is the least color stable compound, with **345-TCIN–X** and **345-TCIN** having comparable color-stability profiles.

The compounds selected exhibit very different color-stability characteristics, and provide an excellent opportunity to explore the structural features in solution that may account for these differences in color stability.

Table 1. Rate and equilibrium constants involved in color loss in selected anthocyanins.

Compound	$k_1 \times 10^2$ (sec^{-1})	k_2 ($sec^{-1}M^{-1}$)	$K_h \times 10^5$ (M)
CyanGXG	6 ± 1	139 ± 1	43 ± 6
345-TMBENZ	8.7 ± 0.6	586 ± 6	14.9 ± 0.8
4-FCIN	5.34 ± 0.03	577 ± 1	9.27 ± 0.06
345-TCIN–X	2.78 ± 0.08	519 ± 20	5.38 ± 0.08
345-TCIN	3.57 ± 0.04	684 ± 52	5.2 ± 0.3

Before a thorough investigation could be undertaken, a molecular modeling protocol had to be developed, which produced models that were validated by data acquired from 2D ^{1}H NMR studies.

C. ^{1}H NMR Studies in Methanol-d_4

1. General. In order to examine the behavior of **CyanGXG**, **345-TMBENZ**, **4-FCIN**, **345-TCIN**, **345-TCIN–X** in their flavylium ion forms, both 1D and 2D ^{1}H NMR studies were conducted in methanol-d_4 that was acidified with trifluoroacetic acid-*d*.[34] The addition of trifluoroacetic acid-*d* was preferred to DCl, because loss of the β-Xyl moiety , which had been observed in methanol-d_4–DCl solutions of anthocyanins over a period of time, was prevented.[34] Methanol-d_4 was selected as the solvent of choice for these studies due to superior spectral dispersion compared to spectra obtained in water. An added advantage of methanol-d_4 over deuterated water was that low-temperature ^{1}H NMR studies—down to −90 °C—could be performed in this medium. This proved to be a powerful tool in ultimately deducing the highly flexible nature of these molecules in solution (see "Low-temperature ^{1}H NMR Studies" section).

2. Analysis of 1D ^{1}H NMR Data. In the study that produced 24 compounds, analysis of the 1D ^{1}H NMR data[34] revealed that the acyl moiety had

a marked effect on the chemical shifts of H-4 and H-8. Comparison of the chemical shifts for H-4 and H-8 in the anthocyanins **CyanGXG**, **345-TMBENZ**, **4-FCIN**, **345-TCIN–X**, and **345-TCIN** illustrates the observations noted for all 24 compounds (For the chemical shifts of the five compounds under discussion, refer to Table 2).[34]

Irrespective of the acyl group at the O-6 Glc terminus of the anthocyanin, the chemical shifts of H-4 are more upfield and more shielded than that of the nonacylated **CyanGXG**.[33,34] Thus, H-4 on these anthocyanins must be close enough to the acyl moiety to experience the anisotropic effect of the benzene ring of the acyl group in question. This phenomenon in which H-4 of monoacylated anthocyanins is shielded is known, and has been interpreted as evidence for intramolecular copigmentation (stacking), which has been invoked

Table 2. Effect of acylation on the chemical shifts of H-4 and H-8.

	H-4 (ppm)	H-8 (ppm)
CyanGXG	8.981	6.964
345-TMBENZ	8.447	6.741
4-FCIN	8.588	not seen[a]
345-TCIN	8.478	6.525
345-TCIN–X	8.663	6.548

a. Exchanges with CD_3OD/TFA-*d*.

to explain the enhanced color stability of monoacylated anthocyanins compared to their nonacylated counterparts.[33,34] Furthermore, an additional effect is noted on the chemical shift of H-8 in only cinnamoylated anthocyanins. The chemical shift of H-8 in the cinnamoylated anthocyanins **345-TCIN** and **345-TCIN–X** is considerably more upfield compared to the corresponding chemical shift in the benzoylated counterpart **345-TMBENZ**. This implies that the exocyclic double bond of the cinnamoyl moiety heavily influences the interaction between the acyl moiety and the flavylium nucleus, and stacking is at a maximum in cinnamoylated anthocyanins—with both H-4 and H-8 being affected by the cinnamoyl moiety.

Further evidence of the crucial role that the exocyclic double bond plays in stacking is seen when the chemical shifts of H-4 and H-8 in the anthocyanin acylated with 3-(4-hydroxyphenyl)propionic acid (HPPA) (not shown here) is compared to its cinnamoylated counterpart (4-hydroxycinnamic acid). The chemical shifts of H-4 and H-8 are (δ 8.821 and δ 6.842, respectively) in the anthocyanin acylated with HPPA *versus* the cinnamoylated anthocyanin (δ 8.524 and δ 6.548, respectively). Clearly H-4 and H-8 are more shielded in the cinnamoylated anthocyanin than the same set of protons in the anthocyanin acylated with HPPA. Thus, in the absence of the exocyclic double bond, these protons do not experience the same anisotropic effects from the acyl moiety and the exocyclic double bond, and they do not stack as readily as in the case of their cinnamoylated counterparts. Moreover the shielding observed in

cinnamoylated anthocyanins is due to the presence of the exocyclic double bond, and not due solely to the extension of the acyl moiety's chain of two methylene units.[34]

The 1D NMR data generated for **CyanGXG**, **345-TMBENZ**, **4-FCIN**, **345-TCIN–X**, and **345-TCIN** demonstrates that long-range intramolecular interactions are operational between the A–C ring of the flavylium nucleus and the acyl moiety. These effects are shown to be the greatest in cinnamoylated anthocyanins, due to an additional effect of the exocyclic double bond. Although this evidence was striking and indicated a strong interaction between the acyl moiety and the flavylium nucleus, any comments about the role of the stacking on the color stability of these compounds could not be substantiated based on 2D representations of these "folded" molecules. For example, this simplistic view could not yield a satisfactory answer to the often-asked question:[29]

> Why are cinnamoylated anthocyanins, such as **345-TCIN** that "stack", less prone to attack of water at the C-2 position of the flavylium nucleus (more color stable), even though one face of the molecule would still be open to attack?

Therefore, realistic 3D models of the compounds that are validated by 2D ^{1}H NMR data were required to study at a molecular level, the events that lead to color loss in these anthocyanins.

3. 2D ^{1}H NMR Studies. With the structural assignments of **CyanGXG**, **345-TMBENZ**, **4-FCIN**, **345-TCIN**, and **345-TCIN–X** in hand, 2D ^{1}H NMR data generated could be used to study the conformations of the anthocyanins.[34] Nuclear Overhauser enhancement spectroscopy (NOESY) experiments were performed at mixing times between 50 and 750 ms to study long-range interactions within **4-FCIN**.[37] However, the intensities of the nuclear Overhauser effects (NOEs) observed in the case of **4-FCIN** were weak, and there was no discernible buildup of the intensity of the NOEs as a function of the mixing time used in several NOESY experiments. This indicates that **4-FCIN**, and molecules like it, have a certain degree of flexibility, and the use of NOESY generated data to validate structures produced from a suitable molecular modeling protocol was not viable. In addition to this finding, low-temperature ^{1}H NMR studies of all five compounds demonstrated the highly flexible nature of these molecules (see the next section). Thus rotating frame Overhauser enhancement spectroscopy (ROESY) data may be used as a diagnostic tool to validate structures produced from molecular modeling protocols, such as quenched molecular dynamics (QMD). Previous studies have demonstrated the utility of this approach to study flexible molecules, such as cyclic peptidomimetics,[38,39] short linear peptides,[40] and α-melanotropins.[41] To date, no one has applied QMD to compounds such as anthocyanins.

ROESY spectra at 20 °C and a mixing time of 500 ms revealed 15, 20, 21,

10, and 17 interactions of **CyanGXG**, **345-TMBENZ**, **4-FCIN**, **345-TCIN–X**, and **345-TCIN**, respectively. Each interaction was categorized depending on their respective intensities. Once assigned as either strong, medium, or weak interactions, each one was assigned a distance range of 1.7 Å–2.5 Å, 1.7 Å–3.2 Å, and 1.7 Å–5 Å, respectively. Thus, if the distance between a certain set of protons, i.e., H-4–H-1^{Gal}, fell into the range that was based on the above categorization, the model could be said to be validated by NMR-derived restraints (see Table 3, 4, 5, 6, and 7 for all the NMR-derived restraints used in the study of **CyanGXG**, **345-TMBENZ**, **4-FCIN**, **345-TCIN–X**, and **345-TCIN**, respectively). This provided a means of generating reasonable structures of these anthocyanins in solution.

Examination of the 2D ^{1}H NMR spectra provided further evidence that long-range interactions are present in these anthocyanins and indicate that the conformation that the molecule adopts in solution may help to explain why monoacylated anthocyanins are more color stable than their nonacylated counterparts. For example, the complete network of these long-range interactions of **4-FCIN** is shown in Fig. 5: a. H-7^{A}–H-1^{Gal}, b. H-8^{A}–H-1^{Gal}, c. H-1^{Gal}–H-4, d. H-2^{Gal}–H-1^{Xyl}.[37] These data will be used to corroborate the validity of structures produced from molecular modeling protocols.

Table 3. NMR-derived restraints for **CyanGXG** in methanol-d_4.

Proton–proton pairs	Volume measured ($\times 10^6$)	Strength of interaction[a]
H-1^{Gal}–H-6^{BGal} (Pro-S)[b]	0.59	W
H-1^{Gal}–H-6^{BGal} (Pro-R)[b]	0.59	W
H-1^{Xyl}–H-2^{Gal}	0.47	W
H-4–H-1^{Gal}	0.45	W
H-4–H-2^{Gal}	0.21	W
H-4^{Gal}–H-6^{BGal} (Pro-R)[b]	–[c]	W
H-4^{Gal}–H-6^{BGal} (Pro-S)[b]	–[c]	W
H-2^{Glc}–H-6^{AGlc} (Pro-R)[b]	–[c]	W
H-2^{Glc}–H-6^{AGlc} (Pro-S)[b]	–[c]	W
H-2^{Glc}–H-2^{Gal}	–[c]	W
H-5^{BaxXyl}–H-4^{Xyl}	–[c]	W
H-1^{Glc}–H-2^{Glc}	–[c]	W
H-5^{BaxXyl}–H-2^{Xyl}	–[c]	W
H-6^{AGlc} (Pro-S)[b]–H-2^{Gal}	–[c]	W
H-6^{AGlc} (Pro-R)[b]–H-2^{Gal}	–[c]	W

a. Strong interaction (S) = 1.7 Å–2.5 Å; medium interaction (M) = 1.7 Å–3.2 Å; weak interaction (W) = 1.7 Å–5 Å. b. Cannot determine whether H-6^{BGal} is Pro-R or Pro-S and so both were used to validate structures generated from modeling protocols. c. An rotating frame Overhauser effect (ROE) that was confirmed by visual inspection of the spectrum, but whose volume could not be measured accurately due to either t_1 noise or overlap of signals. All these were assigned as weak interactions.

Table 4. NMR-derived restraints for **345-TMBENZ** in methanol-d_4.

Proton–proton pairs	Volume measured (× 10^6)	Strength of interaction[a]
H-6'–H-5'	0.64	W
$H\text{-}6^{Gal}$ (Pro R)–$H\text{-}6^{Gal}$ (Pro S)	0.59	W
$H\text{-}3^{Gal}$–$H\text{-}4^{Gal}$	0.35	W
$H\text{-}1^{Glc}$–$H\text{-}3^{Glc}$	0.34	W
$H\text{-}1^{Glc}$–$H\text{-}6^{Gal}$ (Pro S)[b]	0.32	W
$H\text{-}1^{Glc}$–$H\text{-}6^{Gal}$ (Pro R)[b]	0.32	W
$H\text{-}6^{A}$–OMe	0.31	W
$H\text{-}2^{A}$–OMe	0.31	W
$H\text{-}5^{Gal}$–$H\text{-}4^{Gal}$	0.27	W
$H\text{-}1^{Glc}$–$H\text{-}2^{Glc}$	0.26	W
$H\text{-}5^{Gal}$–$H\text{-}3^{Gal}$	0.25	W
$H\text{-}1^{Gal}$–$H\text{-}6^{A}$	0.13	W
$H\text{-}1^{Gal}$–$H\text{-}2^{A}$	0.13	W
H-4–$H\text{-}1^{Gal}$	0.1	W
$H\text{-}1^{Gal}$–$H\text{-}3^{Gal}$	0.096	W
$H\text{-}5^{Gal}$–$H\text{-}1^{Gal}$	0.081	W
$H\text{-}1^{Xyl}$–$H\text{-}3^{Gal}$	0.063	W
$H\text{-}1^{Xyl}$–$H\text{-}2^{Gal}$	–[c]	W
$H\text{-}6^{Glc}$ (Pro R)–$H\text{-}6^{Glc}$ (Pro S)	–[c]	W
$H\text{-}1^{Gal}$–$H\text{-}2^{Gal}$	–[c]	W

a. Strong interaction (S) = 1.7 Å–2.5 Å; medium interaction (M) = 1.7 Å–3.2 Å; weak interaction (W) = 1.7 Å–5 Å. b. Cannot determine whether $H\text{-}6^{BGal}$ is Pro-R or Pro-S and so both were used to validate structures generated from modeling protocols. c. A rotating frame Overhauser effect (ROE) that was confirmed by visual inspection of the spectrum, but whose volume could not be measured accurately due to either t_1 noise or overlap of signals. All these were assigned as weak interactions.

Table 5. NMR-derived restraints for **4-FCIN** in methanol-d_4.

Proton–proton pair	Volume measured ($\times 10^6$)	Strength of interaction[a]
H-6^{AGlc}–H-6^{BGlc}	4.14	S
H-6^{AGal}–H-6^{BGal}	2.72	S
H-1^{Xyl}–H-2^{Gal}	2.5	M
H-4^{Gal}–H-3^{Gal}	2.16	M
H-5^{AeqXyl}–H-5^{BaxXyl}	2.03	M
H-2^{A}–H-8^{A}	1.81	M
H-6^{A}–H-8^{A}	1.81	M
H-2^{A}/6^{A}–H3^{A}/5^{A}	1.79	M
H-1^{Xyl}–H-5^{BaxXyl}	1.17	W
H-7^{A}–H-2^{A}	1.11	W
H-7^{A}–H-6^{A}	1.11	W
H-1^{Xyl}–H-3^{Gal}	1.07	W
H-4–H-1^{Gal}	1	W
H-6^{BGlc} (Pro-S)–H-2^{Glc}	0.751	W
H-7^{A}–H-1^{Gal}	0.742	W
H-6'–H-5'	0.696	W
H-8^{A}–H-1^{Gal}	0.445	W
H-1^{Gal}–H-3^{Gal}	0.325	W
H-6^{BGlc} (Pro-S)–H-4^{Gal}	0.141	W
H-2^{Gal}–H-4^{Gal}	0.132	W
H-7^{A}–H-8^{A}	0.131	W
H-6^{AGal} (Pro-R)–H-4^{Gal}	0.0715	W

a. Strong interaction (S) = 1.7 Å–2.5 Å; medium interaction (M) = 1.7 Å–3.2 Å; weak interaction (W) = 1.7 Å–5 Å.

Table 6. NMR-derived restraints for **345-TCIN–X** in methanol-d_4.

Proton–proton pairs	Volume measured ($\times 10^6$)	Strength of interaction[a]
$H\text{-}6^{AGlc}$–$H\text{-}6^{BGlc}$	1.2	S
$H\text{-}7^{A}$–$H\text{-}2^{A}$	0.39	W
$H\text{-}7^{A}$–$H\text{-}6^{A}$	–[b]	W
$H\text{-}7^{A}$–$H\text{-}8^{A}$	–[b]	W
$H\text{-}8^{A}$–$H\text{-}2^{A}$	–[b]	W
$H\text{-}8^{A}$–$H\text{-}6^{A}$	–[b]	W
$H\text{-}1^{Gal}$–H-4	–[b]	W
$H\text{-}1^{Gal}$–$H\text{-}7^{A}$	–[b]	W
$H\text{-}1^{Gal}$–$H\text{-}3^{Gal}$	–[b]	W
$H\text{-}6^{AGal}$–$H\text{-}6^{BGal}$	–[b]	W

a. Strong interaction (S) = 1.7 Å–2.5 Å; medium interaction (M) = 1.7 Å–3.2 Å; weak interaction (W) = 1.7 Å–5 Å. b. A ROE that was confirmed by visual inspection of the spectrum, but whose volume could not be measured accurately due to either t_1 noise or overlap of signals. All these were assigned as weak interactions.

Table 7. NMR-derived restraints for **345-TCIN** in methanol-d_4.

Proton–proton pairs	Volume measured (× 10^6)	Strength of interaction[a]
H-8^A–H-2^A	3.8	S
H-8^A–H-6^A	3.8	S
H-6^{AGlc}–H-6^{BGlc}	3.2	S
H-7^A–H-2^A	2.6	M
H-7^A–H-6^A	2.6	M
H-4^{Gal}–H-5^{Gal}	1.01	W
H-4^{Gal}–H-2^{Gal}	0.91	W
H-7^A–H-1^{Gal}	0.8	W
H-4–H-1^{Gal}	0.78	W
H-7^A–H-2^{Gal}	0.61	W
H-4–H-2^{Gal}	0.48	W
H-1^{Gal}–H-4^{Gal}	0.27	W
H-1^{Gal}–H-5^{Gal}	0.034	W
H-4^{Gal}–H-3^{Gal}	–[b]	W
H-4–H-3^{Gal}	–[b]	W
H-7^A–H-3^{Gal}	–[b]	W
H-7^A–H-8^A	–[b]	W
H-4^{Xyl}–H-5^{AeqXyl}	–[b]	W

a. Strong interaction (S) = 1.7 Å–2.5 Å; medium interaction (M) = 1.7 Å–3.2 Å; weak interaction (W) = 1.7 Å–5 Å. b. A ROE that was confirmed by visual inspection of the spectrum, but whose volume could not be measured accurately due to either t_1 noise or overlap of signals. All these were assigned as weak interactions.

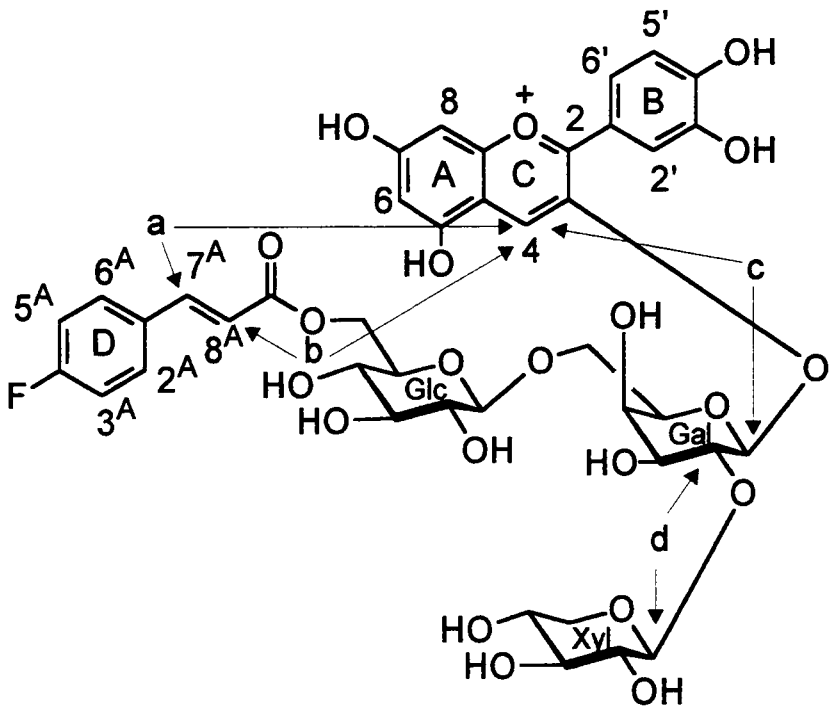


Fig. 5. Network of long-range ROEs in **4-FCIN**.

4. Low-Temperature ^{1}H NMR Studies. The acidic methanolic solutions of anthocyanins offered a unique opportunity to investigate the behavior of these compounds at low temperatures. Previously unpublished results suggested that anthocyanins similar to **4-FCIN**, **345-TCIN–X**, and **345-TCIN** in an acidic medium exhibit a certain degree of flexibility.[42] In these preliminary low-temperature ^{1}H NMR studies, workers suggested that the xylose moiety suffers from considerable internal motions, and this may be important in causing the molecule to contort and fold to shield the C-2 position of the flavylium nucleus. However, there was negligible difference in the color stability of **345-TCIN** and **345-TCIN–X** (see section on "Determination of the Color Stability of Anthocyanins"), a fact that indicates that the β-xylopyranosyl moiety is not crucial in rendering these cinnamoylated anthocyanins more color stable than their nonacylated counterparts. Furthermore, the ^{1}H NMR data of the 24 compounds shows that there is a negligible difference in the chemical shifts of protons in the glycosidic domain in either the benzoylated or cinnamoylated anthocyanins. Clearly the saccharide sub-units, irrespective of the acyl moiety attached at the O-6 Glc terminus, are positioned in such a way that results in the protons in experiencing similar magnetic environments. Thus there must be other nuances in the structure of these anthocyanins in solution that account for the difference in color stability between the various cinnamoylated anthocyanins.

Examination of the aromatic region of the ^{1}H NMR spectra at −20, −40, −60, −80, and −90 °C of the five compounds, **CyanGXG**, **345-TMBENZ**, **4-**

FCIN, **345-TCIN**, and **345-TCIN–X**, reveal that the flavylium nucleus (rings A, C, and B in Fig. 4) is a highly flexible moiety (For low-temperature ^{1}H NMR studies of **CyanGXG**, **345-TMBENZ**, **4-FCIN**, **345-TCIN**, and **345-TCIN–X**, refer to Figs. 6, 7, 8, 9, and 10, respectively). Interestingly the A–C ring system of the flavylium nucleus rotates more rapidly than the 3,4-dihydroxyphenyl ring (ring B), irrespective of the acyl moiety attached to the O-6 Glc terminus of the anthocyanins. For compounds **CyanGXG**, **345-TMBENZ**, and **4-FCIN**, rotation of ring B is severely retarded at -60 °C (see the signals marked H-2', H-6', and H-5' in the Figs.); however, the singlets of H-4 and H-8 are persistent at even -90 °C. This suggests that while rotation at low temperature essentially halts for ring B, considerable motion is retained for the A–C ring system relative to the sugar chain, giving rise to a large number of possible rotational states. Remarkably, when the anthocyanins are cinnamoylated with 3,4,5-trimethoxycinnamic acid, the A–C ring system of the flavylium nucleus behaves very differently (see Figs. 9 and 10). At -90 °C the H-4 singlets become broad doublets, indicating that the machinations of the A–C ring system of the flavylium nucleus is impeded in the presence of this particular acyl moiety.

Figs. 6–10 show that it is not just the flavylium nucleus of the monoacylated anthocyanins that have a high degree flexibility. The aromatic protons H-2^A and H-6^A of the 3,4,5-trimethoxybenzoyl and 3,4,5-trimethoxycinnamoyl moieties in **345-TMBENZ**, **345-TCIN**, and **345-TCIN–X**, respectively, broaden at -80 °C, indicating that the motion of the acyl moieties

Fig. 6. Low-temperature ^{1}H NMR studies of **CyanGXG** in methanol.

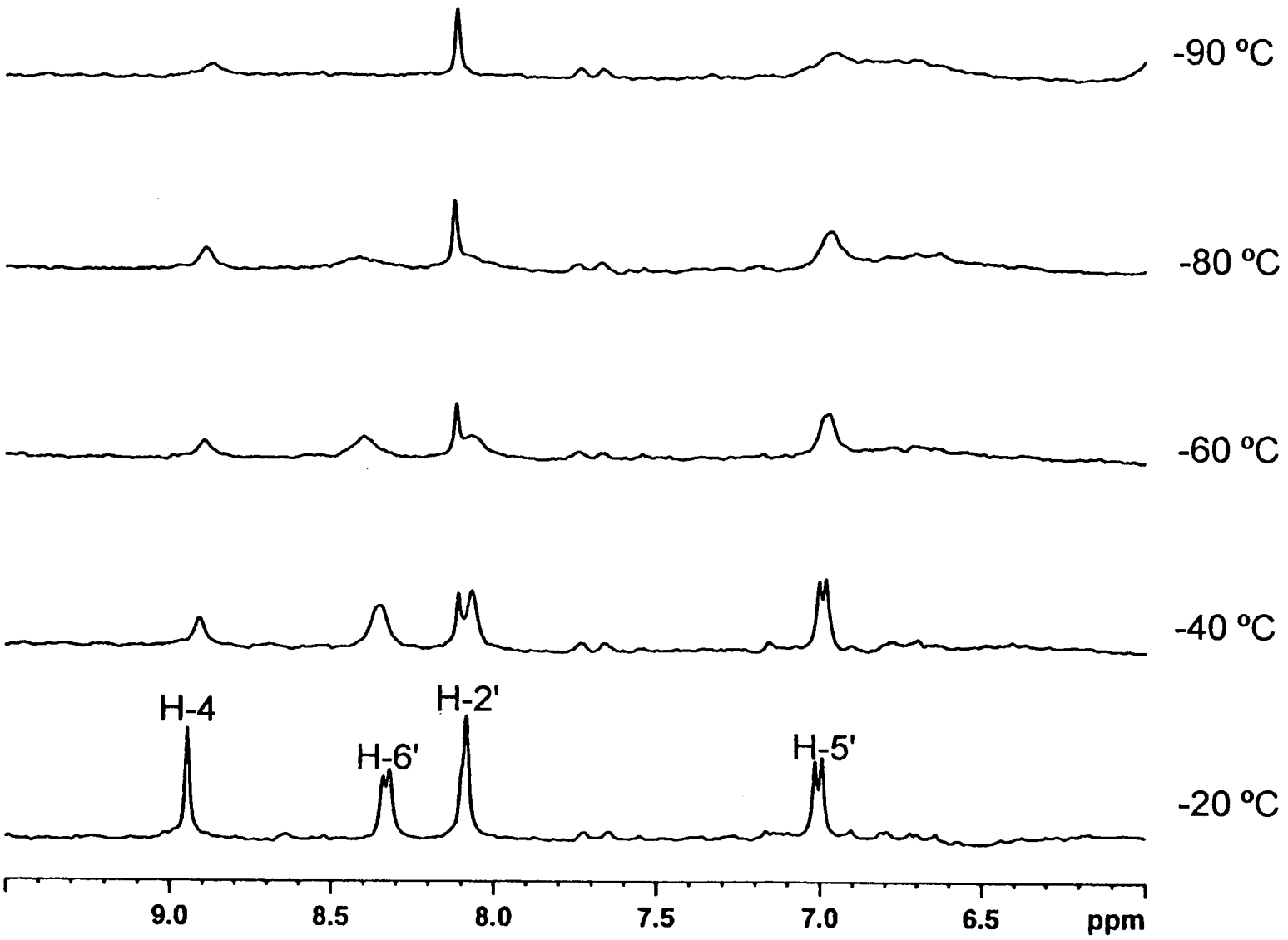

-90 °C
-80 °C
-60 °C
-40 °C
-20 °C
H-4
H-6'
H-2'
H-5'
9.0
8.5
8.0
7.5
7.0
6.5
ppm

Fig. 7. Low-temperature ^{1}H NMR studies of **345-TMBENZ** in methanol.

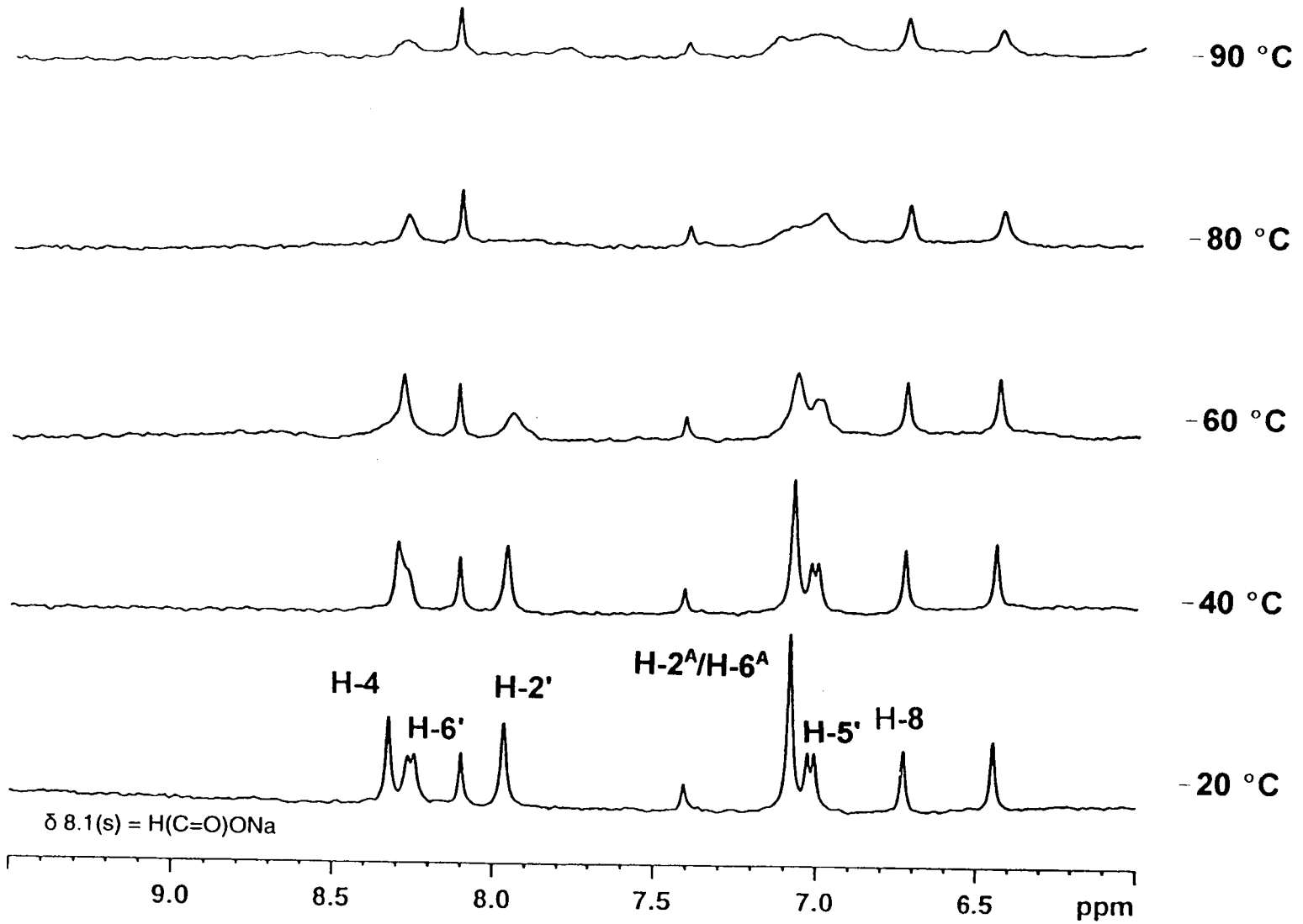

-90 °C
-80 °C
-60 °C
-40 °C
-20 °C
H-4
H-6'
H-2'
H-2^A/H-6^A
H-5'
H-8
δ 8.1(s) = H(C=O)ONa
9.0
8.5
8.0
7.5
7.0
6.5
ppm

Fig. 8. Low-temperature ^{1}H NMR studies of **4-FCIN** in methanol.

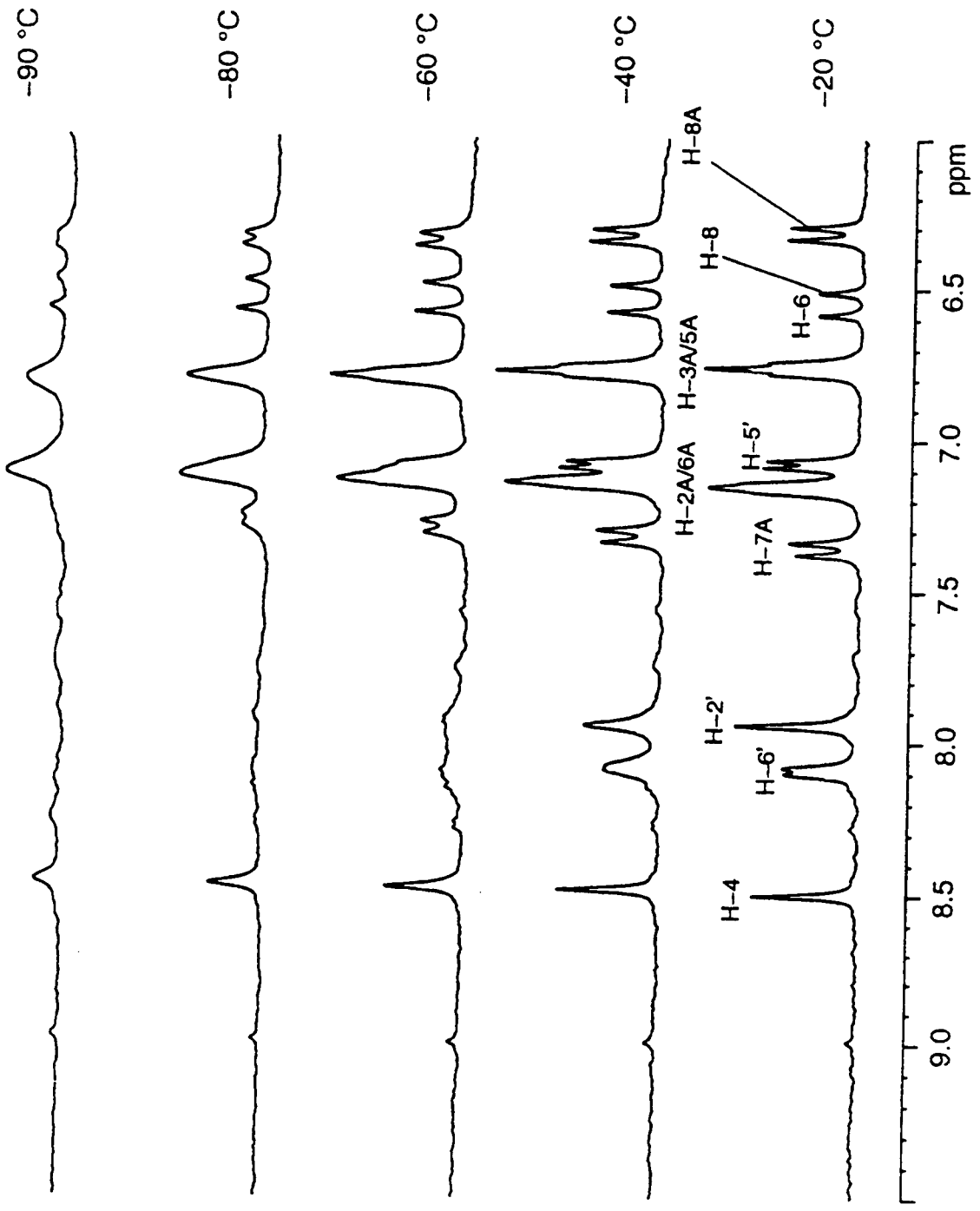

-90 °C
-80 °C
-60 °C
-40 °C
-20 °C
H-8A
H-8
H-6
H-3A/5A
H-5'
H-2A/6A
H-7A
H-2'
H-6'
H-4
9.0
8.5
8.0
7.5
7.0
6.5
ppm

Fig. 9. Low-temperature ^{1}H NMR studies of **345-TCIN** in methanol.

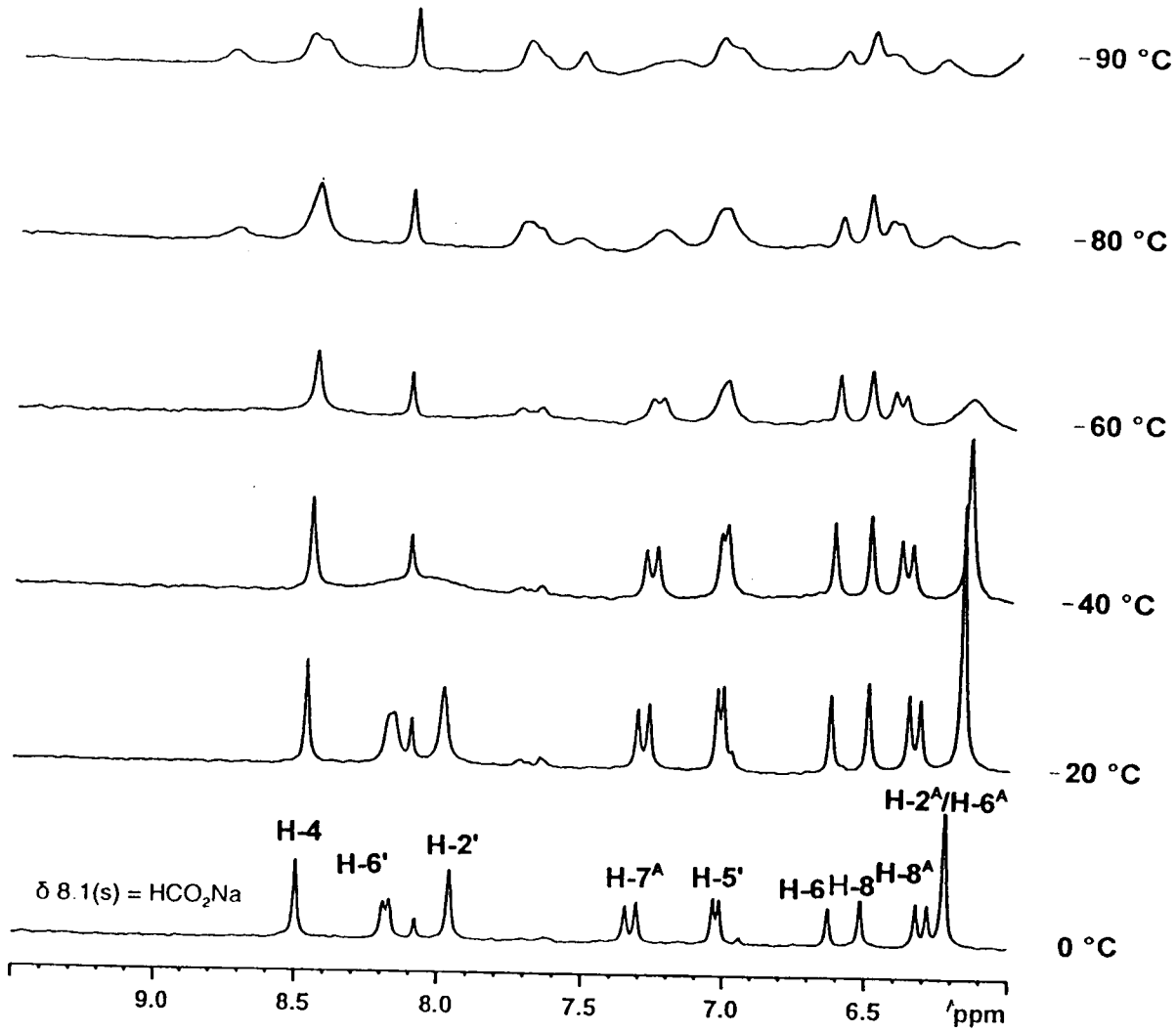
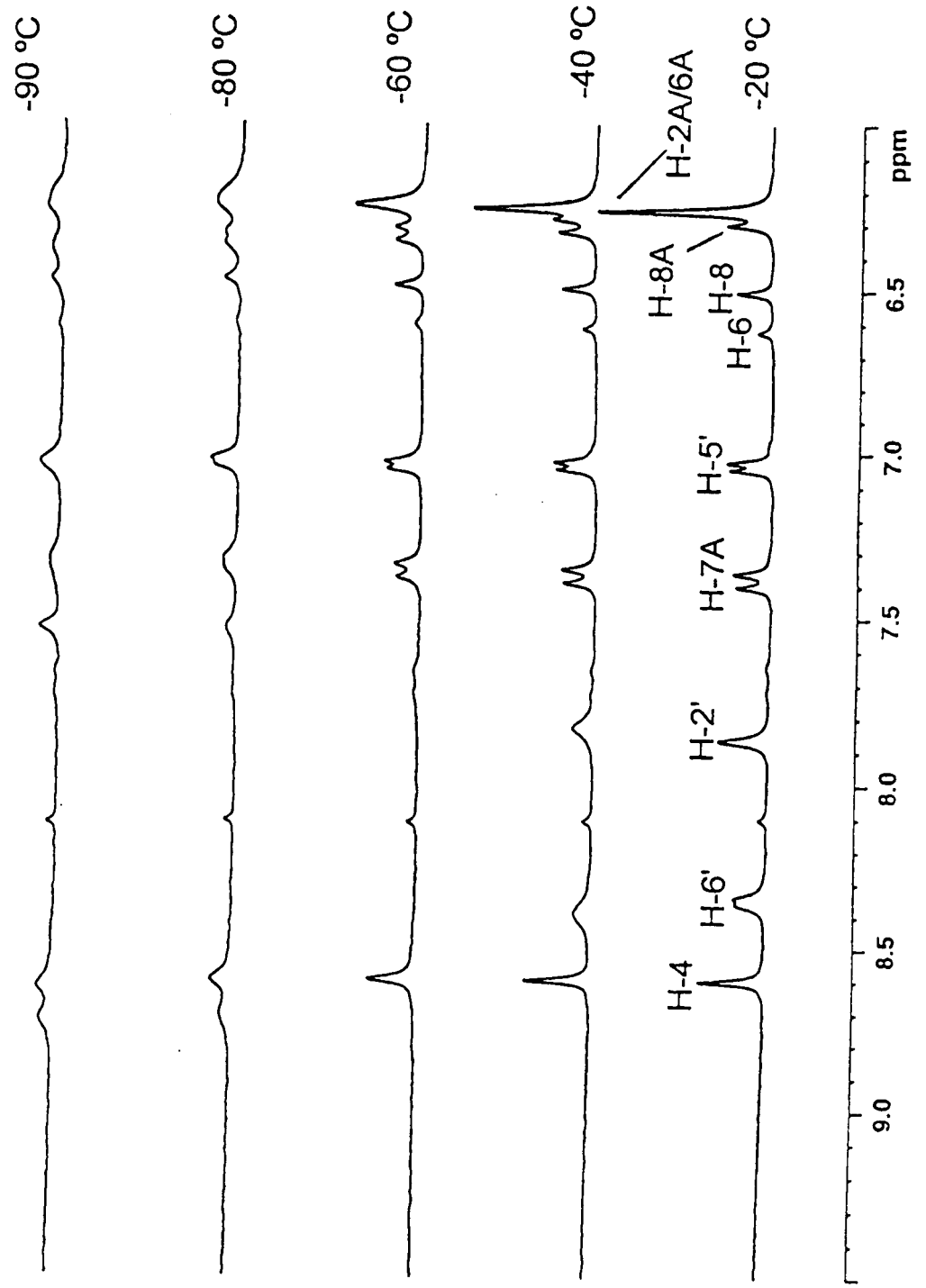

-90 °C
-80 °C
-60 °C
-40 °C
-20 °C
0 °C
H-4
H-6'
H-2'
H-7^A
H-5'
H-6
H-8
H-8^A
H-2^A/H-6^A
δ 8.1(s) = HCO2Na
9.0
8.5
8.0
7.5
7.0
6.5
f ppm

Fig. 10. Low-temperature ^{1}H NMR studies of **345-TCIN–X** in methanol.


-90 °C
-80 °C
-60 °C
-40 °C
-20 °C
H-4
H-6'
H-2'
H-7A
H-5'
H-8A
H-6
H-8
H-2A/6A
9.0
8.5
8.0
7.5
7.0
6.5
ppm

is essentially halted at this temperature (see Figs. 7, 9, and 10). The aromatic protons of the 4-fluorocinnamoyl moiety behave similarly (see Fig. 8). Even the exocyclic double bond in the cinnamoylated anthocyanins **4-FCIN**, **345-TCIN–X** and 345-TCIN is subject to rapid internal motions, which are only diminished at -80 °C. At this temperature the two doublet signals for H-7^A and H-8^A broaden significantly. The exocyclic double bond of anthocyanin **4-FCIN** experiences more internal motions than the corresponding moiety in the anthocyanin acylated with 3,4,5-trimethoxycinnamic acid.

These studies demonstrate that these molecules are subject to considerable internal motions, irrespective of the acyl moiety attached to the 6-O-Glc terminus of the anthocyanin. There are three major functionalities that experience internal motions, that result in the molecule's inherent flexibility: the A–C ring system of the flavylium nucleus, the 3,4-dihydroxyphenyl moiety (ring B), and in the case of cinnamoylated anthocyanins, the exocyclic double bond. In the cinnamoylated anthocyanins investigated, the motions of the A–C ring system are impeded when the anthocyanin is cinnamoylated with 3,4,5-trimethoxycinnamic acid (**345-TCIN** and **345-TCIN–X**). Additionally the flexibility of the exocyclic double bond in the former two compounds is also reduced, compared to the anthocyanin acylated with 4-fluorocinnamic acid (**4-FCIN**).

If molecular models of these anthocyanins are to be useful in studying the molecular events that contribute to the mechanisms of color loss, they would

have to incorporate the flexible nature of these monocinnamoylated anthocyanins, which have been established using both 1D and 2D ^{1}H NMR studies.

D. Molecular Modeling Studies in Methanol

1. Quenched Molecular Dynamics (QMD) Studies. Molecular modeling of anthocyanins using NMR data has been conducted by several groups.[31,43-45] These researchers used both restrained methods or distance geometry programs to construct models of certain anthocyanins. However, these previous attempts to model anthocyanins were totally unsuitable to construct reasonable models of the highly flexible anthocyanins that include compounds **CyanGXG**, **345-TMBENZ**, **4-FCIN**, **345-TCIN**, and **345-TCIN–X**.

Recently, an NMR–QMD protocol has been used by several research groups to study flexible molecules in solution, such as cyclic peptidomimetics,[38,39] short, linear peptides,[40] and α-melanotropins.[41] In these investigations, conformations of the molecules that result from the QMD process are evaluated based on both energy and NMR-derived restraints. The QMD calculation is a two-stage process: a molecular dynamics simulation in a dielectric continuum that represents the solvent used in the ^{1}H NMR studies, which is followed by an exhaustive minimization process. After generating a randomized structure by

performing molecular dynamics simulations from 300 K to a 1000 K, the final structure is subjected to an extensive molecular dynamics simulation at 1000 K. During this simulation a snapshot of the trajectory of the molecule is taken every picosecond. The resulting structures, between 600 and 1000, which have very different consensus folds, are then exhaustively minimized with a suitable force field. By evaluating the conformations based on total energy and NMR-derived restraints, reasonable structures of the molecules are thus generated.

Critical to the suitability of this approach to these anthocyanins was the selection of a force field for the minimization sequence. The force field had to be able to cope with two different domains within the anthocyanin—the charged, aromatic flavylium nucleus and the carbohydrate units that comprise the backbone of these anthocyanins. The only force field that met these requirements was the consistent valence force field (CVFF).[46]

The utility of this QMD–NMR protocol has recently been demonstrated in its application to the study of **4-FCIN** in methanol.[37] An extensive molecular dynamics simulation was performed at 600 K for 1 ns—a snapshot of the molecule was taken every 1 ps. The resulting 1000 structures were evaluated based on their total energy and NMR-derived restraints, which yielded 404 structures. In all prior QMD–NMR studies, several low-energy conformational families were observed.[38-41] Not surprisingly then, the 404 structures produced in this study of **4-FCIN** were categorized into 12 distinct conformational families.

Previous models of anthocyanins, in addition to not taking into account the flexibility of these anthocyanins, yielded only one low-energy conformation.[31,43-45]

The same protocol was adopted for the other anthocyanins. For each anthocyanin under investigation, the 1000 minimized conformations are evaluated based on their total energy. If any of these conformations were greater than 5 kcal mol^{-1} of the global minimum, these were not evaluated any further. The remaining conformations are then validated by the NMR-derived restraints (see Tables 3–7) acquired by ROESY experiments. [37] The results from the QMD calculation are summarized in Table 8.

Table 8. Results of the QMD studies in methanol.

Compound[a]	Total energy (kcal mol^{-1})	NMR-derived restraints satisfied
CyanGXG (715)	141.7 ± 1.0	> 9
345-TMBENZ (511)	197.3 ± 1.7	> 18
4-FCIN (404)	101.3 ± 2.0	> 16
345-TCIN–X (832)	191.6 ± 1.0	> 9
345-TCIN (689)	198.7 ± 1.2	> 12

a. The number in parentheses represents the total number of structures that are within 5 kcal mol^{-1} of the global minimum, and satisfy the NMR-derived restraints.

2. Conformational Families. A summary of the results of each QMD calculation for the five anthocyanins is presented in Table 8. In order to group conformers into conformational families, all 1000 structures for each anthocyanin had to be evaluated based on their total energy, and how well they correspond to the 2D NMR data collected (NMR-derived restraints). As mentioned in the previous Section, all structures that had a total energy greater than 5 kcal mol^{-1} of the global minimum were not considered further. Interestingly, this was found to be the most discriminating method for evaluation of minimized structures, as opposed to the use of NMR-derived restraints. This discovery allowed us to pursue a similar study in water (see the section, "Molecular Modeling Study in Water")—the medium that simulates the conditions found in pharmaceutical and nutraceutical formulations—without validating the models generated with the NMR-derived restraints.

a. Classification of conformations. The structures of **CyanGXG**, **345-TMBENZ**, **4-FCIN**, **345-TCIN–Xyl**, and **345-TCIN** from the above analysis were inspected for their overall folding preferences. The coordinates of each particular conformation were read in from the QMD archive file for each of the compounds studied. In order to perform this classification, the molecule was orientated on the screen such that the galactose residue (β-Gal in Fig. 4) was directed away from the viewer and the acyl moiety (Ring D in Fig. 4) was below the flavylium nucleus (Rings A, B, and C in Fig. 4). If the flavylium nucleus was oriented such

that the nucleus reads "ACB", the conformer in question was classified as "nonflipped" structure (N was used in the code that follows the compound name, for example **345-TCIN–XN**). Conversely, if the flavylium nucleus reads "BCA", the conformer was classified as a "flipped" structure (F was used in the code that follows the compound name, for example, **345-TCIN–XF**). The next aspect of the shape of the minimized structures considered was the alignment of the O-6 position of the β-Gal that is glycosylated with β-Glc. If the β-Glc moiety was forced to be positioned to either the left, or the right, or underneath the flavylium nucleus, the next letter of the compound code was L, R, and U, respectively, for example **345-TCIN–XNR**. Lastly, the relationship of the acyl moiety D to the flavylium nucleus was noted. For example, if the acyl ring D was under the naphthyl portion of the ring (A–C), or the 3,4-dihydroxyphenyl moiety (ring B), or not proximal to any of the units of the flavylium nucleus, the last letters of the code were A–C, B, or D, respectively. When this initial classification was performed for **345-TCIN–X** and **345-TCIN**, the β-Glc came up-and-over the flavylium nucleus. If this occurred in any particular conformation, the term OP was added to the code, for example **345-TCIN–XNUACOP**. In the case of the nonacylated anthocyanin **CyanGXG**, the position the β-Glc, with respect to the flavylium nucleus was considered, i.e., if the β-Glc moiety was underneath the A–C ring system in the "nonflipped" orientation, the code for that conformational family becomes **CyanGXGNUAC**.

Distinct conformational families for each anthocyanin that resulted from the above classification system were proven by considering six dihedral angles, ϕ_1–ϕ_6 (for the dihedral angles measured, see Fig. 11). These data and the RMS deviation values from pairwise superimposition of each conformation within the conformational family for each anthocyanin is given in Tables 9–18.

For the studies of the above compounds, a representative structure of each family was selected based on the lowest energy conformation, which met the greatest number of NMR-derived restraints. These representative structures were used to examine the consensus fold of **CyanGXG**, **345-TMBENZ**, **4-FCIN**, **345-TCIN**, and **345-TCIN–X** in methanol.

Figs. 12–16 show the complete network of long-range rotating frame Overhauser effects (ROEs) and which of the long-range restraints are satisfied by the representative frame from each conformational family for **CyanGXG**, **345-TMBENZ**, **4-FCIN**, **345-TCIN**, and **345-TCIN–X**, respectively. The total number of NMR-derived restraints that is satisfied by these representative structures is also shown in the above Figs.

Although very few of the representative low-energy conformations satisfy all the long-range NMR-derived restraints (8 out of a total of 40 structures), all the conformational families satisfy some of the long-range restraints, which have been derived from ROESY studies at 500 ms. The failure of these low-energy

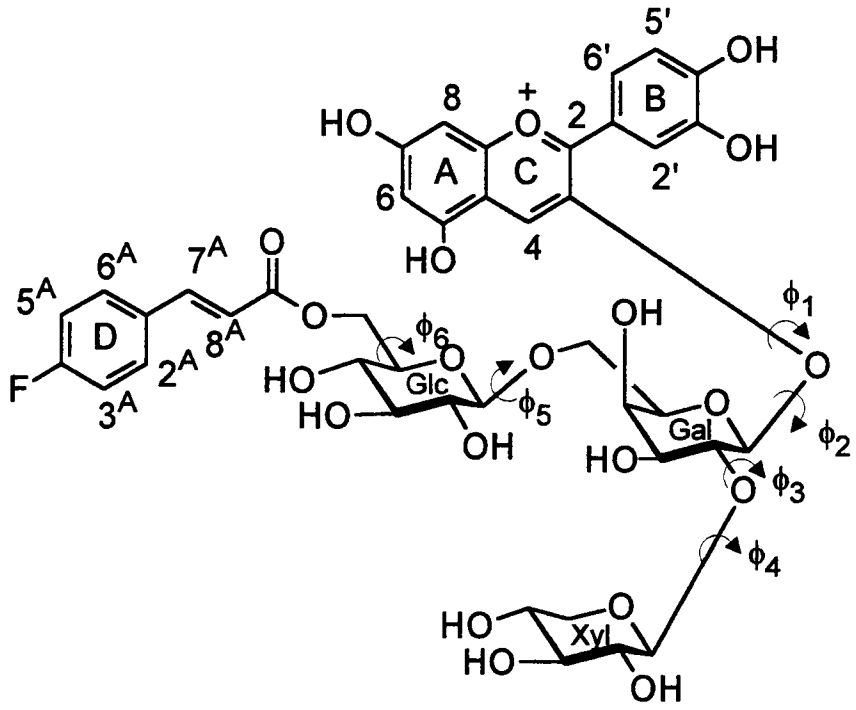


Fig. 11. Dihedral angles of **4-FCIN** used in the classification system.

Table 9. Dihedral angles measured in **CyanGXG**—a study in methanol.

Conformational family [a,b]	ϕ_1 [c]	ϕ_2	ϕ_3	ϕ_4	ϕ_5	ϕ_6
CyanGXGNUB (409)	-80 ± 4°	59 ± 3°	37 ± 25°	-5 ± 6°	126 ± 45°	-55 ± 57°
CyanGXGNUAC (299)	-83 ± 14°	62 ± 4°	42 ± 20°	-2 ± 5°	-2 ± 24°	-44 ± 55°
CyanGXGNRAC (2)	-33°	74°	54°	3°	138°	177°
CyanGXGFUAC (5)	86 ± 1°	47 ± 1°	38 ± 1°	21 ± 0.2°	-7 ± 3°	-39 ± 74°

a. The number in parentheses is the total number of structures in the individual families. b. Values that have no errors indicated in the table have an error less than ± 0.01°. c. The dihedral angles are defined in Fig. 11.

Table 10. RMS deviation value for each conformational family of **CyanGXG** in methanol.

Conformational family	RMS deviation value
CyanGXGNUB	1.78 ± 0.698 Å
CyanGXGNUAC	1.02 ± 0.667 Å
CyanGXGNRAC	0.34 Å
CyanGXGFUAC	0.63 ± 0.091 Å

Table 11. Dihedral angles measured in **345-TMBENZ**—a study in methanol.

Conformational family [a,b]	ϕ_1 [c]	ϕ_2	ϕ_3	ϕ_4	ϕ_5	ϕ_6
345-TMBENZNRAC (452)	-57 ± 44°	17 ± 40°	49 ± 13°	-7 ± 15°	14 ± 28°	-67 ± 6°
345-TMBENZNRD (51)	-97 ± 3°	14 ± 3°	-9 ± 34°	-14 ± 7°	-52 ± 1°	-56 ± 1°
345-TMBENZNLAC (8)	69°	54°	39°	13°	-46°	26°

a. The number in parentheses is the total number of structures in the individual families. b. Values that have no errors indicated in the table have an error less than ± 0.01°. c. The dihedral angles are defined in Fig. 11.

Table 12. RMS deviation values for each conformational family of **345-TMBENZ**—a study in methanol.

Conformational family	RMS deviation value
345-TMBENZNRAC	2.14 ± 0.453 Å
345-TMBENZNRD	1.02 ± 0.259 Å
345-TMBENZNLAC	0.53 ± 0.053 Å

Table 13. Dihedral angles measured in **4-FCIN**—a study in methanol.

Conformational family [a,b]	ϕ_1 [c]	ϕ_2	ϕ_3	ϕ_4	ϕ_5	ϕ_6
4-FCINFRD (58)	77° ± 5°	49° ± 3°	31° ± 19°	11° ± 8°	-3° ± 6°	-64° ± 3°
4-FCINFRB2 (34)	-6.3°	167°	60°	-3.0°	65°	-67°
4-FCINFRB3 (24)	-27°	178°	60°	9°	56°	-66°
4-FCINFRB1 (20)	85° ± 2°	63° ± 3°	50° ± 2°	-7° ± 4°	76° ± 16°	72° ± 2°
4-FCINFRAC (15)	23° ± 17°	35° ± 11°	52° ± 12°	25° ± 12°	17° ± 7°	-170° ± 1°
4-FCINFLD (4)	100° ± 2°	156° ± 3°	30° ± 6°	-7° ± 5°	11° ± 6°	-66° ± 0.1°
4-FCINFRB4 (3)	42°	39°	13°	37°	-7.2°	-65°
4-FCINFUB (2)	-59°	-163°	59°	28°	46°	179°
4-FCINNRAC1 (146)	-85° ± 1°	51° ± 5°	44° ± 31°	1° ± 18°	85° ± 7°	-69° ± 3°
4-FCINNRD (75)	-92° ± 3°	15° ± 7°	25° ± 40°	4° ± 18°	-2° ± 10°	-61° ± 3°
4-FCINNUAC (18)	44°	-53°	67°	15°	43°	-58°
4-FCINNRAC2 (5)	-113°	-38°	51°	29°	28°	-166°

a. The number in parentheses is the total number of structures in the individual families. b. Values that have no errors indicated in the table have an error less than ± 0.01°. c. The dihedral angles are defined in Fig. 11.

Table 14. RMS deviation values for each conformational family of **4-FCIN** in methanol.

Conformational family	RMS deviation value
4-FCINFRD	1.22 ± 0.303
4-FCINFRB2	0.67 ± 0.315
4-FCINFRB3	0.86 ± 0.327
4-FCINFRB1	0.58 ± 0.266
4-FCINFRAC	1.13 ± 0.346
4-FCINFLD	1.12 ± 0.095
4-FCINFRB4	1.05
4-FCINFUB	–
4-FCINNRAC1	0.99 ± 0.391
4-FCINNRD	1.24 ± 0.387
4-FCINNUAC	0.76 ± 0.301
4-FCINNRAC2	0.56 ± 0.330

Table 15. Dihedral angles measured in **345-TCIN–X**—a study in methanol.

Conformational family [a,b]	ϕ_1 [c]	ϕ_2	ϕ_3	ϕ_4	ϕ_5	ϕ_6
345-TCIN–XFLAC (296)	58 ± 8°	-34 ± 20°	–	–	141 ± 32°	-74 ± 20°
345-TCIN–XFRB (104)	-43 ± 21°	-45 ± 5°	–	–	-5 ± 23°	-68 ± 10°
345-TCIN–XFRAC (102)	-78 ± 17°	-42 ± 7°	–	–	0.3 ± 20°	-107 ± 89°
345-TCIN–XFRD2 (13)	1 ± 5°	-65 ± 2°	–	–	-23 ± 2°	-65 ± 1°
345-TCIN–XFUAC (12)	-46 ± 18°	27 ± 21°	–	–	-17 ± 11°	-145 ± 54°
345-TCIN–XFRD1 (5)	-68°	-28°	–	–	-36°	177°
345-TCIN–XFLD (2)	58 ± 2°	-60 ± 4°	–	–	153 ± 3°	-67 ± 5°
345-TCIN–XFUACOP (2)	-111°	-123°	–	–	53°	-174°
345-TCIN–XNLAC (180)	-34 ± 13°	-42 ± 5°	–	–	-13 ± 16°	-64 ± 17°
345-TCIN–XNLB (98)	-78 ± 17°	-42 ± 7°	–	–	0 ± 20°	-107 ± 89°
345-TCIN–XNUACOP (18)	60 ± 2°	-73 ± 4°	–	–	59 ± 15°	-166 ± 11°

a. The number in parentheses is the total number of structures in the individual families. b. Values that have no errors indicated in the table have an error less than ± 0.01°. c. The dihedral angles are defined in Fig. 11.

Table 16. RMS deviation values for each conformational family of **345-TCIN–X**—a study in methanol.

Conformational family	RMS deviation value
345-TCIN–XFLAC	2.34 ± 0.407 Å
345-TCIN–XFRB	1.87 ± 0.607 Å
345-TCIN–XFRAC	1.78 ± 0.622 Å
345-TCIN–XFRD2	2.08 ± 0.741 Å
345-TCIN–XFUAC	1.93 ± 0.738 Å
345-TCIN–XFRD1	0.60 ± 0.060 Å
345-TCIN–XFLD	1.16 Å
345-TCIN–XFUACOP	0.54 Å
345-TCIN–XNLAC	1.39 ± 0.312 Å
345-TCIN–XNLB	2.50 ± 0.301 Å
345-TCIN–XNUACOP	1.73 ± 0.903 Å

Table 17. Dihedral angles measured in **345-TCIN**—a study in methanol.

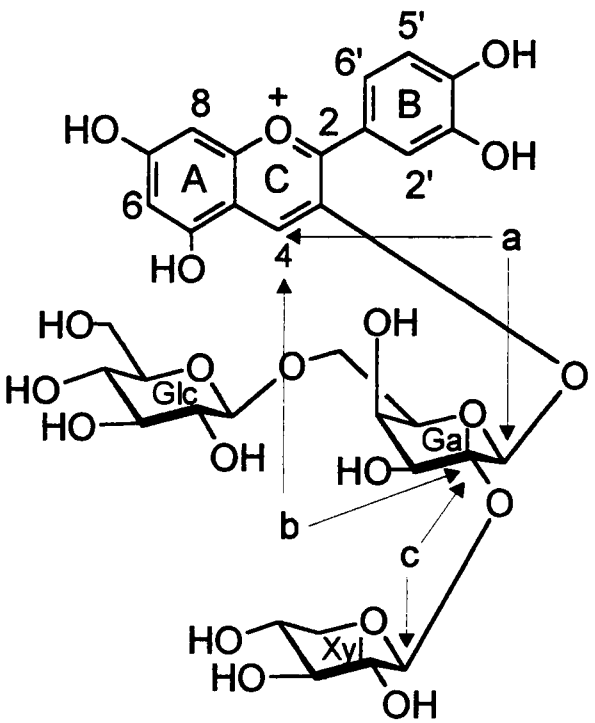
Conformational family [a,b]	ϕ_1 [c]	ϕ_2	ϕ_3	ϕ_4	ϕ_5	ϕ_6
345-TCINFRB (232)	-62 ± 6°	90 ± 1°	37 ± 2°	-32 ± 11°	-15 ± 19°	-66 ± 18°
345-TCINFRAC (167)	-59 ± 8°	96 ± 6°	45 ± 14°	-31 ± 9°	3 ± 26°	-88 ± 80°
345-TCINFRD2 (52)	-35 ± 13°	93 ± 1°	30 ± 11°	-11 ± 24°	-31 ± 7°	-64 ± 3°
345-TCINFLAC (49)	56 ± 3°	91 ± 2°	44 ± 9°	-32 ± 13°	158 ± 8°	-62 ± 2°
345-TCINFRD1 (22)	-69 ± 3°	88 ± 0.2°	37 ± 2°	-37 ± 1	-27 ± 1°	8 ± 177°
345-TCINFUAC (9)	-60 ± 3°	100 ± 4°	55 ± 3°	-25 ± 3°	84 ± 91°	-88 ± 100°
345-TCINFLD (2)	53 ± 3°	91 ± 1°	9 ± 11°	-52 ± 1°	61 ± 117°	-59 ± 7°
345-TCINFUD (1)	-64°	94°	49°	-31°	-28°	-178°
345-TCINNLAC (141)	-53 ± 11°	91 ± 1°	51 ± 14°	-11 ± 9°	131 ± 6°	-57 ± 3°
345-TCINNLD (14)	-58 ± 4°	89 ± 1°	79 ± 39°	-12 ± 7°	133 ± 2°	-62 ± 4°

a. The numbers in parenthesis are the total number of structures in the individual families. b. Values that have no errors indicated in the table have an error less than ± 0.01°. c. The dihedral angles are defined in Fig. 11.

Table 18. RMS deviation values for each conformational family of **345-TCIN** in methanol.

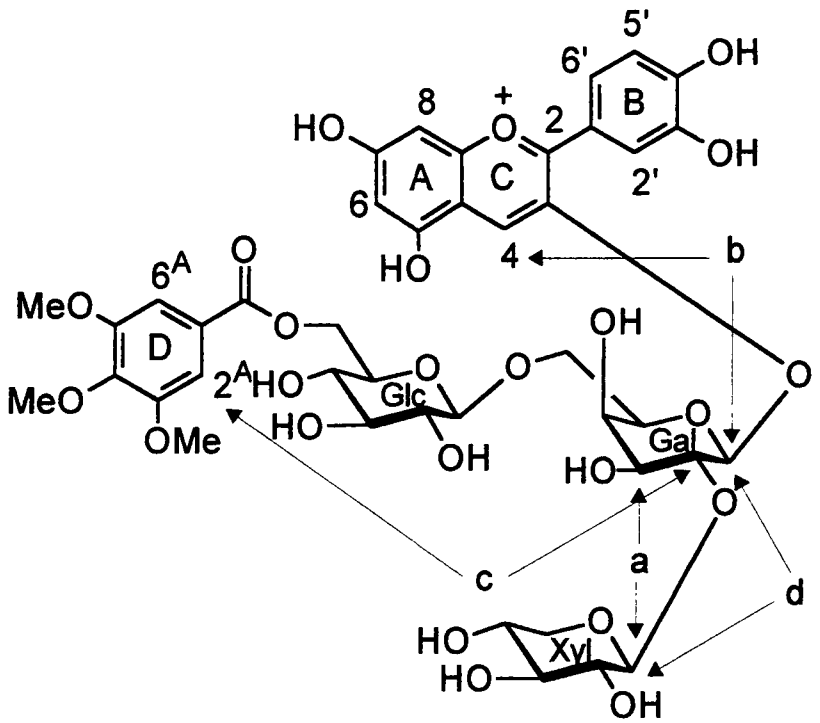
Conformational family	RMS deviation value
345-TCINFRB	2.26 ± 0.56 Å
345-TCINFRAC	2.85 ± 0.823 Å
345-TCINFRD2	1.93 ± 0.663 Å
345-TCINFLAC	1.64 ± 0.798 Å
345-TCINFRD1	1.27 ± 0.285 Å
345-TCINFUAC	2.32 ± 0.525 Å
345-TCINFLD	1.15 Å
345-TCINFUD	–
345-TCINNLAC	2.83 ± 0.443 Å
345-TCINNLD	2.19 ± 0.513 Å

Fig. 12. A complete network of long-range ROEs satisfied in the conformational families of **CyanGXG**.



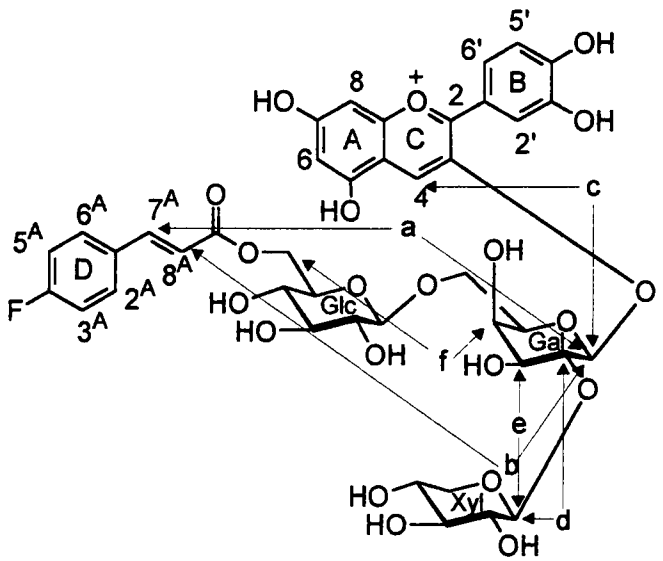
Conformational family	Number of restraints met	Long-range restraints met		
		a	b	c
CyanGXGNUB	11	✓	✓	✓
CyanGXGNUAC	11	✓	✓	✓
CyanGXGNRAC	10	✓	✓	✓
CyanGXGFUAC	10	✓	✗	✓

Fig. 13. A complete network of long-range ROEs satisfied in the conformational families of **345-TMBENZ**.



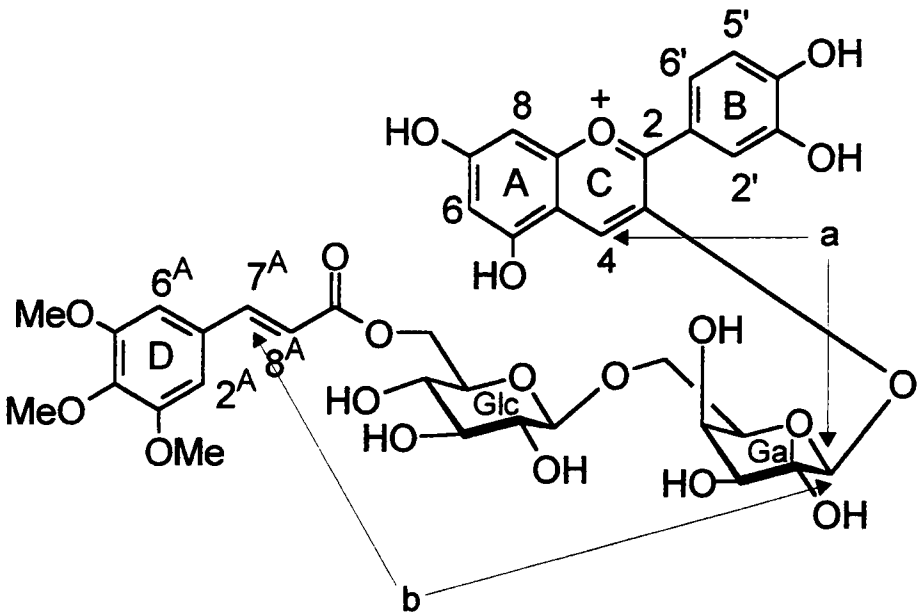
Conformational family	Number of restraints met	Long-range restraints met			
		a	b	c	d
345-TMBENZNRAC	19	✓	✓	✓	✓
345-TMBENZNRD	20	✓	✓	✓	✓
345-TMBENZNLAC	18	✓	✓	✗	✓

Fig. 14. A complete network of long-range ROEs satisfied in the conformational families of **4-FCIN**.



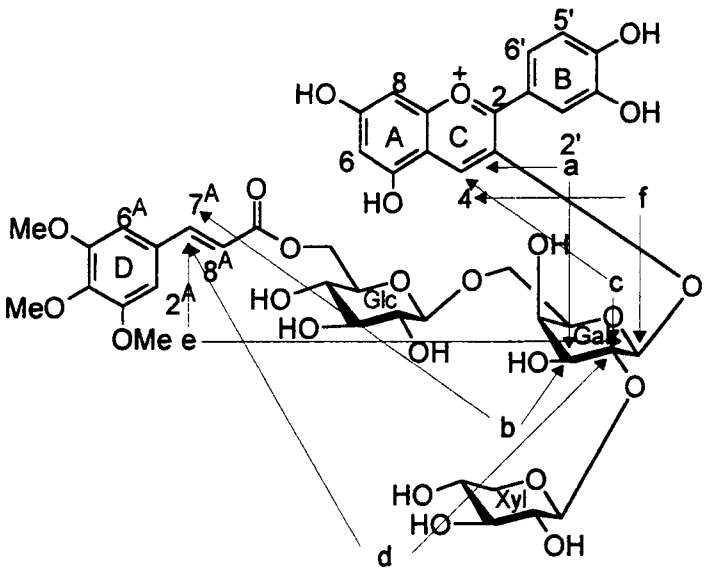
Conformational family	Number of restraints met	Long-range restraints met					
		a	b	c	d	e	f
4-FCINFRD	20	✓	✓	✓	✓	✓	✗
4-FCINFRB2	19	✓	✓	✓	✓	✓	✗
4-FCINFRB3	19	✗	✓	✓	✓	✓	✗
4-FCINFRB1	19	✓	✗	✓	✓	✓	✗
4-FCINFRAC	20	✓	✓	✓	✓	✓	✗
4-FCINFLD	18	✗	✗	✓	✓	✓	✗
4-FCINFRB4	19	✗	✓	✓	✓	✓	✗
4-FCINFUB	18	✗	✗	✓	✓	✓	✗
4-FCINNRAC1	19	✓	✗	✓	✓	✓	✗
4-FCINNRD	20	✓	✓	✓	✓	✓	✗
4-FCINNUAC	19	✗	✓	✓	✓	✓	✗
4-FCINNRAC2	18	✓	✓	✓	✓	✓	✗

Fig. 15. A complete network of long-range ROEs satisfied in the conformational families of **345-TCIN–X**.



Conformational family	Number of restraints met	Long-range restraints met	
		a	b
345-TCIN–XFLAC	9	✓	✗
345-TCIN–XFRB	9	✓	✗
345-TCIN–XFRAC	9	✓	✗
345-TCIN–XFRD2	9	✓	✗
345-TCIN–XFUAC	9	✓	✗
345-TCIN–XFRD1	9	✓	✗
345-TCIN–XFLD	10	✓	✓
345-TCIN–XFUACOP	9	✓	✗
345-TCIN–XNLAC	10	✓	✓
345-TCIN–XNLB	10	✓	✓
345-TCIN–XNUACOP	9	✓	✗

Fig. 16. A complete network of long-range ROEs satisfied in the conformational families of **345-TCIN**.



Conformational family	Number of restraints met	Long-range restraints met					
		a	b	c	d	e	f
345-TCINFRB	13	✓	✗	✗	✗	✗	✓
345-TCINFRAC	13	✓	✗	✓	✗	✗	✓
345-TCINFRD2	14	✓	✓	✓	✗	✓	✓
345-TCINFLAC	14	✓	✗	✓	✗	✓	✓
345-TCINFRD1	13	✓	✗	✓	✗	✗	✓
345-TCINFUAC	13	✓	✗	✓	✗	✗	✓
345-TCINFLD	15	✗	✓	✓	✓	✓	✓
345-TCINFUD	13	✗	✓	✓	✗	✗	✓
345-TCINNLAC	15	✓	✗	✓	✓	✓	✓
345-TCINNLD	14	✓	✗	✓	✗	✓	✓

models to match all the long-range restraints is not surprising. ROE interactions of these molecules more than likely represent an average structure—the existence of an average structure is supported by low-temperature ^{1}H NMR studies (see section, "Low-temperature ^{1}H NMR Studies"). Any specific restraint can be the result of an average between more than one conformation. Thus, a low-energy conformation, which represents a particular conformational family, may not satisfy all the NMR-derived restraints, especially in the case of a flexible molecule.[40] These findings validate that the models thus generated by the QMD–NMR protocol are reasonable representations of the molecules in an acidic methanolic solution.

3. Structural Features of the Conformational Families. Using the above classification system, each anthocyanin of the same conformational class could be compared with one another. These similarities between the individual anthocyanins are not apparent by examination of the dihedral angles in Tables 9–17.

Figs. 17–28 show the representative structures of each conformational family for all five compounds under investigation. Broadly, the conformational families can be separated into two categories: one category where the flavylium nucleus is read "BCA" (flipped) (see Figs. 17–22), and the other category where the flavylium nucleus is read "ACB" (nonflipped) (see Figs. 23–26). Figs. 27 and

Fig. 17. The FLAC conformational families in methanol.

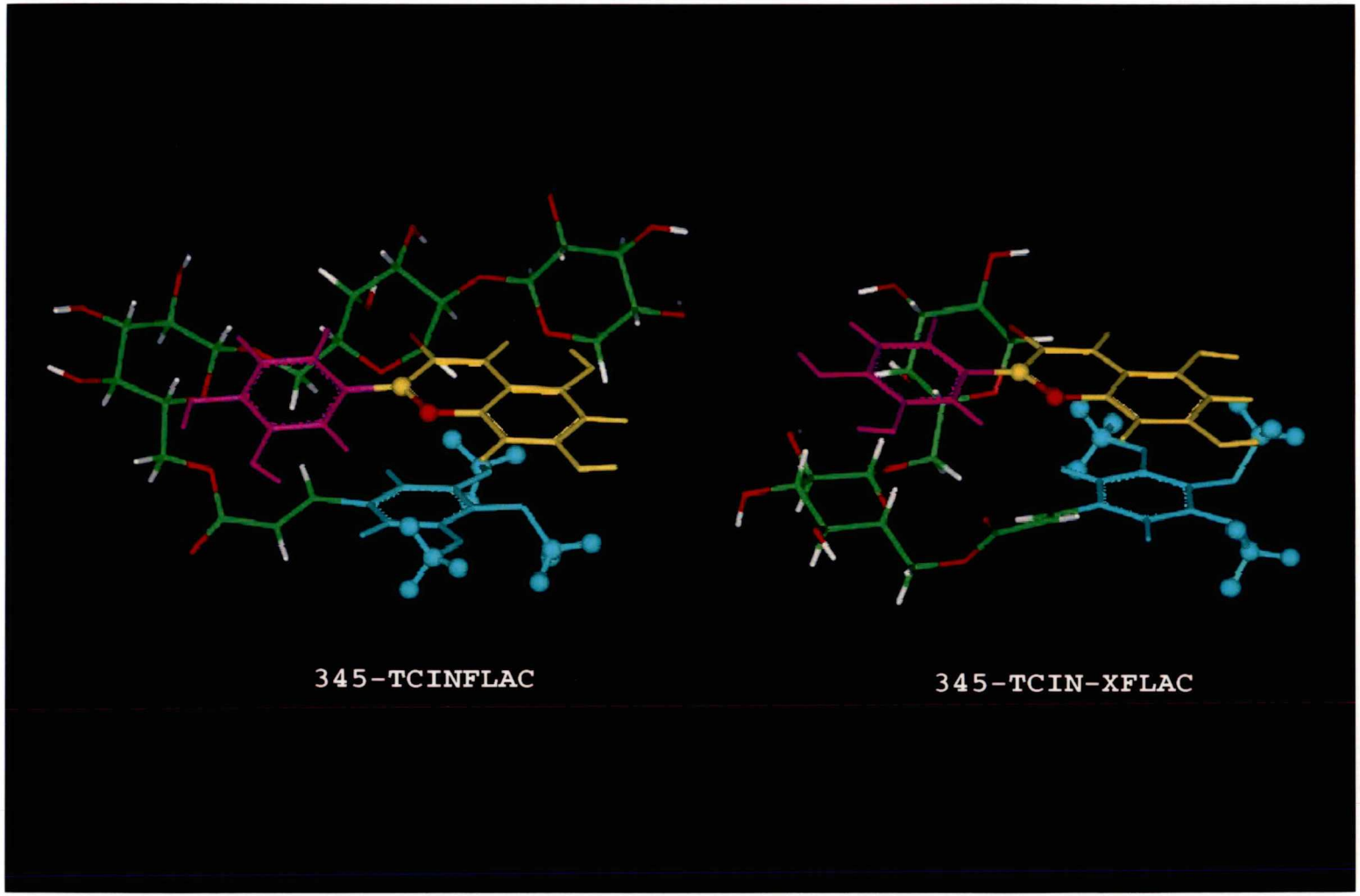

345-TCINFLAC
345-TCIN-XFLAC

Fig. 18. The FLD conformational families in methanol.

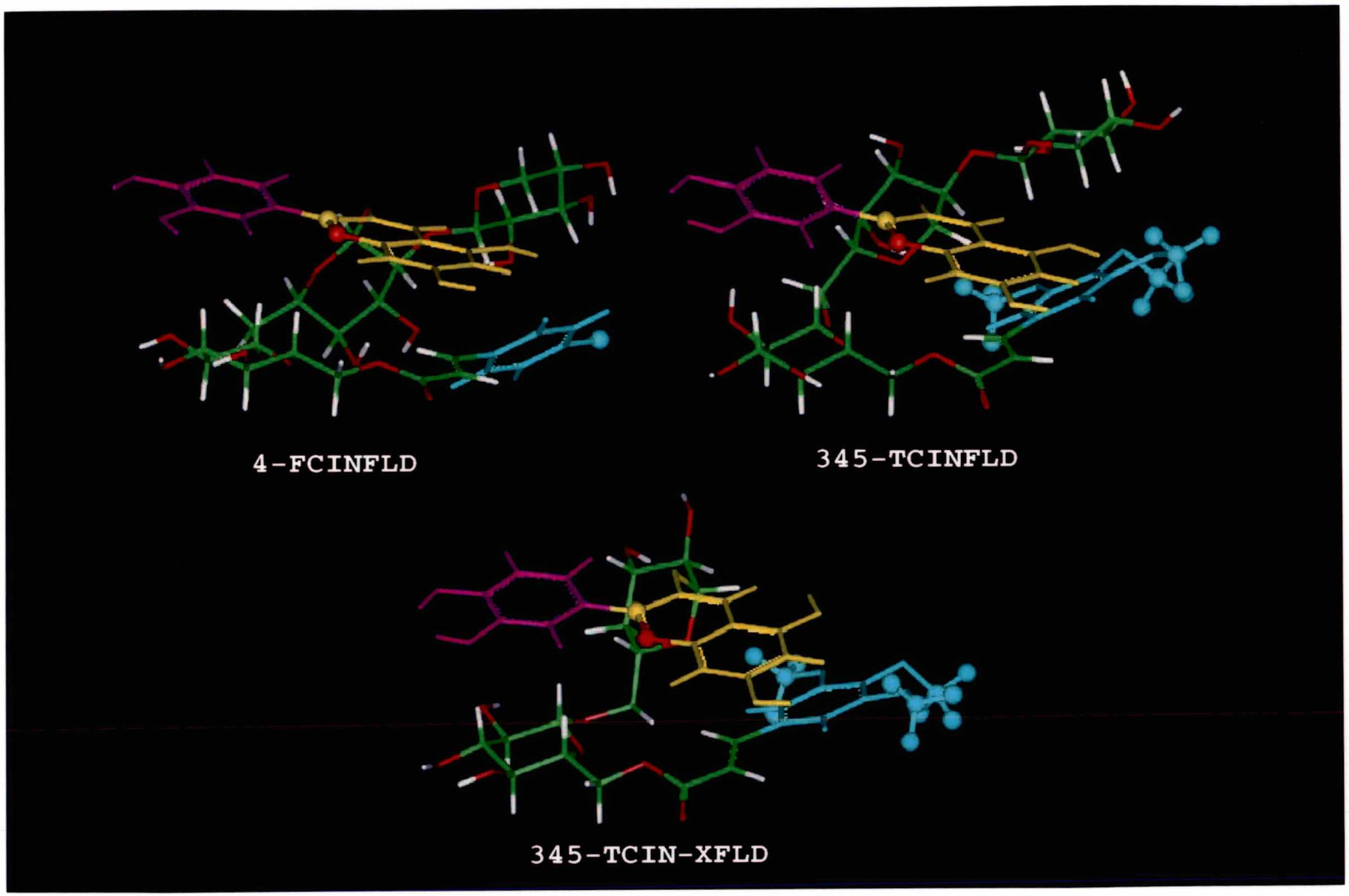

4-FCINFLD
345-TCINFLD
345-TCIN-XFLD

Fig. 19. The FRAC conformational families in methanol.

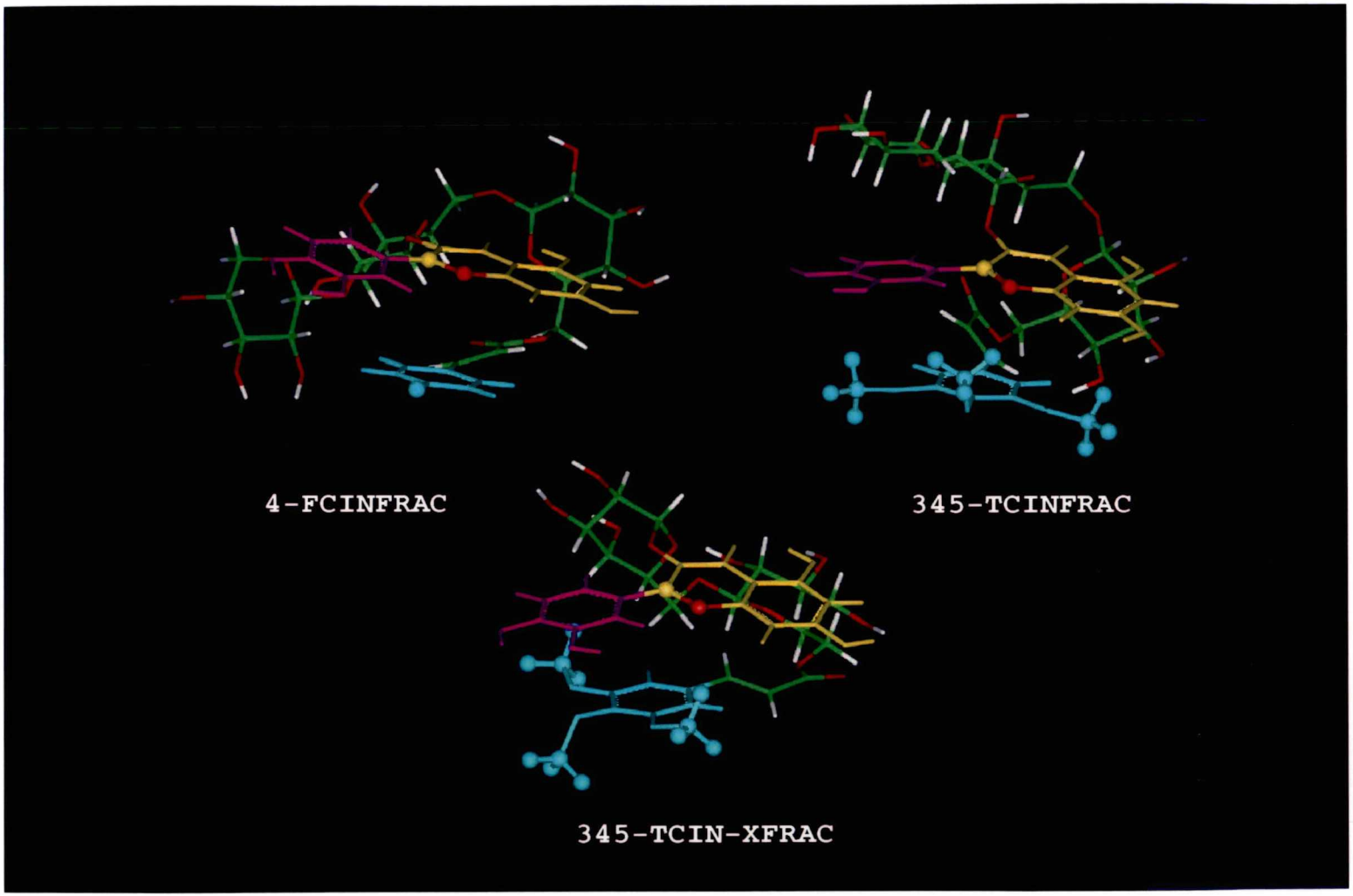

4-FCINFRAC
345-TCINFRAC
345-TCIN-XFRAC

Fig. 20. The FRB conformational families in methanol.

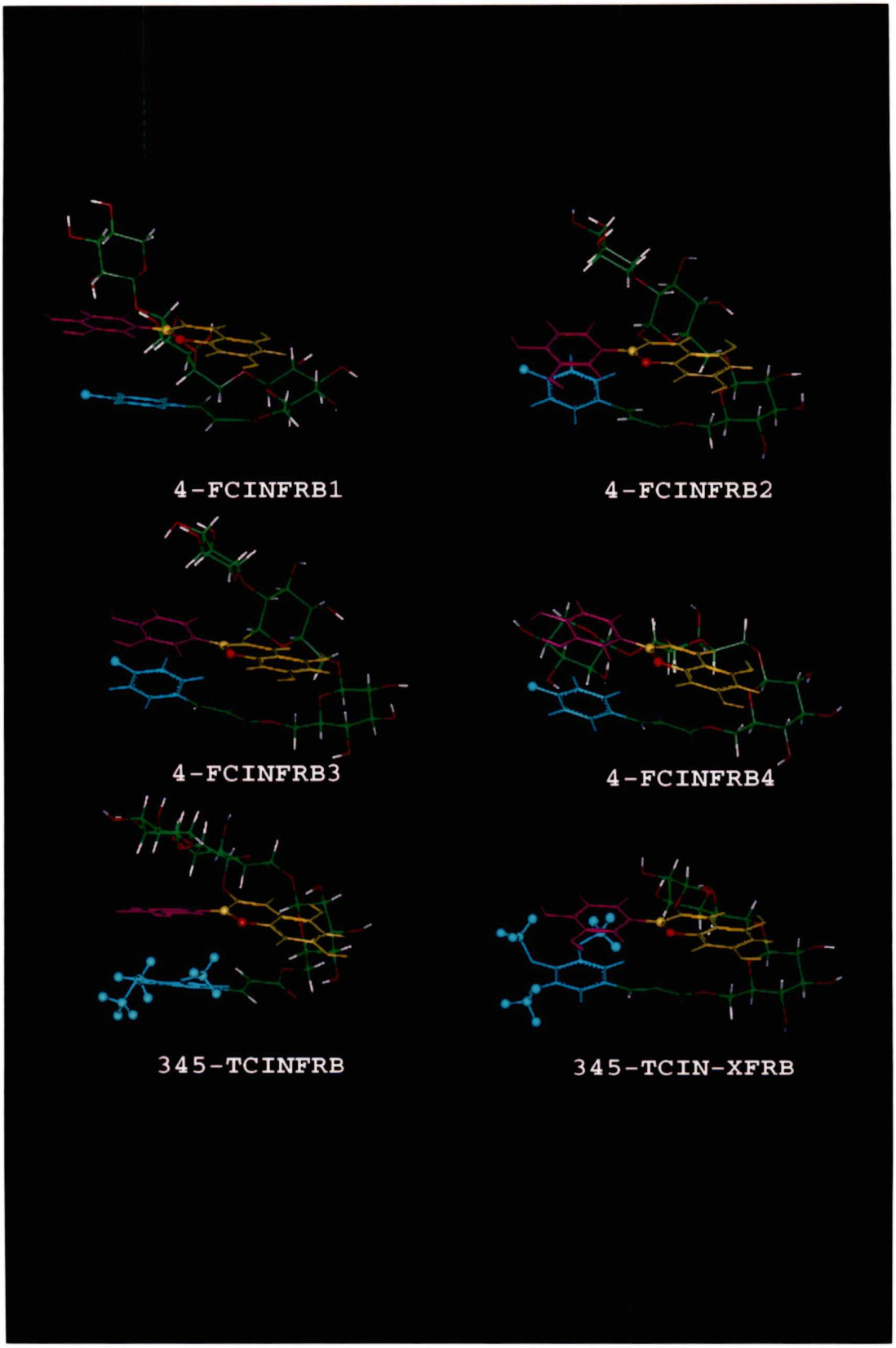

4-FCINFRB1
4-FCINFRB2
4-FCINFRB3
4-FCINFRB4
345-TCINFRB
345-TCIN-XFRB

Fig. 21. The FRD conformational families in methanol.

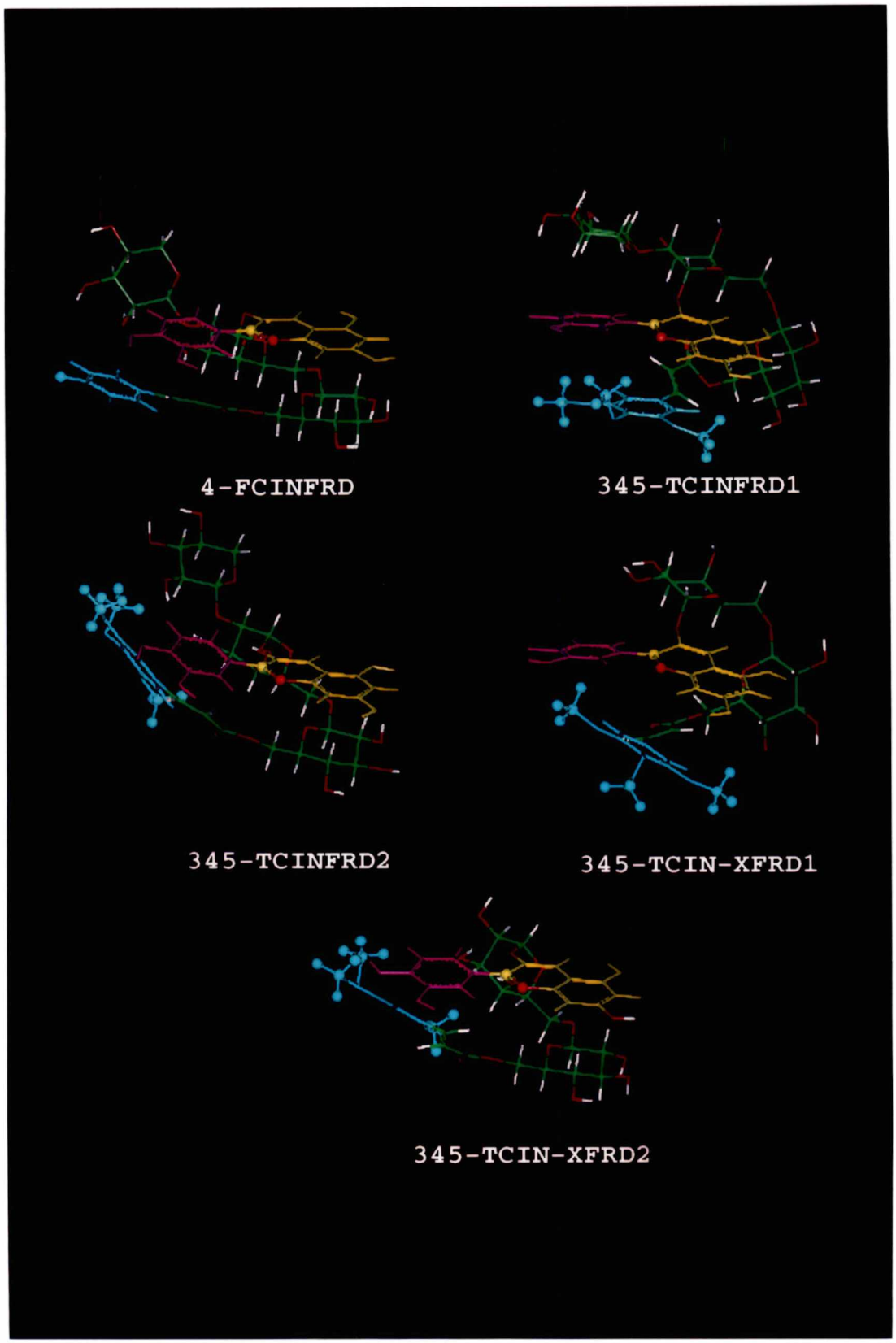

4-FCINFRD
345-TCINFRD1
345-TCINFRD2
345-TCIN-XFRD1
345-TCIN-XFRD2

Fig. 22. The FUAC conformational families in methanol.

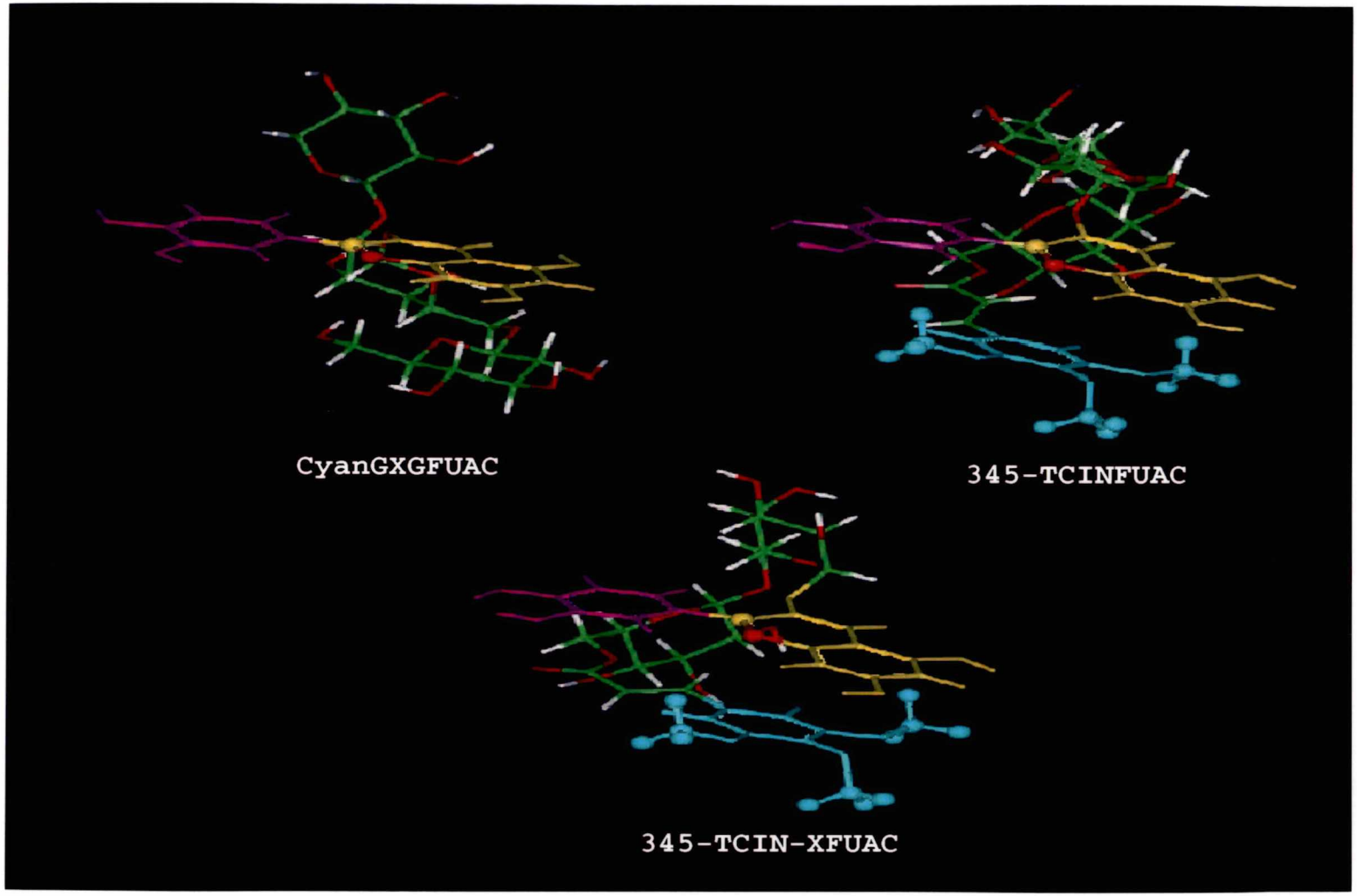

CyanGXGFUAC
345-TCINFUAC
345-TCIN-XFUAC

Fig. 23. The NLAC conformational families in methanol.

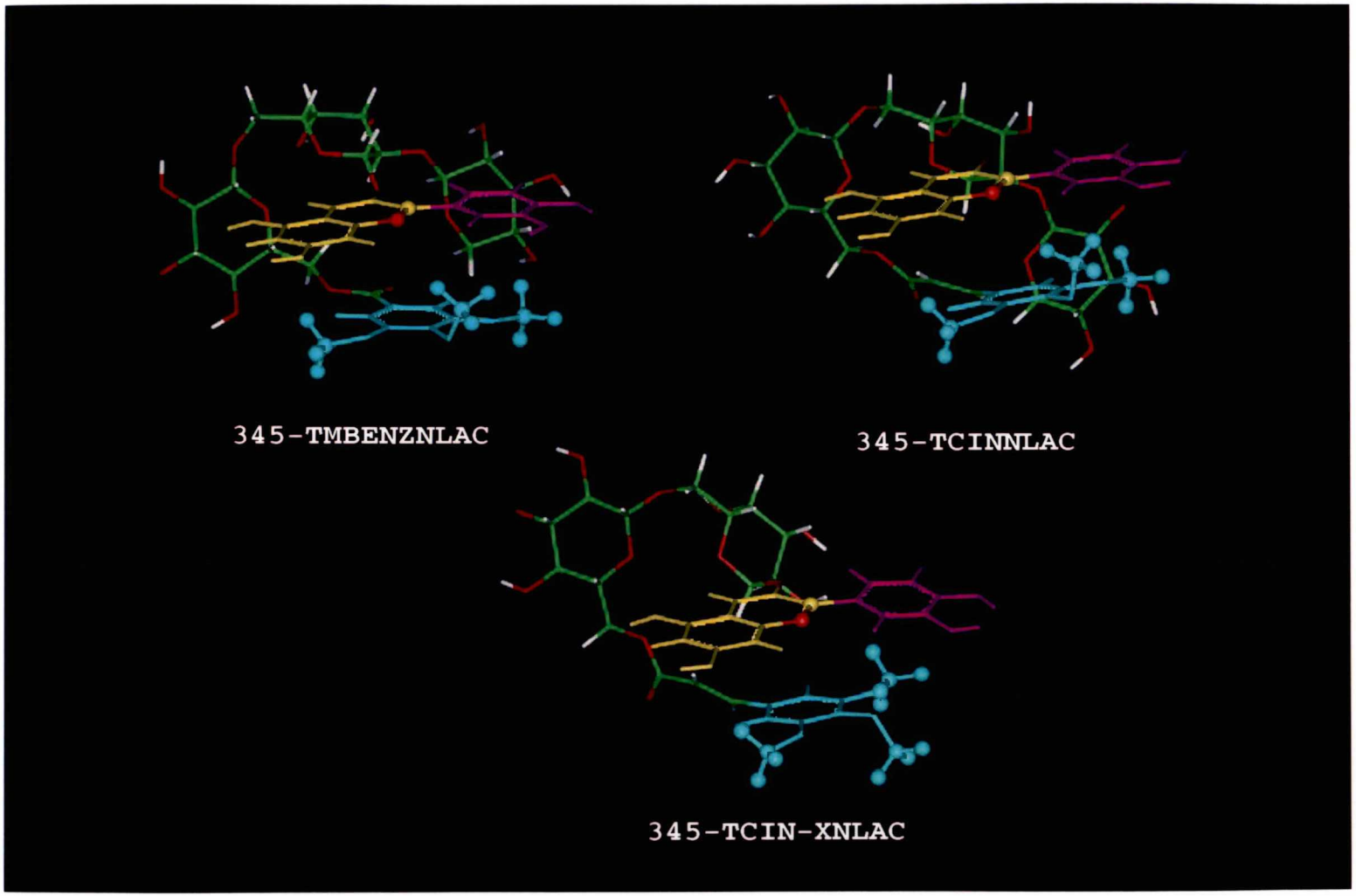

345-TMBENZNLAC
345-TCINNLAC
345-TCIN-XNLAC

Fig. 24. The NRAC conformational families in methanol.

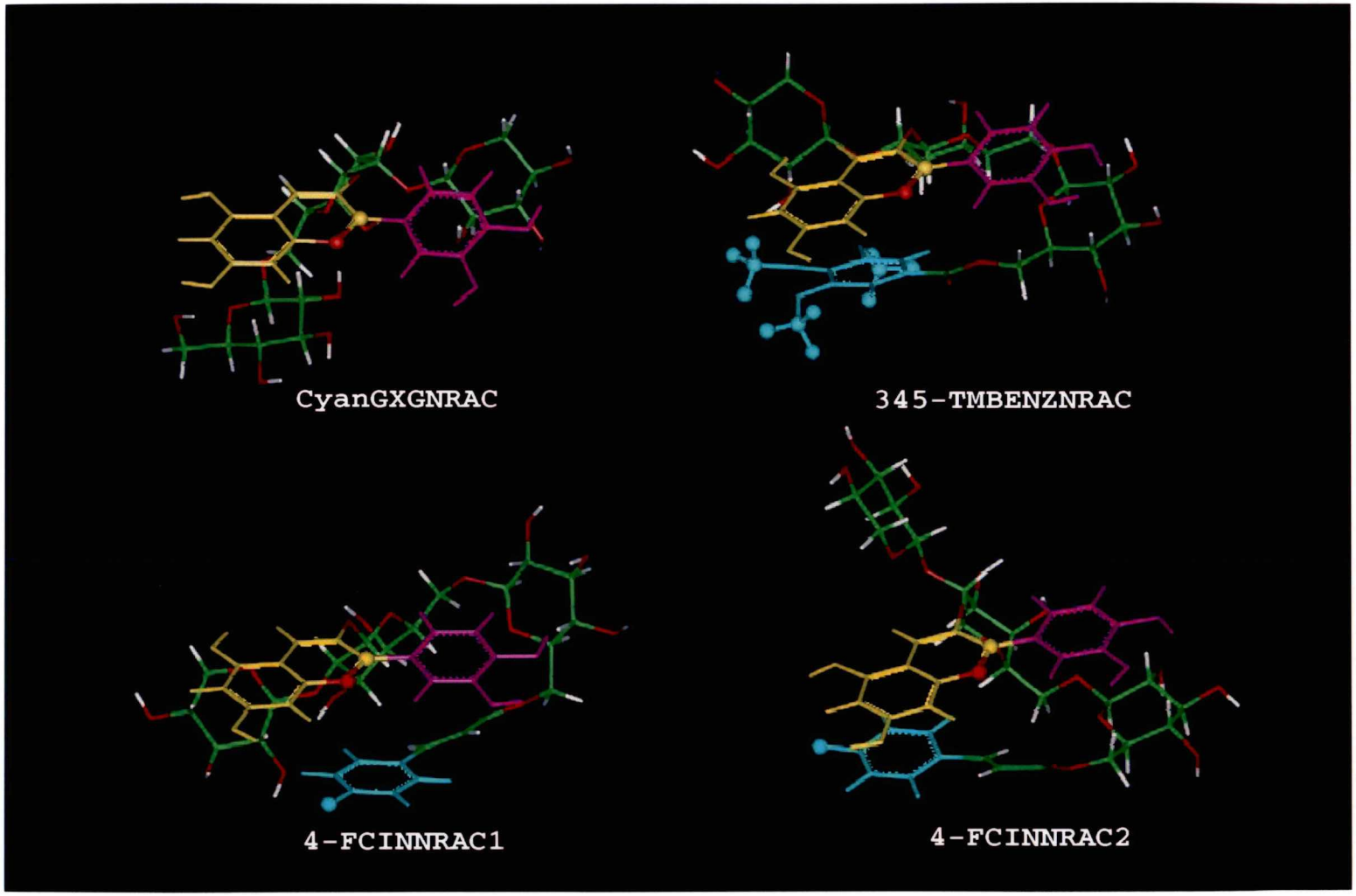

CyanGXGNRAC
345-TMBENZNRAC
4-FCINNRAC1
4-FCINNRAC2

Fig. 25. The NRD conformational families in methanol.

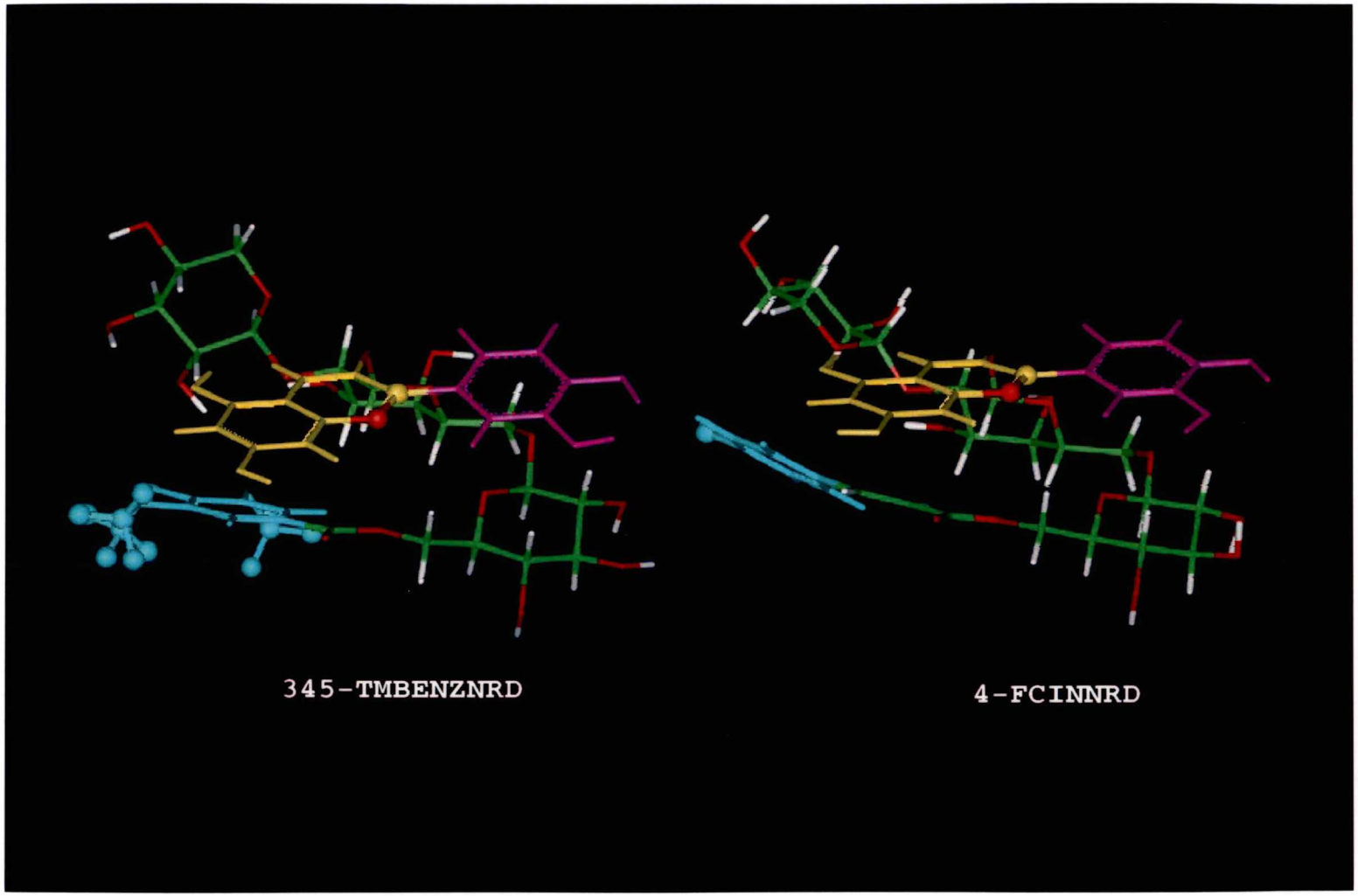

345-TMBENZNRD
4-FCINNRD

Fig. 26. The NUAC conformational families in methanol.

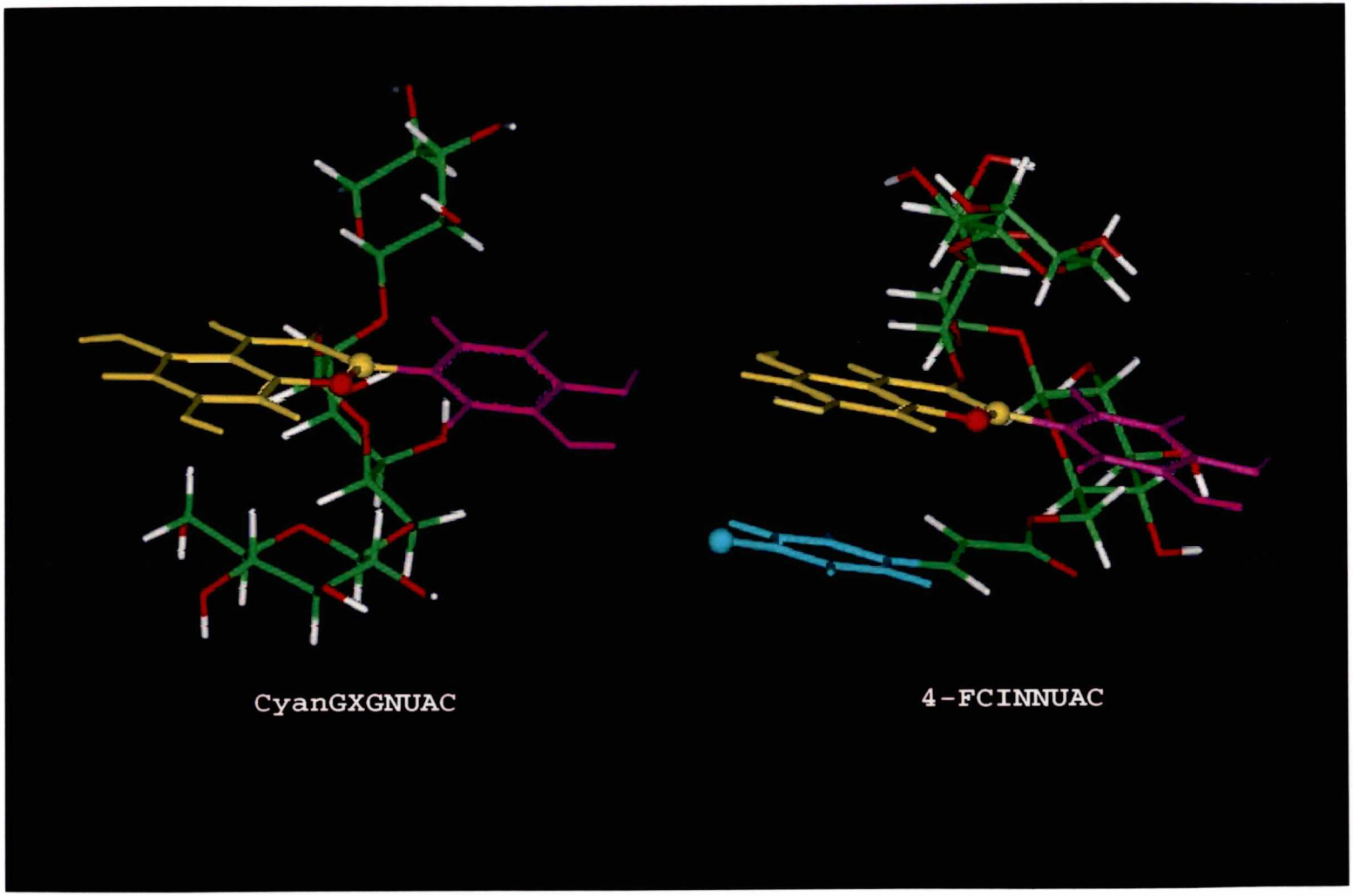

CyanGXGNUAC
4-FCINNUAC

Fig. 27. The OP conformational families in methanol.

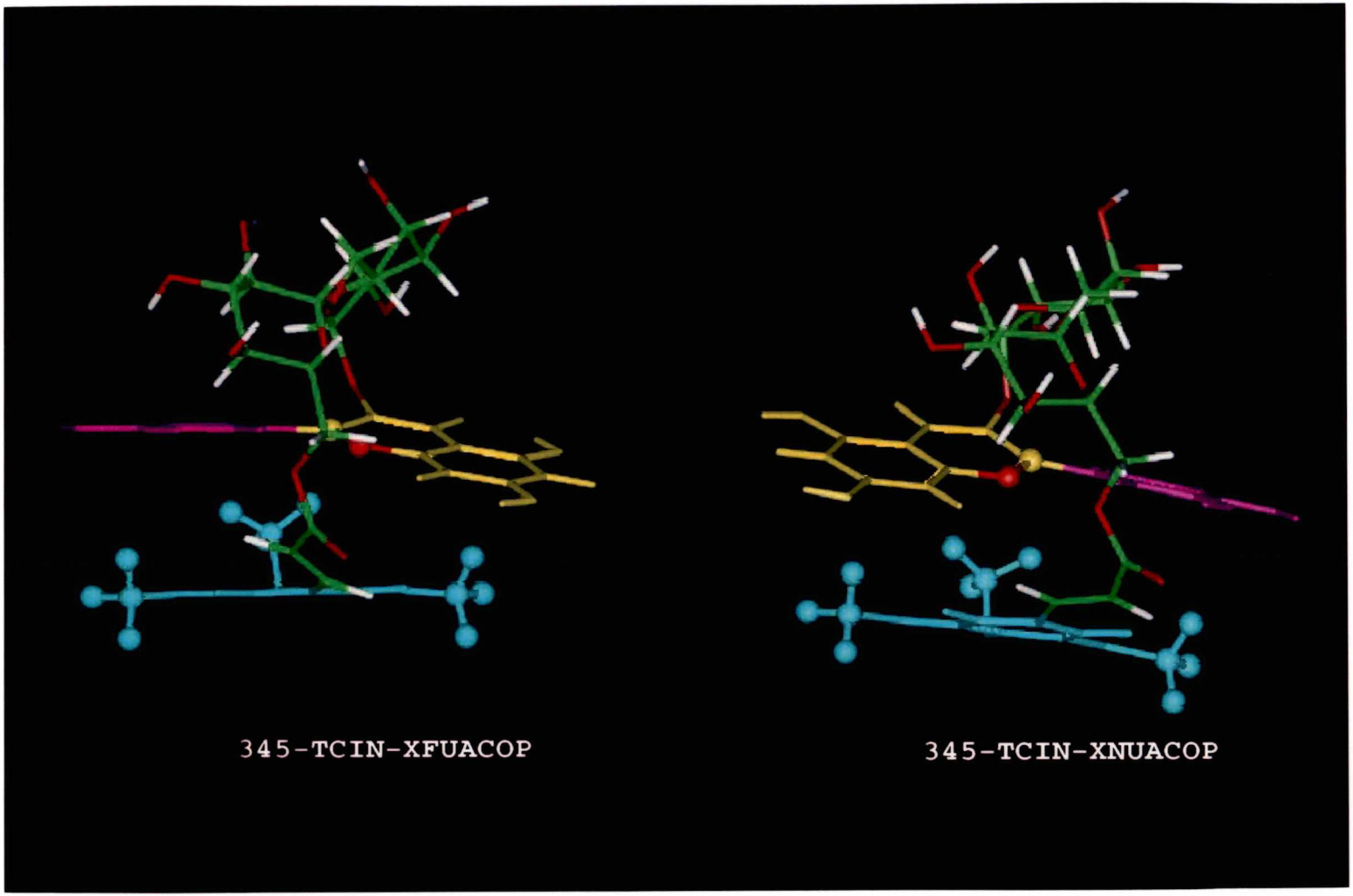
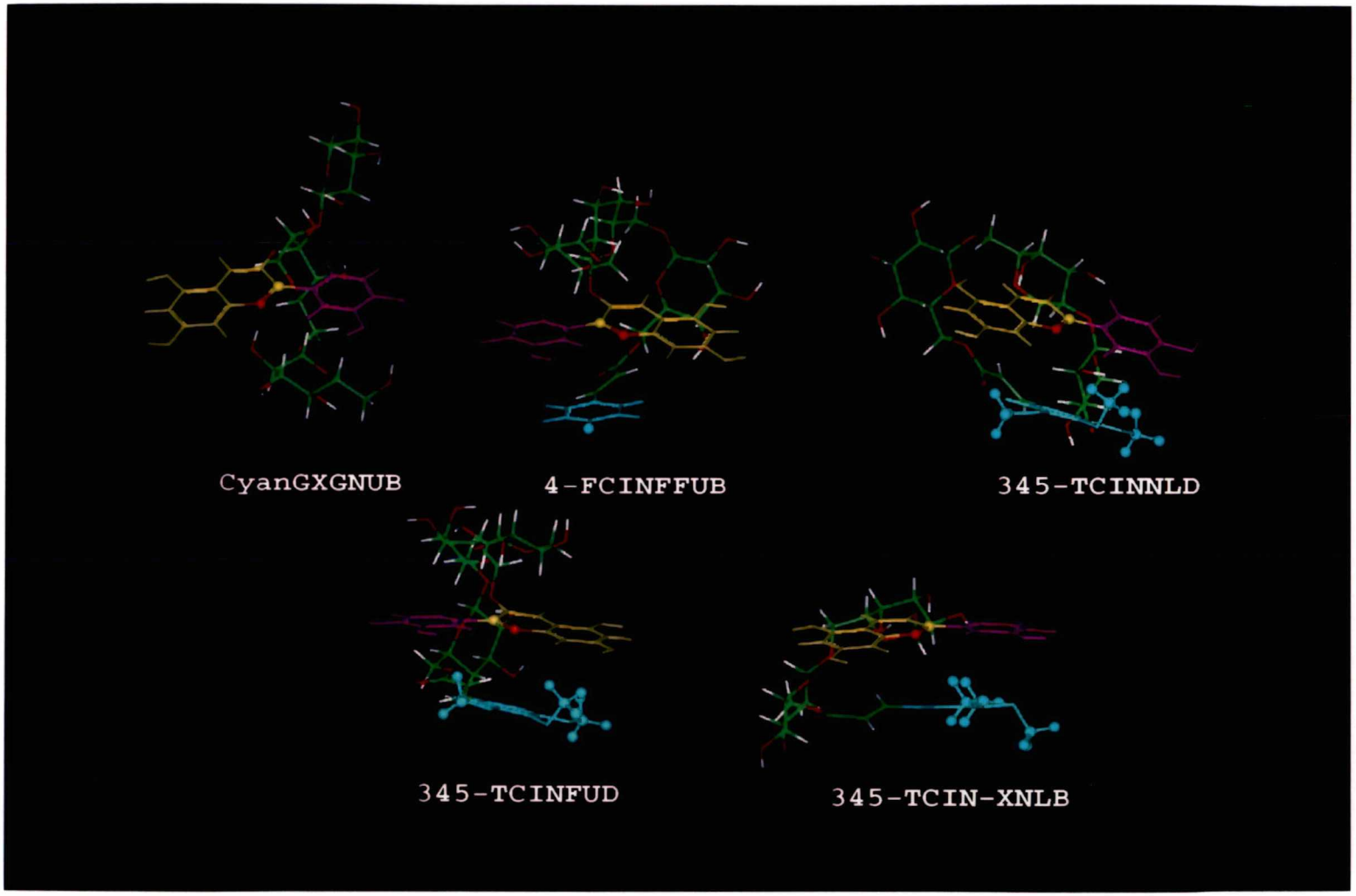

345-TCIN-XFUACOP
345-TCIN-XNUACOP

Fig. 28. Miscellaneous conformational families in methanol.


CyanGXGNUB
4-FCINFFUB
345-TCINNLD
345-TCINFUD
345-TCIN-XNLB

28 show conformational families that are unique to a particular anthocyanin. In order for the viewer to clearly identify the key functionalities within these anthocyanins, ring A–C, ring B, and the acyl moiety has been colored yellow, magenta, and blue, respectively. The C-2 site on the flavylium nucleus ($C=O^+$) is prone to the attack of water at near-neutral conditions results in the loss of color (see Fig. 2). In the above Figs. the C-2 and oxygen atom of the $C=O^+$ is depicted as a yellow and red ball, respectively.

a. FLAC conformational families. In Fig. 17 there are only two anthocyanins that populate this conformational family in methanol, **345-TCIN** and **345-TCIN–X**. If the representative structure for each anthocyanin is viewed from the same perspective, the overall shape of the molecule is comparable—clearly the β-xylopyranose unit does not significantly affect the fold of anthocyanins acylated with 3,4,5-trimethoxycinnamic acid. The perspective of the molecules is the same as the one used to categorize the conformational classes, i.e., the flavylium nucleus (reads "BCA") is oriented towards the viewer, and the β-Gal unit is directed away from the viewer. As the name of the conformational family suggests, the acyl moiety, 3,4,5-trimethoxycinnamic acid attached to the O-6 terminus of the anthocyanins interacts with the A–C ring system of the flavylium nucleus from the left with respect to the β-Gal moiety. The positioning of the exocyclic double bond in these structures implies that the protons will be influenced by the B ring of the flavylium nucleus, and may even stack with this

portion of the flavylium nucleus. This observation in the models supports the analysis of the chemical shift data in the section on the Analysis of 1D ^{1}H NMR Data.

b. FLD conformational families. (Same orientation as above) Three of the five anthocyanins **4-FCIN**, **345-TCIN–X**, and **345-TCIN** exhibit characteristics of this conformational family (see Fig. 18). Irrespective of the acyl moiety on the O-6 Glc terminus, the consensus fold adopted by these molecules is comparable. Like the above conformational family, the O-6 of the β-Gal moiety forces the β-Glc unity to the left with respect to the β-Gal unit. Although, in this family the acyl ring does not stack with any portion of the flavylium nucleus, the exocyclic double bond, however, does interact with the A–C ring system of the flavylium nucleus. In this conformational family, the β-xylopyranose unit does not significantly influence the conformational shape of the molecule; see **345-TCIN–XFLD** and **345-TCINFLD**.

c. FRAC conformational families. (Same orientation) Compounds **4-FCIN**, **345-TCIN**, and **345-TCIN–X** in methanol exhibit structures that adopt this consensus fold (see Fig. 19). In this conformational family the β-linkage between the O-6 Gal and Glc positions the β-Glc moiety to the right, with respect to the Gal moiety. This results in the acyl moiety stacking with the A–C ring system of the flavylium nucleus (reads "BCA"). The representative structures of

4-FCINFRAC and **345-TCIN–XFRAC** show that the exocyclic double bond stacks with A–C ring system.

d. FRB conformational families. (Same orientation) The same compounds **4-FCIN**, **345-TCIN** and **345-TCIN–X** in methanol exhibit the fold that exemplifies the FRB conformational family (see Fig. 20). In the modeling studies performed on **4-FCIN**, it was discovered that the structures that adopted this shape could be sub-categorized into four families; **4-FCINFRB1**, **4-FCINFRB2**, **4-FCINFRB3**, and **4-FCINFRB4**. As with the FRAC family, the flavylium nucleus is read as "BCA", and the Glc moiety is positioned to the right of the molecule, with respect to the β-Gal moiety. Each of the acyl moieties stacks with ring B via arene–arene interactions. The fold that **4-FCINFRB3** adopts is the same as the conformational family **345-TCINFRB**. Similarities are observed when the structure of the conformational family **4-FCINFRB4** is compared to that of **345-TCIN–XFRB**.

If the molecule adopts this particular shape, π–arene and arene–arene interactions are optimal. The configuration that the molecule adopts to cause ring D (blue) to stack with ring B (magenta), causes the exocyclic double bond to be planar enough to interact with the A–C ring system of the flavylium nucleus. Therefore, all parts of the acyl moiety, including the exocyclic double bond, are proximal to the flavylium nucleus, and so maximum overlap is observed via arene–arene and π–arene interactions.

e. FRD conformational familes. (Same orientation) The representative structures of the conformational families **4-FCINFRD**, **345-TCINFRD1**, **345-TCINFRD2**, **345-TCIN–XFRD1**, and **345-TCIN–XFRD2** are shown in Fig. 21. As with the conformation family FRB, the Glc moiety is forced to the right, with respect to the Gal moiety. However, the phenyl ring of the acyl moiety does not interact with any portion of the flavylium nucleus, but the double bond, in certain structures has the required configuration that permits a π–arene interaction between itself and parts of the flavylium nucleus (reads "BCA"). For example, see the structures from the conformational families **4-FCINRFD**, **345-TCINFRD1**, **345-TCIN–XFRD1**, and **345-TCIN–XFRD2**. The exocyclic double bond interacts with ring B, A–C ring system, A–C ring system, and the ring B, respectively.

f. FUAC conformational families. (Same orientation) This conformational family is observed in three anthocyanins, **CyanGXG**, **345-TCIN**, and **345-TCIN–X**, and is depicted in Fig. 22. The FUAC family adopts a very different conformation to the families that have previously been described, in that the Glc moiety does not position to the left or the right of the β-Gal unit, but comes out directly toward the viewer. As with the previous conformational families, the flavylium nucleus is read as "BCA". The structure from **CyanGXGFUAC** has been classified thus, because the Glc moiety resides underneath A–C ring system of the flavylium nucleus, as a result of a number of carbohydrate–arene interactions (CH–π).[47] Representative members of the conformational family

345-TCIN–XFUAC and **345-TCINFUAC** show that the 3,4,5-trimethoxycinnamoyl moiety stacks under the A–C ring system of the flavylium nucleus. In the case of the conformational family **345-TCIN–FUAC**, the β-Xyl moiety is positioned directly above the C-2 of the flavylium nucleus.

g. NLAC conformational families. (Same perspective) Fig. 23 shows the representative structures of the NLAC conformational family of **345-TMBENZ**, **345-TCIN**, and **345-TCIN–X**. In all these structures, the flavylium nucleus is read as "ACB", and the Glc moiety is forced to the left, with respect to the Gal moiety. This causes the 3,4,5-trimethoxycinnamoyl group to stack under the A–C ring system of the flavylium nucleus. The conformational family **345-TMBENZNLAC** demonstrates that in the absence of the exocyclic double bond, the molecule is able to adopt a similar conformation to the cinnamoylated counterparts.

h. NRAC conformational families. (Same perspective) Like the structures from the conformational families in the previous family, the acyl group is positioned underneath the A–C ring system of the flavylium nucleus (reads as "ACB") by the Glc moiety, which contorts to the right, with respect to the Gal unit (see Fig. 24). The shape of the structure from the conformational family **345-TMBENZNRAC** bears a great deal of resemblance to **4-FCINNRAC**.

i. NRD conformational families. (Same perspective) The only molecules that adopt this conformation in methanol is **345-TMBENZ** and **4-FCIN**, are shown in Fig. 25. Neither acyl moiety interacts with any part of the flavylium nucleus

(read as "BCA"); however, the two structures **345-TMBENZNRD** and **4-FCINNRD** exhibit a great deal of similarities to one another, even in the absence of the exocyclic double bond in the anthocyanin **345-TMBENZNRD**.

j. NUAC conformational families. (Same perspective) Fig. 26 shows representative structures of the **CyanGXGNUAC** and **4-FCINNUAC** families. In these structures the Glc moiety comes towards the viewer and forces the acyl moiety to stack under the A–C ring system of the flavylium nucleus (reads "ACB"). The β-xylopyranose moiety positions itself directly above the C-2 position of the flavylium nucleus.

k. FUACOP and NUACOP conformational families. (Same perspective) Fig. 27 shows the representative structures from the conformational families **345-TCIN–XFUACOP** and **345-TCIN–XNUACOP** that are observed in the NMR–QMD protocol in methanol. Unlike the previous conformational families that have been fully described, the glycosidic chain comes up and over the flavylium nucleus, which reads "BCA" and "ACB" in the **345-TCIN–XFUACOP** and **345-TCIN–XNUACOP** families, respectively. In both cases the 3,4,5-trimethoxycinnamoyl moiety stacks under the A–C ring system. These are the only families observed where the Glc unit resides directly above the C-2 position on the flavylium nucleus.

l. Miscellaneous conformational families. (Same perspective) The conformational families depicted in Fig. 28 show the representative structures

from families that only occurred once in the study of the five anthocyanins, which were subjected to the QMD–NMR protocol. The first of these conformational families is **CyanGXGNUB**. The Glc moiety juts out directly towards the viewer and positions itself underneath dihydroxyphenyl ring B (magenta) of the flavylium nucleus (reads "ACB"). Presumably this is as a result of CH–π interactions[47] between the Glc moiety and ring B.

In the structure **4-FCINFUB**, the Glc moiety comes directly towards the viewer, which forces the 4-fluorocinnamoyl functionality to stack with ring B. The fold adopted by the anthocyanin shows that the exocyclic double bond interacts with the A–C ring system of the flavylium nucleus (reads "BCA"). Additionally, the contortion of the molecule results in the β-xylopyranosyl moiety is positioned directly above the C-2 of the flavylium nucleus.

The next two structures shown in Fig. 28 are representatives of conformational families of **345-TCIN**. In both families, the acyl moiety (blue) does not interact with any portion of the flavylium nucleus (reads "ACB" and "BCA" for **345-TCINNLD** and **345-TCINFUD**, respectively). However, the fold that the molecule adopts causes the exocyclic double bond of the 3,4,5-trimethoxycinnamoyl moiety to interact (π–arene) with the different parts of the flavylium nucleus–the A–C ring system and ring B for **345-TCINNLD** and **345-TCINFUD**, respectively.

The final family shown in Fig. 28 is one which results in the monoacylated

anthocyanin **345-TCIN–XNLB**. In this structure, the Glc moiety positions itself to the left, with respect to the Gal moiety, which causes the acyl moiety (blue) and ring B (magenta) of the flavylium nucleus (reads "ACB") to interact (π–arene).

m. Summary. Utilizing the QMD–NMR protocol, the 3D models thus generated exhibit certain characteristics (some of these observations are not apparent from the examination of the representative frames of each compound's conformational families):

1. The flavylium nucleus in structures of these conformational families can be read as "ACB" ("nonflipped") or "BCA" ("flipped"), when viewed from the same perspective.
2. In certain families, the exocyclic double bond interacts with the flavylium nucleus.
3. The acyl moiety on the O-6 Glc terminus of these anthocyanins can interact with either the A–C ring system or ring B of the flavylium nucleus.
4. In certain families, the β-Xyl moiety can position itself over the C-2 of the flavylium nucleus.
5. In the 3,4,5-trimethoxycinnamoylated anthocyanins, the methoxy groups are proximal to the C-2 of the flavylium nucleus.

The most startling discovery in the study of the behavior of these anthocyanins in methanol is that, irrespective of the acyl moiety on the O-6 Glc terminus of the glycosidic domain, they have similar conformations in solution. In the majority of these conformational families, one face of the C-2 of the flavylium nucleus is exposed to possible nucleophilic attack. Thus it became apparent that the shape of the anthocyanin in solution could not be used to explain why certain compounds are more color stable than others.

It became evident that an important feature of these compounds that warrants further investigation is their conformational flexibility, which has been shown by 1D ^{1}H NMR studies. The flexibility of **CyanGXG**, **345-TMBENZ**, **4-FCIN**, **345-TCIN**, and **345-TCIN–X** may result in a conformational state or states, which could be an overture to the processes involved in color loss of the anthocyanins. Furthermore, a combination of the five observations listed above and/or the flexibility of these molecules could account for the observed differences in their color stability. The flexibility of the conformational families was explored.

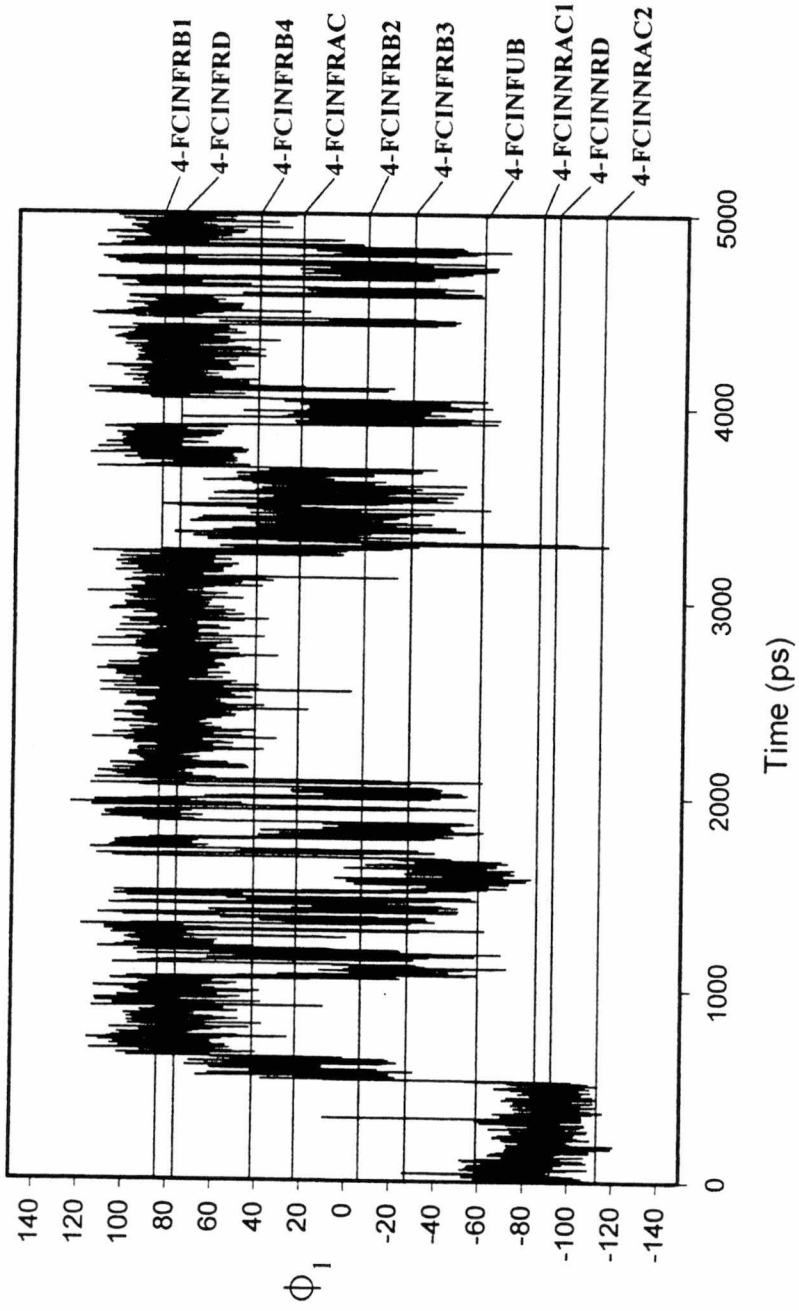
4. Molecular Dynamics Simulations of These Conformational Families. Critical to the acceptance of these models as viable structures of the conformations present in acidic solutions of anthocyanins **CyanGXG**, **345-TMBENZ**, **4-FCIN**, **345-TCIN**, and **345-TCIN–X** is that the various representative

structures can interconvert to one another; this flexibility is indicated by the low-temperature ^{1}H NMR studies. Extensive molecular dynamics simulations in a dielectric continuum of methanol at 400 K applied to the representative structure of the conformational family mimics the conditions experienced by the molecules in acidic methanol. Of particular interest was, can the "flipped" structures convert to "nonflipped" structures? And vice versa?

If this interconversion or "flip" can occur, the acyl moiety on the O-6 Glc terminus of the anthocyanin cannot stack with any portion of the flavylium nucleus. To demonstrate the hypothesis the anthocyanin **4-FCIN** was used. The representative structure of the conformational family **4-FCINNRD**, which is shown in Fig. 25, could conceivably be an intermediate state in the process. Thus, the representative structure of the family was subjected to a molecular dynamics simulation in a dielectric continuum of methanol over 5 ns. The result of this simulation is shown in Fig. 29.

Shown in Fig. 29 is the value of ϕ_1 (this is depicted in Fig. 11) as a function of the simulation time starting with the representative structure of the **4-FCINNRD** family. This dihedral angle was selected as a means to probe the motions about the C-3–O-1^{Gal} (see Table 13). Motion about this bond is essential if the "flip" of the flavylium nucleus within conformational families can occur. The results are in agreement with the discovery that anthocyanins, such

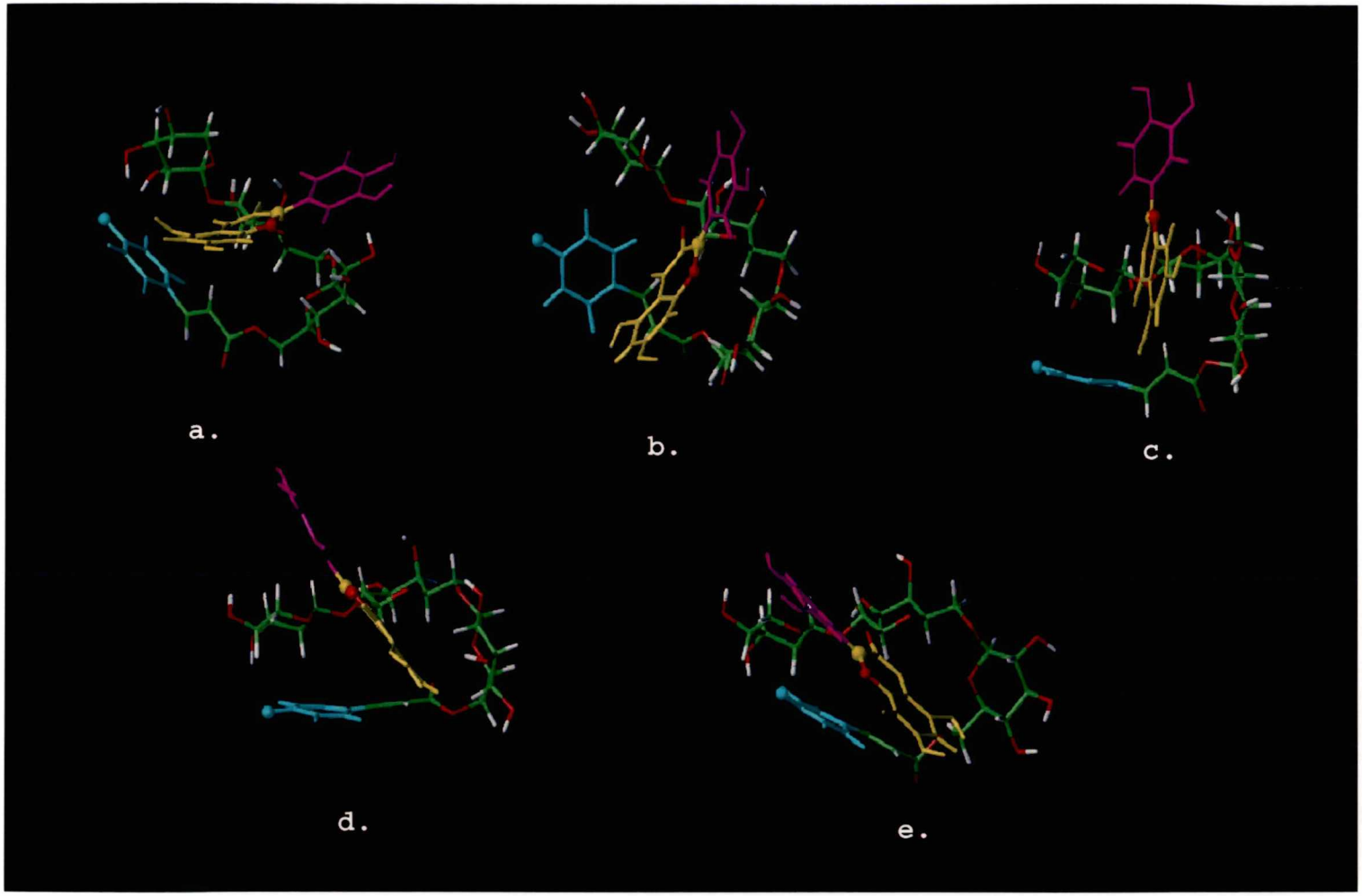
Fig. 29. The dihedral angle ϕ_1 of **4-FCINNRD** as a function of time during a 5 ns molecular dynamics simulation at 400 K in a dielectric continuum of methanol.


4-FCINFRB1
4-FCINFRD
4-FCINFRB4
4-FCINFRAC
4-FCINFRB2
4-FCINFRB3
4-FCINFUB
4-FCINNRAC1
4-FCINNRD
4-FCINNRAC2
140
120
100
80
60
40
20
0
-20
-40
-60
-80
-100
-120
-140
Φ_1
0
1000
2000
3000
4000
5000
Time (ps)

as **4-FCIN** are highly flexible. Nine of the twelve representative structures were populated during the simulation starting with the structure **4-FCINNRD**. The interactions present in these conformational families provide a small barrier to the rapid interconversion of conformational families. These results are consistent with previous studies on acylated anthocyanins that suggested that stacking is a rapid process and there is a distribution of conformations at equilibrium.[29]

Various stages in the "flipping" process along the trajectory of the molecular dynamics simulation are shown in Fig. 30. The molecule **4-FCIN** is oriented where the flavylium nucleus (reads "ACB") is towards the viewer, and the β-Gal unit away from the viewer, i.e, the same perspective used in the classification of these anthocyanins (see Experimental Section). After a certain amount of time, the acyl moiety moves further out of the way of the flavylium nucleus, which provides enough clearance for the flavylium nucleus to move (see structure "a" in Fig. 30). Thus from a congested state that is evident in the **4-FCINNRD** family of structures, the C-2 attack site becomes more prone to the deleterious nucleophilic attack by a water molecule. The congestion at C-2 is further relieved as the flavylium nucleus moves close to, and perpendicular to the glycosidic domain (see structures "b" and "c", respectively). Unlike the stacked conformational families, the conformation "c" is prone to attack from both faces of the flavylium nucleus. From this conformation, the flavylium nucleus can

Fig. 30. Conformations in the "flipping" process of **4-FCINNRD** in methanol.


a.
b.
c.
d.
e.

return to its original orientation, i.e., it can be read as "ACB", or can it invert and be read as "BCA". In the conformation "d" the flavylium nucleus moves past the perpendicular and results in a congested conformation "e", which is similar to the structures of the **4-FCINFRD** family.

Thus the flavylium nucleus can rotate about the glycosidic bond between C-3 of the flavylium nucleus and the β-Gal unit of the anthocyanin. In itself, this is not that remarkable as the flavylium nucleus has been shown to move more rapidly than the dihydroxyphenyl ring (ring B, marked magenta); however, the fact that C-2 can become more prone to attack through these motions indicate that this could be an important factor in the processes responsible for color loss in monoacylated anthocyanins. Moreover, subtle changes in the environment around C-2 may account for the differences observed in the color stability of the anthocyanins under investigation.

In order to prove this hypothesis, a molecular visualization method, such as MOLCAD[48-62] would be extremely useful.

5. Molecular Visualization of Conformational Families Using *M*olecular *C*omputer *A*ided *D*esign (MOLCAD). The computer program MOLCAD has been used to study various properties of carbohydrates, such as sucrose and cyclodextrins.[51,56,58,59] The first stage in this visualization method is that a water molecule is rolled over the surface of the molecule in question. A

Connolly surface[63] is thus generated and permits various properties of these structures to be projected onto the surface. In this investigation, three molecular properties using the MOLCAD module on SYBYL were studied: the molecular lipophilic potential (MLP), the molecular local curvature (MLC), and molecular electrostatic potential (MEP). Mapping the MLP property on the surface of the molecule, graphically represents the lipophilicity of areas of the molecule; highly hydrophobic areas are shown as brown, whereas highly hydrophilic areas are shown as blue. The topography of the molecule can be studied by generating the MLC property on the surface of the molecule; the convex areas and concave areas of the molecule, shown as white and blue, respectively. The property MEP shows areas within the molecule that are electropositive and electronegative, shown as red and purple, respectively.

Figs. 31–33 show MLP, MLC, and MEP of the "flipping" process of the representative structure from the **4-FCINNRD** family, respectively. Unlike the previous depiction of this flipping process in Fig. 30, the process is viewed from a different perspective. Each structure in the Figs. is oriented where the C-2 position (shown as a yellow ball in each of these Figs.) of the flavylium nucleus directly faces the viewer. Fig. 31 shows the MLP property mapped on a Connolly surface of intermediates of the "flipping" process of the representative structure of the conformational family **4-FCINNRD**. In structure "a" the micro-environment surrounding the C-2 position of the flavylium nucleus reveals that

Fig. 31. The "flipping" process of **4-FCINNRD** in methanol as visualized by Molecular Lipophilic Potential (MLP).

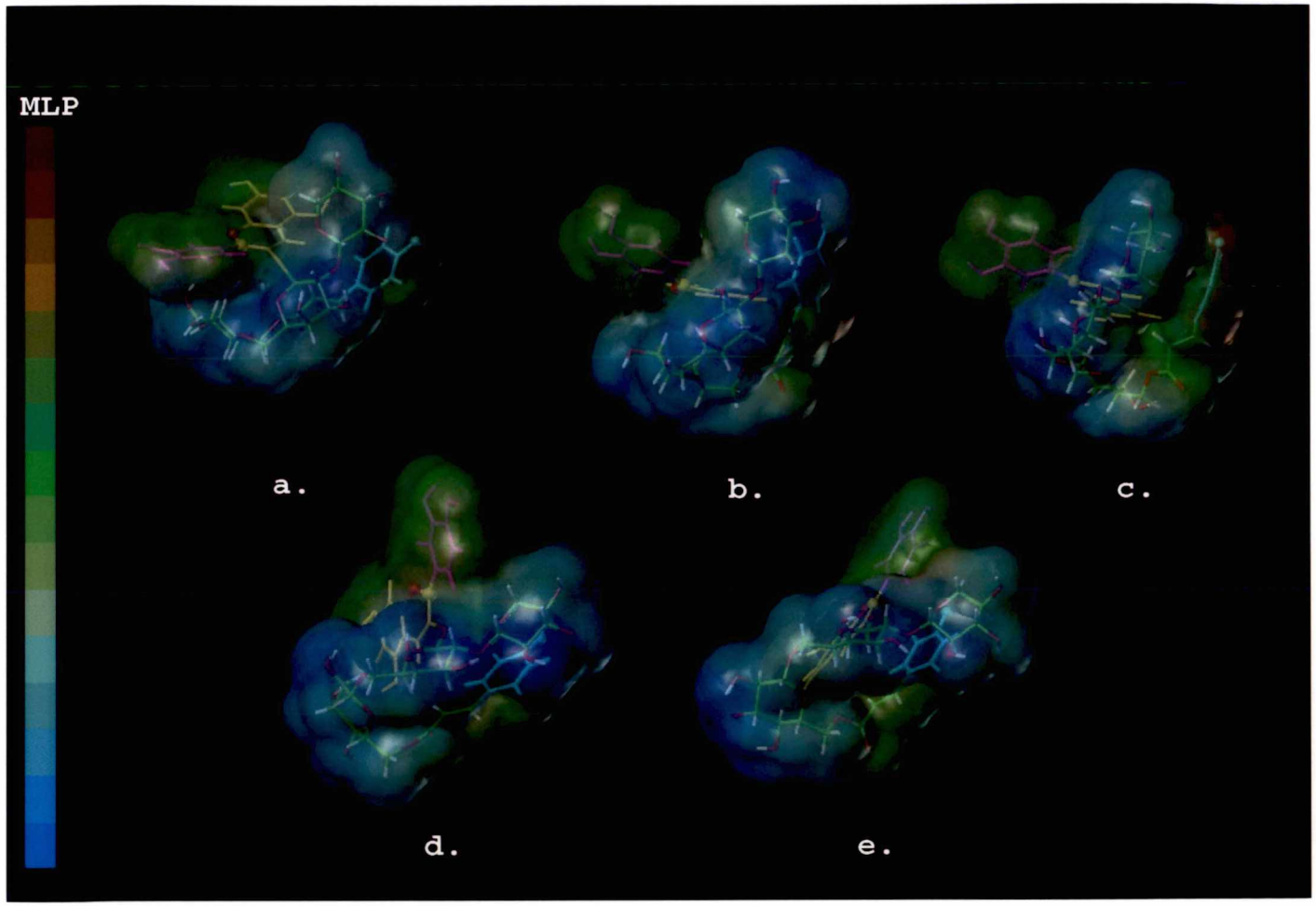

MLP
a.
b.
c.
d.
e.

Fig. 32. The "flipping" process of **4-FCINNRD** in methanol as visualized by Molecular Local Curvature (MLC).

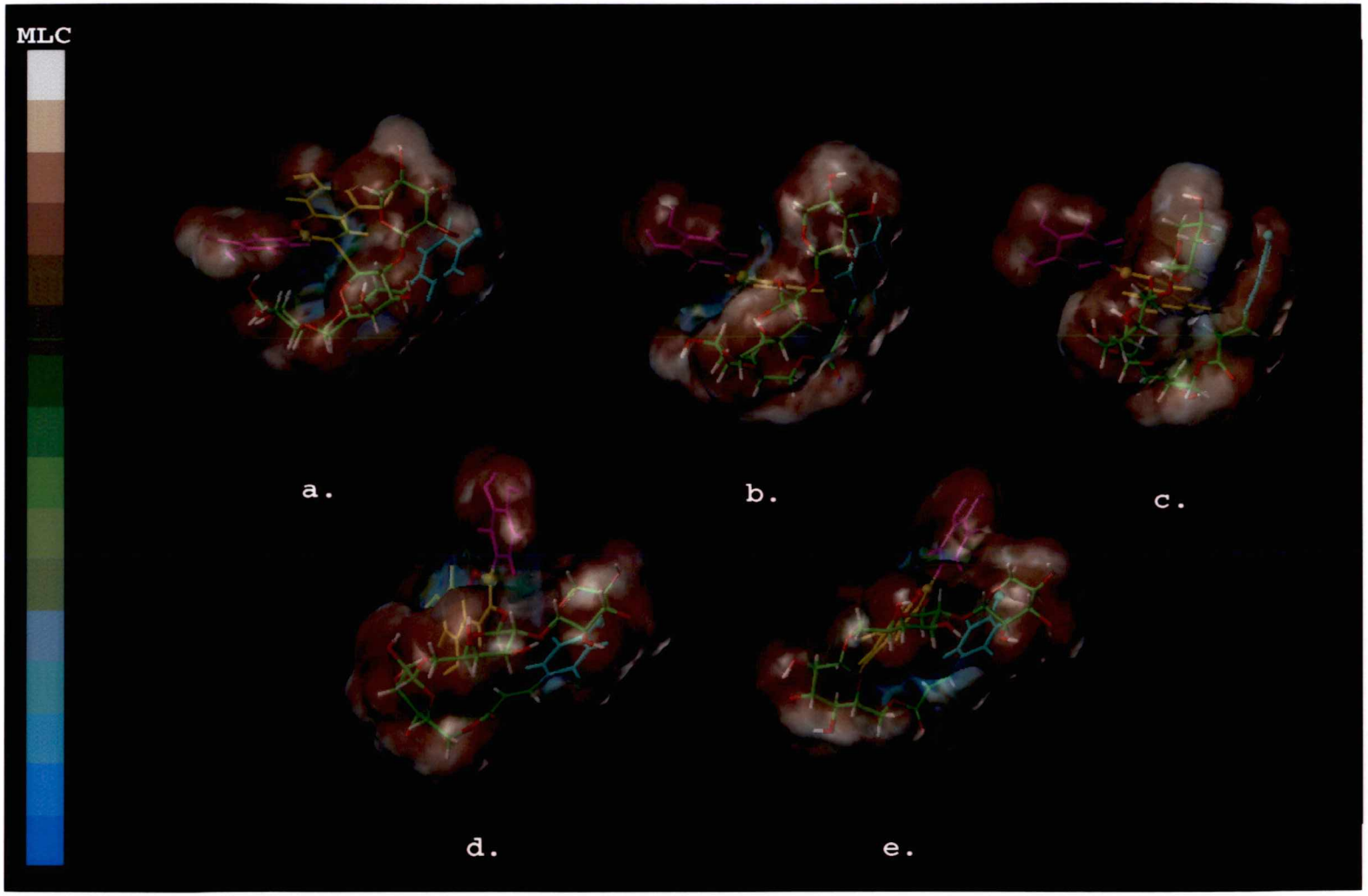
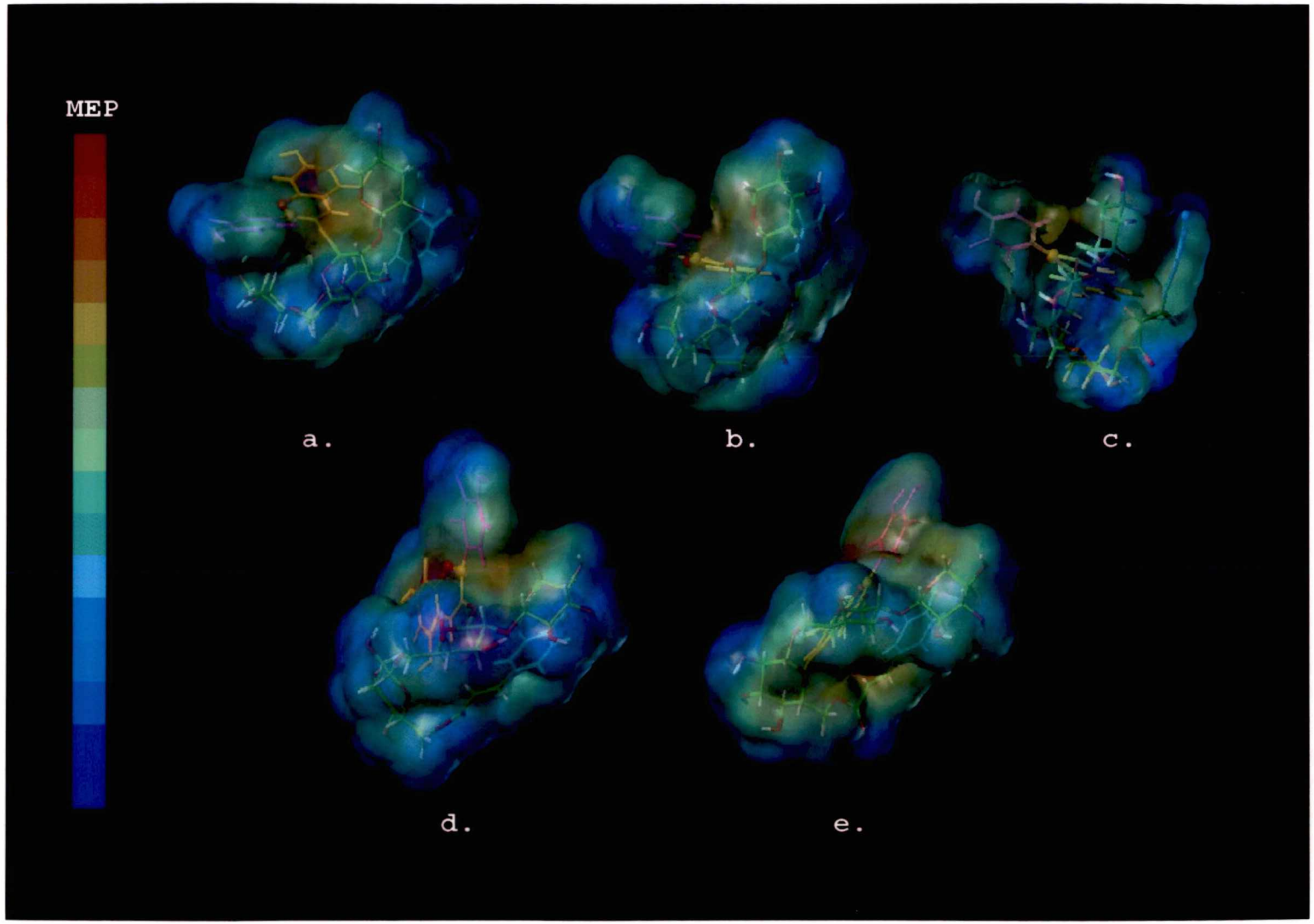

MLC
a.
b.
c.
d.
e.

Fig. 33. The "flipping" process of **4-FCINNRD** in methanol as visualized by Molecular Electrostatic Potential (MEP).


MEP
a.
b.
c.
d.
e.

is situated in a pocket of moderate hydrophobicity (green-brown coloration). As the molecule progresses through the previously described stages of the "flipping" process, the property of the pocket surrounding the reaction center becomes more hydrophilic (see structures "b", "c", and "d", and the blue region surrounding the C-2 atom). When the molecule returns to folded state, which is similar to the conformational family **4-FCINFRD**, the micro-environment surrounding the C-2 position of the flavylium nucleus still remains fairly hydrophilic, i.e., shown as a blue region. This suggests that the "flipped" structure has a micro-environment surrounding C-2 that is more hydrophilic than the "nonflipped" counterpart (structure "a").

As the "flipping" process progresses "a"→"e", the topography of the **4-FCIN** molecule changes (shown in Fig. 32), revealed by mapping the MLC property. In structures "a" and "e", the strategic $C=O^+$ bond is inaccessible as it is in a convex region, which is shown as brown areas in Fig. 32, i.e., the water molecule that was used in the construction of the Connolly surface, was unable to approach close to the flavylium nucleus). However, in the intermediates of the "flipping" process (see "b", "c", and "d"), C-2 becomes more accessible, and intimate contact with the incoming nucleophile can occur. Moreover, by mapping the MLP property (see Fig. 31) the micro-environment surrounding $C=O^+$ of the flavylium nucleus in these three structures encourages the approach of water molecules.

Areas within the molecule that are either electropositive or electronegative can be revealed by mapping the MEP property (see Fig. 33). Electropositive and electronegative areas are shown as red and purple regions, respectively. Structures "a", "b", "c", and "d" show that the $C=O^+$ resides in a pocket of moderate electropositivity and thus promotes the deleterious attack of water on this strategic bond. However, in the "flipped" structure "e", the micro-environment is more electronegative than the other structures.

For deleterious attack of the nucleophile on the C-2 position of the A–C ring system of the flavylium nucleus, two criteria have to be satisfied, (1) the reaction center must be exposed along the Bürgi–Dunitz trajectory,[64] which governs attack of nucleophiles on the carbonyl moiety, and (2) the micro-environment surrounding the C-2 position encourages the nucleophile to approach the reaction center. In the "flipping" process of this conformational family, the micro-environment of the site becomes more hydrophilic, accessible, and more electropositive. Thus throughout the "flipping" process the reaction site ($C=O^+$) becomes more prone to nucleophilic attack than the same site in the folded conformations.

Using MOLCAD as a means of molecular visualization establishes that the micro-environment surrounding the C-2 position of the flavylium nucleus changes and promotes nucleophilic attack. However, the flexibility of anthocyanins in methanol cannot be directly correlated to the color-stability data of these

compounds, which was acquired in water. In order to establish the physical behavior of anthocyanins and their color-stability data, reasonable models of the anthocyanins in water needed to be generated.

E. Molecular Modeling Studies in Water

1. General. The aim of this entire investigation was to correlate the physical behavior of the anthocyanins with color-stability data, which was acquired in water according to a technique by Dangles and co-workers.[29] Thus reasonable models of these molecules in water needed to be generated. Prior to these studies, models of anthocyanins in methanol were successfully generated using a QMD–NMR protocol, which has been detailed in Section D of the Results and Discussion chapter. This protocol could be easily adapted to mimic the conditions experienced in aqueous medium. Two cinnamoylated anthocyanins **4-FCIN** and **345-TCIN** were selected as candidates for the QMD protocol.

2. QMD Studies. At the time of writing this document, no 2D ^{1}H NMR data are available. Prior studies in methanol that are described in Section D of this dissertation suggest that the main means of identifying invalid structures is achieved by rejecting the structures that have a total energy, which is 5 kcal

mol^{-1} greater than the global minimum. Thus in the absence of NMR-derived restraints, the structures produced from the QMD calculations in a dielectric continuum to mimic water (ϵ = 80) were evaluated solely on total energy considerations.

From the 1000 structures produced in each of the QMD calculations that mimic aqueous medium, their evaluation based on the total energy yielded 641 and 724 structures for **4-FCIN** and **345-TCIN**, respectively, and average total energy of anthocyanins **4-FCIN** and **345-TCIN** was 174.2 ± 1.4 and 201.6 ± 1.0 kcal mol^{-1}, respectively. After the structures were initially categorized according to Section D.2, 7 and 8 conformational families from anthocyanins **4-FCIN** and **345-TCIN**, respectively, were generated. The "flipped" structures of **4-FCIN** and **345-TCIN** in water are depicted in Figs. 34 and 36, respectively. The "nonflipped" structures of **4-FCIN** and **345-TCIN** in water are shown in Figs. 35 and 37, respectively. As with the studies in methanol, the distinct conformational families that result from the QMD calculation in water were characterized using the same dihedral angles (ϕ_1–ϕ_6). These data along with RMS deviation values from pairwise superimposition of each conformation within the conformational family for **4-FCIN** are given in Tables 19 and 20, and for **345-TCIN** Tables 21 and 22.

3. Conformational Families. The representative structures of each

Fig. 34. "Flipped" conformational families of **4-FCIN** in water.

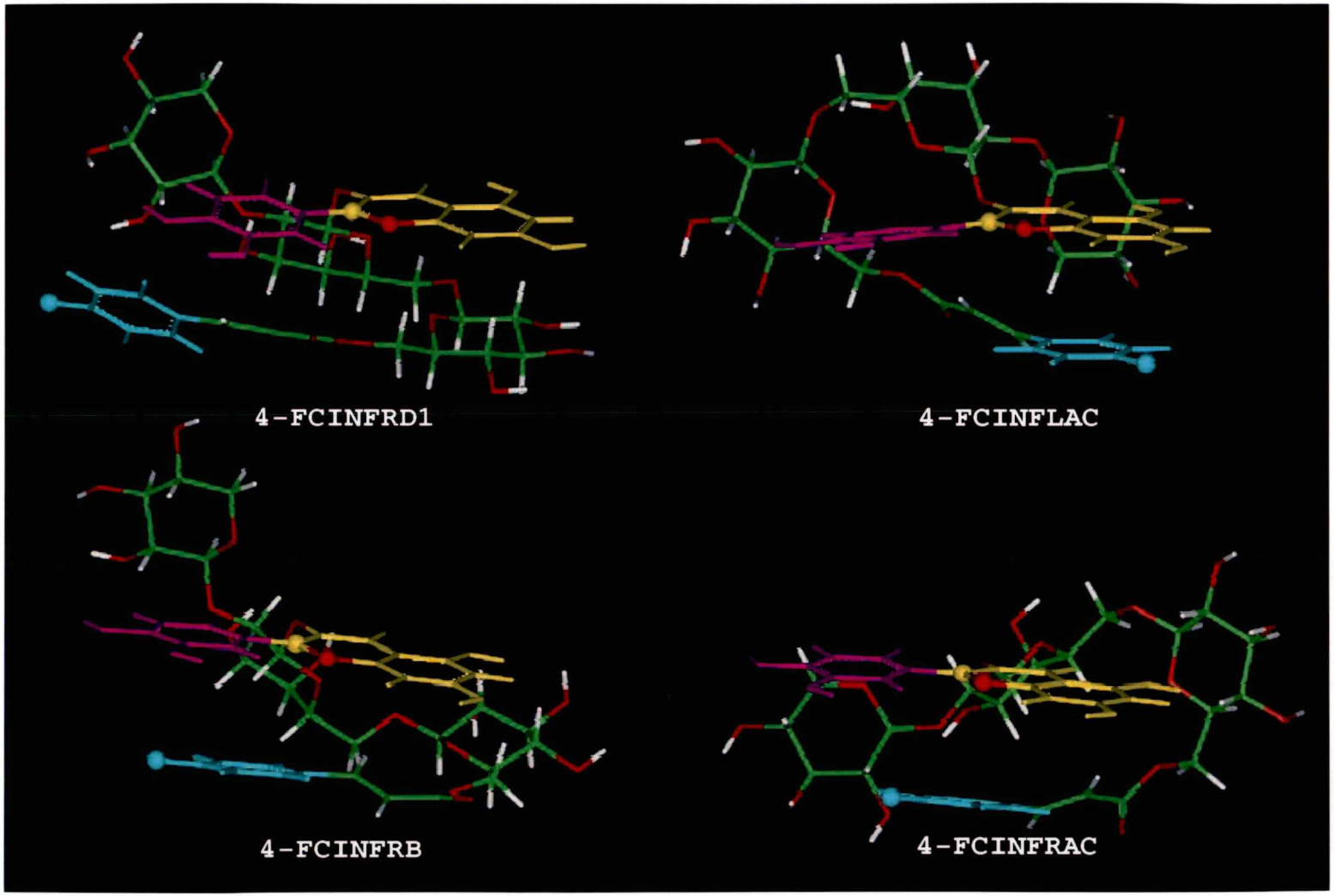

4-FCINFRD1
4-FCINFLAC
4-FCINFRB
4-FCINFRAC

Fig. 35. "Flipped" conformational families of **345-TCIN** in water.

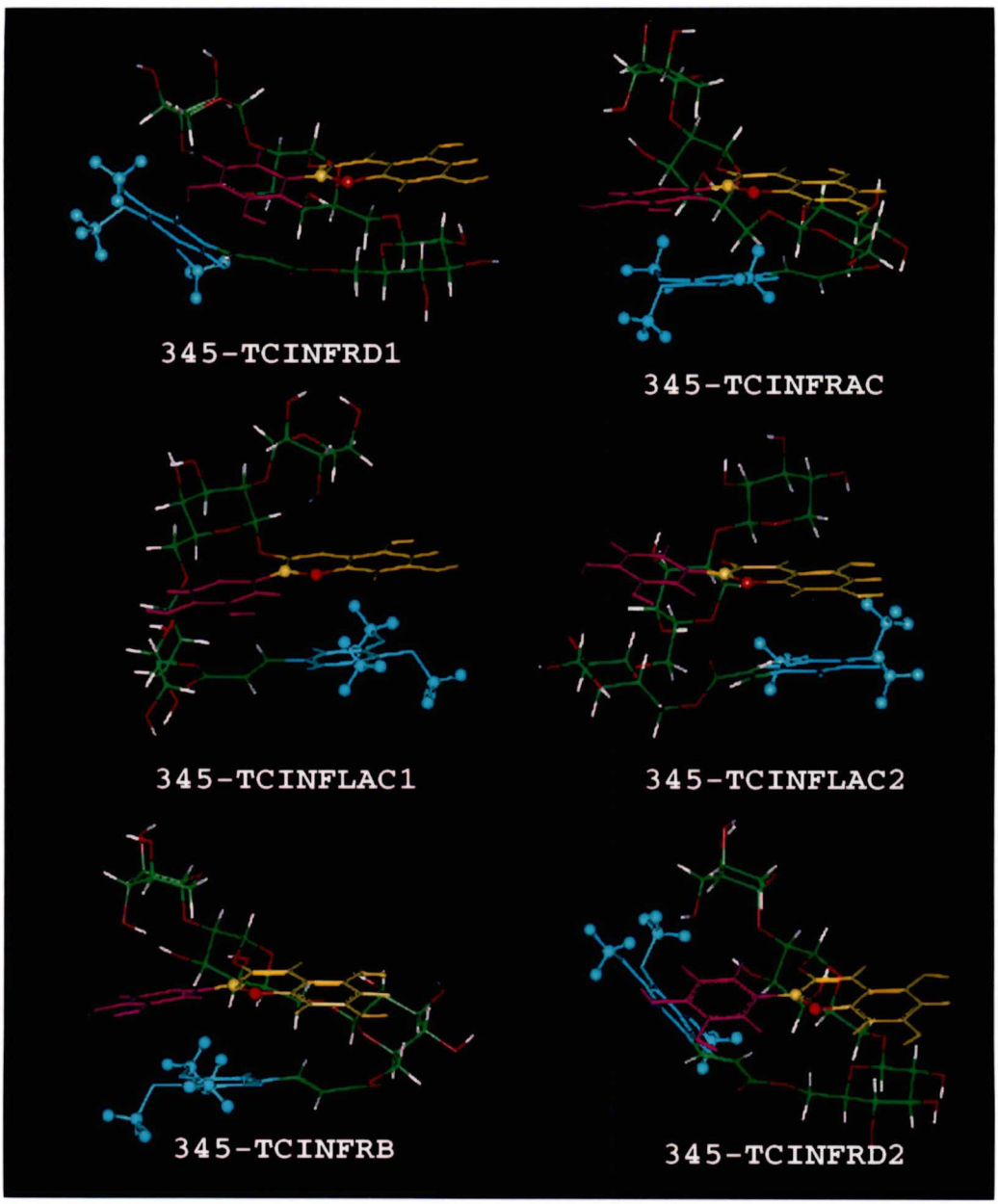

345-TCINFRD1
345-TCINFRAC
345-TCINFLAC1
345-TCINFLAC2
345-TCINFRB
345-TCINFRD2

Fig. 36. "Nonflipped" conformational families of **4-FCIN** in water.

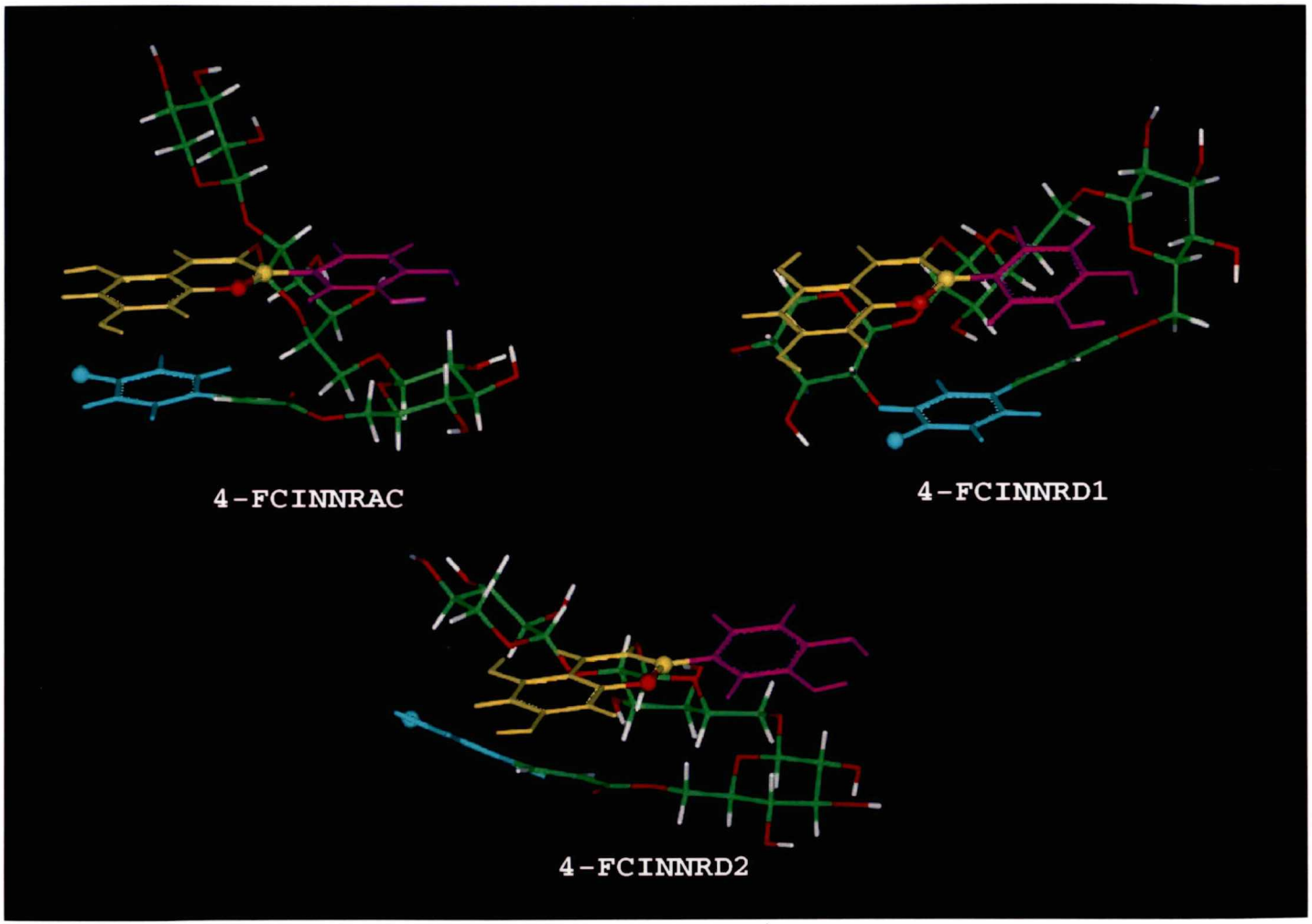

4-FCINNRAC
4-FCINNRD1
4-FCINNRD2

Fig. 37. "Nonflipped" conformational families of **345-TCIN** in water.

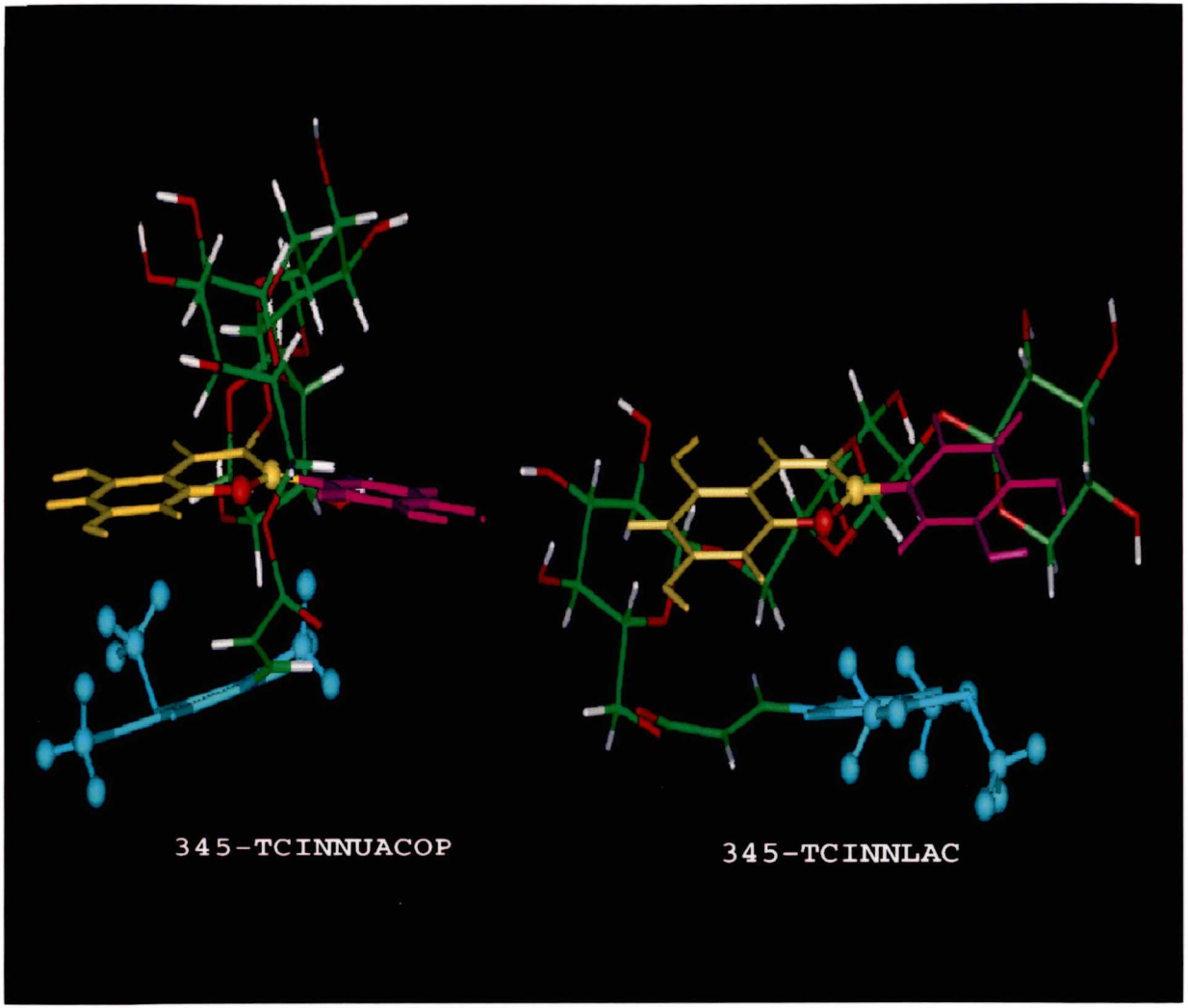

345-TCINNUACOP
345-TCINNLAC

Table 19. Dihedral angles measured in **4-FCIN** in water.

Families [a,b]	ϕ_1 [c]	ϕ_2	ϕ_3	ϕ_4	ϕ_5	ϕ_6
4-FCINFRD (130)	77 ± 5°	49 ± 2°	26 ± 18°	12 ± 5°	-45 ± 4°	-64 ± 1°
4-FCINFLAC (46)	-86 ± 4°	3 ± 0.3°	57 ± 0.1°	3 ± 1°	-35 ± 3°	-43 ± 2°
4-FCINFRAC(23)	30 ± 15°	36 ± 7°	42 ± 16°	26 ± 11°	-34 ± 8°	-144 ± 39°
4-FCINFRB (19)	42 ± 54°	108 ± 55°	54 ± 4°	-1 ± 8°	29 ± 15°	-70 ± 3°
4-FCINNRAC (209)	-85 ± 2°	51 ± 6°	52 ± 27°	-17 ± 18°	45 ± 6°	-67 ± 2°
4-FCINNRD2 (209)	-93 ± 2°	9 ± 5°	39 ± 35°	-4 ± 7°	-44 ± 7°	-63 ± 2°
4-FCINNRD1 (5)	-114 ± 0.6°	-40 ± 2°	53 ± 3°	29 ± 0.1°	-22 ± 2°	-166 ± 1°

[a] The numbers in parenthesis are the total number of structures in the individual families. [b] Values that have no errors indicated in the table have an error less than ± 0.01. [c] The dihedral angles are defined in Figure 1.

Table 20. RMS deviation value for each conformational family of 4-FCIN.

Conformational family	RMS deviation value
4-FCINFRD	1.06 ± 0.361 Å
4-FCINFLAC	0.71 ± 0.280 Å
4-FCINFRAC	0.87 ± 0.406 Å
4-FCINFRB	1.21 ± 0.495 Å
4-FCINNRAC	1.22 ± 0.271 Å
4-FCINNRD2	0.63 ± 0.140 Å
4-FCINNRD1	1.33 ± 0.264 Å

Table 21. Dihedral angles measured in **345-TCIN** in water.

Families [a,b]	ϕ_1 [c]	ϕ_2	ϕ_3	ϕ_4	ϕ_5	ϕ_6
345-TCINFRD1 (320)	-19 ± 16°	-54 ± 8°	26 ± 26°	-17 ± 21°	30 ± 12°	-61 ± 17°
345-TCINFRAC (244)	-29 ± 16°	-22 ± 30°	30 ± 18°	-22 ± 17°	65 ± 15°	-67 ± 11°
345-TCINFLAC1 (81)	-52 ± 6°	39 ± 5°	18 ± 31°	1 ± 21°	22 ± 16°	-168 ± 16°
345-TCINFLAC2 (57)	58 ± 15°	-18 ± 25°	19 ± 32°	-19 ± 19°	59 ± 146°	-61 ± 4°
345-TCINFRB1 (12)	-50 ± 15°	-38 ± 6°	28 ± 35°	-8 ± 31°	41 ± 21°	-19 ± 66°
345-TCINFRD2 (1)	-2°	-64°	33°	-27°	19°	-68°
345-TCINNUACOP (8)	61°	-72°	43°	-31°	85°	-177°
345-TCINNLAC (1)	-101°	-58°	52°	-9°	166°	-58°

[a] The numbers in parenthesis are the total number of structures in the individual families. [b] Values that have no errors indicated in the table have an error less than ± 0.01. [c] The dihedral angles are defined in Figure 11.

Table 22. RMS deviation value for each conformational family of **345-TCIN**.

Conformational family	RMS deviation value
345-TCINFRD1	2.16 ± 0.603 Å
345-TCINFRAC	2.37 ± 0.519 Å
345-TCINFLAC1	2.60 ± 0.159 Å
345-TCINFLAC2	1.96 ± 0.459 Å
345-TCINFRB	1.93 ± 0.581 Å
345-TCINNUACOP	0.83 ± 0.496 Å
345-TCINNLAC	one structure
345-TCINFRD2	one structure

conformational family for both **4-FCIN** and **345-TCIN** are shown in Figs. 34–37. Although these structures were not validated by NMR-derived restraints, several of the conformational families have a similar shape as the families produced in the studies in methanol. This suggests that, assuming similar long-range interactions within the molecule are observed in water, the models of anthocyanins produced are reasonable. Additionally, the representative structures from the "flipped" families for both of the anthocyanins under investigation, i.e., **4-FCINFRD** and **345-TCINFRD1** closely resemble one another, and similarly the representative structures of **4-FCINFRB**, and **345-TCINFRB** show commonalities to one another (see Fig. 21 and 20, respectively). Thus, irrespective of the acyl group on the O-6 Glc terminus of the anthocyanins, the conformational families these anthocyanins populate can be the same. Moreover, the "flipping" process that exists in methanol could exist in water and explain the differences in the anthocyanin's color stability.

4. Structural Features of the Conformational Families. In Figs. 34–37 the representative structures from each conformational family are depicted according to the classification system previously described (see Section D.2), i.e., the flavylium nucleus faces towards the viewer, and the β-Gal unit is facing away from the viewer. Like the structures of **CyanGXG**, **345-TMBENZ**, **4-FCIN**, **345-TCIN**, and **345-TCIN–X** in methanol, the strategic $C=O^+$ in the C-2 position

of the flavylium nucleus is shown as a yellow and red ball, respectively.

Salient features of these conformational families are the same as those observed in the studies in methanol. Like the studies performed in methanol, the characteristics are based on the 3D model, as well as the Figs. that feature the representative structures of each conformational family. These observations are summarized below:

1. The flavylium nucleus in structures of these conformational families can be read as "ACB" ("nonflipped") or "BCA" ("flipped"), when viewed from the same perspective.
2. In certain families, the exocyclic double bond interacts with the flavylium nucleus.
3. The acyl moiety on the O-6 Glc terminus of these anthocyanins can interact with either the A–C ring system or ring B of the flavylium nucleus.
4. In certain families, the β-Xyl moiety is positioned over the C-2 of the flavylium nucleus.
5. In the 3,4,5-trimethoxycinnamoylated anthocyanin, the methoxy groups are proximal to the C-2 of the flavylium nucleus.

The similarities between the conformational families for the anthocyanins in water suggest that the overall shape of these cinnamoylated anthocyanins in solution is not critical to explain the differences in the color stability of this type of compounds. Thus, as with the studies in methanol, the differences in the physical behavior of these compounds in solution could explain the different color-stability profiles of these cinnamoylated anthocyanins.

5. Molecular Dynamics Simulations of These Conformational Families. In the simulation studies in methanol (see Section D.4), the structure that represents **4-FCINNRD** was shown to be flexible and converted to structures that were similar to other conformational families. By performing a 5 ns molecular dynamics simulation in a dielectric continuum to mimic water ($\epsilon = 80$), the motions of these particular anthocyanins could be established. Figs. 38–40 and Figs. 41–42 show ϕ_1 as a function of time for the duration of the simulation for the representative structures from selected conformational families of **4-FCIN** and **345-TCIN**, respectively.

As with the studies in methanol, the representative structures where the acyl moiety is not interacting with any portion of the flavylium nucleus (the codes for these structures end with a D) were subjected a 5 ns molecular dynamics simulation in a dielectric continuum of water. The results of the simulations suggest that the structures of **4-FCIN** with a similar consensus fold as their

Fig. 38. The dihedral angle ϕ_1 of **4-FCINNRD1** as a function of time during a 5 ns molecular dynamics simulation at 400 K in a dielectric continuum of water.

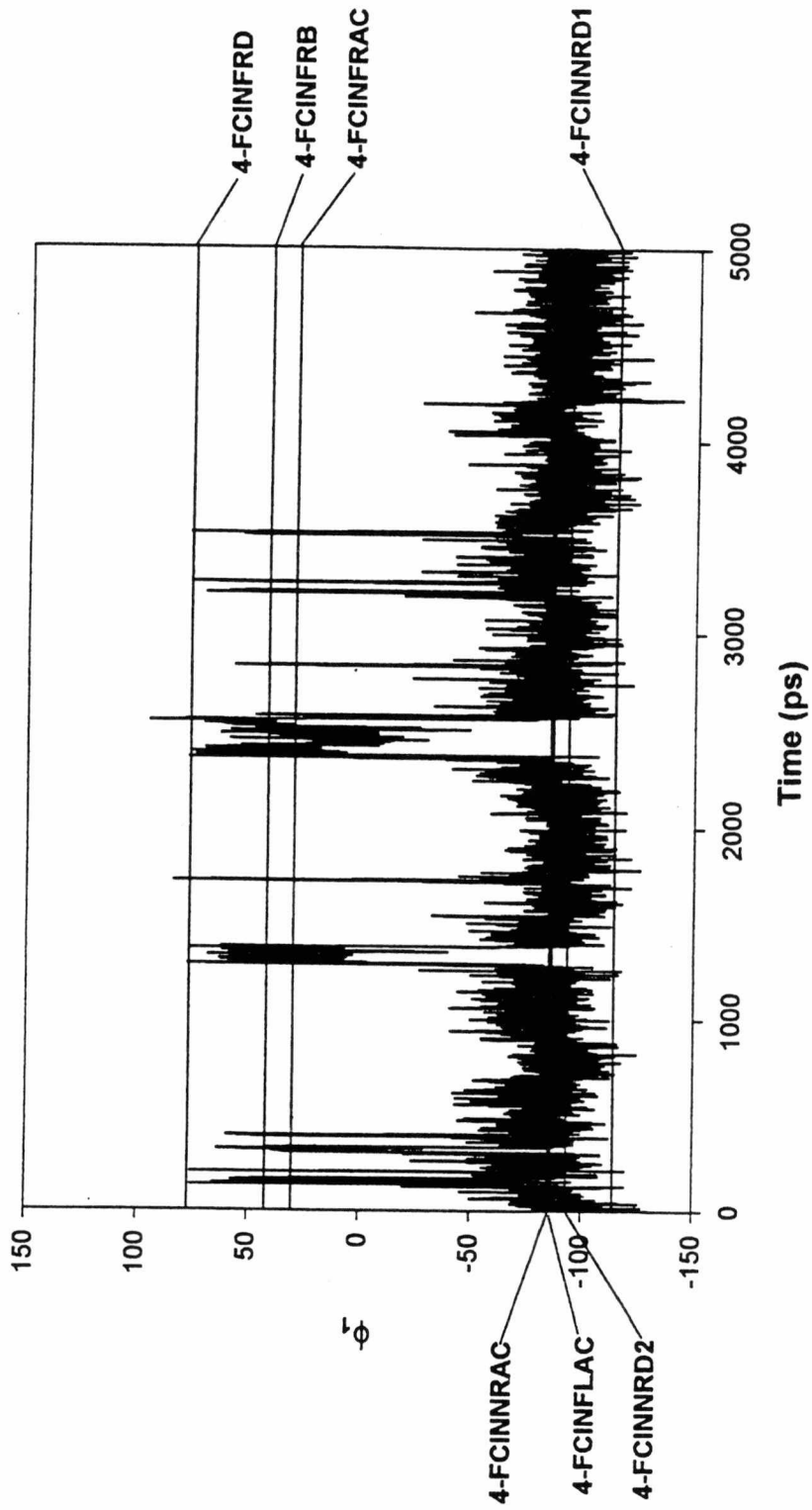

4-FCINFRD
4-FCINFRB
4-FCINFRAC
4-FCINNRD1
4-FCINNRAC
4-FCINFLAC
4-FCINNRD2
150
100
50
0
-50
-100
-150
0
1000
2000
3000
4000
5000
Time (ps)

Fig. 39. The dihedral angle ϕ_1 of **4-FCINFRD1** as a function of time during a 5 ns molecular dynamics simulation at 400 K in a dielectric continuum of water.

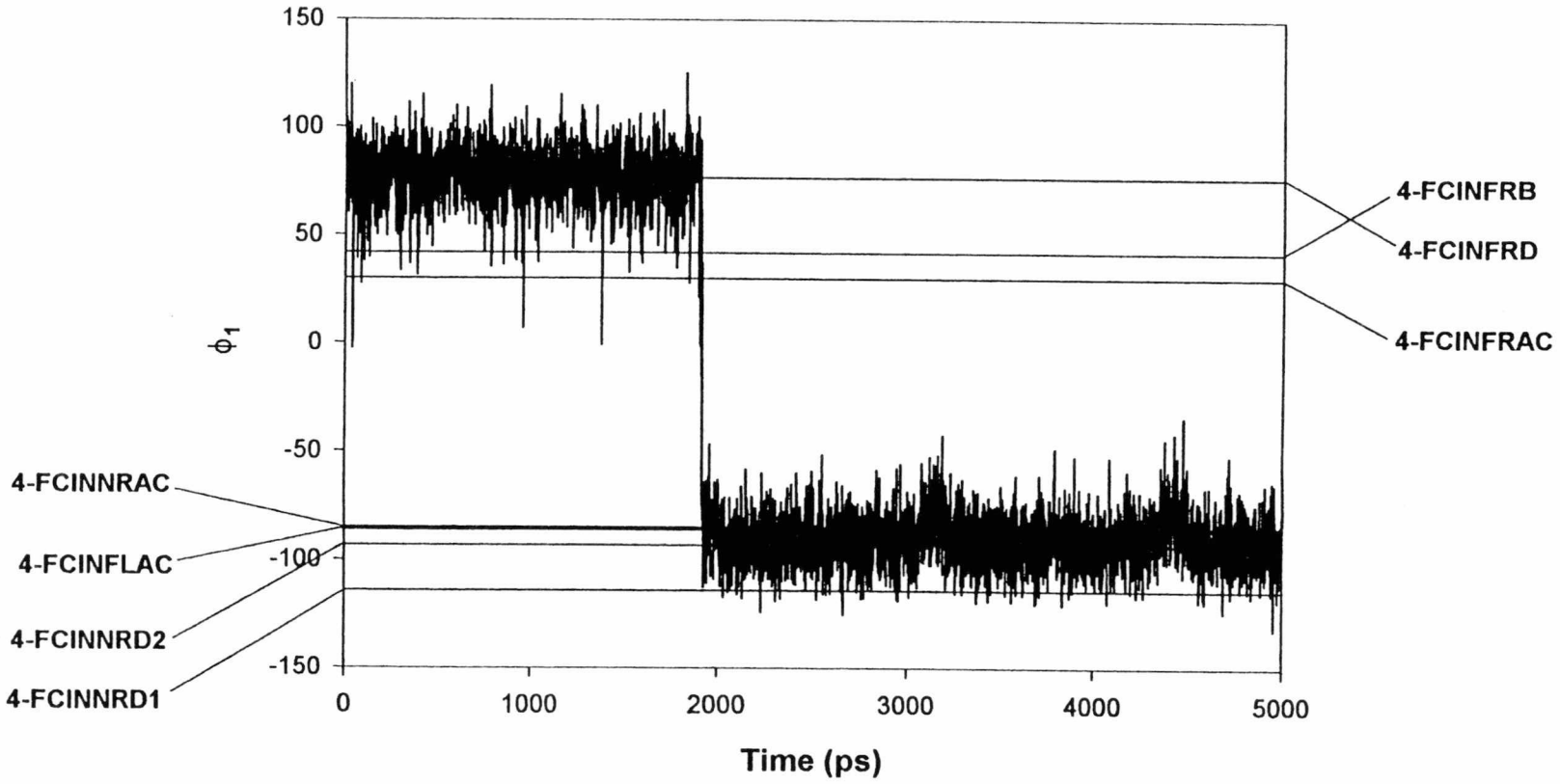
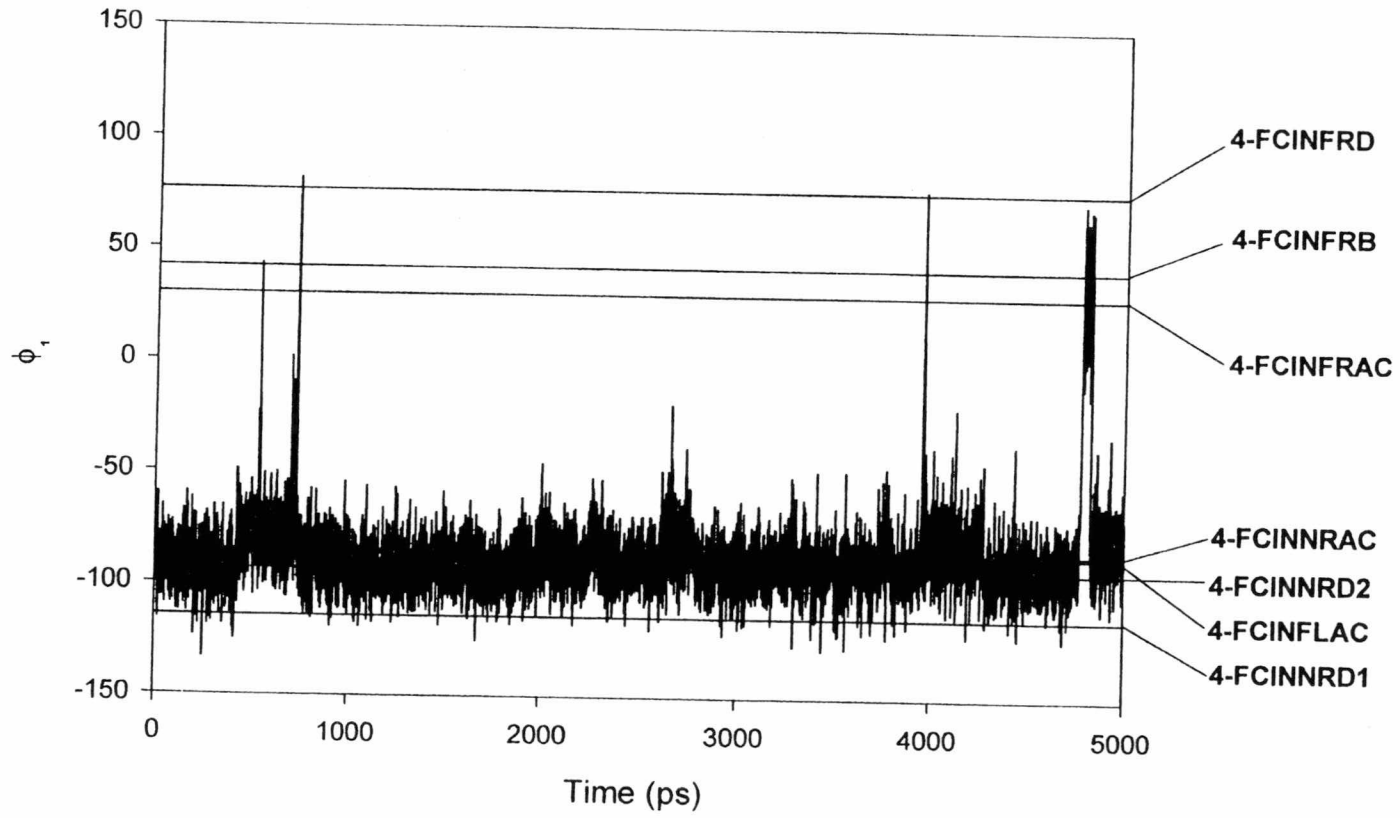

150
100
50
0
-50
-100
-150
ϕ_1
0
1000
2000
3000
4000
5000
Time (ps)
4-FCINFRB
4-FCINFRD
4-FCINFRAC
4-FCINNRAC
4-FCINFLAC
4-FCINNRD2
4-FCINNRD1

Fig. 40. The dihedral angle ϕ_1 of **4-FCINNRD2** as a function of time during a 5 ns molecular dynamics simulation at 400 K in a dielectric continuum of water.


150
100
50
0
-50
-100
-150
ϕ_1
0
1000
2000
3000
4000
5000
Time (ps)
4-FCINFRD
4-FCINFRB
4-FCINFRAC
4-FCINNRAC
4-FCINNRD2
4-FCINFLAC
4-FCINNRD1

counterparts in methanol are not as flexible (compare Figs. 38–40 to Fig. 29). Although the structures do interconvert and the "flipping" process in water does occur, they reside longer in that particular conformational shape than their counterparts in methanol. However, the structures of **345-TCIN** that were subjected to extensive molecular dynamics simulations revealed that these do not spend any time in a particular conformation (shown in Figs. 41–42) and the clearly defined "flipping" process, which is apparent in the certain conformational families of **4-FCIN** are not observed for families of **345-TCIN**. The difference in the behavior of **4-FCINFRD** and **345-TCINFRD1** is shown in Figs. 39 and 41–42, respectively. The structures "a" → "e" show the intermediates involved in the "flipping" process of **4-FCINFRD** (see Fig. 43). A similar series of events occurs in water as observed in methanol (for the "flipping" process in methanol, see Fig. 30). In structure "a" the flavylium nucleus is facing the viewer and reads "BCA" from left to right. The strategic $C=O^{+}$ is marked as a yellow and red ball, respectively. As the intermediate "a" progresses to "b" the 4-fluorocinnamoyl moiety moves closer to the β-Xyl moiety, which provides enough clearance for the flavylium nucleus to rotate perpendicular to the glycosidic chain. This orientation is clearly shown in "c" and "d". In this position the flavylium nucleus can revert to the original position, or it can position itself where the flavylium nucleus now reads "ACB", i.e., the "nonflipped" orientation.

Very different behavior is exhibited when **345-TCINFRD1** is subjected to

Fig. 41. The dihedral angle ϕ_1 of **345-TCINFRD1** as a function of time during a 5 ns molecular dynamics simulation at 400 K in a dielectric continuum of water.

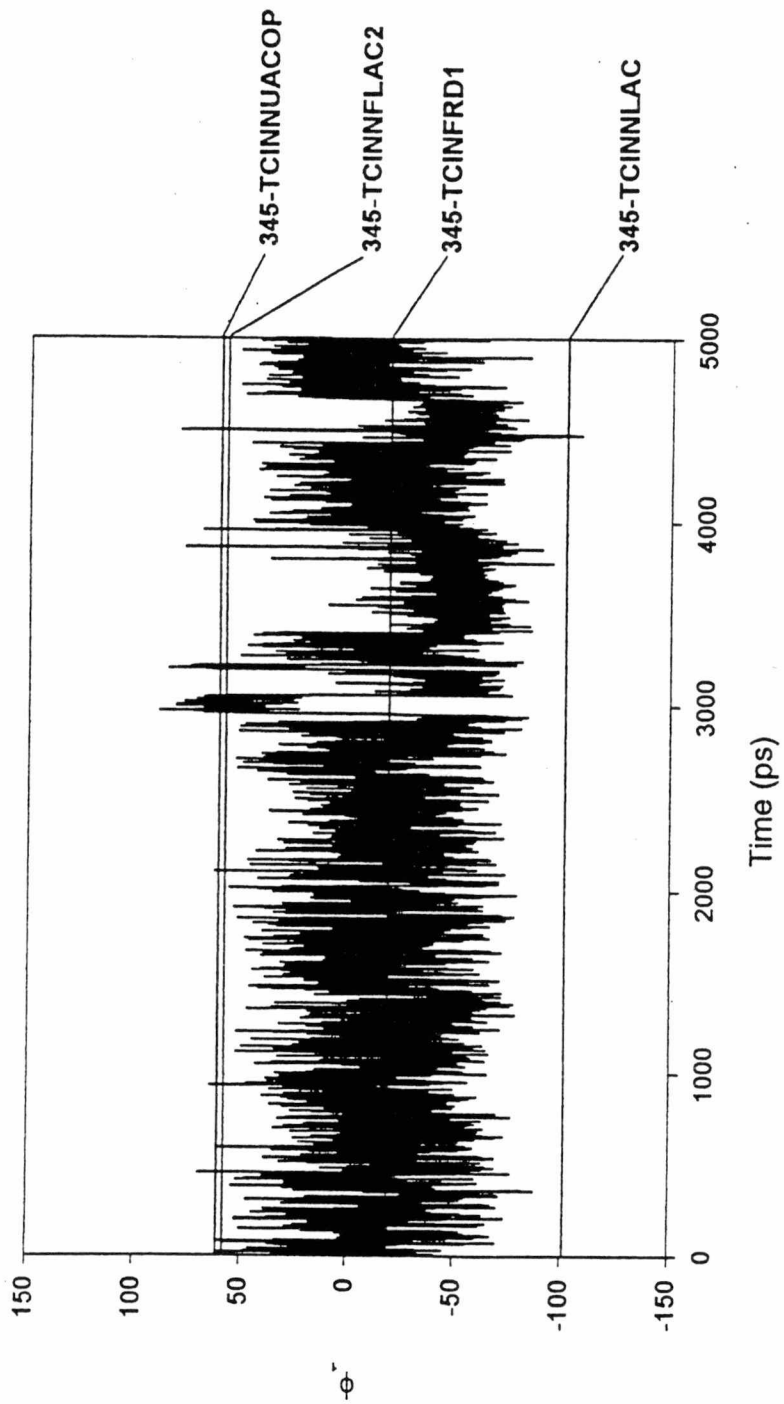

345-TCINNUACOP
345-TCINNFLAC2
345-TCINFRD1
345-TCINNLAC
150
100
50
0
-50
-100
-150
0
1000
2000
3000
4000
5000
Time (ps)

Fig. 42. The dihedral angle ϕ_1 of **345-TCINFRD2** as a function of time during a 5 ns molecular dynamics simulation at 400 K in a dielectric continuum of water.

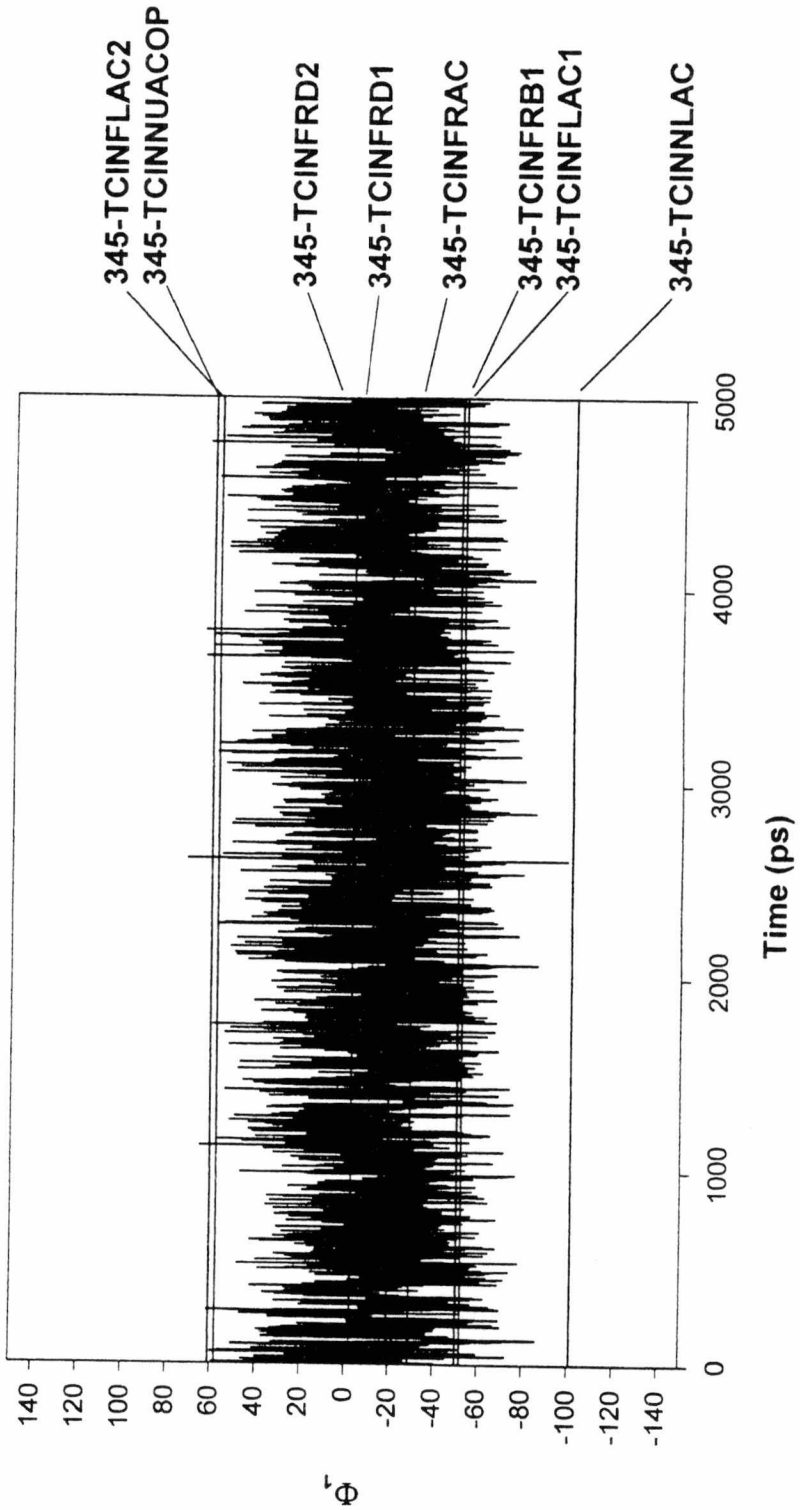
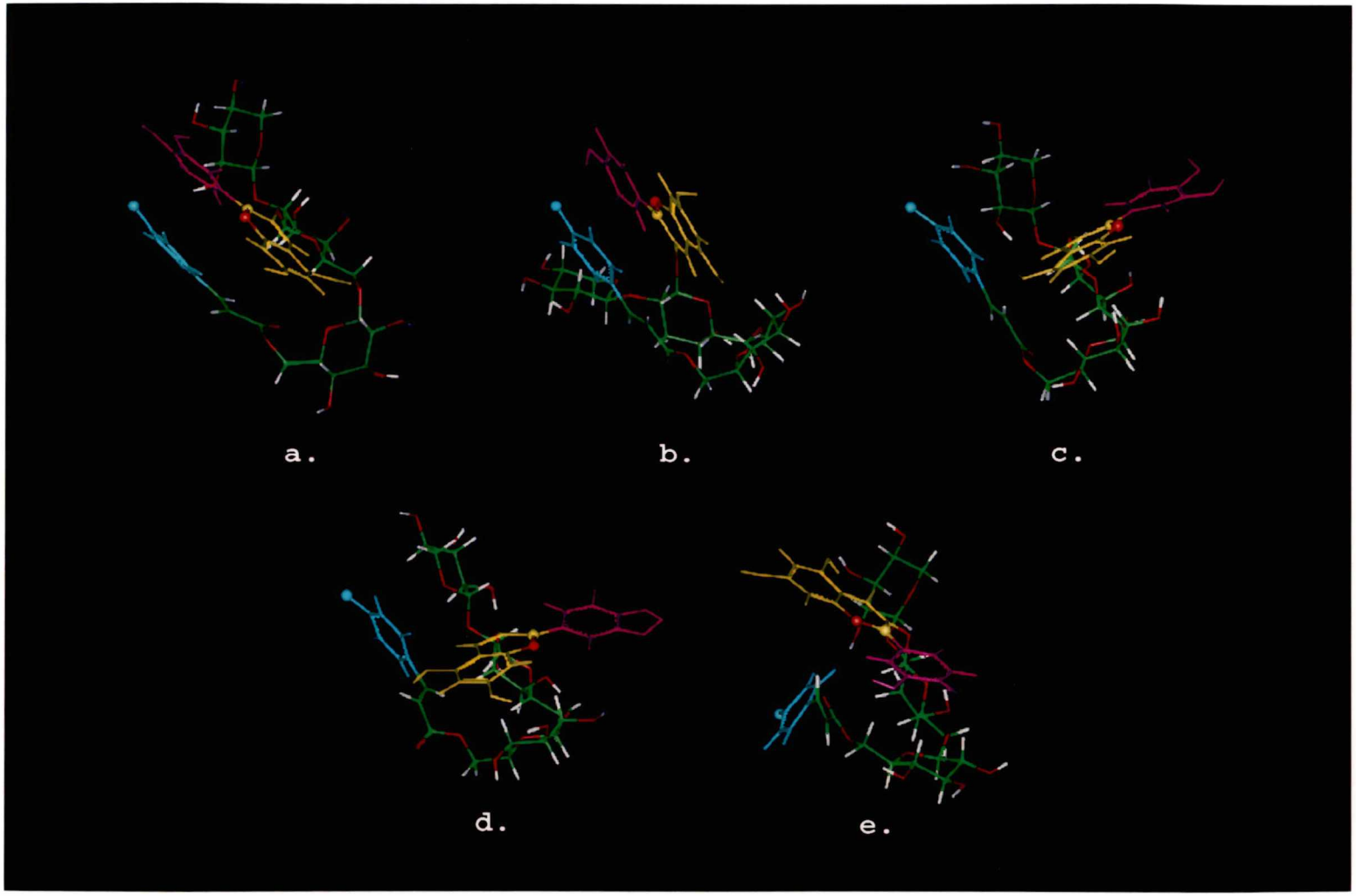
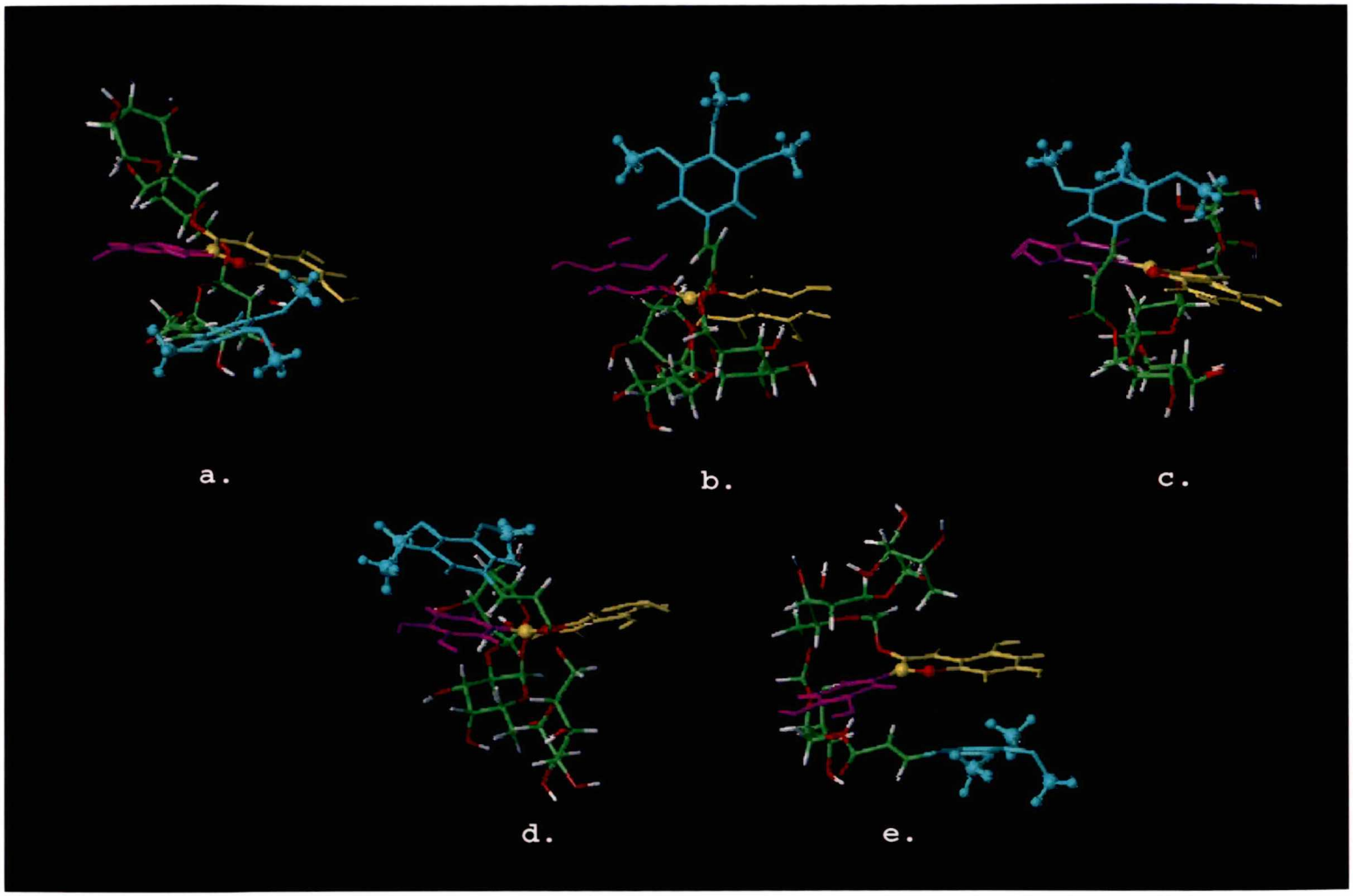

345-TCINFLAC2
345-TCINNUACOP
345-TCINFRD2
345-TCINFRD1
345-TCINFRAC
345-TCINFRB1
345-TCINFLAC1
345-TCINNLAC
140
120
100
80
60
40
20
0
-20
-40
-60
-80
-100
-120
-140
0
1000
2000
3000
4000
5000
Time (ps)
Φ1

Fig. 43. Conformations in the "flipping" process of **4-FCINNRD** in water.


a.
b.
c.
d.
e.

extensive molecular dynamics simulations in a dielectric continuum that mimics water. The unusual motions of the molecule are shown in Fig. 44. Interestingly, the 3,4,5-trimethoxycinnamoyl moiety folds over the flavylium nucleus, thus protecting both faces of the nucleus from the deleterious attack of water at the C-2 position (see structures "b", "c",and "d"). The final structure "e" shows that the flavylium nucleus reads "BCA" as in the initial structure. Thus, unlike the conformational family **4-FCINFRD**, the representative structure of the family **345-TCINFRD1** and **345-TCINFRD2** does not "flip". The failure for the latter structure to "flip" implies that there is not enough clearance for the flavylium nucleus to move. Clearly, the sterically demanding methoxy groups could cause the congestion necessary to prevent the motion necessary for the flavylium nucleus to "flip". Additionally, the exocyclic double bond in this structure retains intimate contact with the flavylium nucleus. This π–arene interaction prevents the acyl moiety moving beyond the flavylium nucleus, closer to the β-Xyl moiety, which normally precipitates the rapid rotation of the flavylium nucleus. The strength of the interaction compared to that found in **4-FCIN** is considerably greater. This stems from the electron richness of the double bond in the anthocyanin **345-TCIN**, which results from through conjugation of the *p*-OMe group. Thus, the differences in the physical behavior of the anthocyanins under investigation may be result of both steric and electronic factors. Visualization of these structures with MOLCAD [48-62] could lead to further explanations of the differences in the color-stability profiles of these anthocyanins.

Fig. 44. Conformations in the "flipping" process of **345-TCINFRD** in water.


a.
b.
c.
d.
e.

6. Molecular Visualization of the Dynamics of 4-FCIN and 345-TCIN Using MOLCAD.[63] (For further details about MOLCAD refer to Section D.5) As with the studies of **4-FCIN** in methanol, molecular visualization of the intermediates involved in the "flipping" process in water was performed using MOLCAD. By mapping MLP, MEP, and MLC on the surface of the conformations of **4-FCIN**, the properties of the pocket that encases the strategic $C=O^+$ bond (yellow and red ball, respectively) can be examined. The C-2 attack site of the flavylium nucleus is analogous to a protonated carbonyl.

Nucleophilic attack at the carbon atom of this moiety is governed by the Bürgi–Dunitz trajectory,[64] which dictates that the incoming nucleophile approaches the reaction center at 109° to π-plane. In Figs. 45–47, the $C=O^+$ bond of the **4-FCIN** conformations is positioned to face the viewer. Thus sighting down the bond, the viewer can establish the conditions that the incoming water molecule experiences. Although this is a qualitative analytical tool to establish the conditions in the micro-environment around C-2, trends in the properties of various anthocyanins can be readily established.

The MLP mapped onto the surface of the molecule indicates the hydrophilic nature of areas within the molecule (see Fig. 45). The structures "a" and "b" show that the strategic $C=O^+$ bond of the flavylium nucleus is in a

Fig. 45. The "flipping" process of **4-FCINFRD1** in water as visualized by Molecular Lipophilic Potential (MLP).

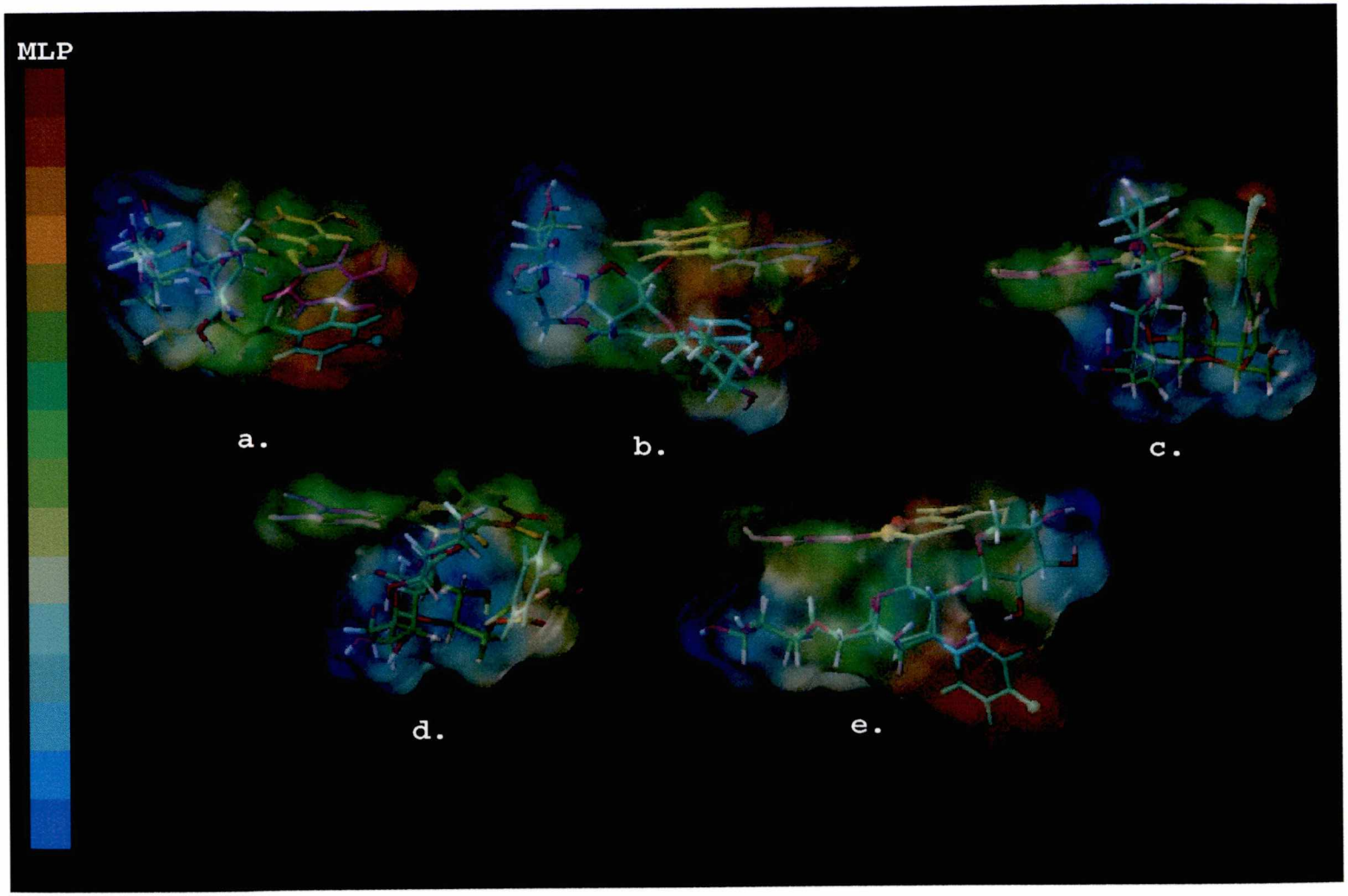

MLP
a.
b.
c.
d.
e.

Fig. 46. The "flipping" process of **4-FCINFRD1** in water as visualized by Molecular Electrostatic Potential (MEP).

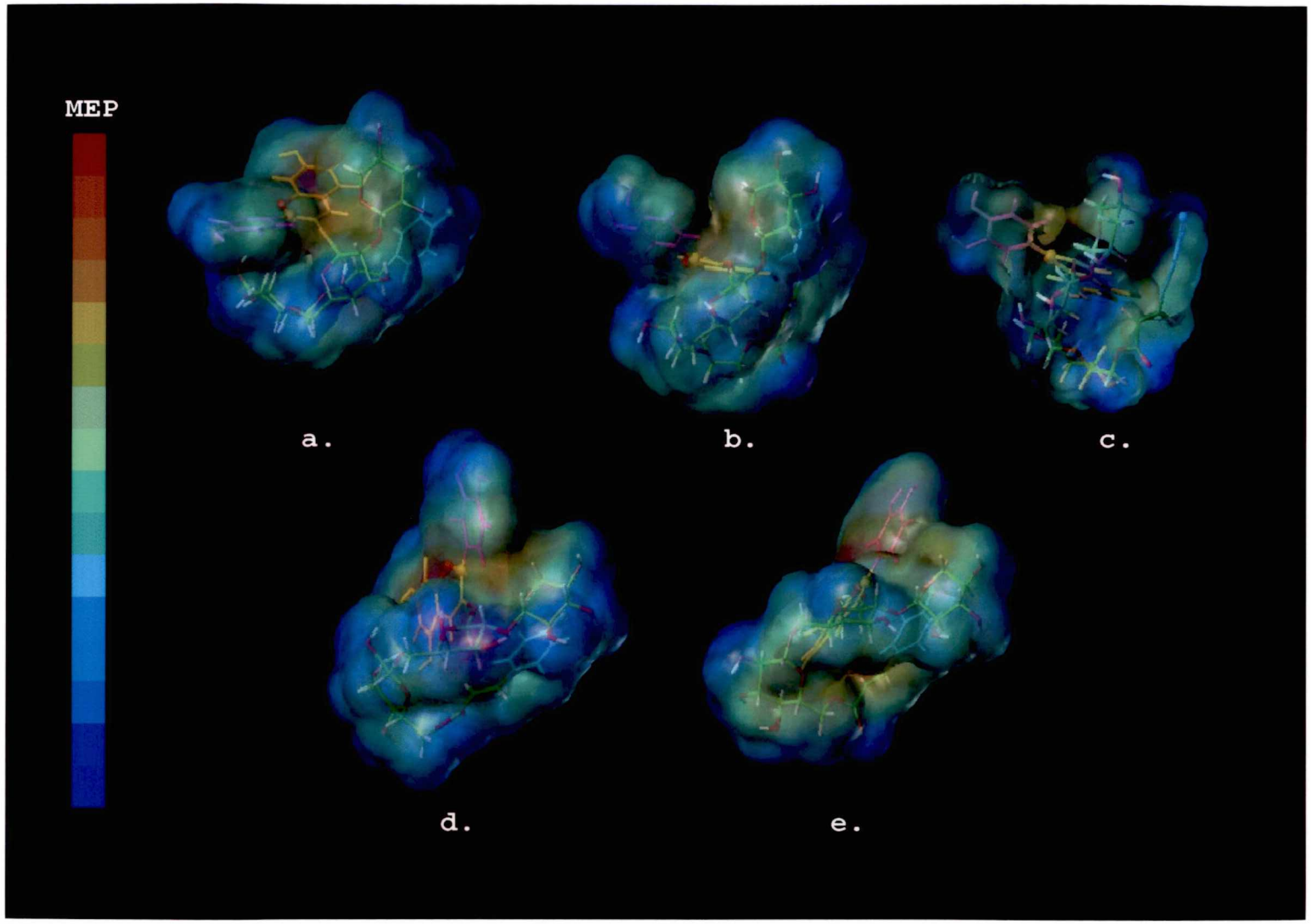
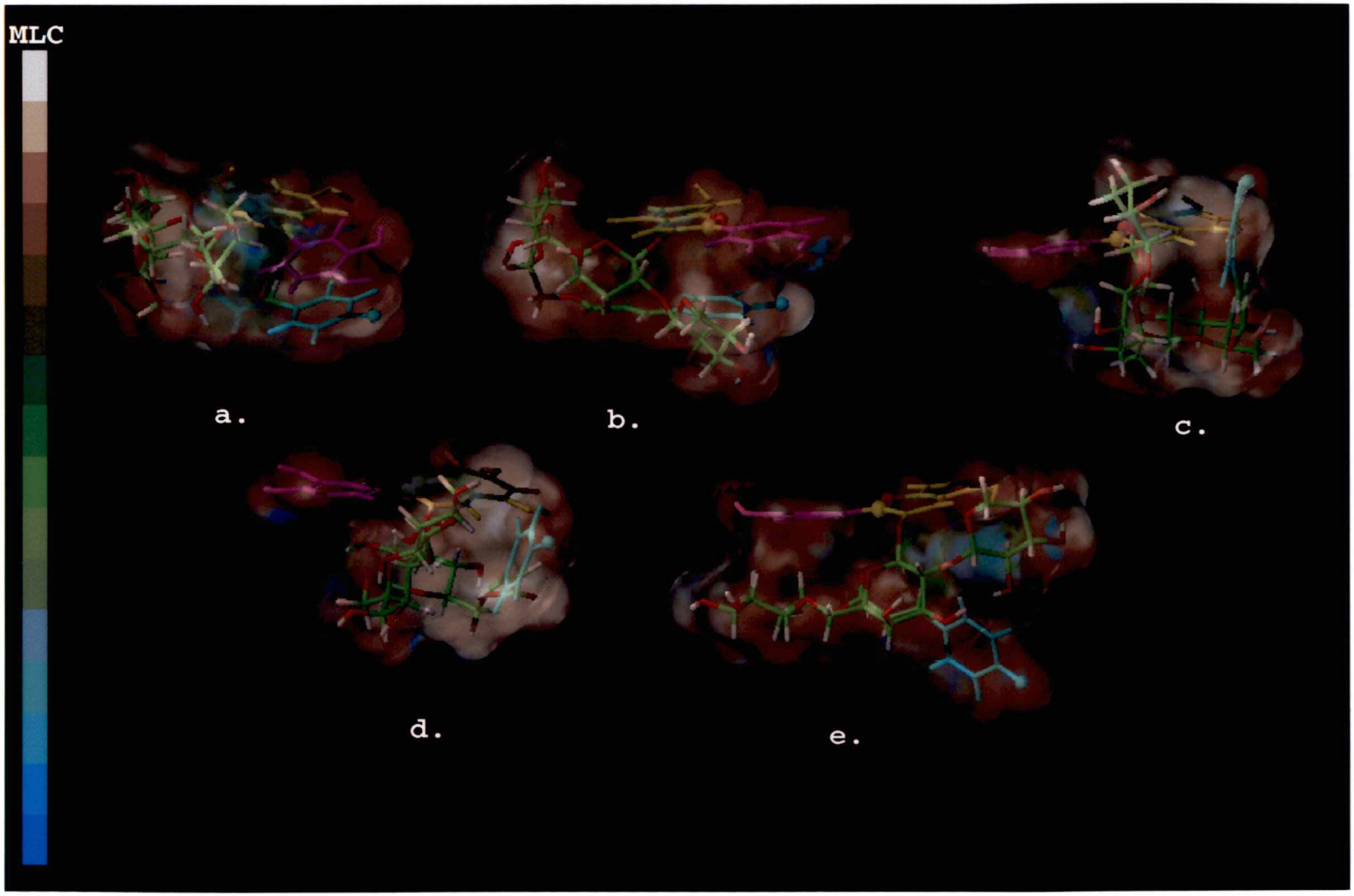

MEP
a.
b.
c.
d.
e.

Fig. 47. The "flipping" process of **4-FCINFRD1** in water as visualized by Molecular Local Curvature (MLC).


MLC
a.
b.
c.
d.
e.

moderately hydrophobic pocket (green). However, as the "flip" of **4-FCINFRD** progresses, the structures "c" and "d" show that the region around C-2 position of the flavylium nucleus becomes bluer. This indicates that the pocket is becoming more hydrophilic. In the final structure shown in Fig. 45, the area around the $C=O^+$ bond returns to its original hydrophobicity (green/brown). Thus, during the "flipping" process of **4-FCINFRD** in water, mapping ("a" → "e") MLP reveals that the micro-environment surrounding the C-2 attack site becomes more hydrophilic.

Mapping the MEP onto the surface of the intermediates involved in the "flipping" process of **4-FCINFRD** is particularly revealing (see Fig. 46). The electrostatic potential remains essentially unaltered throughout the entire process. Moreover, the local curvature, which is visualized by mapping the MLC property, remains unaltered through the "flipping" process (see Fig. 47). These findings suggest that the MLP property may be more sensitive to changes in the conformational states of these anthocyanins in water than the other two properties that were mapped.

As demonstrated in the prior study, MOLCAD is a powerful tool to reveal the properties of the micro-environment of C-2 of monocinnamoylated anthocyanins. Mapping of MLP, MEP, and MLC property on the surface of conformational states involved in the motions of **345-TCINFRD1** in water is shown in Figs. 48–50, respectively. The conformations of the anthocyanins are

Fig. 48. The "flipping" process of **345-TCINFRD1** in water as visualized by Molecular Lipophilic Potential (MLP).

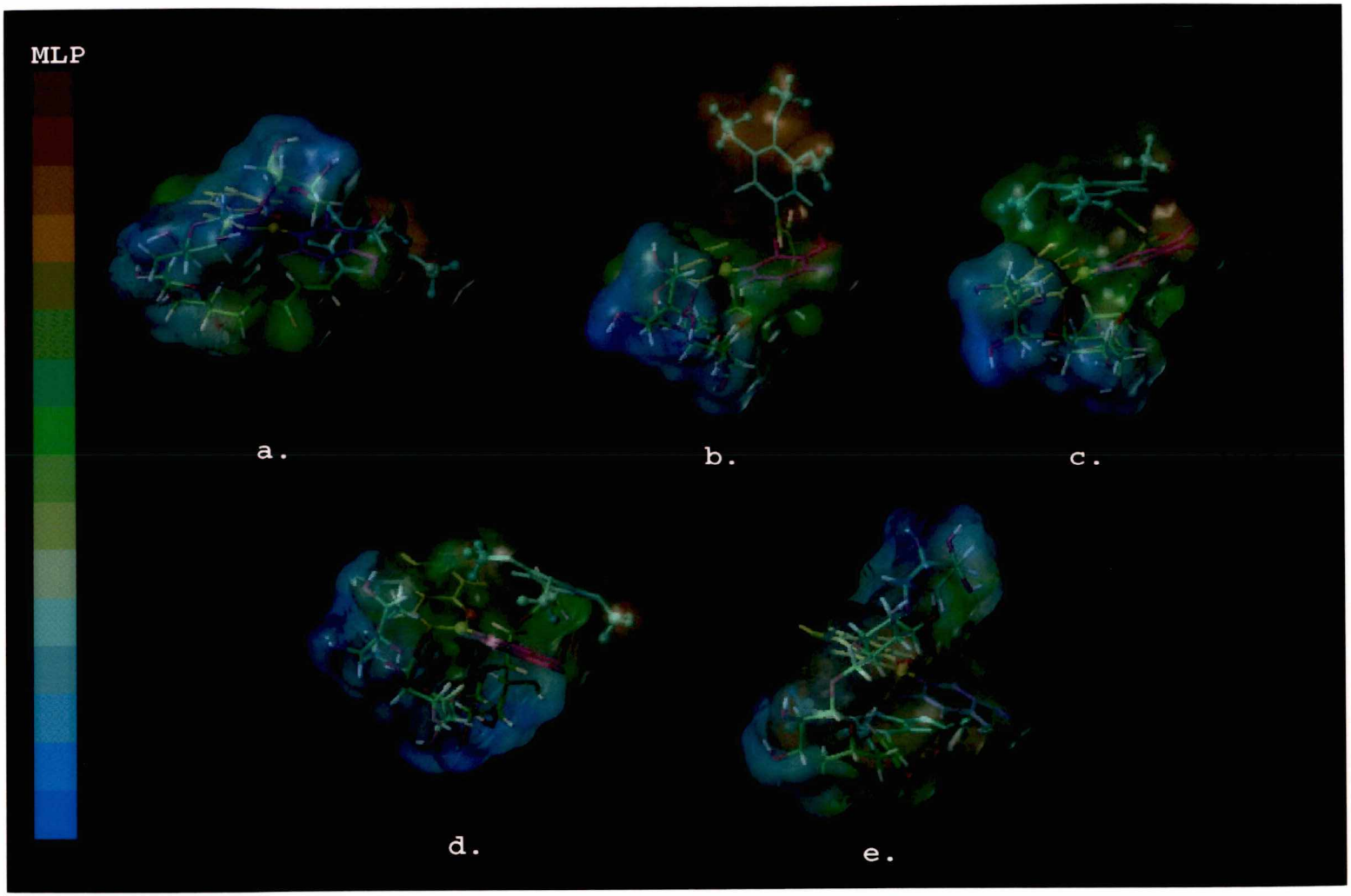

MLP
a.
b.
c.
d.
e.

Fig. 49. The "flipping" process of **345-TCINFRD1** in water as visualized by Molecular Electrostatic Potential (MEP).

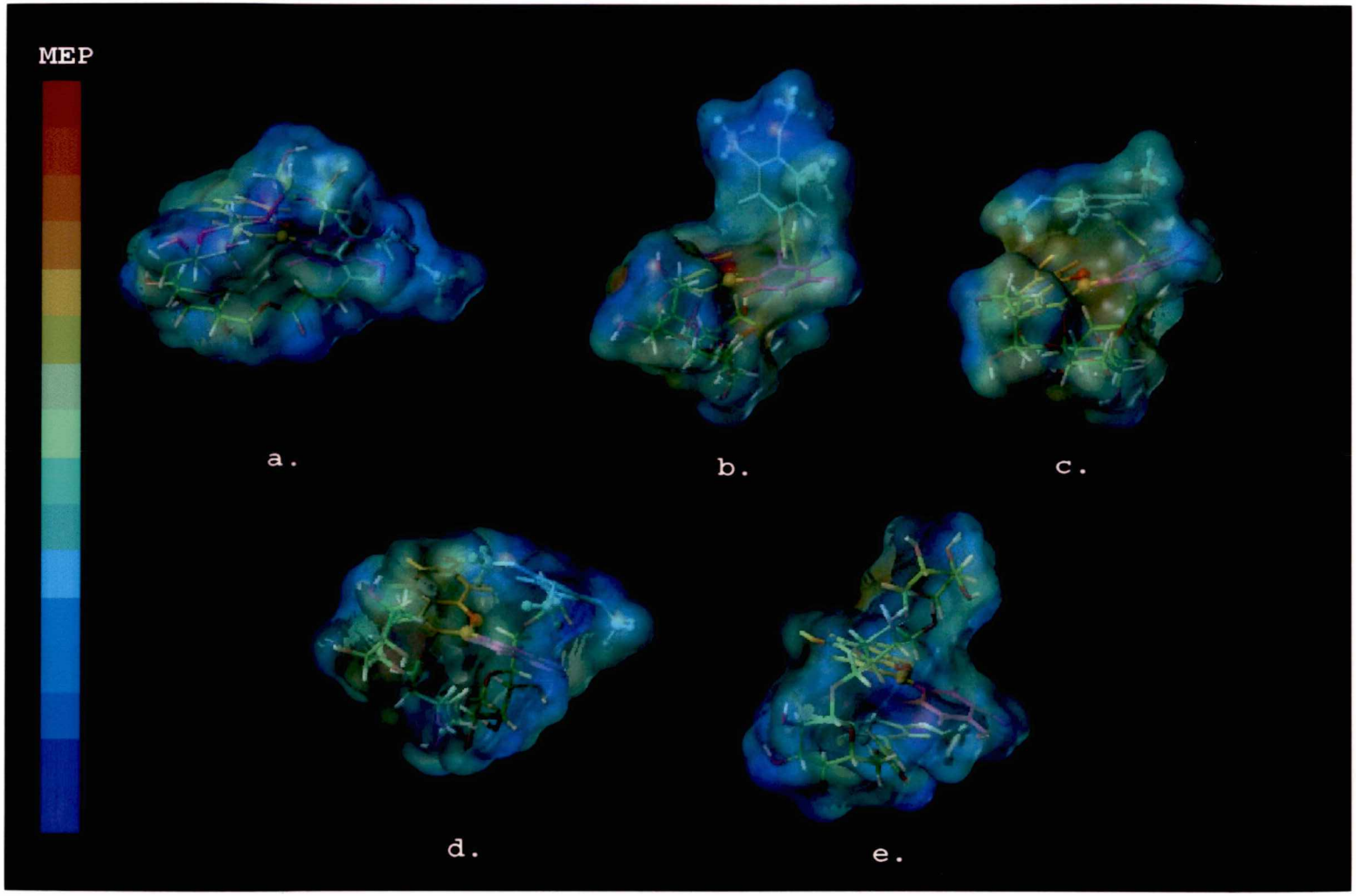
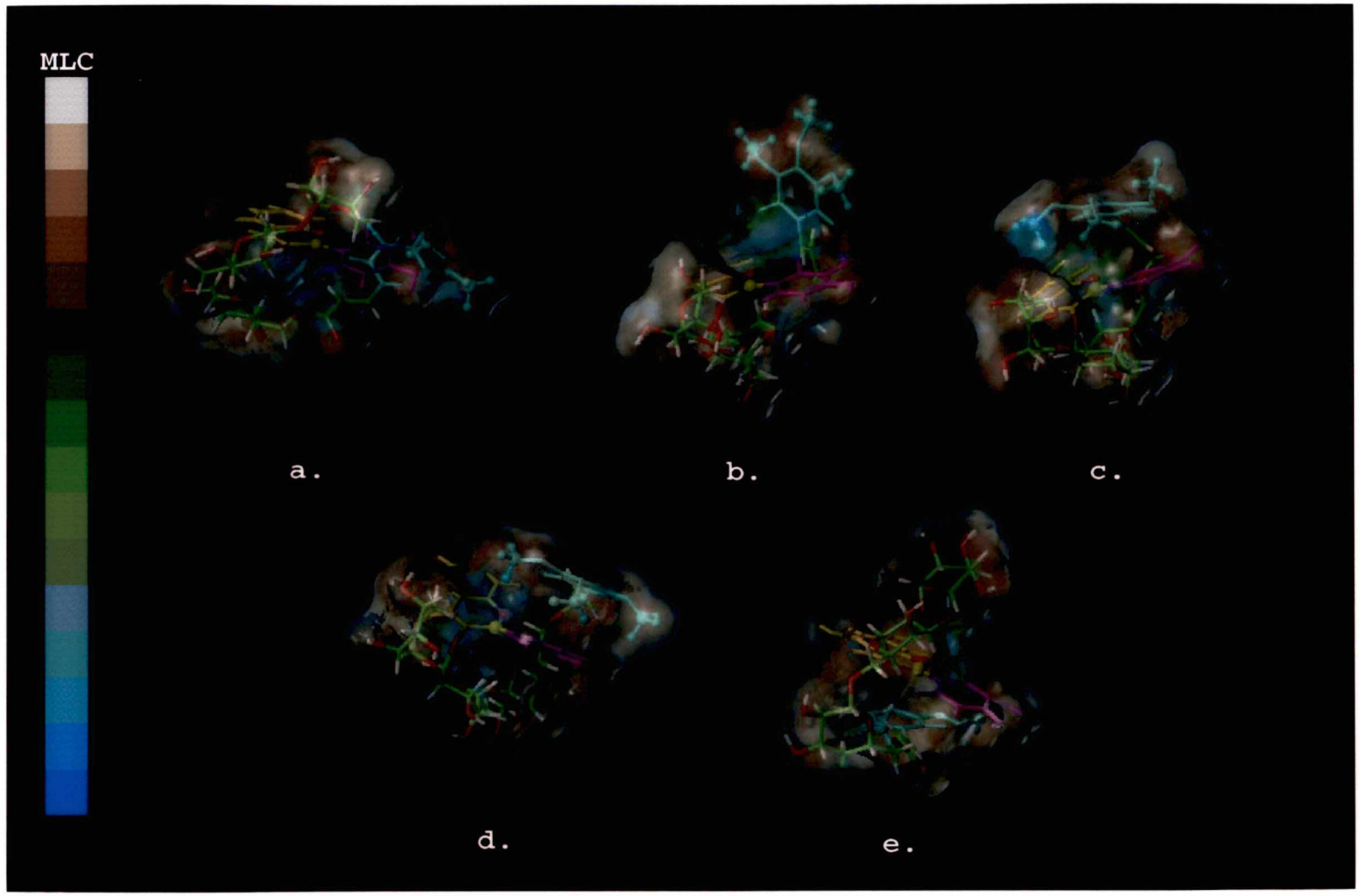

MEP
a.
b.
c.
d.
e.

Fig. 50. The "flipping" process of **345-TCINFRD1** in water as visualized by Molecular Local Curvature (MLC).


MLC
a.
b.
c.
d.
e.

shown in each of these Figs. from the same perspective as the Figs., which involved **4-FCIN**, i.e., the C-2 attack site faces the viewers. Unlike the behavior of the representative structure of **4-FCINFRD** in a dielectric continuum of water, the motions of **345-TCINFRD1** observed shows that the micro-environment of C-2 becomes more hydrophobic (see Fig 48). This is indicated by the blue region in structure "a", which makes way to a dark-green region in "b", "c", and "d". In the final structure "e", the region surrounding the C-2 position is the most hydrophobic (khaki) of all five structures.

In Fig. 49 the MEP property has been mapped onto the surface of conformations of the **345-TCIN**, which are involved in the motions of the molecule in water. In progressing from "a" → "e", the electrostatic potential of the micro-environment encapsulating the C-2 position does change. Structures "a" and "e" show that the region surrounding C-2 is more electronegative (bluish) than the same region in structures "b", "c", and "d" (orangish)–conformation "d" is more electronegative than "b" and "c".

Accessibility of the C-2 in **345-TCIN** to the incoming water molecule can be revealed by mapping the MLC property on the surfaces of these conformational states (see Fig. 50). The more susceptible the $C=O^+$ bond is to attack by a water molecule the bluer the region surrounding the C-2 position. This indicates a concave region where the C-2 position of the flavylium nucleus is exposed. In "a" the strategic $C=O^+$ bond is more exposed (dark blue) than in

the final structure "e" (brown). The intermediates "b", "c", and "d" show that the site of deleterious attack at the C-2 becomes less exposed, but not as protected as the final structure "e".

MOLCAD has revealed that the micro-environment of the C-2 position of the flavylium nucleus changes throughout dynamics simulations in a dielectric continuum of water. Correlation of this discovery to their color stability would permit researchers to design more color-stable monocinnamoylated anthocyanins.

F. Correlating the Behavior of Monocinnamoylated Anthocyanins in Water to Their Color Stability Data

1. General. In order to rationally design a "super color-stable" monocinnamoylated anthocyanin, there has to be a relationship of the structure of the anthocyanin to their color stability. The equilibrium constant of hydration of the C-2 position of the flavylium nucleus, K_h is an excellent measure of the color stability these anthocyanins. The smaller the value, the greater the color stability (see Table 1). Thus **345-TCIN** is a more color-stable anthocyanin than **4-FCIN**.

2. Ratio of "Flipped" to "Nonflipped" Conformers. When the QMD

protocol[37] was performed on **345-TCIN** and **4-FCIN** in a dielectric continuum of water to most closely model natural conditions, we observed ratios of "flipped" to "non-flipped" conformers (see IV.F.3) for each that were quite divergent: 79:1 "flipped:nonflipped" for **4-FCIN** and 1:2 "flipped:nonflipped" for **345-TCIN**. We feel that the difference observed in these ratios is quite significant, as compounds **4-FCIN** and **345-TCIN**, while different in their K_h values, do not represent extremes in color stabilities; thus the ratios should be highly sensitive indicators to differences in color stability. Extension of these studies to other monocinnamoylated anthocyanins could lead to an excellent means of judging the color stability of heretofore unmade anthocyanins.

3. Flexibility of the Monocinnamoylated Anthocyanins. In order to determine the flexibility of the anthocyanins under investigation, the representative structure of select conformational families, where the acyl moiety does not interact with any portion of the flavylium nucleus, has been subjected to a 5 ns molecular dynamics simulation in a dielectric continuum of water (400 K). By viewing dihedral angle ϕ_1 as a function of time, and establishing the interconversion of various conformational families, the flexibility can be established. Another powerful tool used to ascertain the flexibility of these anthocyanins was the visual inspection of the molecule during the simulation. Of the two anthocyanins, the compound **345-TCIN**, the most color-stable

anthocyanin investigated, was the most inflexible. There are two reasons that may account for this difference, (1) the π–arene and, or arene–arene interaction is considerably stronger in **345-TCIN** than the same interaction in **4-FCIN**; thus, preventing the motion of the flavylium nucleus, (2) the sterically demanding methoxy groups results in congestion rendering the motion of the flavylium nucleus difficult, or shields the reaction center from attack by water molecules.

Examination solely of the color-stability data of anthocyanins, illustrate the impact a sterically demanding moiety has on the color-stability of monocinnamoylated anthocyanins. Recently, in a study where the color-stability data of all 24 compounds was reported, an anthocyanin acylated with 2-methoxycinnamic acid was found to have a comparable K_h value to that of **345-TCIN** ($5.0 \pm 0.2 \times 10^{-5}$ M *cf* $5.2 \pm 0.2 \times 10^{-5}$ M, respectively).[36] This indicates that the 2-OMe group is proximal to the strategic $C=O^+$ bond, either protecting the reaction center, or preventing the motion of the flavylium, which will render the C-2 site more exposed. Since the electron-donating ability of the 2-OMe group is the same as the 4-OMe group in **345-TCIN**, steric factors are clearly important.

4. Micro-environment Surrounding C-2. Molecular visualization using MOLCAD is an extremely powerful tool to probe the properties of region surrounding the C-2. Of the three properties mapped on the surface of these

molecules, the MLP property best correlates to the susceptibility of the C-2 position to the deleterious hydration reaction. This property reveals hydrophilic and hydrophobic areas within the molecule. During the "flipping" process of **4-FCINFRD**, the micro-environment of C-2 becomes more hydrophilic, thus potentially encouraging the attack of water at this strategic $C=O^+$ bond. However, the internal motions of the anthocyanin **345-TCIN** indicate that the pocket, which encompasses C-2, becomes more hydrophobic, thus potentially discouraging the attack of water at this strategic $C=O^+$ bond. Moreover, this would suggest that **345-TCIN** is more color stable than **4-FCIN**, a finding which is substantiated by the experimentally determined color-stability data.

Considerable motions of these highly flexible compounds result in subtle changes in the characteristics of the micro-environment of C-2, which can be evaluated using MOLCAD. These characteristics appear to be different for each cinnamoylated anthocyanin; thus, providing a possible means to explain the differences the color stability of this series of anthocyanins.

IV. EXPERIMENTAL

A. Materials and Methods

All the carboxylic acids used were obtained from Aldrich Chemical Company, Milwaukee, WI. The deuterated solvents used in the NMR studies were obtained from both Aldrich Chemical Company, Milwaukee, WI and Cambridge Isotopes Laboratory, Cambridge MA. Negligible difference was observed between the solvents from the two sources. Mass spectra were measured by FABMS in the positive-ion mode in thioglycerol[32] and by ESIMS in the positive-ion mode in 50% MeOH–H_2O, except when noted otherwise. ESIMS was performed with a Quattro-II mass spectrometer (Micro-Mass, Inc., Manchester, UK). UV-vis spectra were measured in 1% v/v concd HCl in 95% MeOH, and vis spectra were measured in 0.1 M acetate + 0.1 M phosphate adjusted to pH 2.0 and to pH 6.0 (HCl) within an hour of preparing the solution using a Hitachi Model U-2000 UV-vis spectrophotometer (Hitachi Instruments, Inc., San Jose, CA). Unless otherwise stated, all other materials were available from a number of different suppliers.

B. Biological Material

Work in section B, C, and D that follow were performed by Dr. Donald K. Dougall and co-workers in the Botany Department. Procedures are included here for background information.

The wild carrot (*Daucus carota* spp *carota*) cell clone used in these studies was WC63-1-9-1-13-1[65], and a subline was selected from it for increased anthocyanin yield.

C. Culture Preparation

For each acid tested, a concentration that gave little or no growth inhibition and the best level of total and novel anthocyanin in the tissue was selected experimentally. For purification of the novel anthocyanins, 1.5–2 L of culture in 100-mL portions was grown for 12 days, with the chosen concentration of the individual carboxylic acids in Me_2SO added (1% of culture volume) at days 4 and 8. The tissue was filtered on Miracloth (Calbiochem–Novabiochem Intl., San Diego, CA.) washed with water, frozen in liquid nitrogen, and stored at -80 °C.

D. Isolation of Anthocyanins

The frozen tissue was extracted overnight in a refrigerator with 10 mL/g fresh weight of methanol containing 5% v/v formic acid. The filtered extract was concentrated approximately five-fold in vacuo at less than 30 °C to remove methanol, extracted twice with 0.5 volumes of CH_2Cl_2, and then twice with 0.5 volumes of EtOAc. The aqueous residue was chromatographed on Amberlite XAD-7 resin (Sigma Chemical Co., St. Louis, MO) (2.5 × 20 cm or 4 × 20 cm) using a gradient from 0.1% formic acid in water to 0.1% formic acid in methanol. The fractions containing the novel anthocyanin were selected by HPLC using either a μBondapak C_{18} column (3.9 × 300 mm, Waters Associates, Inc., Milford, MA.), or a Microsorb-MV C_{18} column (4.6 × 250 mm, Rainin Inst. Co., Woburn, MA), and either isocratic mixtures of or gradients of (a) 5% formic acid in water, and (b) 5% formic acid plus 55% methanol plus 10% acetonitrile in water. The combined fractions were concentrated under reduced pressure and chromatographed on a C_{18} reversed-phase column (1.5 × 44 cm, 28–40 μm, E. Merck, Gibbstown, NJ.) with a gradient from 5% formic acid in water to 5% formic acid plus 55% methanol plus 10% acetonitrile in water. The fractions containing the novel anthocyanin were combined and concentrated under reduced pressure. In some cases two novel anthocyanins were separated on the C_{18} reversed-phase column and were treated separately. The new anthocyanins

were then chromatographed on a lipophilic Sephadex LH-20 column (2.5 × 20 cm, Pharmacia Biotech, Inc., Piscataway, NJ) with 0.1% formic acid in water as the solvent. The fractions containing the desired anthocyanin were combined, concentrated in vacuo, dissolved in 0.1% formic acid and stored frozen. In the cases of **345-TMBENZ**, the anthocyanin after chromatography on Sephadex LH-20 was rechromatographed on a PVP column (Polyclar AT > 0.2 mm, 2.5 × 20 cm), eluted with 0.1% formic acid in water, and the fractions containing the novel anthocyanin were selected and treated as above. Compound **345-TMBENZ**, at this stage, was still contaminated with a component absorbing at 280 nm that was removed by semipreparative chromatography on a 4.8 × 300 mm C_{18} μBondapak column eluted isocratically with a mixture of 0.1% formic acid and 80% methanol.

Compound **CyanGXG** was prepared from **345-TCIN** that had been chromatographed on Amberlite XAD-7 and C_{18} media as described above. The anthocyanin (30 mg) in water at room temperature was treated with stirring, under nitrogen, with an equal volume of 1.8 N KOH for 7 min, followed by 5 volumes of N formic acid. The deacylated product was purified by chromatography as above on C_{18} reversed phase and on Sephadex LH-20 columns.

Compound **345-TCIN–X** was prepared from an NMR sample of **345-TCIN** in CD_3OD and DCl that had been observed to lose the xylose residue. The

sample was chromatographed on C_{18} reversed phase and on Sephadex LH-20 columns to give pure **345-TCIN–X**. Xylose was removed preparatively from **345-TCIN** by partial hydrolysis in 5 N HCl at 25 °C for 60 to 72 h, and the products were chromatographed on C_{18} reversed phase and on Sephadex LH-20 columns to give pure **345-TCIN–X**.

E. ^{1}H NMR Data Acquisition

1. Sample Preparation. ^{1}H NMR spectra were measured using a Bruker AMX 400 spectrometer as previously described,[35] except that CF_3CO_2D was substituted for DCl to avoid the observed partial hydrolysis of xylose from the compounds. This change made no observable difference to the spectrum of **345-TCIN**, which demonstrates that spectra measured in either acid can be directly compared. For some compounds, the assignment of peaks to specific protons was done from 2D spectra, and in other cases by analogy to compounds where the assignments had been determined from 2D spectra.

2. 2D ^{1}H NMR Studies. In the NOESY experiments, a total of 256 FIDs of 2K datapoints were collected with a total of 64 scans per FID with a spectral width of 3205 Hz. The data were zero-filled to 1K points in t_1 and multiplied by the sine^2 window function in both dimensions before Fourier transformation. The

mixing times used were 50–750 ms (the mixing time of 500 ms gave the strongest NOEs), and the transmitter offset was placed on the H_2O resonance, which was irradiated with a lower power pulse during a relaxation delay of 2 s to suppress the water signal. All processing was performed with FELIX 95 software (Biosym/Molecular Simulations) on a Silicon Graphics Indigo2 workstation.

ROESY experiments on the anthocyanins in methanol-d_4 were performed as follows. A ROESY spectrum[66] was acquired at 500 ms on a Bruker AMX-400 at 293 K. Processing was performed as previously described for the NOESY experiments. The volumes of all the cross-peaks were measured in the Felix 95 NMR processing program (BIOSYM/ Molecular Simulations). For the structure validation for **CyanGXG**, **345-TMBENZ**, **4-FCIN**, **345-TCIN–X**, and **345-TCIN**, 15, 20, 22, 10, and 18 ROEs were categorized as strong (1.7–2.5 Å), medium (1.7–3.2 Å), and weak (1.7–5.0 Å), respectively. The NMR-derived restraints are shown in Tables 3–7 for **CyanGXG**, **345-TMBENZ**, **4-FCIN**, **345-TCIN–X**, and **345-TCIN**, respectively.

F. Molecular Modeling

1. General Procedures. All molecular mechanics and molecular dynamics calculations were carried out with the CVFF force field[46] interfaced with Insight II/*Discover* (BIOSYM/Molecular Simulations) operating on a Silicon

Graphics Indigo^2 workstation. All calculations were carried out *in vacuo* with a dielectric continuum of 32.6 and 80.0 to mimic methanol and water, respectively. Molecular dynamics calculations were carried out using the Verlet Leapfrog Integrator using a time step of 1 fs and an equilibration time of 0.1 ps. All simulations were done at constant temperature under canonical ensemble (NVT) conditions. Molecular dynamics simulations on the twelve representative structures were run over a 5 ns time period at 400 K.

QMD simulations were carried out using the general protocol of Burgess and co-workers to treat flexible molecules.[38,39] A random structure of each anthocyanin **CyanGXG**, **345-TMBENZ**, **4-FCIN**, **345-TCIN–X**, and **345-TCIN** was subjected to conjugate gradient minimization until the root-mean-squared (RMS) energy derivative was less than 0.0001 kcal mol^{-1} Å^{-1} and then heated from 300 K to 600 K over 30 ps by increasing the temperature by 10 K every 1 ps. An equilibration step followed that consisted of molecular dynamics at 600 K for 10 ps. The resulting conformation was then subjected to 1 ns of molecular dynamics at 600 K, and snapshots of the conformations were taken every 1 ps to yield 1000 conformers. Each conformer was then subjected to conjugate gradient minimization until the RMS energy derivative was less than 0.0001 kcal mol^{-1} Å^{-1}. The final molecular dynamics and minimization steps of the QMD protocol were performed with the aid of an input file. (To view the file for the simulations in methanol and water, refer to p 342 and p 343, respectively in the Appendix A.)

In order to establish that the conformational space was thoroughly explored, Rachmandran plots were constructed of ϕ_1 *vs* ϕ_2 of the 1000 conformations in both the history and archive file for each of the compounds. A table of ϕ_1 and ϕ_2 was constructed with the aid of the Decipher module in InsightII/*Discover*. To produce the graphs, the text file was then imported into a SigmaPlot file (SPSS, Inc., Chicago, IL).

2. Evaluation of the Conformers in Methanol. Each of the 1000 minimized structures were evaluated on the basis of energy and the number of NMR restraints met. Conformers of **CyanGXG**, **345-TMBENZ**, **4-FCIN**, **345-TCIN–X**, **345-TCIN** were further evaluated if their energy was within 5 kcal mol^{-1} of the global minimum and satisfied at least 9 of the 15, 18 of the 20, 16 of the 22, 9 of 10, and 12 of the 18 NMR-derived distance restraints, respectively. This analysis of **CyanGXG**, **345-TMBENZ**, **4-FCIN**, **345-TCIN–X**, and **345-TCIN**, yielded 715, 511, 404, 832, 689 structures, respectively. A table of six dihedral angles ϕ_1–ϕ_6 (refer to Fig. 11) and the total energy was constructed in the Decipher module of InisightII/*Discover* package (as detailed above) for each of the anthocyanins investigated.

3. Classification System. The structures of **CyanGXG**, **345-TMBENZ**, **4-FCIN**, **345-TCIN–X**, and **345-TCIN** from the above analysis were inspected for

their overall folding preferences. The coordinates of each particular conformation were read in from the QMD archive file for each of the compounds studied. In order to perform this classification, the molecule was orientated on the screen such that the galactose residue (**β-Gal** in Fig. 3) was directed away from the viewer and the acyl moiety (Ring **D** in Fig. 3) was below the flavylium nucleus (Rings **A**, **B**, and **C** in Fig. 3). If the flavylium nucleus was oriented such that the nucleus reads **"ACB"**, the conformer in question was classified as "non-flipped" structure (**N** was used in the code that follows the compound name, for example **345-TCIN–XN**). Conversely, if the flavylium nucleus read **"BCA"** that was classified as a "flipped" structure (**F** was used in the code that follows the compound name, for example **345-TCIN–XF**). The next aspect of the "shape" of the minimized structures considered was the alignment of the O-6 position of the **β-Gal** that is glycosylated with **β-Glc**. If the **β-Glc** moiety was forced to be positioned to either the left or the right or underneath the flavylium nucleus, the next letter of the compound code was **L**, **R**, and **U**, respectively, for example **345-TCIN–XNR**. Lastly, the relationship of the acyl moiety **D** to the flavylium nucleus was noted. For example, if the acyl ring **D** was under the naphthyl portion of the ring (**A–C**), or the 3,4-dihydroxyphenyl moiety (ring **B**), or not proximal to any of the units of the flavylium nucleus, the last letters of the code were **A–C**, **B**, or **D**, respectively. When this initial classification was performed for **345-TCIN–X** and **345-TCIN**, the **β-Glc** came up-and-over the flavylium nucleus. If this occurred

in any particular conformation, the term **OP** was added to the code, for example **345-TCIN–XNUACOP**. In the case of the nonacylated anthocyanin **CyanGXG**, the position the β-Glc, with respect to the flavylium nucleus was considered, i.e., if the β-Glc moiety was underneath the A–C ring system in the "nonflipped" orientation, the code for that conformational family becomes **CyanGXGNUAC**.

For each anthocyanin studied, the code for each conformation, such as **345-TCIN–XNRAC** was entered into a spreadsheet using QuatroPro Corel Corporation, Orem, UT, on an IBM clone personal computer, which contained the following data: the total energy, the total number of NMR-derived restraints met, and the six measured dihedral angles ϕ_1–ϕ_6 (refer to Fig. 11).. In the case of each compound, conformations that had the same code were grouped together and then made into separate worksheets within the spreadsheet notebook. The families of conformations were then further sub-classified based on energy, RMS deviation values, and the values of the dihedral angles given in Tables 9–18. This treatment yielded 4, 3, 12, 11, and 10 families of **CyanGXG**, **345-TMBENZ**, **4-FCIN**, **345-TCIN–Xyl**, and **345-TCIN**, respectively. The RMS deviation value was calculated for the structures in each family and is an average of the pairwise deviations when each conformer was superimposed on one conformer of the family. This operation was performed by the construction of a separate archive file (Analysis module of InsightII/*Discover*) for each family using the existing QMD archive file. With the aid of the Get Molecule button under the Molecule

button in InsightII/*Discover*, all the conformations can be superimposed on the first one. Compiling the RMS data so generated allowed the RMS deviation value in the Tables to be determined. For the studies of the above compounds, a representative structure of each family was selected based on the lowest energy conformation, which met the greatest number of NMR-derived restraints.

4. Evaluation of the Conformers From the QMD Study in Water. Each of the 1000 conformers produced were evaluated solely on the basis of energy. The minimized structures were further evaluated as above without consideration of NMR-derived restraints. In the case of **4-FCIN** and **345-TCIN** this process yielded 641 and 724 structures, respectively. Utilizing the methods above, these were categorized into 7 and 8 distinct conformational families, respectively. (Refer to Tables 19–22).

G. Evaluation of Conformers with *Mol*ecular Computer *A*ided *D*esign (MOLCAD)[48-62]

Selected structures from the conformational families or the extensive molecular dynamics study were saved as .mol2 files in InsightII/*Discover* (and then imported onto an SGI O^2 that supports SYBYL (Tripos, Inc. St Louis, MO) modeling package. In the SYBYL program, the structures of interest were read

into the program. Prior to using the MOLCAD module,[63] the charges on the molecule were calculated using the Gastieger–Huckel method. Once the charges had been calculated, a Connolly surface was constructed in the MOLCAD module. Various surfaces could then be projected onto the Connolly surface that permit the viewer to visualize different properties of the molecule. If the molecular lipophilic potential (MLP) surface was selected, this mode depicted the regions of hydrophilicity (blue regions) and hydrophobicity (brown regions) of the molecule. If the molecular local curvature (MLC) surface is selected, areas that are convex and concave are shown. If molecular electrostatic potential (MEP) surface is selected, areas of high and low electron density can be observed.

H. Determination of Equilibrium Constants

These were performed in accordance with the protocol established by Brouillard and co-workers.[29]

V. CONCLUSIONS

Low-temperature ^{1}H NMR studies on anthocyanins **CyanGXG**, **4-FCIN**, **345-TMBENZ**, **345-TCIN–X**, and **345-TCIN** have shown that these compounds in acidified methanol-d_4 are highly flexible. Despite of their inherent flexibility, reasonable molecular models have been successfully generated using the QMD–NMR protocol (see Section III.D and III.E). Unlike the molecular modeling studies in methanol, the structures produced in water have not been validated by NMR-derived restraints at this time.

Prior modeling studies suggest that anthocyanins, which resemble the structure of the anthocyanins under investigation, result in a single predominant conformation.[3] However, utilizing the QMD–NMR protocol with a dielectric continuum of both water and methanol, several distinct conformational families of each anthocyanin are produced. Interestingly, irrespective of the acyl moiety attached to O-6 Glc terminus of the anthocyanin, the families for different anthocyanins possess the same consensus fold. A summary of the important structural features from the conformational families found in water follows:

1. The flavylium nucleus in structures of these conformational families can be read as "ACB" ("nonflipped") or "BCA" ("flipped"), when viewed from the same perspective.

2. In certain families, the exocyclic double bond interacts with the flavylium nucleus.
3. The acyl moiety on the O-6 Glc terminus of these anthocyanins can interact with either the A–C ring system or ring B of the flavylium nucleus.
4. In certain families, the β-Xyl moiety can position itself over the C-2 of the flavylium nucleus.
5. In the 3,4,5-trimethoxycinnamoylated anthocyanins, the methoxy groups are proximal to the C-2 of the flavylium nucleus.

Furthermore, by subjecting structures from select conformational families of **4-FCIN** and **345-TCIN** to a 5 ns molecular dynamics simulation in a dielectric continuum of water, which is approximates the medium used experimentally to determine the color stability data, the flexibility of these molecules can be gaged. As the forces of attraction in the stacking of these molecules are weak, interconversion between conformational families occurs—a "flipped" conformer (flavylium nucleus reads "BCA") can "flip" to a "nonflipped" (flavylium nucleus reads "ACB") conformer. However, this only occurs in conformational families of **4-FCIN**, and not **345-TCIN**.

In order to study the stereoelectronic factors that cause the anthocyanins

under investigation to have different color-stability profiles, the characteristics of the intermediates adopted from the motions of each molecule during the simulations were studied. These mimic the behavior of these molecules in acidic aqueous medium, and permit the micro-environment around C-2 to be probed using the molecular visualization technique MOLCAD.[63] By mapping the MLP property onto the surfaces of these intermediates, the hydrophilicity surrounding the strategic $C=O^+$ bond can be determined. This site in the more flexible **4-FCIN** was found to be more hydrophilic than in the relatively inflexible **345-TCIN**.

As a result of these studies on **4-FCIN** and **345-TCIN**, three methods to correlate the color stability of monocinnamoylated anthocyanins to structure are proposed:

1. The ratio of "flipped" to "nonflipped" conformers that result from the QMD, or the QMD–NMR protocol. For example, the ratio for **4-FCIN** and **345-TCIN** was 1:2 and 79:1, respectively, i.e., the greater the ratio the greater the color stability.

2. The conformational flexibility of the monocinnamoylated anthocyanins as revealed by extensive molecular dynamics simulations (5 ns) in a dielectric continuum of water. This

can be judged by studying a plot of ϕ_1 against time for the duration of the simulation.

3. The micro-environment surrounding the strategic $C=O^+$ bond in intermediates during the molecular dynamics simulation in a dielectric continuum of water, which can be determined by using the MLP property in the MOLCAD module. The more hydrophilic the pocket is, the more prone it is to the deleterious attack of a water molecule.

It has become clear from this work described herein, and in this laboratory[32-37] that anthocyanins of the general structure 6-O-(substituted cinnamoyl)-β-D-glucopyranosyl-(1→6)-β-D-galactopyranosyl-(1→O^3)-cyanidins (see Fig. 3) are more stable than their nonacylated counterparts due to the following key factors. Moreover, these factors can be used to explain the different color-stability profiles of the fifteen monocinnamoylated anthocyanins:

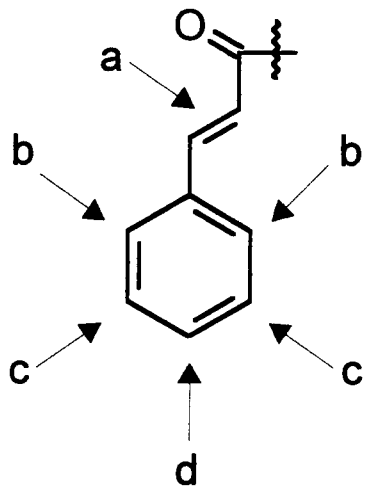
- The conformational flexibility of these compounds as revealed by molecular dynamics simulations in a dielectric continuum of water;
- The influence of substituents on the acyl moiety on the

electron richness of the aromatic system and the exocyclic double bond;

- The steric bulk of the substituents.

These factors and their points of origin are shown graphically in Fig. 51. Color stability of a monocinnamoylated anthocyanin correlates to the flexibility of the anthocyanin, which is judged by molecular dynamics simulations in a dielectric continuum of water, and physical inspection of the intermediates. Our studies suggest that if the powerfully electron-donating substituents are attached in either the *ortho*- or *para*-positions, the compounds are more color stable compounds. As a result, the electron-rich exocyclic double bond can form stronger interactions (π–arene) with parts of the flavylium nucleus and reduce the flexibility of the anthocyanin. Furthermore, the strategic positioning (2/6- or 3/5- position on the cinnamic acid residue) of a sterically demanding group on the cinnamoyl moiety, such as a methoxy further reduces the flexibility of the monocinammoylated anthocyanin.

If these *structure–activity relationships*, and hypotheses can be extended to other monocinnamoylated anthocyanins, rational design of a "super color-stable" monocinnamoylated anthocyanin could be achieved. The plan is described further in the next section.[1]



a. Electron density of exocyclic double bond
b. Bulky, electron-donating substituents
c. Electron-donating substituents
d. Electron-donating substituents

Fig. 51. Factors that impact color stability of cinnamoylated anthocyanins.

IV. FURTHER WORK

This section is an excerpt from a research proposal submitted to the USDA. It represents the strategy that will be employed by the author and co-workers to design a "super"color stable monocinanmoylated anthocyanin (citations refer to the bibliography that is found in "References" section):[67]

> "**General.**—The developments outlined in the Progress Report—advances in the biosynthesis, isolation, characterization, as well as insights in increasing color stability via substituent effects as determined by physicochemical studies and molecular modeling—when taken together, allow us to now launch a program, based on sound scientific principles, to design and carry out the biosynthesis of anthocyanins that will have enhanced color stability. Such an approach is reminiscent of that of *rational design,* which is the very basis for research in areas such as drug design, where *structure–activity relationships* (SAR) are developed among congeners or analogues in a orderly, predictable fashion to achieve a predetermined goal. Our systems allow us to incorporate a variety of carboxylic acids into acylated anthocyanin products. Our plan is to rely upon our modeling to guide us in

selecting candidates for tissue culture development, then proceed to validate the model with experimentally determined color stability measurements. Detailed color-stability studies will then be carried out on the best compounds. Our goal is to identify in this project period an acylated anthocyanin that is suitable for industrial production and development as a food colorant. Spinoffs from these studies may well benefit evaluation of other anthocyanin types that hold promise as useful products.

Plan of Research.—Our plan is to (a) evaluate seven of the compounds currently in hand via our NMR–molecular modeling approach in order to fully validate the methods we have developed. To date, two compounds, **345-TCIN** and **4-FCIN**, which represent respectively a relatively color-stable and a moderately color-unstable compound, have been subjected to the full QMD protocol in aqueous media. We will then (b) model a number of acylated candidate compounds, whose acyl groups will serve to probe critical stereoelectronic phenomena. Then (c) from the more promising modeled candidates, we will choose the best for synthesis, followed by in-depth color-stability studies. The final phase (d) will be to gather essential data to promote a candidate

or two for possible development as a food colorant. These steps are discussed in depth in the paragraphs that follow. Details of experimental protocol are presented under Research Methods.

a. Validation of our NMR–molecular modeling methods.—When the QMD protocol[37] was performed on **345-TCIN** and **4-FCIN** in a dielectric continuum of water (see Progress Report, p. 6, bottom) to most closely model natural conditions, we observed ratios of "flipped" to "non-flipped" conformers (for terminology, see Progress Report) for each that were quite divergent: 79:1 "flipped:nonflipped" for **345-TCIN** and 1:2 "flipped:nonflipped" for **4-FCIN.** We feel that the difference observed in these ratios is quite significant, as compounds **345-TCIN** and **4-FCIN**, while different in their K_h values, do not represent extremes in color stabilities; thus the ratios should be highly sensitive. These studies will be extended to [other monocinnamoylated]compounds **CyanGXG**, **5**, **13**, **14**, **17**, and **18** in a continuum of water. We expect to see a trend in the ratios that reflects experimentally measured color stability among these compounds. It is essential that 2D NMR studies in water are conducted alongside the modeling work to (a) provide assignments for all resonances in the

^{1}H NMR spectra and (b) to make use of NMR-derived restraints from the ROESY spectra to experimentally validate the models. Details are provided in the Research Methods section and in the manuscript[37] in Appendix B.

b. Molecular computer-aided design (MOLCAD) [see Section IV.E.5]

c. Lead optimization strategies.—Of the compounds examined in depth by both modeling and color stability measurements, the 3,4,5-trimethoxycinnamoyl derivative **345-TCIN** (see Progress Report) is selected as the lead compound on which to develop strategies for enhancement of color stability.[68]

It has become clear from the work performed in this laboratory[32-37] that anthocyanins of the general structure 6-*O*-(substituted cinnamoyl)-β-D-glucopyranosyl-(1→6)-β-D-galactopyranosyl-(1→O^3)-cyanidins (see Fig. 2) are more stable than their nonacylated counterparts due to the following key factors:

- The influence of substituents on the acyl moiety on the

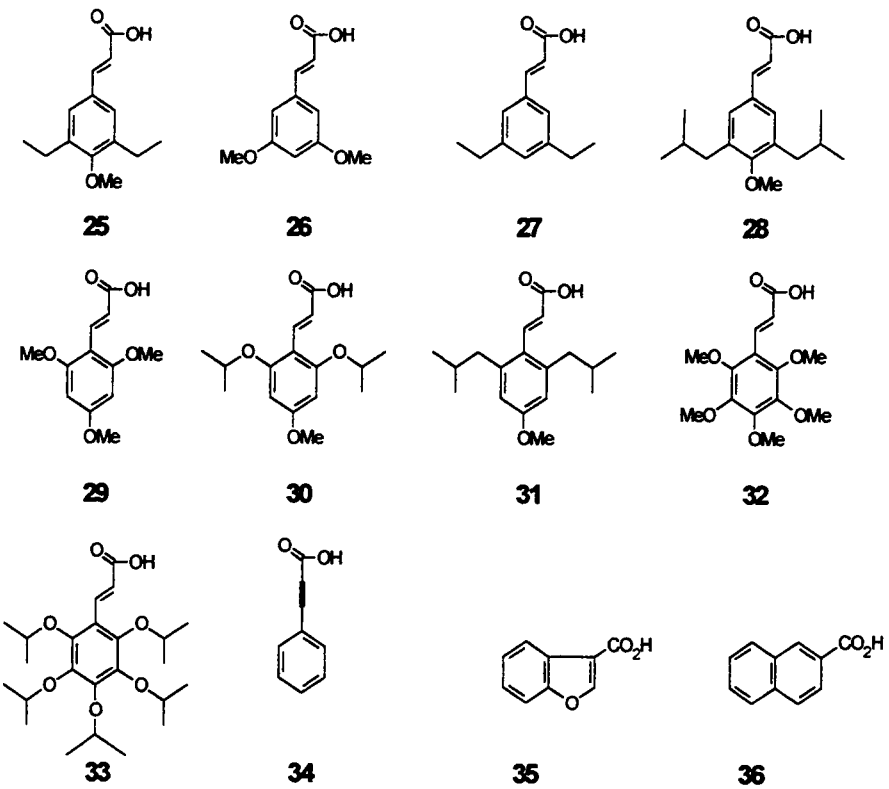
electron richness of the aromatic system and the exocyclic double bond;

- The steric bulk of the substituents;
- The conformational flexibility of these compounds as revealed by molecular dynamic simulations in a dielectric continuum of water.

These factors and their points of origin are shown graphically in [Fig. 51 in the Conclusions section of this document].

The strategy that we will use is outlined in the following list of eight steps. The strategy is designed to further explore the above factors that affect the color retention properties of cinnamoylated anthocyanins similar to **5–19**.[69] Furthermore, the protocols outlined permit the rational design of the next-generation of highly color-stable monoacylated anthocyanins:[70]

1. Construct molecular models of the twelve proposed compounds (refer to Fig. 52 for suggested acyl groups) using QMD in a dielectric continuum of water. Choose candidate compounds that show maximum ratios of



Compound **25** can be synthesized from an aldehyde precursor;[71] compounds **26**, **34**, and **36** are commercially available;[72] compound **27** is accessible via the aldehyde;[73] compound **28** can be prepared in an analogous manner to the synthesis of 3,5-diisopropyl-4hydroxycinnamaldehyde;[71] compound **29** is commercially available;[74] compound **30** can be readily synthesized from 2,6-dihydroxy-4-methoxybenzaldehyde;[75] compound **31** can be prepared in analogous manner to the 2,6-dimethyl derivative;[76] compound **32** and **33** can be prepared from the same aldehyde;[77] the synthesis of compound **35** (3-bezofurancarboxylic acid) is well known.[78]

Fig. 52. Carboxylic acids to be used in the rational design of a "super" color stable monoacylated anthocyanin.

2. "flipped":"nonflipped" families of conformers. Use MOLCAD[55,57,61,62] to examine the environment around the reactive $C=O^+$.

3. Purchase or synthesize requisite substituted carboxylic acids that have been identified by molecular modeling as the acids that will lead to monoacylated anthocyanins that behave similarly to **345-TCIN**. See [Fig. 52] for structures of a plausible set of carboxylic acids.

4. After the best candidates have been identified using modeling methods, begin preliminary small-scale tissue-culture studies to determine optimum conditions for production of the anthocyanin.

5. Do scaled-up tissue cultures for the isolation of mg-amounts of anthocyanin. Isolate, purify, and assess purity of the product by HPLC.

6. With the compound in hand perform characterization studies, i.e., NMR and ROESY experiments, as well as mass spectrometry.

7. Measure the color stabilities of the novel anthocyanins using pH-jump experiments.[29]

8. Correlate the color stability data to both the ratio of "flipped":"nonflipped" families of conformations found in step 1, above.

9. Subject the most promising candidates to long-term evaluation of their color stabilities at 25 °C.

Modeling targeted acylated anthocyanins. The strategy in this investigation is to model a variety of anthocyanins monoacylated with substituted cinnamoyl groups and related carboxylic acid groups and determine what acyl moieties give rise to compounds that indicate protection from attack by water at C-2. Using this information, one can then proceed with selecting a smaller group of compounds for biosynthesis. This approach will be less time consuming, as producing a new anthocyanin itself is very labor intensive, and many of these new, proposed anthocyanins will require synthesis of the carboxylic acids, most of which are not

commercially available. The carboxylic acids chosen will be selected from those in [Fig. 52]; however, as our studies progress, we undoubtedly will need to consider other acids.

In order to optimize the color stability in our proposed set of anthocyanins, we must fully assess the stereoelectronic effects that are operative in the substituted cinnamoyl esters. It is important to factor out steric from electronic effects at key positions on the benzene ring of the acyl moiety [(see Fig. 51)]. Molecular models of anthocyanins acylated with **25–28** [(see Fig. 52)] will be constructed, and the compounds will be examined by the QMD protocols. Ethyl groups, which are isosteric with MeO and are not significantly electron donating, are proposed to probe the question of which is the more important effect—steric or electronic. Compound **28** permits further exploration of this complex issue by increasing steric bulk at the 3- and 5-positions.

Analysis of the of the experimentally derived color stabilities for the monomethoxy-substituted compounds **11–13** indicate that a MeO group in the 2-position is the most color stable of the group, comparing favorably with the 3,4,5-trimethoxy-substituted

compound **345-TCIN** (see data in Table 1, Appendix A). Thus a single MeO group at C-2 functions extraordinarily well, apparently shielding the $C=O^+$ attack site in addition to contributing to increased electron density in the acyl moiety. Thus anthocyanins that result from the cinnamic acids **29–31** will allow this effect to be investigated. Additionally, strongly electron-donating substituents at both the *ortho* and *para* positions of these compounds will increase the electron density of the exocyclic double bond, which is essential in their color stability.

As we currently understand the phenomena associated with color stability, anthocyanins acylated with highly sterically hindered and powerfully electron-donating groups such as those derived from carboxylic acids **32** and **33** should yield the most color-stable monocinnamoylated anthocyanin generated to date.

Compound **34** will be examined to determine whether such a rigid, linear acetylenic system can orient itself to interact with the flavylium nucleus. Compounds **35** and **36** are proposed to model interactions of larger aromatic systems which may π-bond over a larger area with the flavylium moiety. Other polycyclic aromatics could also be considered.

Carboxylic acid synthesis. The carboxylic acids **26–33** are all substituted cinnamic acids, for which general synthetic procedures are well known to the organic chemist. For example, most cinnamic acids are synthesized from the aromatic aldehyde by condensation with the appropriate aldol-type reagents via the well-known Claisen, Knoevenagel, or Perkin condensations.[79,80] We anticipate minimal problems in producing a variety of the acids needed for this project, e.g., those listed in [Fig. 52]. References for preparation or purchase of these acids are provided in [Fig. 52]."

REFERENCES AND NOTES

LIST OF REFERENCES AND FOOTNOTES

1. Excerpts are from a research proposal submitted to the USDA that was based on the work of Neil A. Whittemore.

2. Willstätter, R.; Everest, A. E. Unterschungen über die Anthocyane; I. Über den Farbstoff der Kornblume. *Justus Liebigs Ann. Chem.* **1913**, *401*, 189–232.

3. Goto, T.; Kondo, T. Structure and Molecular Staking of Anthocyanins–Flower Color Variation. *Angew. Chem., Int. Ed. Engl.* **1991**, *30*, 17–33, and references therein.

4. Andersen, Ø.; Opheim, S.; Aksnes, D. W.; Frøstein, N. A. Structure of Petanin, an Acylated Anthocyanin Isolated from *Solanum tuberosum*, using Homo- and Hetero-nuclear Two-dimensional Nuclear Magnetic Resonance Techniques. *Phytochem. Anal.* **1991**, *2*, 230–236.

5. Shibata, K.; Shibata, Y.; Kasiwagi, I. Studies in Anthocyanins: Color Variation in Anthocyanins. *J. Am. Chem. Soc.* **1919**, *41*, 208–220.

6. Kondo, T.; Ueda, M.; Isobe, M.; Goto, T. A New Molecular Mechanism of Blue Color Development with Protocyanin, a Supramolecular Pigment from Cornflower, *Centaurea cyanus*. *Tetrahedron Lett.* **1998**, *39*, 8307–8310.

7. Brouillard, R. In *The Flavonoids*; Harborne, J. B., Ed.; Chapman and Hall: London, 1988, pp 525–538.

8. Brouillard, R. Chemical structure of anthocyanins. In *Anthocyanins as Food Colors*; Markakis, P., Ed.; Academic Press: New York, 1982, pp 1–40.

9. Francis, F. J. Food Colorants: Anthocyanins. *CRC Crit. Rev. Food Sci. Nutr.* **1989**, *28*, 273–314.

10. Mazza, G.; Miniati, E. *Anthocyanins in Fruits, Vegetables, and Grains*; CRC Press: Boca Raton, FL, 1993.

11. Goto, T.; Kondo, T.; Tamura, H.; Imagawa, H.; Iino, A.; Takeda, K. Structure of Gentiodelphin, an Acylated Anthocyanin Isolated from *Gentiana makinoi,* that is Stable in Aqueous Solution. *Tetrahedron Lett.* **1982**, *23*, 3695–3698.

12. Idaka, E.; Yamakita, H.; Ogawa, T.; Kondo, T.; Yamamoto, M.; Goto, T. Structure of Three Diacylated Anthocyanins Isolated from Red Cabbage, *Brassica oleracea*. *Chem. Lett.* **1987**, 1213–1216.

13. Kondo, T.; Yamashiki, J.; Kawahori, K.; Goto, T. Structure of Lobelinin A and B, Novel Anthocyanins Acylated with Three and Four Different Organic Acids, Respectively. *Tetrahedron Lett.* **1989**, *30*, 6055–6058.

14. Kondo, T.; Ueda, M.; Goto, T. Structure of Ternatin B1, a Pentaacylated Anthocyanin Substituted on the B-Ring Asymmetrically with Two Long Chains. *Tetrahedron Lett.* **1990**, *46*, 4749–4756.

15. Terahara, N.; Saito, N.; Honda, T.; Toki, K.; Osajimas, Y. Acylated Anthocyanins of *Clitoria ternatea* Flowers and their Acyl Moieties. *Phytochemistry* **1990**, *29*, 949–953.

16. Terahara, N.; Saito, N.; Honda, T.; Toki, K.; Osajimas, Y. Structure of Ternatin A1, the Largest Ternatin in the Major Blue Anthocyanins from *Clitoria ternatia* Flowers. *Tetrahedron Lett.* **1990**, *31*, 2921–2924.

17. Yoshida, K.; Kondo, T.; Goto, T. Unusually Stable Monoacylated Anthocyanin from Purple Yam, *Dioscorea alata*. *Tetrahedron Lett.* **1991**, *32*, 5579–5580.

18. Yoshida, K.; Kondo, T.; Kameda, K.; Kawakishi, S.; Lubag, A. J. M.; Mendoza, E. M. T.; Goto, T. Structures of Alatanin A, B and C Isolated from Edible Purple Yam, *Dioscorea alata*. *Tetrahedron Lett.* **1991**, *32*, 5575–5578.

19. Lu, T. S.; Saito, N.; Yokoi, M.; Shigihara, A.; Honda, T. Acylated Pelargonidin Glycosides in the Red-Purple Flowers of *Pharbitis nil*. *Phytochemistry* **1992**, *31*, 289–295.

20. Lu, T. S.; Saito, N.; Yokoi, M.; Shigihara, A.; Honda, T. Acylated Peonidin Glycosides in the Violet-Blue Cultivars of *Pharbitis nil*. *Phytochemistry* **1992**, *31*, 659–663.

21. Gläßgen, W. E.; Wray, V.; Strack, D.; Metzger, J. W.; Seitz, H. U. Anthocyanins from Cell Suspension Cultures of *Daucus carota*. *Phytochemistry* **1992**, *31*, 1593–1602.

22. Gläßgen, W. E.; Hofmann, R.; Emmerling, M.; Neumann, G. D.; Seitz, H. U. Structure Elucidation of Saccharides in Anthocyanins and Flavanols by Means of Methylation Analysis and Gas Chromatography. *J. Chromatogr.* **1992**, *598*, 81–87.

23. Gläßgen, W. E.; Seitz, H. U.; Metzger, J. W. High-Performance Liquid Chromatography/Electrospray Mass Spectrometry and Tandem Mass Spectrometry of Anthocyanins from Plant Tissues and Cell Cultures of *Daucus carota* L. *Biol. Mass Spectrom.* **1992**, *21*, 271–277.

24. Idaka, E.; Suzuki, K.; Yamakita, H.; Ogawa, T.; Kondo, T.; Goto, T. Structure of Monoacylated Anthocyanins Isolated from Red Cabbage, *Brassica oleracea*. *Chem. Lett.* **1987**, 145–148.

25. Johansen, O.-P.; Andersen, Ø. M.; Nerdal, W.; Aksnes, D. W. Cyanidin 3-[6-(*p*-coumaroyl)-2-xylosyl-glucoside]-5-glucoside and Other Anthocyanins from Fruits of *Sambucus canadensis*. *Phytochemistry* **1991**, *30*, 4137–4141.

26. Lu, T. S.; Saito, N.; Yokoi, M.; Shigihara, A.; Honda, T. An Acylated Peonidin Glycoside in the Violet-blue Flowers of *Pharbitis nil*. *Phytochemistry* **1991**, *30*, 2387–2390.

27. Odake, K.; Terahara, N.; Saito, N.; Toki, K.; Honda, T. Chemical Structures of Two Anthocyanins from Purple Sweet Potato, *Ipomea batatas*. *Phytochemistry* **1992**, *31*, 2127–2130.

28. Saito, N.; Lu, T. S.; Yokoi, M.; Shigihara, A.; Honda, T. An Acylated Cyanidin 3-Sophoroside-5-glucoside in the Violet-Blue Flowers of *Phabitis nil*. *Phytochemistry* **1993**, *33*, 245–247.

29. Dangles, O.; Saito, N.; Brouillard, R. Kinetic and Thermodynamic Control of Flavylium Hydration in the Pelargonidin–Cinnamic Acid Complexation. Origin of the Extraordinary Flower Color Diversity of *Pharbitis nil*. *J. Am. Chem. Soc.* **1993**, *115*, 3125–3132.

30. Dangles, O.; Saito, N.; Brouillard, R. Anthocyanin Intramolecular Copigment Effect. *Phytochemistry* **1993**, *34*, 119–124.

31. Yoshida, K.; Kondo, T.; Goto, T. Intramolecular Stacking Conformation of Gentiodelphin, a Diacylated Anthocyanin from *Gentiana makinoi*. *Tetrahedron* **1992**, *48*, 4313–4326.

32. Baker, D. C.; Dougall, D. K.; Gläßgen, W. E.; Johnson, S. C.; Metzger, J. W.; Rose, A.; Seitz, H. U. Effects of supplied cinnamic acids and biosynthetic intermediates on the anthocyanins accumulated by wild carrot suspension cultures. *Plant Cell, Tissue Organ Cult.* **1994**, *39*, 79–91.

33. Dougall, D. K.; Baker, D. C.; Gakh, E.; Redus, M. Biosynthesis and Stability of Monoacylated Anthocyanins. *Food Technol.* **1997**, *51*, 69–71.

34. Dougall, D. K.; Baker, D. C.; Gakh, E. G.; Redus, M. A.; Whittemore, N. A. Anthocyanins from wild carrot suspension cultures acylated with supplied carboxylic acids. *Carbohydr. Res.* **1998**, *310*, 177–189.

35. Gakh, E. G.; Dougall, D. K.; Baker, D. C. ^{1}H NMR Studies of Monoacylated Anthocyanins From the Wild Carrot: Part 1. Inter- and Intramolecular Interactions in Solution. *Phytochem. Anal.* **1998**, *9*, 28–34.

36. Redus, M. A.; Baker, D. C.; Dougall, D. K. Constants for the Dehydration and Deprotonation Reactions of Some Monoacylated and Glycosylated Cyanidin Derivatives. *J. Agric. Food Chem.* **1998**, submitted.

37. Whittemore, N. A.; Cox, J. R.; Dougall, D. K.; Baker, D. C. The Conformational Flexibility of a Monoacylated Anthocyanins in Methanol Revealed by Quenched Molecular Dynamics and NMR Spectroscopy. *Carbohydr. Res.* **1999**, manuscript in preparation.

38. Burgess, K.; Lim, D.; Mousa, S. A. Synthesis and Solution Conformation of Cyclo[RGDRGD]: A Cyclic Peptide with Selectivity for the V 3 Receptor. *J. Med. Chem.* **1996**, *39*, 4520–4526.

39. Lim, D.; Burgess, K. Spirocyclic Peptidomimetics Featuring 2,3-Methanoamino Acids. *J. Am. Chem. Soc.* **1997**, *119*, 9632–9640.

40. Cutts, R. J.; Howlin, B. J.; Mulholland, F.; Webb, G. A. Low-Energy Conformations of Delicious Peptide, a Food Flavor. Study by Quenched Molecular Dynamics and NMR. *J. Agric. Food Chem.* **1996**, *44*, 1409–1415.

41. Al-Obeidi, F.; O'Connor, S. D.; Job, C.; Hruby, V. J.; Pettitt, B. M. NMR and quenched molecular dynamics studies of superpotent linear and cyclic α-melanotropins. *J. Peptide Res.* **1998**, *51*, 420–431.

42. Whittemore, N. A.; Cox, J. R.; Baker, D. C.; Dougall, D. K.; Gakh, E. **1998**, unpublished results.

43. Nerdal, W.; Anderson, Ø. M. Evidence for Self-association of the Anthocyanin Petanin in Acidified, Methanolic Solution using Two-Dimensional Nuclear Overhauser Enhancement NMR Experiments and Distance Geometry Calculations. *Phytochem. Anal.* **1991**, *2*, 263–270.

44. Hoshino, T. An Approximate Estimate of Self-association Constants and the Self-stacking Conformation of Malvin Quinonoidal Bases Studied by ^{1}H NMR. *Phytochemistry* **1991**, *30*, 2049–2055.

45. Nerdal, W.; Anderson, Ø. M. Intermolecular Aromatic Acid Association of an Anthocyanin (Petanin) Evidenced by Two-Dimensional Nuclear Overhauser Enhancement of Nuclear Magnetic Resonance Experiments and Distance Geometry Calculations. *Phytochem. Anal.* **1992**, *3*, 182–189.

46. Dauber-Osguthorpe, P.; Roberts, V. A.; Osguthorpe, D. J.; Wolff, J.; Genest, M.; Hagler, A. T. Structure and Energetics of Ligand Binding to Proteins: *Escherichia coli* Dihydrofolate Reductase–Trimethoprim, a Drug–Receptor System. *Proteins: Struct., Funct. Genet.* **1988**, *4*, 31–47.

47. Nishio, M.; Hirota, M.; Umezawa, Y. *The CH/π Interaction: Evidence, Nature, and Consequences*; Wiley-VCH: New York, 1998.

48. Brickmann, J.; Bertling, H.; Bussian, B. M.; Goetze, T.; Knoblauch, M.; Waldherr-Teschner, M. MOLCAD - interactive molecular computer graphics on high-performance computers. *Tagungsber. - Vortragstag., Ges. Dtsch. Chem., Fachgruppe Chem.-Inf.* **1987**, *3rd*, 93–111.

49. Brickmann, J.; Waldherr-Teschner, M.; Demuth, R. Molecular models from the personal computer. *Prax. Naturwiss., Chem.* **1987**, *36*, 25–27.

50. Knoblauch, M.; Waldherr-Teschner, M. MOLCAD—new development of molecular modeling software for superworkstations. In *Software-Entwickl. Chem. 3, Proc. Workshops "Comput. Chem."*, 3rd ed., Springer: Berlin, Germany, 1989; 357–361.

51. Lichtenthaler, F. W.; Immel, S.; Kreis, U. Evolution of the structural representation of sucrose [1]. *Starch/Staerke* **1991**, *43*, 121–132.

52. Lichtenthaler, F. W.; Immel, S.; Kreis, U. Old roots-new branches: evolution of the structural representation of sucrose. *Carbohydr. Org. Raw Mater., Dev. Workshop*, 1991; VCH, Weinheim, Fed, 1991; 1–32.

53. Pang, L.; Lucken, E. A. C.; Weber, J.; Bernardinelli, G. Structural investigations and modeling of cavities in clathrates. *J. Comput.-Aided Mol. Des.* **1991**, *5*, 285–291.

54. Kielkiewicz, J.; Brickmann, J. Calixarenes - cyclic calyciform aromatic hydrocarbons and the potential uses of computer graphics in their study. *Polimery (Warsaw)* **1992**, *37*, 251–6.

55. Lichtenthaler, F. W.; Immel, S. Sucrose, sucralose and fructose: correlations between hydrophobicity potential profiles and AH-B-X assignments. In *Sweet-Taste Chemorecept., [Minisymp.]*, 1993; Elsevier, London, UK, 1993; 21–53, 8 plates.

56. Lichtenthaler, F. W.; Immel, S. Molecular modeling of saccharides. Part 4. Cyclodextrins, cyclomannins, and cyclogalactins with five and six (1 → 4)-linked sugar units: a comparative assessment of their conformations and hydrophobicity potential profiles. *Tetrahedron: Asymmetry* **1994**, *5*, 2045–2060.

57. Brickmann, J.; Goetze, T.; Heiden, W.; Moeckel, G.; Reiling, S.; Vollhardt, H.; Zachmann, C.-D. Interactive visualization of molecular scenarios with MOLCAD/SYBYL. In *Data Visualization Mol. Sci.*, 1995; Addison-Wesley, Reading, Mass, 1995; 83–97.

58. Lichtenthaler, F. W.; Immel, S. Molecular modeling of saccharides. Part 14. The lipophilicity patterns of cyclodextrins and of non-glucose cyclic oligosaccharides. *J. Inclusion Phenom. Mol. Recognit. Chem.* **1996**, *25*, 3–16.

59. Lichtenthaler, F. W.; Immel, S. Molecular modeling of saccharides. 11. Towards understanding formation and stability of cyclodextrin inclusion complexes: computation and visualization of their molecular lipophilicity patterns. *Starch/Staerke* **1996**, *48*, 145–154.

60. Hinds, T. A.; Drake, R. R.; Compadre, C. M. Analysis of the binding modes of substrates and inhibitors of the herpes simplex virus type I thymidine kinase (HSV-I TK) using 3D QSAR and molecular surface properties. In *Abstracts of Papers*, 213th National Meeting of the American Chemical Society, San Francisco, April 13–17; American Chemical Society, Washington, DC, 1997; MEDI 264.

61. Hinds, T. A.; Drake, R. R.; Hurlburt, B. K.; Compadre, C. M. Computational strategy to design drug specific Herpes Simplex Virus type I thymidine kinases for gene therapies. In *Abstracts of Papers*, 216th National Meeting of the American Chemical Society, Boston, August 23–27; American Chemical Society, Washington, DC, 1998; COMP 031.

62. Brard, F.; Petit, S.; Coquerel, G.; Gilbert, D.; Koutouzov, S.; Perez, G.; Tron, F. Modeling of anti-nucleosome immunoglobulin Fv domains: analysis of electrostatic interactions. *Mol. Immunol.* **1998**, *34*, 793–807.

63. *SYBYL Graphics Manual*; 6.4 ed.; Tripos Associates, Inc.: St. Louis, MO, 1997.

64. Bürgi, H. B.; Dunitz, J. D.; Schefter, E. J. Geometrical reaction coordinates. II. Nucleophilic addition to a carbonyl group. *J. Am. Chem. Soc.* **1973**, *95*, 5065–5067.

65. Dougall, D. K.; Vogelien, D. L. Anthocyanin Yields of Clonal Wild Carrot Cell Cultures: Effects of Serial Cloning Plus Selection for High or Low Yield. *Plant Cell, Tissue Organ Cult.* **1990**, *23*, 79–91.

66. Hwang, T.-L.; Shaka, A. J. Cross relaxation without TOCSY: transverse rotating-frame Overhauser effect spectroscopy. *J. Am. Chem. Soc.* **1992**, *114*, 3157–3159.

67. The codes used in this excerpt are consistent with the codes used throughout the dissertation and not in the original research proposal.

68. Compound **7** was selected as the lead rather than **5**, because the cinnamic acids that bear a 4-OMe could be more readily synthesized or procured than 4-OH species. The difference in the color stability of **10** and **11** suggests that there is a negligible difference between the two substituents (see Table 1, Appendix A).

69. It is noted that the 6-*O*-cinnamoylated anthocyanins are in general more stable that other acylated compounds so far examined.

70. This strategy parallels the approach of the pharmaceutical industry to identify viable drug candidates.

71. Nurfina, A. N.; Reksohadiprodjo, M. S.; Timmerman, H.; Jenie, U. A.; Sugiyanto, D.; Van Der Goot, H. Synthesis of some symmetrical curcumin derivatives and their antiinflammatory activity. *Eur. J. Med. Chem.* **1997**, *32*, 321–328.

72. Aldrich cat. # D13,400-7; P3,120-5 and 18,024-6, respectively.

73. Platzer, N.; Ronzani, N.; Lang, C.; Lange, C. Conformational study of anticholinesterase carbamates in the furylbenzene series by proton and carbon-13 NMR spectroscopy. *Org. Magn. Reson.* **1982**, *18*, 14–19.

74. Pfaltz and Bauer, Inc cat # T26140.

75. Gia, O.; Anselmo, A.; Conconi, M. T.; Antonello, C.; Uriarte, E.; Caffieri, S. 4'-Methyl Derivatives of 5-MOP and 5-MOA: Synthesis, Photoreactivity, and Photobiological Activity. *J. Med. Chem.* **1996**, *39*, 4489–4496.

76. Qian, X.; Russell, K. C.; Boteju, L. W.; Hruby, V. J. Stereoselective total synthesis of topographically constrained designer amino acids: 2',6'-dimethyl-β-methyltyrosines. *Tetrahedron* **1995**, *51*, 1033–1054.

77. Brossi, A.; Sharma, P. N.; Takahashi, K.; Chiang, J. F.; Karle, I. L.; Seibert, G. Tetramethoprim and pentamethoprim: synthesis, antibacterial properties and x-ray structures. *Helv. Chim. Acta* **1983**, *66*, 795–800.

78. Buttery, C. D.; Knight, D. W.; Nott, A. P. The generation and synthetic utility of dianions derived from benzofurancarboxylic acids. *J. Chem. Soc., Perkin Trans. 1* **1984**, 2839–2843.

79. Norman, R. O. C. *Principles of Organic Synthesis*, 2nd ed.; Chapman and Hall: London, 1978, pp 231–237.

80. Gross, H.; Bischoff, C.; Höft, E.; Gründemann, E. *Preparative Organic Chemistry*, Hilgetag, G.; Martini, A., Eds.; Wiley: London, 1972.

PART TWO:

DESIGN AND SYNTHESIS OF ELECTROACTIVE OLIGODEOXYNUCLEOTIDES. PROBES FOR NUCLEIC ACID HYBRIDIZATION

I. INTRODUCTION

A. Nucleic Acids[1-3]

1. General. The information presented in this section on nucleic acids is an overview of a huge field, which recently has become a partnership between biology and chemistry. Contributors to the elucidation of the structure of both deoxyribonucleic acid and ribonucleic acid are too numerous to mention in this section (for a detailed account of the early studies, and modern developments, refer to Reference 1).

2. Structure of Deoxyribonucleic Acid (DNA). Each piece of single-stranded or double-stranded DNA (ss-DNA and ds-DNA, respectively) is a linear array of monomers called nucleotides. These "building blocks" are monophosphate esters of nucleosides and are components of both DNA and RNA. A nucleotide is constructed from three residues: a nucleobase, a pentose sugar, and a phosphate residue. In Fig.1 the major bases are shown. There are two distinct families: the monocyclic structures (pyrimidines) or fused-ring structures (purine). The major purine bases are adenine (A) and guanine (G), and the major pyrimidine bases are cytosine (C), thymine (T), and uracil (U)—uracil is only found in RNA. The nucleosides that afford the nucleotides

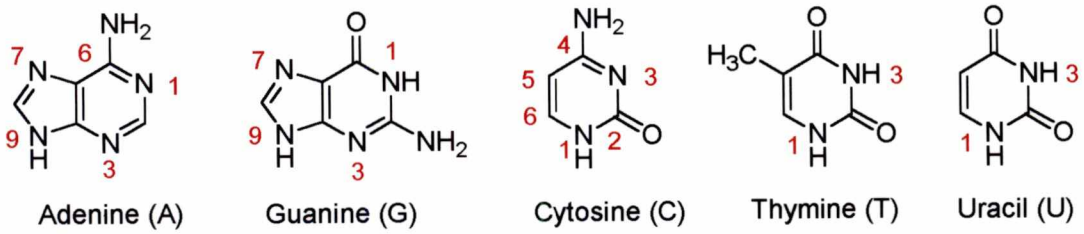


Fig. 1. Structures of the five major bases in nucleic acids.

found in DNA are shown in Fig. 2. Unlike RNA, DNA has a backbone that is comprised of 2′-deoxynucleosides. The meteoric explosion of the field only occurred in the 1970s when reasonable amounts of DNA could be synthesized.

3. Synthesis of DNA. Since the pioneering work of Khorana to synthesize oligomers of deoxyribonucleic acid (DNA) that led to the eventual synthesis of an entire gene,[4] massive developments have resulted in facile preparation of oligodeoxynucleotides (ODNs). The two main methods that are routinely used in laboratories throughout the world are (1) the polymerase chain reaction (PCR)[5-7] and (2) the phosphoramidite solid-phase synthesis methodology.[8]

a. Polymerase chain reaction (PCR).[5,6,9] The polymerase chain reaction (PCR) allows DNA from a selected region of a genome to be amplified by more than a millionfold, provided that the sequences on either side of the section of interest are known. Since many purified DNA polymerases from *Thermus aquaticus*, which have resistance to high temperatures, and synthetic DNA ODN primers[10] are now commercially available, there has been an explosion in the use of this technique to prepare DNA. Furthermore, this method has made it possible to clone specific DNA sequences rapidly without the need of the living cell. It is this characteristic that has led the PCR technique to be an essential tool in modern forensics.

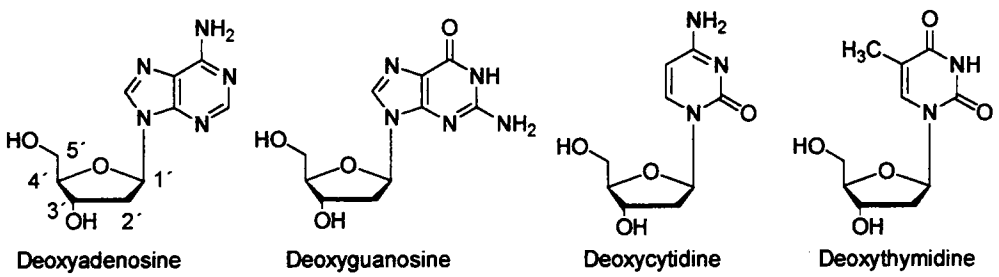


Fig. 2. Structures of the four 2′-deoxynucleosides.

Portions of the sequence that surround the region to be amplified are used to design two synthetic DNA ODNs (A and B), each complementary to the ends of the DNA double-helix. These ODNs serve as primers for in vitro DNA synthesis, which is catalyzed by the DNA polymerase, and determine the ends of the final DNA fragment that is obtained.

Each cycle of the reaction requires a high temperature (95 °C) to separate the two strands of the DNA double-helix (step 1). Subsequent cooling (37–65 °C) of the DNA in the presence of a large excess of the two primers affords the annealed mixture. The specific primers are annealed to their complementary sequences on opposite strands of the target DNA, with their 3′-ends pointing toward each other (step 2). This is exploited by incubating with DNA polymerase and the four 2′-deoxyribonucleotide triphosphates so that the regions of DNA adjacent to the primers are selectively synthesized (step 3). In this cycle, each strand of the target DNA sequence is copied once to give a twofold amplification. The newly synthesized strand contains a binding site for the primer used for copying the *other* strand. A second round of denaturation, annealing, and primer extension results in a fourfold amplification.

For effective DNA amplification, 20–30 cycles of the reaction mixture are required, which results in the production of 2^{20-30} copies of the original target DNA. Each cycle lasts only approximately five minutes, compared to the standard cloning procedures that require several days. By modifying the

nucleotides there is a means to obtain modified single-strands of the section of interest.

b. Phoshphoramidite methodology.[8,1] The strategy closely parallels the innovative synthetic methodology used to produce peptides, which was developed by Merrifield.[11-13]

The essence of the solid-phase synthesis (SPS) of oligodeoxynucleotides (ODNs) is that a building block is heterogeneously coupled to another residue bound to an insoluble support. Highly efficient coupling is achieved by the use of large excesses of soluble building blocks. As the support is insoluble in the reaction medium, the excess of reagents can easily be removed by copious wash cycles. The entire series of steps has been automated, and ODNs are routinely prepared on automated synthesizers.

The 2′-deoxynucleoside that will be the 3′-terminus of the growing ODN is attached by means of a linker arm to a solid support. In Fig. 3, the coupling of a 2′-deoxynucleoside to derivatized controlled pore glass beads (CPG) is shown. Growth of the desired ODN sequence is built from the 3′-to-5′-terminus. The building blocks that are routinely used are phoshporamidites.

In Fig. 4, the processes involved in the preparation of ODNs using phosphoramidite methodology are shown. The removal of the 5′-*O*-(4,4'-dimethoxytrityl) moiety (DMT) of the supported nucleoside is readily effected by treatment of the surface-modified beads with either dichloroacetic acid or

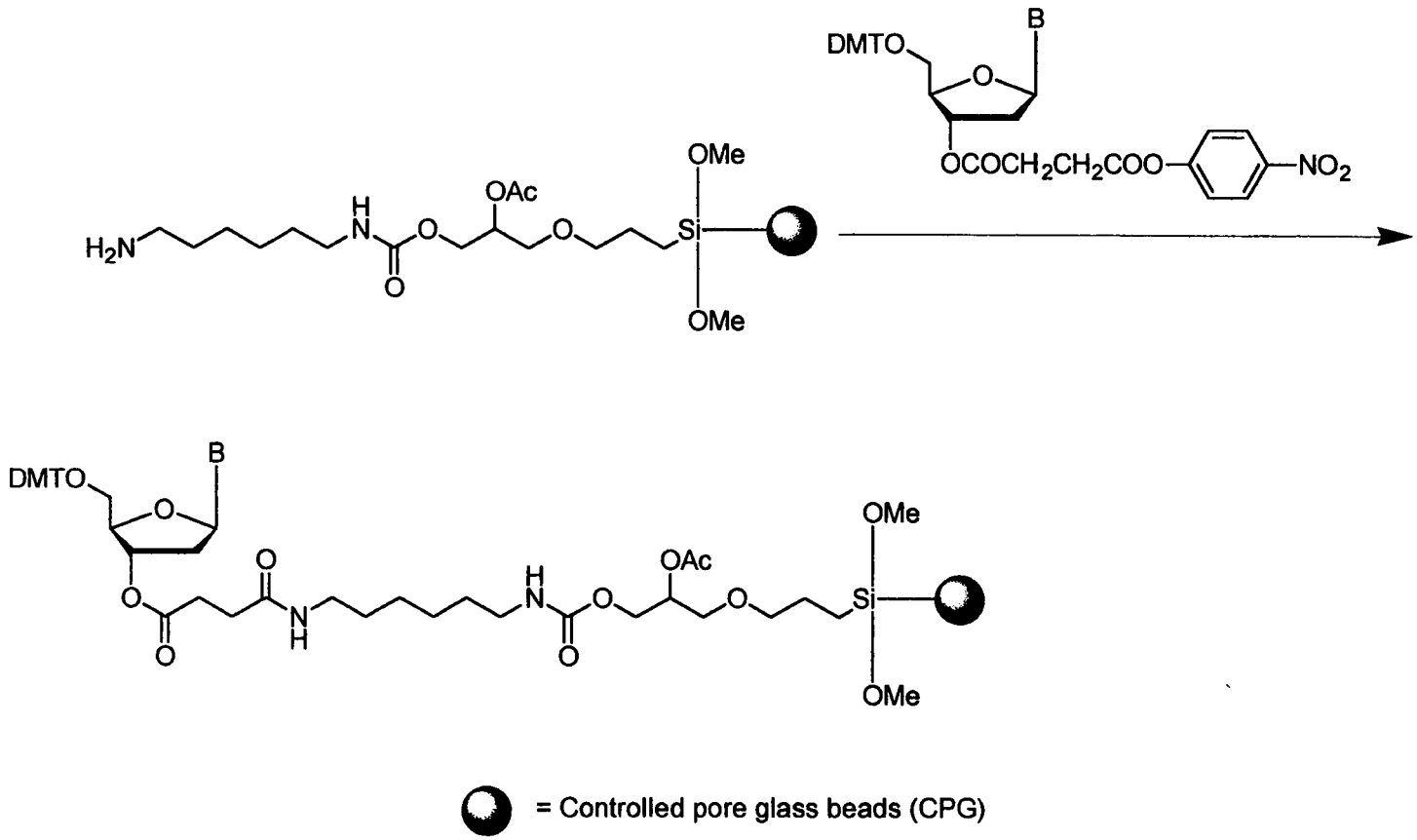


Fig. 3. Attachment of a 2′-deoxyribonucleotide to CPG.

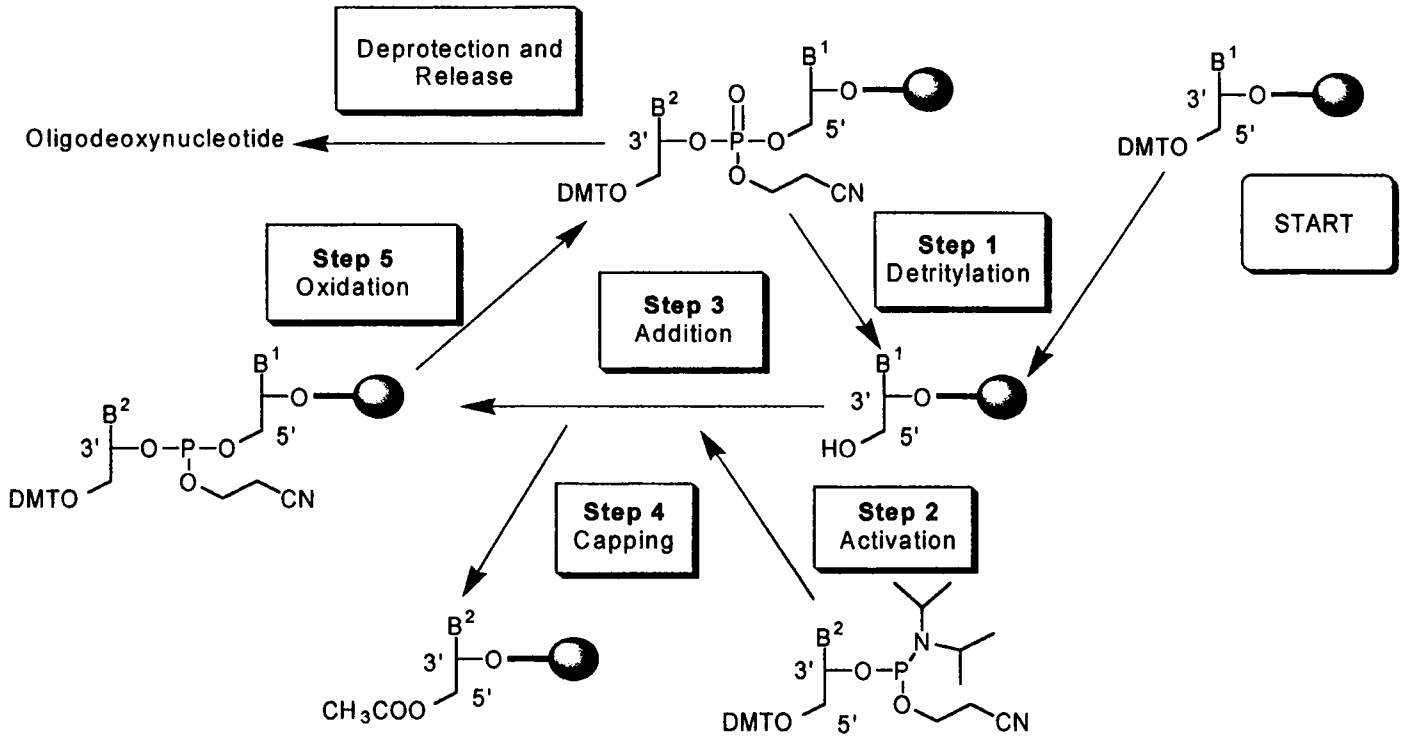


Fig. 4. Schematic of the solid-phase synthesis of oligodeoxynucleotides by the phosphoramidite method.

trichloroacetic acid (TCA) (step 1). Activation of the phosphoramidite building block readily occurs when it is mixed with tetrazole in acetonitrile solution (step 2). The activated compound adds readily to the growing ODN chain (step 3). In the previous coupling step, there may be some chains that failed to react. Capping these chains results in a limited number of failure sequences, i.e., those chains missing an internal residue. This is accomplished by the treatment of the support with acetic anhydride and *N*-methylimidazole (step 4). The phosphotriester functionality in the growing ODN is readily achieved by the oxidation of the phosphite with iodine and water (step 5). The hydrogen iodide produced in this step is then neutralized with either pyridine or 2,6-lutidine. A 20-mer is produced by repeating steps 1–5 a further 18 times. Concomitant removal of protection groups and cleavage from the solid support is readily achieved by reacting the CPG beads in concentrated (concd) ammonia for 5 h at 50 °C. The end-result can also be accomplished by treating the beads with concd ammonia at room temperature for approximately 24 h.

4. Nucleic Acid Hybridization.[14] Hybridization of nucleic acids occurs when two complementary strands "pair" with one another. This event occurs because of the hydrogen bonding between the bases along the backbone of different strands of DNA. These interactions that were first identified by Watson and Crick and are shown in Fig. 5 in red. Base A is complementary with T, and

the base C is complementary with G. These and other more complex interactions cause the duplex formed to adopt the immediately recognized helical structure of DNA.

On hybridization of two complementary sequences, a small quantity of energy is released via the formation of each hydrogen bond and the stacking of each nucleobase. The total of this energy determines the stability of the double helix (duplex). There is only a slight variation in energy between the deoxyribo- and ribo-duplexes; thus, most experiments can be conducted with either, despite the fact that deoxyribo-duplexes are less stable. However, since ODNs are relatively easy to prepare, oligomeric DNA probes are preferred.

B. Probes for Nucleic Acid Hybridization[2]

1. General. There has been much work recently into the various methods of detecting nucleic acid hybridization using DNA probes.[15,14] Current gene probe assay techniques are labor intensive and time consuming, taking anything from several hours to days to complete. The major time-consuming step is most frequently the hybridization detection step.

If there is an ODN with complementary antiparallel nucleotide sequence, this ODN binds specifically to single-stranded nucleic acids to form a double helix. Therefore, biological processes involving these nucleic acids can be

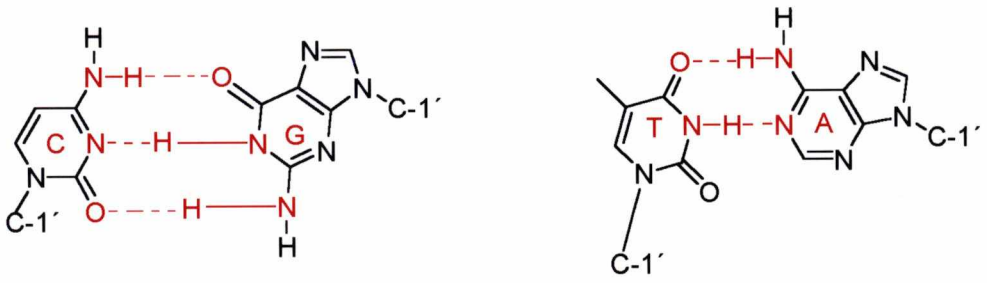


Fig. 5. Watson-Crick base-pairing for C:G (left) and T:A (right).

modulated by addition of the respective ODNs. The effects of these ODNs and the fields of potential application can be broadened by the introduction of chemically modified bases. For example, replacement of one of the phosphate groups on an ODN would result in a loss of negative charge, thereby increasing its lipophilicity. Also, an ODN carrying a reactive group can modify its binding partner.

DNA in the helical form is considered unreactive in the living cell. However, single-stranded RNA and DNA (ss-RNA and ss-DNA) are relatively reactive; for instance, DNA is replicated and transcribed, and mRNA is used as a template in the biosynthesis of proteins. Therefore, ODNs of complementary and antiparallel sequence can bind to these single-strands, thus forming a double helix via Watson–Crick base pairing (see Fig. 5). This type of binding can find two different applications:

1. An ODN labeled in some way can provide detection of the complementary sequence in solution. This complementary sequence can either be localized in an extract, a cell, or a tissue. Therefore, labeled ODNs can be used for the identification of specific sequences.
2. The ODNs can also be used for inhibition. This can be thought of as the single-strand being suppressed, as the

single-strand region is converted into the arrested form of the double-helix.

These two factors can find interest in the detection and localization of a messenger RNA or its gene. This is commonly referred to as antisense technology and has recently been the subject of a review.[16] The first antisense ODN, Vitravene™ (fomivirsen sodium injectable) to be approved for marketing in the US by the Federal Drug Administration (FDA) (September 16, 1998),[17] is excellent in the treatment of cytomegalovirus (CMV) retinitis in acquired immune deficiency syndrome (AIDS) patients.[18] Apart from the treatment of diseases, a suitably designed ODN (probe) can be used to detect specific bacterial or viral sequences in biological specimens. Detection normally occurs through the use of a reporter group attached to the probe ODN.

There are several types of labels for DNA probes used in the detection of the hybridization step. The most common label is a radioisotope,[14] although several nonradioactive labels have recently been explored.[15,19] These tend to be preferred to the radioactive labels for reasons of safety and convenience. Such nonradioactive labels include fluorescent agents[20-23,15] enzymatic agents,[14] and, more recently, electroactive agents.[24]

2. Methods of Labeling and Detection. (For a detailed discussion of the functionalization of ODNs via phosphoramidites, see the review by Beaucage and Iyer.[25])

a. Radioactive labels.[15,14] Radioactive labels are direct labels, where the radioactivity incorporated into the probe molecules may be directly detected. Although nonradioactive labels may be preferable, radioactive labels are still considered as the "gold standard" of probes because of their sensitivity to detection. The most common technique to label ODNs is the enzymatic incorporation of the radioisotopes ^{32}P or ^{35}S at the 5′-end of the phosphodiester.

The choice of labeling method is dictated by the nature of the probe. Uniform labeling of double-stranded DNA probes may be accomplished by nick translation,[26] random priming, and by PCR with one or more radioactive 2′-deoxynucleotide triphosphates. Single-stranded DNA probes may be prepared by primer extension from a single-stranded DNA template, by run-off polymerization, or by asymmetric PCR using *thermus aquaticus* (Taq) polymerase.

Double-stranded DNA may be labeled at the 3′-end via replacement synthesis using T4 DNA polymerase. The 3′-end of oligodeoxynucleotides and double-stranded DNA also may be labeled using a terminal transferase by addition of one or more radioactive nucleotides. The 5′-hydroxyl on an ODN, or on a DNA after treatment with alkaline phosphatase, may be phosphorylated

using gamma ^{32}P-labeled ATP and T4 polynucleotide kinase. Simultaneous application of probes labeled with different radioisotopes is unusual, but has recently been used to compare two-dimensional restriction enzyme fingerprint patterns of DNA from two strains of *Escherichia coli*.[15]

b. Nonradioactive labels. The importance of discovering alternatives to radioactive labels is best summarized by this quote from Kessler in his nonradioactive labeling and detection methods:[19]

> "During the last two decades the use of nonradioactive markers instead of radioisotopes has gained increasing importance in bioanalysis. Major disadvantages of isotope use, such as rapid decay, radiation exposure, the need of specific isotope facilities, and the elimination of radioactive waste by trained personnel, have been overcome by the development of nonradioactive labeling and detection techniques. In contrast to radioisotopes, the nonradioactive modification groups are characterized by long-term stability, general, rapid, but also easy-to-handle modification procedures, by the existence of highly sensitive detection systems, and by the avoidance of hazardous materials."

(i) Fluorescent reporter groups—The use of fluorescent ODN probes is well established and the basis of commercial DNA analyzers. Reviews of the older literature on this topic are available,[15,27] and a summary of recent attempts to improve detection of the hybridization event was given by Thiel et al.,[28] who used surface plasmon resonance imaging to differentiate between ss- and ds-DNA.

In simple cases the modified ODN is substituted with a colored, chemiluminescent, or fluorescent marker. Suitable substituents include fluorescein, isoluminol, and rhodamine compounds. The linkage of a dye to the ODN can be accomplished in a variety of ways: for example, via the 3′-*O*-phosphate.[15]

Ability to directly attach different fluorescent dyes to different probe molecules allows the simultaneous detection of hybridization and/or biosynthetic products involving more than one probe. Based on differential hybridization of mismatched and perfectly matched primers, a competitive PCR color complementation test is available to detect human mutations and polymorphism.

Many fluorescent dyes are commercially available as fluorimetric reporter groups attached to avidin, or streptavidin, or attached to primary or secondary antibodies.

(ii) Enzyme-linked ODNs—Enzyme-linked ODN probes can be used for the recognition of an RNA or DNA sequence with high sensitivity comparable to

that of radioactively labeled compounds.[15] The enzyme is designed to multiply a signal, such as the production of a colored or fluorescent compound.

The enzyme can be linked to the ODN directly, or, alternatively, the enzyme can be linked to any agent that immediately binds in situ to the enzyme. In the first instance an enzyme and an ODN might be linked through a bifunctional reagent, or by UV irradiation: normally, a spacer of about 30 atoms in length is used. (An example of this type of probe is described in the next section.) After the hybridization event, the alkaline phosphatase (ALP)-catalyzed degradation of *p*-nitrophenyl phosphate to *p*-nitrophenol allows colorimetric detection of the target phage sequence.

Alternatively, ALP can initiate the formation of 5-bromo-4-chloroindolyl phosphate and nitroblue tetrazolium, also assayed colorimetrically.[15] This enzyme can also cleave 4-methylumbelliferone phosphate, which leads to a fluorescent adduct.

The enzyme need not be linked directly to the ODN. Instead, the ODN can be coupled to any agent that binds in situ to the enzyme. This antibody variation of the system requires that the ODN carries an antigenic substituent such as digoxigenin, 5-bromo-2′-deoxyuridine, or fluorescein.

An antibody linked to the enzyme then binds to the antigenic group, and the enzyme generates a signal. The most widely used of these assays is the biotin–(strept)avidin system.

(iii) The ODN–biotin–avidin–XXX system—Biotin-linked ODNs in solutions, extracts, or tissue specimens form very tight and specific aggregates of the biotin group and the protein avidin or streptavidin.[15] Avidin can be easily coupled to further agents suitable for recognition, such as ALP. In this instance a chromogen is converted into a chromophore or visa versa.

The linking of biotin to an ODN can be facilitated chemically or enzymatically, usually through a spacer of about 10 atoms.[15] In the simple case, biotin and the ODN are linked unspecifically through a bifunctional reagent.

Most of the coupling procedures form specific linkages so that the number of biotin residues per ODN is known. In most cases, a nucleotide derivative already substituted with all or part of the spacer is used in conjunction with an automated ODN synthesis. The ODN is biotinylated after the synthesis is complete.

Suitable nucleotide derivatives are 8-substituted adenosine and 5-substituted 2′-deoxyuridine.[20,21] Furthermore, biotinylation can use a terminal phosphate group or a terminal hydroxyl group for attachment.[20,21] Finally, biotinylation of ODNs also can be accomplished by adding a biotin-carrying nucleotide using an appropriate polymerase.

The synthesis of many biotinylated ODNs,[20,21] has promoted their use in nucleic acid recognition assays. Under optimal assay conditions, these assays are sensitive enough to detect one nucleobase exchange in a target sequence.

(iv) Electrochemical methods—An alternative property to those routinely used with ODNs is the development of techniques for the detection of hybridization that utilize the redox behavior of certain electroactive compounds.[29]

A modified electrode surface incorporating an electroactive probe would have many attractive features common to modern electroanalytical techniques. These include in situ analysis of small volumes and possibly no requirement for washing of excess reactants from the surface reaction layer. Ideally, a surface-attached ODN with an attached electroactive group would mimic natural DNA, which gives well-defined faradaic signals for ss-DNA and not ds-DNA.[30-32] An ideal tag for this purpose would give a persistent signal, preferably electrochemically reversible, in a potential region well removed from where natural DNA and RNA are electroactive, such that the signal could be easily interrogated in a sensor configuration. ODNs with attached electroactive groups or tags have been reported on by several groups.[33-37] These applications have involved chromatographic separation of the ss- and ds-DNAs with electrochemical detection of the tag, although Xu and Bard used electrochemical luminescence to detect ds-DNA with an end-tethered $Ru(bpy)_3^{2+}$ group.[38]

The above strategy can be contrasted to other electrochemical means to detect ds-DNA that have appeared in recent years, many of which involve the use of electroactive intercalators that selectively bind to double-helix structures. Most of these methods require the addition of a solution species, the intercalator,

to perform the analysis. Thus hybridization can be detected by the preconcentration or binding of the intercalator to a surface-confined DNA molecule, which leads to an increase in the signal. Transition metal complexes, which bind to DNA to give electroactive complexes,[39-41] have been used in this manner,[40,42-45] as have a variety of other species including a Hoechst dye,[46] ethidium, [47] methylene blue,[48] daunomycin,[49] and aromatic amines.[50] Other electrochemical approaches involve the enhancement of the electrocatalytic current for oxidation of ds-DNA by intercalating redox couples,[51-54] use of the $Fe(CN)_6^{3-/4-}$ couple as a permeability marker,[55] and an attenuation of the poly(pyrrole) doping process by a tethered ODN in the double helix form.[56]

II. STATEMENT OF THE PROBLEM

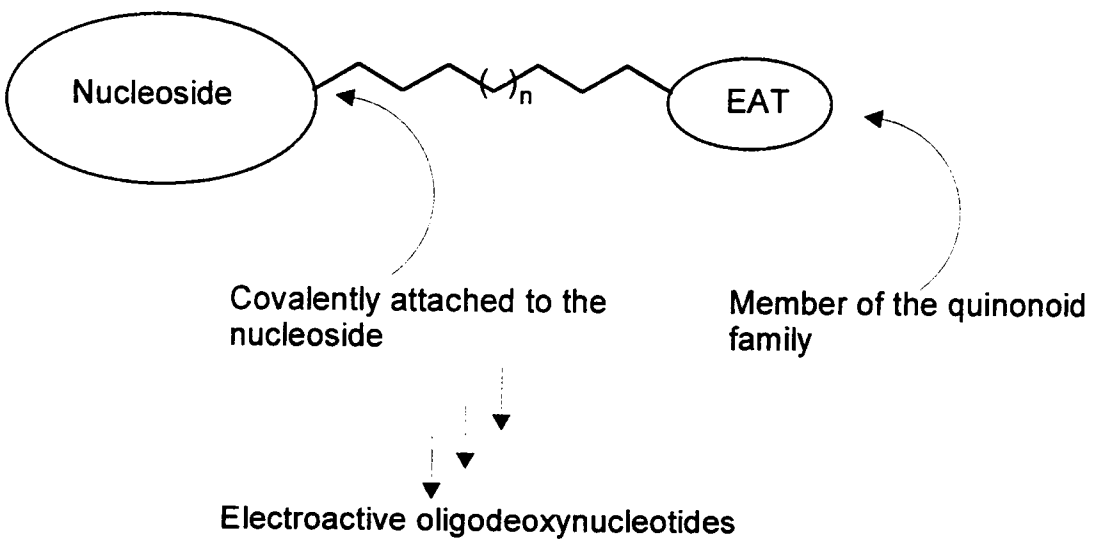
Since the discovery and widespread use of radioactively labeled oligodeoxynucleotides (ODNs), considerable effort has been expended to find alternatives that are cheaper and not as hazardous as their radioactive predecessors.[22] Probes tagged with UV or fluorescently active groups have typically been employed.[15] The objective of this study was to design and synthesize labeled nucleosides that bear an electrochemically active group, which can be used in the preparation of ODN oligomers, and assess their usefulness as a probe of nucleic acid hybridization (see Fig. 6).

Critical to their use as probes for nucleic acid hybridization is that the characteristic signal, albeit an electrochemical or fluorescence signal, should be markedly different in double-stranded DNA (ds-DNA) compared to the single-stranded DNA (ss-DNA), and be persistent. Additionally, the signal should not overlap with any signals that result from DNA itself. Thus, the judicious selection of an electroactive reporter group that possesses these properties is critical in the success of a probe.

Molecules in the quinonoid family give a persistent, electrochemically reversible quinone/hydroquinone couple in aqueous solutions.[57] An added advantage is that the electrochemical reversibility occurs in a potential region distinct from where natural RNA and DNA are electroactive. This would permit

the interrogation of ODNs bearing these electroactive reporter groups in a sensor configuration.[24]

Thus single or multiple incorporation of a suitable quinone–monomer bioconjugate into an ODN via either the phosphoramidite methodology or polymerase chain reaction (PCR) technology—utilizing the 5′-triphosphate of the conjugate—would provide entry into a series of electroactive ODNs, which can be used as possible probes to detect nucleic acid hybridization.



EAT = Electroactive tag

Fig. 6. Strategy to synthesize electroactive oligodeoxynucleotides.

III. RESULTS AND DISCUSSION

A. Overall Strategy

The key strategy underpinning this work is outlined in Fig. 6. Essential to the synthesis of electroactive ODNs is the preparation of suitable precursors that have the desired electroactive reporter group covalently attached to the nucleoside. Through the design of this electroactive conjugate, the electroactive ODNs could be secured via either standard phosphoramidite or PCR methodology (for further details on the synthesis of DNA utilizing these methods, see section I.A.3). The point of attachment of these tags can be either to the nucleobase[58] or to the glycone. However, it is imperative that the attachment of the electroactive tag (EAT) does not dramatically affect the hybridization of the ODN with its complementary strand on the surface of a working electrode.[59] Failure of these ODNs to hybridize would render them unacceptable as probes for nucleic acid hybridization.

B. Synthesis of C-8 Modified 2′-Deoxyadenosine (First-generation Electroactive Bioconjugates)

1. Review of the Literature. In addition to the use of these modified C-8 purine nucleosides (for numbering of the purine ring system, refer to Fig. 2) as building blocks to create ODNs that have been used as probes for nucleic acid hybridization,[60,20,61,23] these compounds have been used to design antisense ODNs[62] and ODNs that do not possess the adenine base at a certain position in the sequence, i.e., DNA with abasic sites.[63,64] These modified nucleosides were all obtained by treating 8-bromo-2′-deoxyadenosine[65] with a variety of nucleophiles.

Reaction of this 8-bromo-2′-deoxyadenosine[65] with[65] thiols results in the covalent attachment of a linker arm to the C-8 position. Pieles and co-workers[62] successfully attached a thiol tether indirectly via 8-mercapto-2′-deoxyadenosine[66] and used this intermediate to build a psoralen adduct located in an ODN, which upon hybridization and irradiation, formed a sequence-specific cross-link to a target sequence. Two groups have attached thiol linker arms directly to the C-8 position of 2′-deoxyadenosine using the common intermediate of 8-bromo-2′-deoxyadenosine.[60,63,64] Roduit and co-workers treated 8-bromo-2′-deoxyadenosine with an acylated ω-aminothiol.[60] Synthesis of the phosphoramidite of this modified nucleoside was then used in the preparation of

ODNs. A standard deprotection with concd ammonia of the resultant ODN then unveiled the terminal amino moiety, appended to the C-8 position, and permitted facile conjugation with commonly used reporter groups, such as biotin.

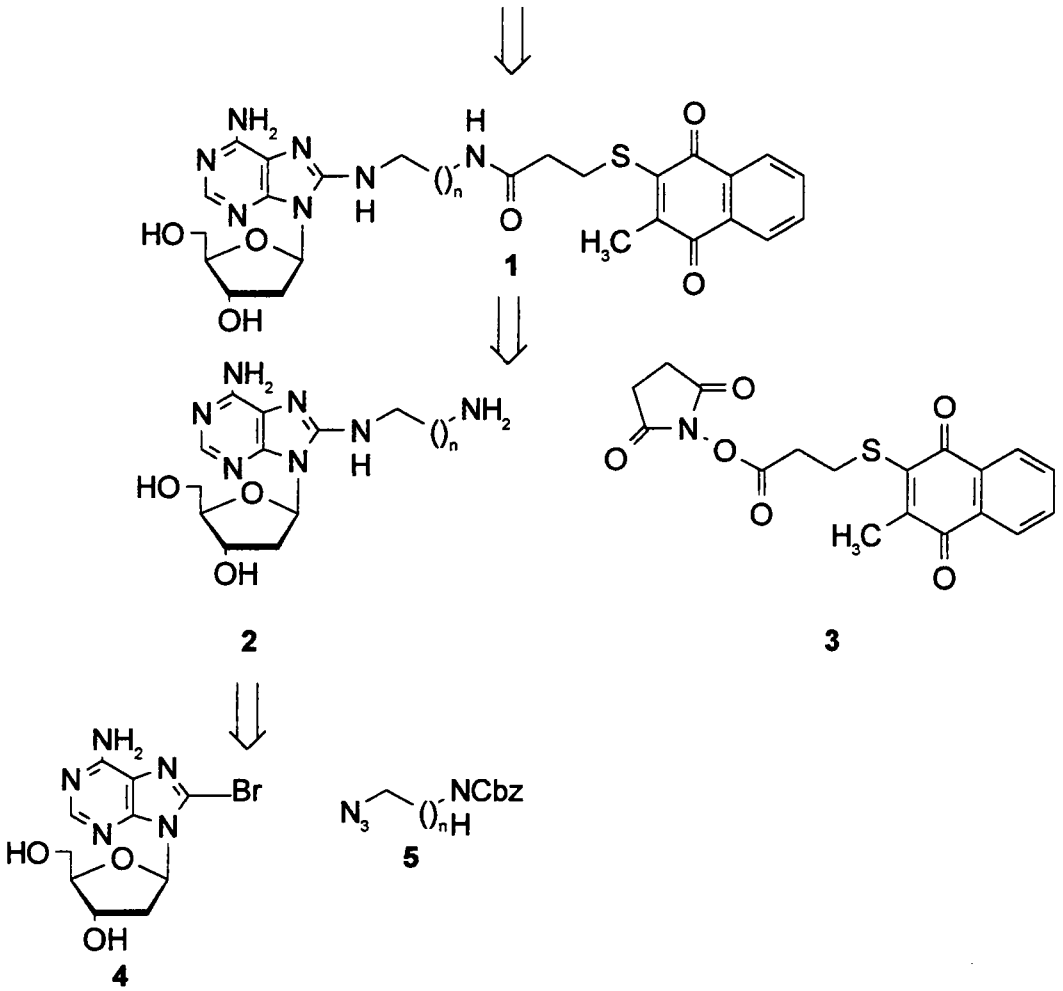
Direct treatment of 8-bromo-2′-deoxyadenosine with 1-propanethiol resulted in a modified nucleoside that was used to incorporate an abasic site into an ODN.[63,64] An abasic site is defined as a nucleotide moiety that does not possess a nucleobase, but the glycone moiety remains intact. Since hydrolytic cleavage of adenine was greatly accelerated by the C-8 substitution of an electron-withdrawing moiety,[64] oxidation with potassium persulfate (oxone) of the thiol modified ODN afforded the strongly electron-withdrawing sulfoxide moiety. Thus an abasic site was introduced into the ODN by selective hydrolytic cleavage of the thiol modified adenine base.[63]

Aliphatic amino tethers have been attached to the C-8 position of adenine. Displacement of the 8-Br group was readily effected by treatment of this invaluable precursor with diamines.[20,61,23] Coupling of the amino moiety at the terminus of these linker arms to a variety of fluorescent reporter groups, such as dansyl[23] and fluorescein,[20] yielded probes for nucleic acid hybridization. However, even though these fluorescent groups attached via a linker arm to the C-8 position of 2′-deoxyadenosine may have electrochemical signatures, no research group has exploited this characteristic of these common fluorescent labels.

Since 2′-deoxyadenosine has been modified in the C-8 position in a number of ways, it was selected as a suitable nucleoside that would allow entry into electroactive ODNs that bear quinone moieties. Thus the retrosynthetic analysis shown in Scheme 1 was devised to achieve this goal.

2. Retrosynthetic Analysis. The key to the synthesis of naphthoquinone–2′-deoxyadenosine conjugate **1** was the procurement of a C-8 modified nucleoside **2**. Compounds such as **2** have been prepared by others by heating 8-bromo-2′-deoxyadenosine (**4**) with the appropriate diamine in ethanol under reflux.[20,23] However, in our hands, attempts to prepare the hexamethylamino derivative **2** (where n = 5) with 1,6-diaminohexane failed to yield the desired compound. An alternative to this route relied on securing a monoprotected "masked" diamine compound **5**—the azido moiety acts as a "masked" amino functionality.[67] Orthogonal protection of a diamine is achieved indirectly by protecting the amino group of any ω-aminoalcohol with the benzyloxycarbonyl (Cbz) group and converting the hydroxyl moiety to a "masked" amine via the mesylate. The Cbz protecting group was selected for two reasons: (1) the azido functionality can be reduced to the amine without affecting the integrity of the Cbz group, and (2) the removal of the Cbz group of the terminal amino moiety of the tether can be readily achieved without affecting the purine ring system.[68] With **2** in hand, the naphthoquinone conjugate could be readily

Electroactive oligodeoxynucleotides

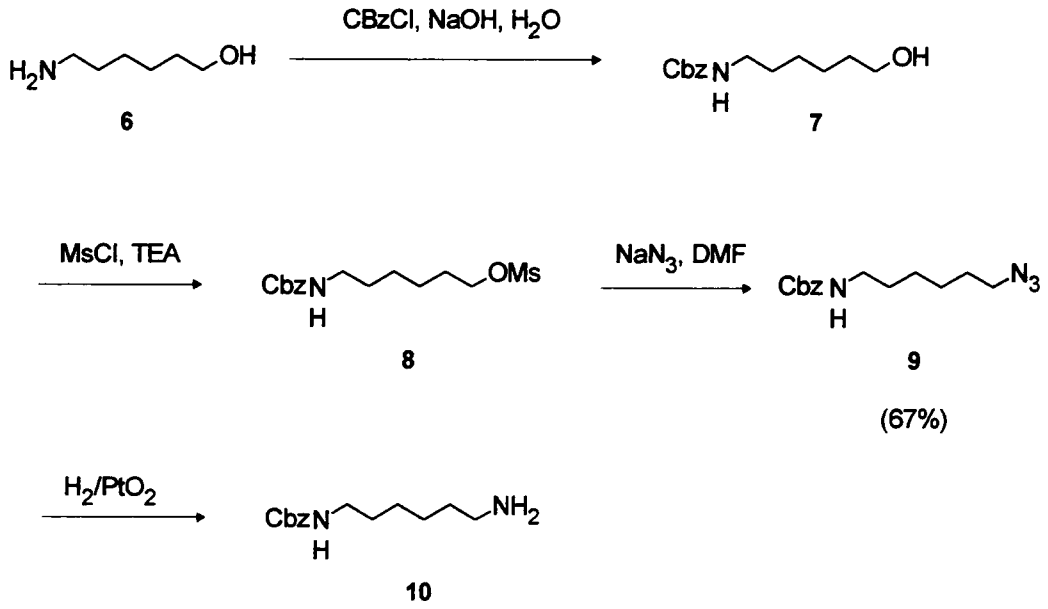


Scheme 1. Retrosynthetic analysis of the synthesis of electroactive bioconjugates.

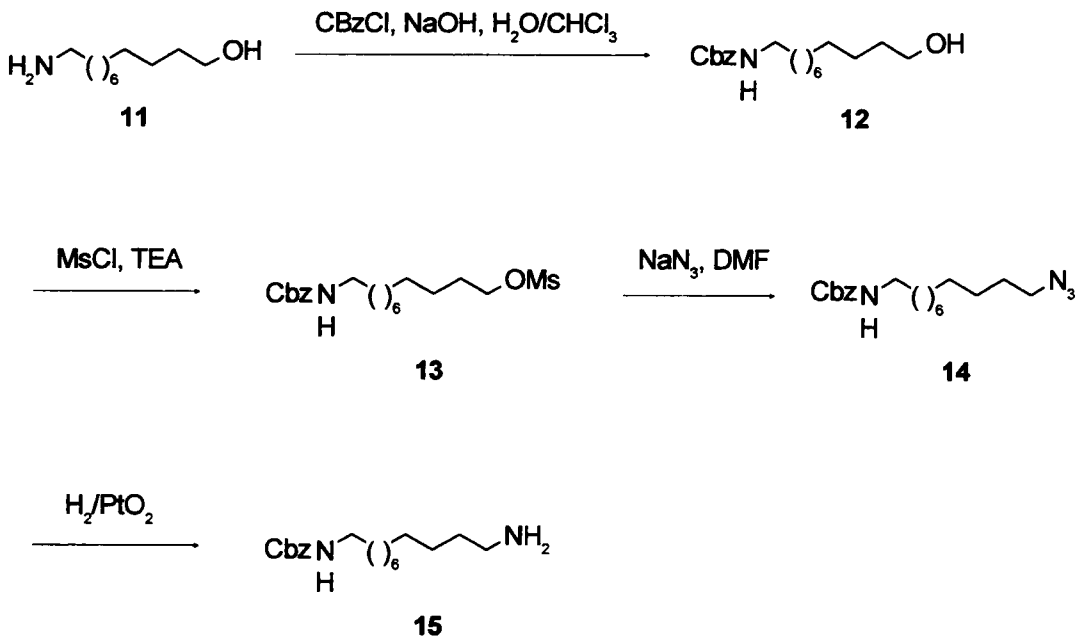
prepared using the *S*-(2-methyl-1,4-naphthoquinonyl-3)-β-mercaptopropionic acid *N*-Hydroxysuccinimide (NHS) ester, which has been used by Rokita to form [2+2] cycloadducts between this naphthoquinone moiety at the 5′-terminus of an ODN and thymine bases in a complementary ODN.[69] If the conjugate **1** could be secured, electroactive ODNs can be prepared using either PCR or phosphoramidite methodology. Additionally, studying the electrochemical signature of the monomer **1** would be an excellent model that would allow the development of techniques that would permit the studying electroactive ODNs in general.

3. Preparation of Monoprotected Diamines. The strategies involved in securing the hexylamino and undecylamino "masked" monoprotected diamines are shown in Schemes 2 and 3, respectively. Monoprotection of difunctional, symmetrical compounds is notoriously difficult to carry out without the formation of the bis-adduct and a subsequent loss of yield.[70] Atwell and Denny, and Ponpipom and Rupprecht have prepared compound **15** from 1,6-diaminohexane and benzyl chloroformate (CbzCl) in total yields of 34%[71] and 35%,[72] respectively—both research groups prepared the hydrochloride salt. To date, there have been no reports of the preparation of the C_{11} analog.

The 1-aminohexan-6-ol (**6**) is commercially available; however, **11** had to be prepared from 11-aminoundecanoic acid. Reduction of the carboxylic acid



Scheme 2. Synthesis of monoprotected diamine **10**.



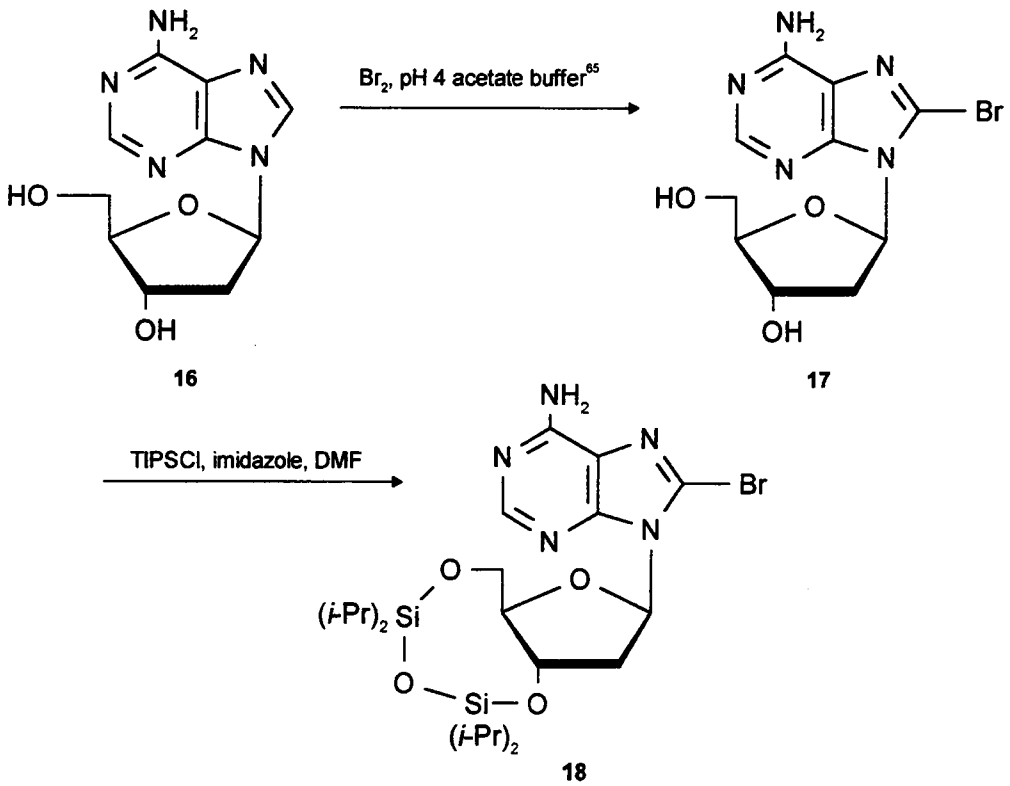
Scheme 3. Synthesis of monoprotected diamine **15**.

function was readily achieved by treating the acid with boron trifluoride·etherate and borane in tetrahydrofuran (THF) heated under reflux.[73,74] The strategy outlined in Schemes 2 and 3 shows that with the ω-amino alcohols **6** (Scheme 2) and **11** (Scheme 3) in hand, selective protection of the amino moiety is performed by the treatment of the alcohol with CbzCl under Schotten–Baumann conditions.[75] Several alternative methods, which are similar to the one we ultimately used, have been used to provide the monoprotected amino alcohol **6**.[76-79] The unaffected hydroxyl moiety can be readily converted to the mesylates **8**[80,81] and **13** (Schemes 2 and 3, respectively), which in turn can be displaced by the azide to yield **9** and **14** (Schemes 2 and 3, respectively). Atmospheric hydrogenation of the azido moiety over platinum(IV) oxide, left the Cbz protective group unscathed, but yielded the amines **10** and **15** (Schemes 2 and 3, respectively).[82]

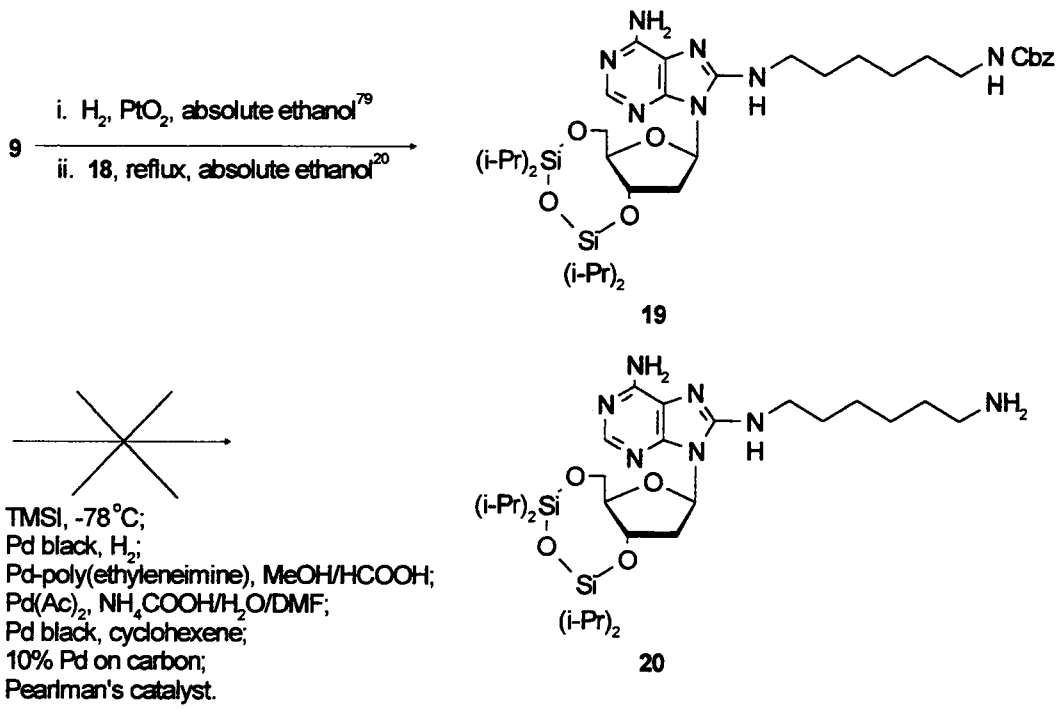
4. Attachment of the Hexylamino Linker Arm. In order to evaluate these new "masked" monoprotected diamines, such as **9**, as a means to attach a hexylamino linker arm to the C-8 position of 2′-deoxyadenosine, a series of experiments was performed with the isolated amine **10** and 8-bromo-2′-deoxyadenosine. When the two compounds were heated under reflux in ethanol, the desired C-8 adduct was not observed. Since the purity of the amino compound was questionable, a reevaluation of the strategy was carried out.

Since the final step in constructing the conjugate **1** is the reaction of "free" amino moiety at the terminus of linker arms of variable length, conceivably, the 3′- and 5′-hydroxyls of the C-8 modified nucleoside may lead to undesired ester formation. Markiewicz and co-workers have used the tetraisopropyldisiloxane-1,3-diyl (TIPDSi) protecting group to simultaneously protect the 3′- and 5′-hydroxyls to great effect with a variety of nucleosides.[83-85] Markiewicz et al. have generally used this protective group strategy on ribonucleosides,[83-85] and other groups have used this strategy to simultaneously protect the 3′- and 5′-hydroxyls of unmodified[86] and C-8 modified 2′-deoxyadenosine.[62] Another considerable advantage of this procedure is that the fully protected nucleoside was more easily handled than the "free" nucleoside. However, the TIPDSi ultimately proved to be a blockade to the entry of the conjugate **1** (see Scheme 5, and subsequent discussion). The TIPDSi group was installed by treating 8-bromo-2′-deoxyadenosine (**17**)[65,66] with 1,3-dichloro-1,1,3,3-tetraisopropyldisiloxane in the presence of imidazole (see Scheme 4).[83]

Additionally, the in situ reduction of the "masked" amine **9** and subsequent treatment of the "free" amine **10** with silyl protected 8-bromo-2′-deoxyadenosine was thought to be the best method to achieve the coupling between **10** and **18**.



Scheme 4. Preparation of protected 8-Br-2′-deoxyadenosine **18**.

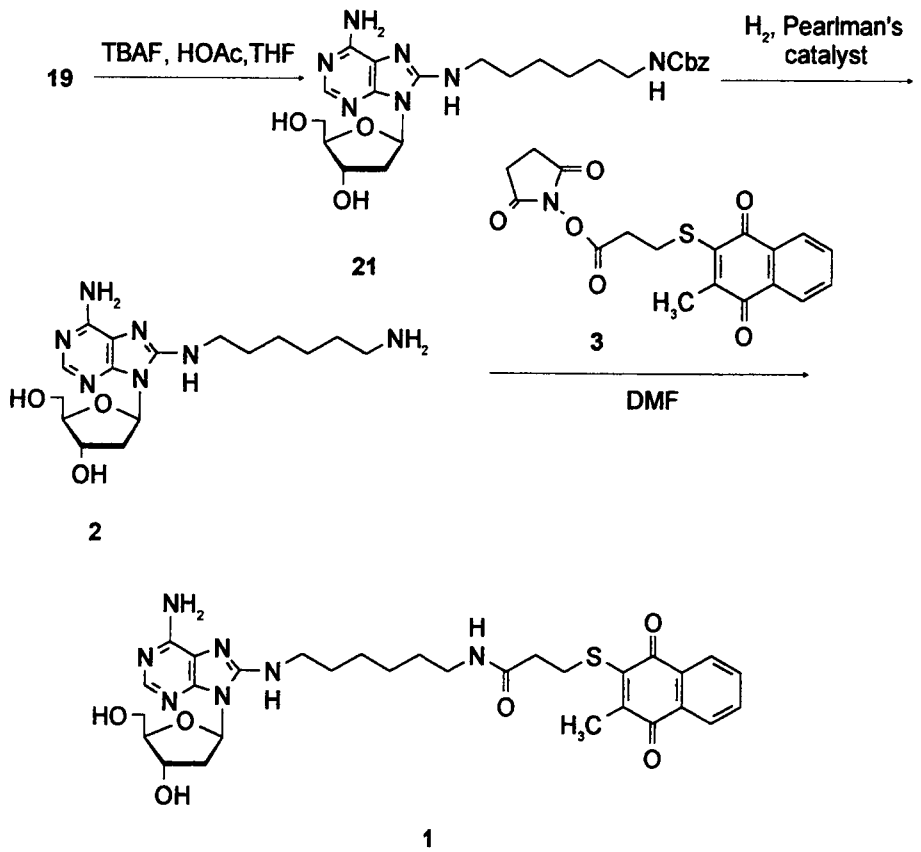


Scheme 5. Attempted preparation of silyl compound **20**.

As shown in Scheme 5, the newly adopted strategy was vindicated. However, with the nearly completely protected C-8 modified nucleoside **19** in hand, removal of the Cbz moiety on the terminus of the hexylamino linker arm using a variety of methods proved to be unsuccessful.[68]

5. Synthesis of the Naphthoquinone–2′-Deoxyadenosine Conjugate 1. In a last-ditch effort to secure the naphthoquinone conjugate **1**, the TIPDSi was completely removed by treatment of **19** with tetrabutylammonium fluoride in the presence of acetic acid (see Scheme 6). Hydrogenolysis of the Cbz protecting group on **21** was accomplished under an atmosphere of hydrogen in the presence of Pearlman's catalyst [palladium(II) hydroxide, 20 wt. % Pd (dry basis) on carbon][87] in absolute ethanol. Co-evaporation of **2** with anhydrous pyridine and subsequent treatment with *S*-(2-methyl-1,4-naphthoquinonyl-3)-β-mercaptopropionic acid *N*-Hydroxysuccinimide (NHS) ester(**3**)[69] in DMF afforded the NQ–conjugate **1**.

6. Electrochemical Studies on the Novel Naphthoquinone–2′-Deoxyadenosine Conjugate 1 (First-generation Bioconjugate).[88] A cyclic voltammogram (cv) was performed on an acidified, aqueous solution of the NQ conjugate **1**. The electrochemical signature produced was characteristic of the $2H^+/2e^-$ hydroquinone/quinone couple signal observed for other quinonoidal



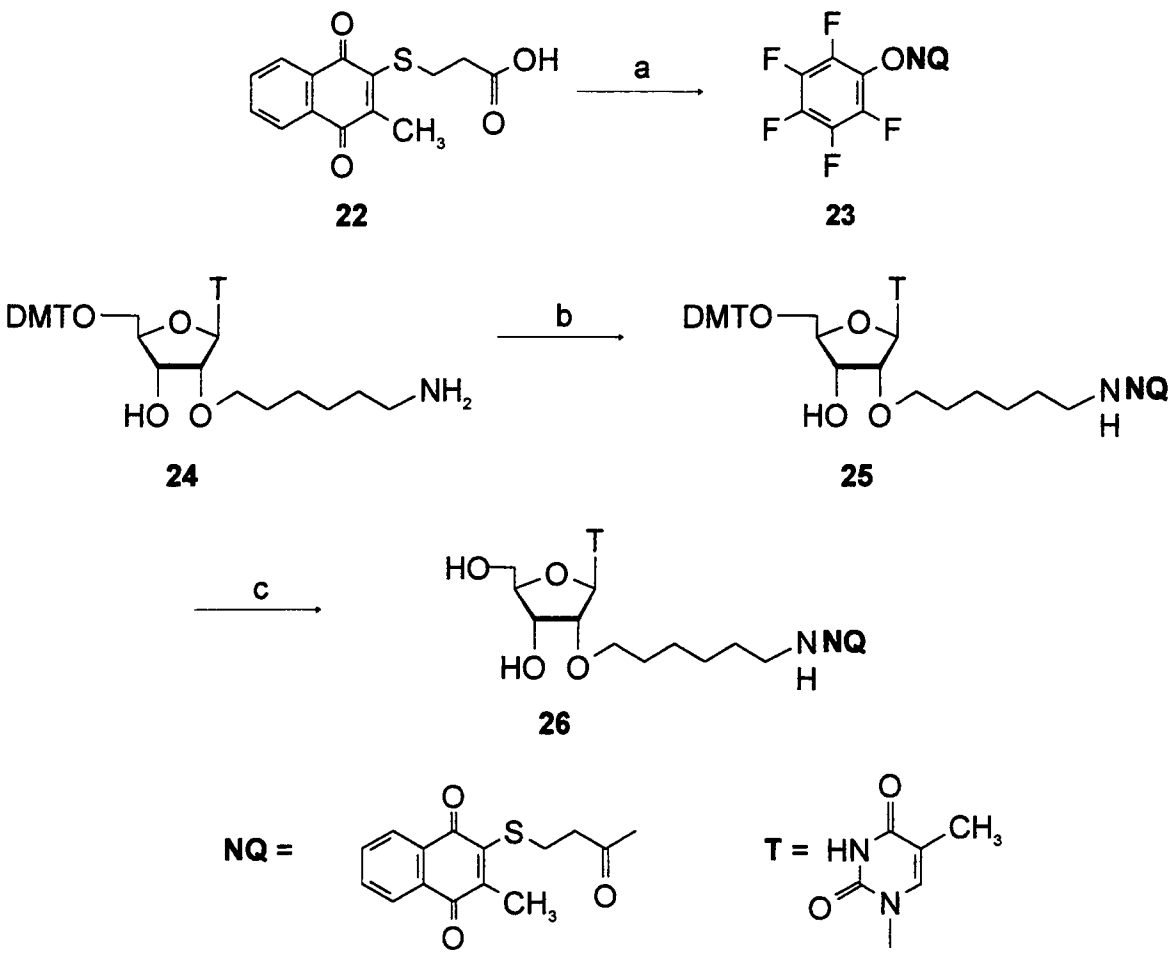
Scheme 6. Synthesis of the first-generation electroactive naphthoquinone–2′-deoxyadenosine conjugate **1**.

compounds in aqueous systems.[57] However, as a result of presenting this work,[89] C-8-modified electroactive nucleosides as convenient building blocks in the preparation of electroactive ODNs were no longer pursued (for the reasons this approach was abandoned, see Section III.C).

C. Synthesis of 2′-*O*-Modified Nucleosides (Second-generation Electroactive Bioconjugates)[24]

1. General. After presenting the results detailed in Section III.B at the 212th National Meeting of the American Chemical Society in Orlando, FL,[89] we became aware that the use of C-8 modified nucleosides was flawed.[90] Hybridization of certain base-modified ODNs is difficult[91] compared to the well documented hybridization properties of 2′-O-modified ODNs, which have shown potential as antisense therapeutic agents.[92] Moreover, these modified ODNs produce duplexes that have a greater stability than their unmodified counterparts.[93] Thus was launched a collaboration with the pioneers of these modifications, Isis Pharmaceuticals, Inc., Carlsbad, CA.[94-97]

2. Synthesis 1,4-Naphthoquinone–Thymidine (NQ–Thymidine) Bioconjugates. Scheme 7 shows a synthetic outline for the preparation of a NQ–thymidine conjugate. The novel conjugate **25** was obtained by the reaction

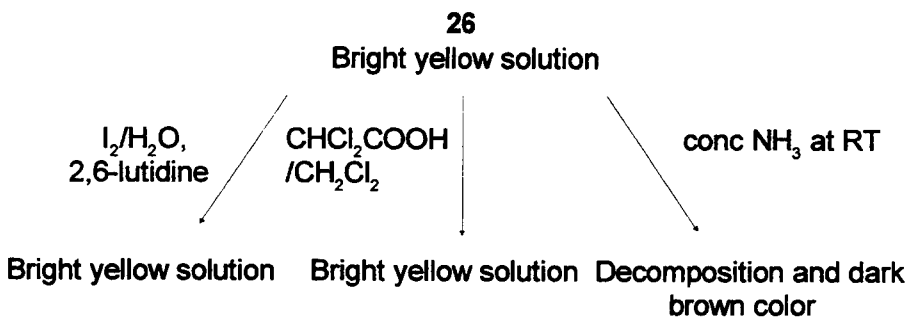


[a]Reagents: (a) DCC, pentafluorophenol, CH_2Cl_2, 0 °C → room temperature over the course of 12 h; (b) pyr, CH_2Cl_2, **23**, 0 °C for 50 min, room temperature for 3 h; (c) 3% (v/v) dichloroacetic acid in CH_2Cl_2, 10 min.

Scheme 7.[a] Synthesis of the second-generation electroactive naphthoquinone–thymidine conjugates **25** and **26**.

of the free amine **24**[98] with *S*-(2-methyl-1,4-naphthoquinonyl-3)-β-mercaptopropionic acid pentafluorophenyl ester (**23**).[69] With **25** in hand, (a) the electroactive phosphoramidite could be prepared, and (b) the free ribonucleoside **26** could be obtained by removal of the 5′-*O*-(4,4'-dimethoxytrityl) (DMT) group with dichloroacetic acid.[99] Compound **26** could be used as a model compound in electrochemical studies of electroactive ODNs in aqueous systems.

However, before the synthesis of the 3′-*O*-phosphoramidite of the NQ–thymidine conjugate was carried out by Isis Pharmaceuticals, Inc., Carlsbad, CA, the stability of the NQ moiety upon treatment with the solutions routinely used in automated ODN synthesis (this study is shown in Scheme 8)[99] needed to be established. This was achieved by (a) monitoring the color of solutions, and (b) by performing TLC on the resultant solutions. The detritylation and oxidation solutions (see Fig. 4) did not affect the integrity of the NQ moiety. However, in the presence of concd ammonia, which is used to completely deprotect the synthetic ODN, the intense, bright yellow solution rapidly darkened, and quickly became a dark-brown color. Presumably either a 1,4-Michael addition of ammonia to the NQ moiety occurred[100] or the quinone methide of the NQ moiety formed and underwent further reaction.[101] For each scenario, further deleterious reactions could result, and decomposition of the NQ–thymidine bioconjugate may even be a combination of both reaction pathways that



Scheme 8. Can the NQ moiety survive the conditions experienced in the automated ODN synthesizer?

eventually leads to the formation of a polymer. As a consequence of these observations, further work with NQ bioconjugates was abandoned (for the implications that this study has to the future development of conjugates that bear novel EATs, see Section VI).

3. Synthesis of 9,10-Anthraquinone–Uridine (AQ–Uridine) Bioconjugates. As explained in the previous section, the NQ conjugate could not be used to secure electroactive ODNs, because of the incompatibility of the reporter group in the final deblocking step in the synthesis of ODNs.[99] This discovery could explain why Rokita and Chatterjee chose to install the same NQ moiety at the 5′-terminus of an already assembled synthetic ODN; i.e., the NQ–ODN was not constructed using a phosphoramidite building block in an automated ODN synthesizer.[69] Thus alternative quinonoidal species were sought that could act as EATs.

a. General. Ample precedent exists in the literature that AQ–ODN conjugates are known to survive the conditions experienced in the oligonucleotide synthesizer.[102,103] As with the NQ moiety, the AQ tag would give the desired, persistent electrochemical signature, but not succumb to the deleterious reactions that the NQ moiety would undergo.

Although the work described in this section focuses on the electrode reactions of 2′-*O*-modified AQ–ODN bioconjugates, others have prepared ODNs

with tethered quinone groups for different applications. An increase in stability has been noted for nucleic acid duplexes modified at the sugar 2′-position,[93] including several studies using pendant AQ groups.[103-105] Rokita and co-workers have used tethered quinones for photochemical methylation of DNA with known sequences at specific sites,[69,106] and Gasper and Schuster found photooxidation of GG sites in a DNA double-helix possessing an end-tethered anthraquinone group.[107] Cohen and co-workers utilized 5′-linked AQ–ODNs to demonstrate that AQ derivatives can be delivered to target nucleic acids (mRNA or DNA).[102] AQ tags were chosen for the present study since they can withstand the conditions required for the solid-phase synthesis of ODNs,[93,107] while also exhibiting a two-electron electrode reaction characteristic of the quinone/hydroquinone couple. The formal potential of this couple is well separated from potentials of redox reactions associated with the ODNs. In addition, the electrochemical signal provides a means to study interfacial electron and proton transfer reactions of immobilized oligonucleotide probes on electrode surfaces.

b. Preparation of novel AQ–ODNs. Entry to the novel oligomers **27a–c** and **28** was crucial for this study (refer to Fig. 7). The key intermediate in the synthetic sequence was the electroactive phosphoramidite **29** (see Fig. 8). Additionally, the strategy provided access to the free nucleoside **31** that was required to establish the experimental conditions for observation of the distinctive electrochemical signature of the quinone moiety.

5'-d(A**U***G CAT TCT GCC CCC AAG AG)-3'

27a

5'-d(ATG CAT TC**U*** GCC CCC AAG AG)-3'

27b

5'-d(A**U***G CAT TC**U*** GCC CCC AAG AG)-3'

27c

5'-d(GA**U***CT)-3'

28

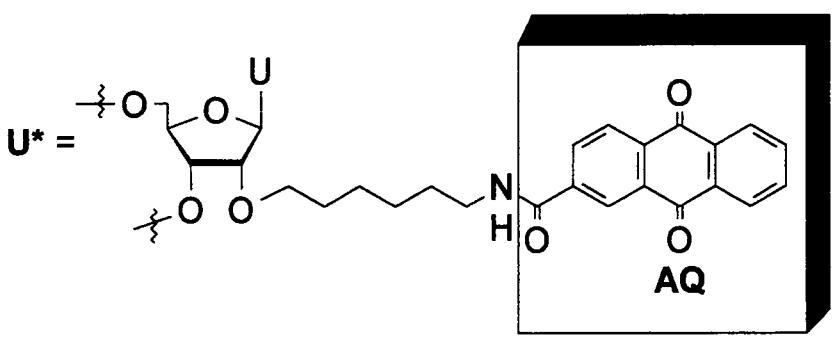
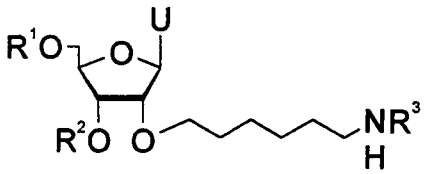


Fig. 7. Electroactive AQ–ODN bioconjugates prepared using phosphoramidite methodology.



29: R^1 = DMT; R^2 = (i-Pr)$_2$N $-P\begin{smallmatrix}\diagup\\ O\end{smallmatrix}\!\!\sim\!\!CN$; R^3 = **AQ**

30: R^1 = DMT; R^2 = H; R^3 = H

31: R^1 = H; R^2 = H; R^3 = **AQ**

3'-d(TAC GTA AGA CGG GGG TTC TC)-5'

32

3'-d(GAG AAC CCC CGT CTT ACG TA)-5'

33

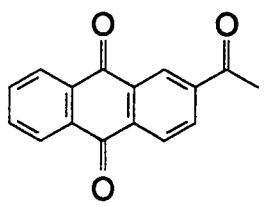
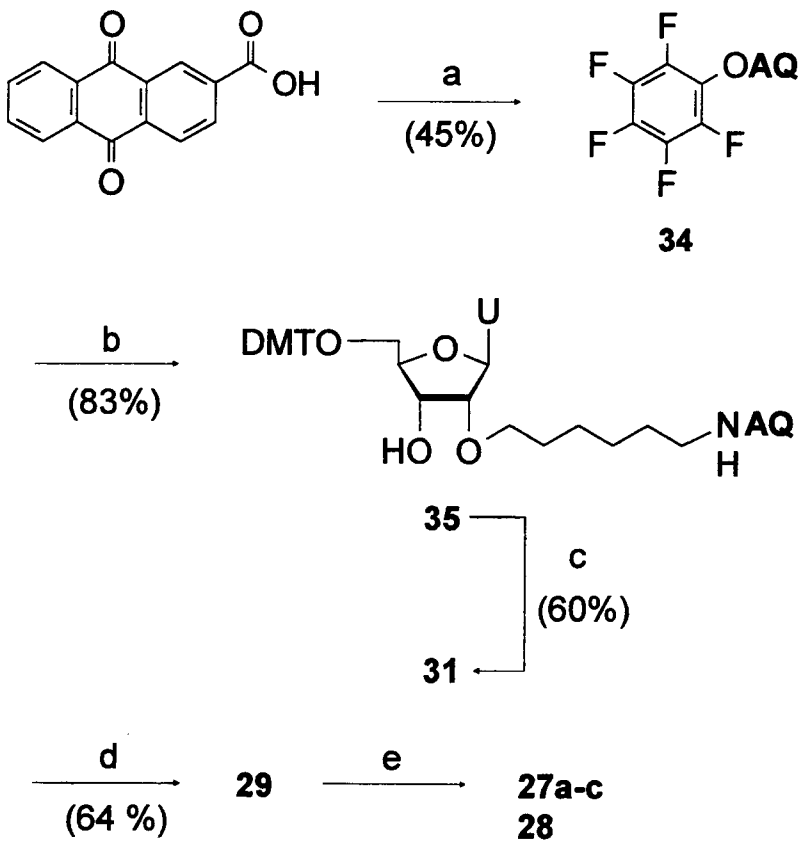
AQ = 

Fig. 8. Building blocks in the synthesis of electroactive AQ–ODN conjugates.

Compound **34** was synthesized utilizing DCC to condense the commercially available 9,10-anthraquinone-2-carboxylic acid with pentafluorophenol (Scheme 9). Addition of **34** to **30**[96] in the presence of pyridine secured the modified nucleoside **35**. With this essential intermediate in hand, (a) the phosphoramidite **29** was prepared by Isis Pharmaceuticals, Inc., Carlsbad, CA, using standard methodology[96] and, (b) removal of the 5′-*O*-(4,4′-dimethoxyltrityl) (DMT) group was readily achieved with a 3% (v/v) dichloroacetic acid in CH_2Cl_2 solution[99] to afford the free ribonucleoside **31**. A standard protocol was performed to obtain AQ–ODNs **27a–c** and **28** from **29** on an automated oligonucleotide synthesizer.[97] Prior to removal of the terminal DMT group, the resulting oligomers were purified using reversed-phase HPLC.

D. Electrochemical Studies[108]

In order to develop suitable protocols for the study of the electrochemical behavior of **27a–c**, extensive electrochemical studies on **28** and **31** were required.[108] Furthermore, before **27a–c** could be assessed as probes for nucleic acid hybridization, the melting temperatures (T_m) of these novel electroactive ODNs had to be established.



[a]Reagents and conditions: a. DCC, 2,3,4,5,6-pentafluorophenol, CH_2Cl_2, 0 °C - RT over 12 h; b. **4**, pyr, CH_2Cl_2, 0 °C for 50 min, RT for 3 h; c. 3% (v/v) $Cl_2CHCOOH$ in CH_2Cl_2, 10 min; d. Diisopropylammoniumtetrazolide, 2-(cyanoethyl)-*N,N',N',N*-tetraisopropyl phosphoramidite, CH_2Cl_2, RT over 12 h. e. Automated ODN synthesizer.

Scheme 9.[a] Synthesis of electroactive AQ–ODN conjugates **27a–c** and **28**.

E. Hybridization Studies

To determine the T_m of the electroactive 20-mers **27a–c**, the tagged 20-mer and its complementary strand were placed in a buffer, and the melting/annealing process was followed by monitoring the UV absorption spectrum as a function of temperature. Additionally, this buffer solution offered the advantage that it could be used for electrochemical studies to be performed simultaneously, i.e., the presence of ds-DNA could be confirmed, and then using the same solution, cyclic voltammetry on this species could be carried out. Fig. 9 shows a cooling absorbance trace for a solution of **27a** plus its complementary strand, which exhibits a melting point at 66 °C. Interestingly, the melting temperatures of the untagged duplex, i.e., **32•33**, and the duplexes of the AQ–ODNs were approximately the same, indicating that the tethered AQ group is not intercalated in the duplex structure. In pH 7.4, 0.1 M phosphate buffer containing 0.05 M NaCl and 5 mM EDTA, the $T_m(\Delta T_m)$ values were 66.4, 68.3(1.9), 68.4(2.0) and 69.1(2.7) °C for the duplexes of **32** with **33**, **27a**, **27b**, and **27c**, respectively. Somewhat larger ΔT_m values were seen for 2′-*O*-modified ribonucleotides with an intercalating substituent, 2-aminoanthraquinone, tethered on shorter linker arms.[104]

Cyclic voltammetry experiments were run in parallel with the melting curves. In these experiments, solutions containing equimolar amounts of a

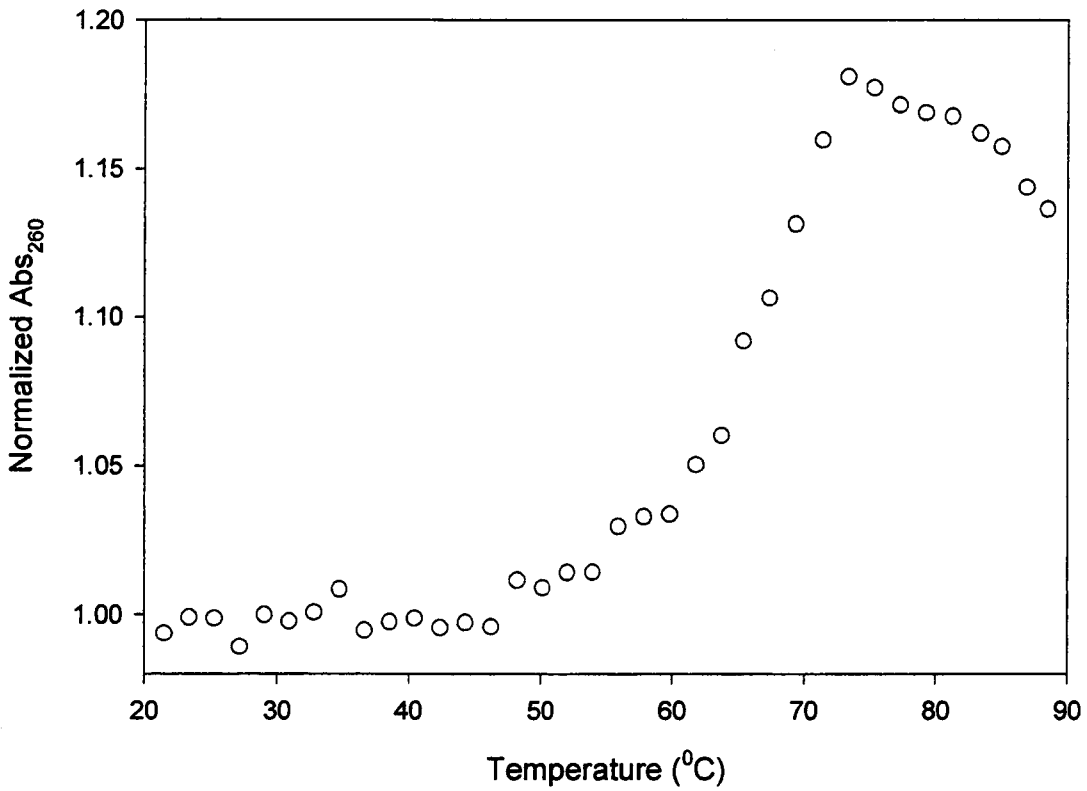


Fig. 9. Typical melting curve for 0.35 μM **27a** and **32** in pH 6.83 0.1 M phosphate buffer, with 0.1 M NaCl.

tagged AQ-ODN and either its complementary (**32**) or a non-complementary (**33**) ODN species were split into two parts and subjected to both CV and UV-vis analysis. The resulting voltammograms for compound **27a** are shown in Figures 10 and 11 for a pH 7.4 phosphate buffer. The CVs marked A in these figures were obtained on solutions containing **27a** at a concentration sufficient to give a limiting surface coverage of the AQ-ODN. Addition of the complementary strand to the solution resulted in an attenuation of the signal; refer to CV marked B in Figure 10. However, this result cannot be distinguished from simple competitive adsorption of an untagged ODN since essentially identical behavior was seen when the experiment was repeated with a non-complementary sequence; see CV marked B in Figure 11.

Significantly, however, when the solution containing **27a** and its complement was annealed at 90 °C, followed by slow cooling to room temperature, the resulting CV obtained on the solution was further attenuated and shifted to slightly more negative potential; see CV marked C in Figure 10. The corresponding CV obtained on the control solution with the non-complementary species **33**, CV marked C in Figure 11, was not attenuated. These results are best understood if the hybridization is slow in these dilute solutions at room temperature. In this case, the attenuation seen in the CVs marked B in Figures 10 and 11 could be due to competitive adsorption as described elsewhere.[108]

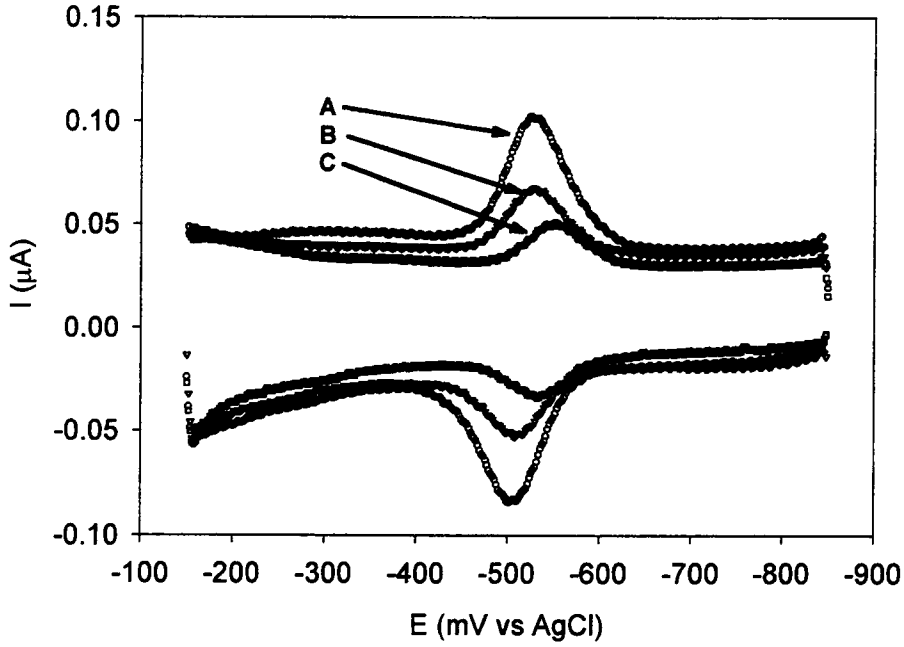


Fig. 10. Cyclic voltammetry of **27a** plus complementary 20-mer **32**. (A) 0.695 μM **27a** in pH 7.4 phosphate buffer (0.1 M), 0.05 M NaCl, 5 mM EDTA; (B) Addition of equal amount of compound **32** at room temperature; (C) After heating to 90 °C and cooling to room temperature; sweep rate: 0.1 V s^{-1}.

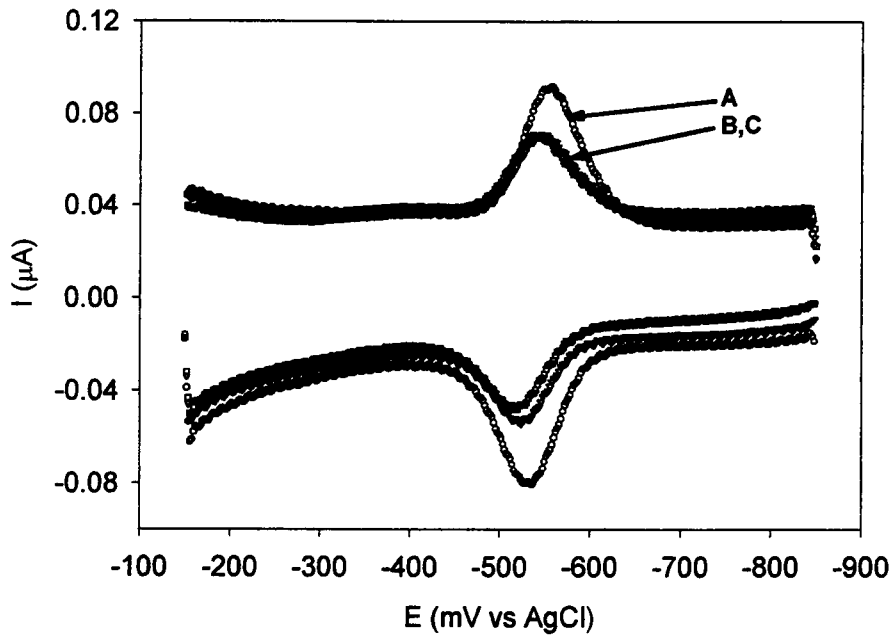


Fig. 11. Cyclic voltammetry of **27a** plus noncomplementary 20-mer **33**.

Conditions same as Figure 10.

While the further attenuation seen in the CV marked C of Figure 10 appears to be related to formation of the duplex species in solution, the physical phenomenon responsible for this effect is not clear. One possibility is that the duplex **27a•32** species is electroinactive or not adsorbed on the electrode surface and that the signal obtained after solution hybridization is due to adsorbed **27a** in equilibrium with a decreased concentration of **27a** in the bulk of the solution. Alternatively, the duplex **27a•32** might adsorb on the electrode with a larger footprint (i.e., surface area per adsorbate) than the combined footprints of the tagged and untagged 20-mers. More likely, the duplex **27a•32** is electroactive, but has a weaker attraction for the electrode surface than the single-strand ODNs since the DNA bases are not free to interact with the surface, so that when the duplex is formed in solution, the surface layer is no longer at saturation coverage. In any case, the possibility of a simple in situ electrochemical detection of the hybridization event based on these results is problematic without a different strategy and further modification of the electrode surface.

IV. EXPERIMENTAL

A. General Methods

All reactions were monitored by thin-layer chromatography (TLC). Adsorption chromatography was carried out using E. Merck silica gel products: (a) TLC on 0.2 mm aluminum-backed plates, (b) column chromatography using 230–400 mesh silica gel. Visualization of the TLC plates was by 254 nm UV light and by spray–heat development using a *p*-anisaldehyde–sulfuric acid reagent[109] (reagent A) and ninhydrin solution (reagent B).[110] The solvent systems for adsorption chromatography were A, 1:1 ethyl acetate–hexanes; B, 95:5 dichloromethane–methanol; C, 3:1 ethyl acetate–hexanes; D, 9:1 dichloromethane–methanol; E, 99:1 dichloromethane–methanol; F, 65:35:trace ethyl acetate–hexanes–triethylamine; G, 70:30 ethyl acetate–hexanes; H, 2:1 ethyl acetate–hexanes; I, 1:2 ethyl acetate–hexanes; J, 99:1 dichloromethane–hexanes; K, 99:1 chloroform–methanol; L, 97.5:2.5 dichloromethane–methanol; M, 98:2 dichloromethane–methanol. All reactions were carried out under a nitrogen atmosphere unless otherwise indicated. Solvents were evaporated at aspirator vacuum at about 25 °C unless otherwise indicated. Melting points were determined on a Thomas–Hoover capillary melting point apparatus and are uncorrected. Elemental analyses were

furnished by Atlantic Microlab, Inc., Atlanta, GA. ^{1}H and ^{13}C NMR spectra were recorded at 400.13 and 100.61 MHz, respectively, unless stated otherwise. ^{19}F spectra were recorded on a Jeol FX90Q spectrometer at 84.24 MHZ using an external standard of trifluoroacetic acid-*d*. ^{31}P spectra were recorded at 161.9 MHZ using an external standard of phosphoric acid (85%) at 37 °C.

Infrared spectra were acquired on a Perkin-Elmer 710B spectrophotometer (Perkin-Elmer Corporation, Norwalk, CT) against a polystyrene film standard (1601 cm^{-1}).

Positive-ion electrospray mass spectra of the 2′-*O*-modified nucleosides were acquired on a Quattro-II quadrupole instrument (Micromass Inc, Manchester, UK) by infusion (5 μL/min) of a ca. 1 μM solution of the analyte in methanol. Data were averaged in the "multi-channel acquisition" mode over a 2-min acquisition period. Conversely, negative-ion electrospray mass spectra of the unmodified ODNs were obtained on the same instrument by infusion (5 μL/min) of a ca. 1 μM solution of the analyte in 1:1 methanol–water that contains 0.15% triethylamine. The averaging of the data was performed as above.

The detritylation, oxidation, and deblocking solutions used in the compatibility testing of the NQ–2′-*O*-thymidine conjugate were the same as those used in the automated synthesizer to prepare ODNs via phosphoramidites.[99]

The AQ–ODNs were synthesized using a Perspective Biosystems Expedite 8901 Nucleic Acid Synthesis System (PE Applied Biosystems, Foster City, CA).

Certain reactions of the C-8 modified nucleosides were monitored on reversed-phase HPLC. This was performed on a Beckman 421 equipped with an Altex Model 153 analytical detector, Beckman Ultrasphere ODS column (46 mm × 250 mm), and a linear strip-chart recorder (Beckman Coulter, Inc., Fullerton, CA). The solvent systems used for reversed-phase HPLC (N) 90:10 methanol–pH 6.86 phosphate buffer (200 fold dilution of a solution prepared using Gram-Pac®, Fisher Scientific, Fair Lawn, NJ), (O) 60:40 methanol–pH 6.86 phosphate buffer, and (P) 50:50 methanol–pH 6.86 phosphate buffer. The isocratic solvent system employed to study the hydrogenolysis of **19** was solvent N using a flow rate of 2 mL/min (method A). The analytical purity of the free C-8 modified nucleoside **21** was assessed using solvent system O and a flow rate of 1.5 mL/min (method B). Hydrogenolysis of **21** was performed utilizing solvent system P and a flow rate of 1.5 mL/min (method C).

Preparative reversed-phase HPLC on the monotritylated AQ–ODNs was performed on a Waters 600E instrument (260 nm) equipped with a Waters Delta Pak C4 column (7.8 × 300 mm) and a Waters 991 integrator (Waters Corp., Milford, MA). The solvent systems used for reversed-phase HPLC were Q, 50 mM triethylammonium acetate at pH 7.0; R, acetonitrile. The gradient system

employed was 95:5 Q–R for 5 min with a linear increase to 4:6 Q–R over 50 min (method D) using a flow-rate of 2.5 mL/min. Purity of the AQ–ODNs was determined utilizing a Waters Delta Pak C4 column (3.9 × 300 mm) and the same gradient system, as above at a flow rate of 1.5 mL/min (method E).

Additional analysis of the AQ–ODNs was conducted with capillary gel electrophoresis (CGE). An 100-μL aliquot of the ODN (0.2 ODs) was injected into a Beckman P/ACE System 5000 Capillary Gel Electrophoresis unit, coupled to a UV–vis detector (Beckman and Coulter, Inc., Fullerton, CA) that was equipped with a column (27 cm in total length with an effective length of 20 cm) of 12% linear polyacrylamide in a buffer of 7M urea and 0.2M bis tris borate. A voltage of 500 V/cm was supplied to the column at ca. 40 °C. A typical analysis was completed in 12 min (method A).

Prior to acquisition of the negative-ion electrospray mass spectra of the AQ–ODNs on a HP 59987A Series II API 5989A Mass Spectrometer (Hewlett-Packard Co., Palo Alto, CA), ca. 0.5 ODs was desalted by osmosis from water that contained ammonium hydroxide using an Millipore VS 0.025 μm filter (Millipore Corp., Bedford, MA). After 1 h the purified sample was then dissolved in 1:1 2-propanol–water (100 μL). Before the sample was infused into the spectrometer, a 2.5-μL aliquot of piperidine (100 mM) was added.

A Shimadzu UV-2101PC UV–vis scanning spectrophotometer (Shimadzu Corp., Kyoto, Japan) was used to determine ϵ_{max} of the novel AQ–ODNs. Melting

points of the ODNs were determined using an HP Model 8452A diode array spectrophotometer equipped with a HP Model 89090A Peltier temperature controller (Hewlett-Packard Co., Palo Alto, CA).

The electrochemical studies were performed using a hanging mercury dropping electrode, HMDE (EG&G, Oak Ridge, TN). The electrode area was 0.0225 cm^2 for most of the voltammetric experiments; details are given elsewhere.[111] The reference electrode was a Ag/AgCl wire immersed directly in the test solution. A Cypress Model CS-2Ra (Cypress Systems, Inc., Lawrence, KS) potentiostat was used.

B. Materials and Solvents

Solutions of non-modified phosphoramidites (0.1 M) were used as purchased from PE Applied Biosystems, Foster City, CA. 5′-d(ATG CAT TCT GCC CCC AAG AG)-3′ (**33**) was supplied by Operon Technologies, Inc., Alameda, CA. The other unmodified ODN 5′-d(CTC TTG GGG GCA GAA TGC AT)-3′ (**32**) was furnished by Isis Pharmaceuticals, Carlsbad, CA. The entire amount of the ODNs were diluted to 10 mL with sterile deionized water. Anhydrous solvents were prepared as follows: tetrahydrofuran (THF) was distilled from the benzophenone ketyl radical (Na/benzophenone); dichloromethane and pyridine were distilled from calcium hydride at atmospheric

pressure; *N*,*N*-dimethylformamide (DMF) was distilled from calcium hydride under vacuum; 1,4-dioxane was distilled from lithium aluminum hydride; triethylamine distilled from calcium hydride.

Unless otherwise stated all chemicals were purchased from Aldrich Chemical Company, Milwaukee, WI.

C. Synthesis of C-8 Modified Nucleosides (First-generation Electroactive Conjugates)[2,3]

Preparation of 6-(*N*-Benzyloxycarbonylamino)hexanol (7). A solution of 6-amino-1-hexanol (**6**) (10.0 g, 85.6 mmol) in 1 M NaOH (42.6 mL) was made in a flask. The mixture was cooled to 0 °C under nitrogen, and benzyl chloroformate (14.6 mL) and 1 M NaOH (42.6 mL) were added alternatively over 15 min. Once the addition was complete, the mixture was warmed to room temperature. The progress of the reaction was monitored by TLC (R_f = 0.28; solvent H), which was complete after 3 h. The white solid that formed was filtered and washed with ice water and triturated in hexanes overnight to remove the non-polar impurities. The product **7** was filtered and dried in a vacuum oven (19.8 g, 92%): R_f = 0.28 (solvent H); mp 79–82 °C (lit.[79] 79–80 °C); ^{1}H NMR (250 MHz, $CDCl_3$): δ 7.35 (5 H, s, Ar–**H**), 5.10 (2 H, s, Ar–CH_2), 4.75 (1 H, br s, **NH**), 3.63 (2 H, t, J = 6.25, CH_2–OH), 3.20 (2 H, br q, J = 6.31, CH_2–NH–), 1.52

(5 H, br s, –O*H*, CH_2–CH_2–CH_2 –OH), 1.36 (4 H, br CH_2–CH_2–CH_2 –NH); ^{13}C NMR (62.9 MHz, $CDCl_3$): δ 156.44, 136.56, 128.39, 127.96, 66.49, 62.47, 40.81, 32.43, 29.82, 26.28, 25.22. Anal. Calcd for $C_{14}H_{21}NO_3$: C, 66.91; H, 8.42; N, 5.57; O, 19.10. Found: C,66.78; H, 8.36; N, 5.59.

Preparation of 6-(*N*-Benzyloxycarbonylamino)-1-*O*-(methylsulfonyl)hexanol (8). To a cooled solution of **7** (15.0 g, 60 mmol) in anhydrous dichloromethane (360 mL) was added triethylamine (41.6 mL, 298 mmol), and the solution was stirred at 0 °C. Methanesulfonyl chloride (5.6 mL, 72 mmol) was added dropwise over 10 min, under nitrogen. The reaction mixture was warmed to room temperature, and the reaction, followed by TLC (R_f = 0.49; solvent H), was complete after 6 h. The crude reaction mixture was evaporated to dryness, and the white solid was subjected to column chromatography (solvent I → solvent A). The oil thus obtained turned to a white solid **8** when dried on the vac-line (16.6 g, 84%): R_f = 0.49 (solvent H); mp 32–35 °C; ^1H NMR (250 MHz, $CDCl_3$): δ 7.33 (5 H, s, Ar–**H**), 5.09 (2 H, s, Ar-CH_2), 4.78 (1 H, br s, NH), 4.21 (2 H, t, *J* =6.41 Hz,–CH_2–OMs), 3.18 (2 H, m, –CH_2–NH), 2.99 (3 H, s, –OSO_2–CH_3), 1.73 (2 H, m, CH_2–CH_2–OMs), 1.44 (6 H, m, CH_2 s); ^{13}C NMR (62.9 MHz, $CDCl_3$): δ 156.35, 136.59, 128.40, 127.97, 77.51, 77.00, 76.50, 69.81, 66.47, 40.75, 37.25, 29.68, 28.91, 25.97, 24.9. Anal. Calcd for $C_{15}H_{23}NO_5S$: C, 54.69, H, 7.04, N, 4.25, S, 9.73, O, 24.28. Found: C, 54.69; H, 7.08; N, 4.29; S, 9.77.

Preparation of 1-Azido-6-(*N*-benzyloxycarbonylamino)hexane (9). To a stirred solution of **8** (26.3 g, 79.8 mmol) in dry DMF (35 mL) was added sodium azide (10.4 g, 160 mmol). After 22 h the reaction mixture still contained starting material as shown by TLC. The reaction was stopped, and the DMF was removed under vacuum. The residue was washed in ethyl acetate–water (60 mL:100 mL, respectively) mixture and then with brine (100 mL). The combined aqueous layer was extracted with ethyl acetate (50 mL). The organic extracts were combined, and the solvent was removed *in vacuo*. The resulting oil was subjected to column chromatography (solvent I). The starting material **7** was recovered by continued elution with solvent A. The combined organic extracts were dried ($MgSO_4$) and then evaporated to dryness to afford **9** [11.6 g, 59%, based on recovered starting material (2.8 g)]: R_f = 0.9 (solvent H); ^{1}H NMR (250 MHz, $CDCl_3$): δ 7.35 (5 H, s, Ar–**H**), 5.09 (2 H, s, Ar-C**H**$_2$), 4.74 (1 H, br s, – **NH**), 3.23 (4 H, m, C**H**$_2$–N_3 and –C**H**$_2$ –NH), 1.62–1.36 (8 H, m, CH_2 s); ^{13}C NMR (62.9 MHz, $CDCl_3$): δ 156.31, 136.55, 128.34, 127.91, 77.51, 77.00, 76.49, 66.42, 51.17, 40.78, 29.71, 28.58, 26.22, 26.09. Anal. Calcd for $C_{14}H_{20}N_4O_2$: C, 60.85; H, 7.29; N, 20.27; O, 11.58. Found: C, 60.67; H, 7.20; N, 20.15.

Preparation of 6-(*N*-Benzyloxycarbonylamino)hexylamine (10). Compound **9** (1.0 g, 3.6 mmol) was added to a suspension of platinum(IV) oxide (4.2 mg, 0.18 mmol) in absolute ethanol (60 mL). The flask containing the reaction mixture was then evacuated and filled with hydrogen at atmospheric

pressure. The reaction mixture was stirred for 4 h, filtered through Celite, and evaporated to approximately 40 mL. Due to the difficulty in isolating pure amine **10**, the ^{1}H NMR data is presented here and the assumption is made that amine is formed in 100% yield: ^{1}H NMR (250.13 MHz, $CDCl_3$): δ 1.2–1.6 (overlapping resonances and H_2O, 9H), 2.25 (s, 3H. Exchanges with D_2O), 2.70 (t, J = 6.86 Hz, 2H), 3.18 (q, J = 6.5 Hz, 2H), 4.81 (bs, 1H. Slowly exchanges with D_2O), 5.09 (s, 2H), 7.35 (s, 5H).

Synthesis of 8-Bromo-3′,5′-*O*-(1,1,3,3-tetraisopropyldisiloxane-1,3-diyl)-2′-deoxyadenosine (18). To a solution of imidazole (0.9 g, 13.2 mmol) in anhydrous DMF (20 mL) was added 8-bromo-2′-deoxyadenosine[65] (1.0 g, 3.0 mmol). After cooling the solution to 0 °C, 1,3-dichloro-1,1,3,3-tetraisopropyldisiloxane (1.1 mL, 3.34 mmol) was added dropwise. A sandy-brown solid formed immediately. The solution was allowed to warm up gradually to RT, and the reaction was stopped after 1.75 h by removing the solvent *in vacuo*. To the crude reaction mixture was added dichloromethane (50 mL). The sandy-brown precipitate was filtered under vacuum, and the filtrate was evaporated *in vacuo*. The crude reaction mixture was dissolved in the minimum amount of dichloromethane (ca. 2 mL), and this solution was subjected to column chromatography (solvent J), which afforded **18** as an off-white, amorphous solid (1.02 g, 59%): ^{1}H NMR (250.13 MHz, $CDCl_3$): δ 0.9–1.30 (overlapping resonances, 28H), 2.50–2.7 (m, 1H), 3.15–3.28 (m, 1H), 3.85–3.95 (m, 1H), 5.46

(bd, J = 7.97 Hz, 2H), 5.40–5.60 (overlapping resonances, 3H), 6.28 (dd, J = 2.49 Hz, J = 8.78 Hz, 1H), 8.22 (s, 1H); ^{13}C NMR (62.9 MHz, DMSO-d_6): δ 12.0, 12.11, 12.47, 12.64, 12.87, 16.76, 16.85, 17.02, 17.13, 17.29, 37.55, 62.76, 72.11, 83.65, 84.21, 119.41, 126.72, 149.53, 152.25, 154.95. Anal. Calcd for $C_{22}H_{38}BrN_5O_4Si_2$: C, 46.14; H, 6.69; Br, 13.95; N, 12.23; O, 11.18; Si, 9.81. Found: C, 46.19; H, 6.65; Br, 14.05; N, 12.15.

Synthesis of 8-[6-(*N*-Benzyloxycarbonylamino)hexylamino]-3′,5′-*O*-(1,1,3,3-tetraisopropyldisiloxane-1,3-diyl)-2′-deoxyadenosine (19). Compound **9** (2.0 g, 3.6 mmol) was added to a suspension of platinum(IV) oxide (82 mg, 0.18 mmol) in absolute ethanol (ca. 50 mL). The flask was then evacuated and filled with hydrogen at atmospheric pressure. The reaction mixture was stirred for 1.5 h, filtered through Celite, and evaporated to a total volume of ca. 40 mL.

To the solution of **10** described above (assuming a complete conversion from the azide precursor **9**, (1.8 g, 7.2 mmol), **18** (1.03 g, 1.8 mmol) was added. The solution was heated to reflux for 24 h. The solvent was removed *in vacuo*, and the crude reaction mixture was subjected to column chromatography (chloroform → solvent K) to afford a brownish paste. Lyophilization of the paste with deionized water (2 × 20 mL) on a Virtis Freezemobile 5SL (Virtis Company, Inc., Gardiner, NY) afforded a brown, glassy material [1.1 g, 82% (based on recovered starting material)]: t_R = 8.6 min (HPLC, method A); ^{1}H NMR (250.13

MHz, $CDCl_3$): δ 0.90–1.20 (overlapping resonances, 28H), 1.20–1.40 (bs, 4H), 1.40–1.55 (bm, 2H), 1.50–1.65 (bm, 2H), 2.4–2.55 (m, 1H), 3.00–3.20 (overlapping resonances, 3H), 3.20–3.50 (overlapping resonances, 3H), 3.80–3.95 (bm, 2H), 3.95–4.05 (bm, 1H), 4.9–5.05 (bm, 1H), 5.08 (s, 2H), 5.26 (overlapping resonances, 2H), 5.67 (s, 2H), 6.16 (dd, J = 3.32 Hz, J = 7.63 Hz, 1H), 7.30 (bs, 5H), 8.09 (s, 1H); ^{13}C NMR (62.9 MHz, $CDCl_3$): δ 12.34, 12.75, 12.96, 13.17, 16.75, 16.82, 17.01, 17.17, 17.35, 26.08, 26.23, 29.17, 29.51, 29.67, 37.90, 40.69, 42.67, 62.35, 66.35, 71.20, 76.49, 82.43, 84.73, 117.45, 127.85, 128.29, 136.54, 149.27, 149.50, 151.98, 152.02, 156.36. Anal. Calcd for $C_{36}H_{59}N_7O_6Si_2$: C, 58.27; H, 8.01; N, 13.21; O, 12.94; Si, 7.57. Found: C, 58.33; H, 8.05; N, 13.08.

Attempted hydrogenolysis of compound 19. *a. Trimethylsilyl iodide.* To a round-bottom flask of **19** (8 mg, 0.01 mmol), and dichloromethane (1 mL) and cooled to -78 °C (dry ice/acetone) was added trimethylsilyl iodide (TMSI) (1.8 μL, 0.013 mmol).[112] After 1.25 h the reaction was stopped, due to the formation of many byproducts, as judged by reversed-phase HPLC (method A). The reaction was abandoned at this point.

b. Catalytic hydrogenation using gaseous hydrogen. Pd black was freshly prepared by placing palladium(II) chloride in an atmosphere of hydrogen. The black solid was filtered and washed with copious amounts of absolute ethanol. The damp catalyst was added to fresh absolute ethanol and **19** (17 mg, 0.02

mmol), and the mixture was then placed in an atmosphere of hydrogen. The progress of the reaction was monitored by reversed-phase HPLC (method A). After 3 h, more freshly prepared Pd black (11 mg) was added, and the flask was re-evacuated and placed in an atmosphere of hydrogen. Negligible reaction, as judged by HPLC, had occurred after 3 h.

Additionally, the hydrogenolysis of **19** with Pearlman's catalyst[87] and 10% Pd on carbon was attempted; however, under similar conditions as above there was no reaction.

c. Catalytic hydrogenation using hydrogen-transfer. In a similar fashion, attempts were made to secure **20** under hydrogen-transfer conditions. Pd-poly(ethyleneimine) in methanol–formic acid,[113] palladium(II) acetate in ammonium formate–water–DMF,[114] and Pd black in cyclohexene[115] all failed to yield the desired amine **20**.

Synthesis of 8-[6-(*N*-Benzyloxycarbonylamino)hexylamino]-2′-deoxyadenosine (21). To a solution of **19** (1.8 g, 2.4 mmol) and acetic acid (0.14 mL, 2.4 mmol) in anhydrous THF (10 mL), which was cooled to 0 °C, was added 1 M tetrabutylammonium fluoride (TBAF) in THF (4.8 mL, 4.8 mmol). The reaction was monitored by reversed-phase HPLC (method A) and was complete after 30 min (the starting material was entirely consumed). In order to remove the fluoride byproducts from the reaction, the crude reaction mixture was passed through a pad of coarse silica gel in a fritted glass funnel under vacuum. The

pad was washed copiously with reagent grade THF (800 mL). The solvent was removed *in vacuo,* and the crude reaction mixture was adsorbed onto silica gel and subjected to column chromatography (solvent L → solvent B), which afforded **21** (0.9 g, 75%): t_R = 5.5 min (HPLC using method B); ^{1}H NMR (DMSO-d_6): δ 1.28 (bs, 4H), 1.36–1.39 (m, 2H), 1.41–1.43 (m, 2H), 1.95–1.20 (m, 1H), 2.64–2.68 (m, 1H), 2.97 (q, J = 6.45 Hz, 2H), 3.67 (bs, 2H), 3.88 (d, J = 1.93 Hz, 1H), 4.39 (bs, 1H), 4.99 (s, 2H), 5.27 (d, J = 3.82 Hz, 1H. Exchanges with D_2O), 5.74 (t, J = 5.28 Hz, 1H. Exchanges with D_2O), 6.35 (dd, J = 5.81 Hz, J = 9.27 Hz, 1H), 6.44 (s, 2H. Exchanges with D_2O), 6.93 (t, J = 5.30 Hz, 1H. Exchanges slowly with D_2O), 7.20 (t, J = 5.38 Hz, 1H), 7.32 (m, 5H), 8.119 (s, 1H); ^{13}C NMR (DMSO-d_6): δ 26.09, 26.19, 28.66, 29.38, 37.63, 40.22, 42.25, 61.62, 65.05, 71.38, 82.93, 116.98, 127.66, 128.29, 137.28, 148.37, 149.27, 151.09, 152.23, 156.06.

Preparation of *S*-(2-Methyl-1,4-naphthoquinon-3-yl)-β-mercaptopropionic Acid *N*-Hydroxysuccinimide (NHS) ester (3). Compound **3** was prepared from the acid[116] according to the procedure of Chatterjee and Rokita.[69]

Hydrogenolysis of 8-[6-(*N*-Benzyloxycarbonylamino)hexylamino]-2′-deoxyadenosine (21). The consumption of the starting material **21** was monitored by reversed-phase HPLC (method C). To a solution of Pearlman's catalyst[87] (12 mg) in absolute ethanol (2 mL) was added compound **21** (20 mg,

0.2 mmol). Air was removed from the flask, and the reaction mixture was placed under an atmosphere of hydrogen and stirred for 1 h. The reaction was judged to be complete, i.e., all of compound **21** was consumed, by reversed-phase HPLC. The mixture was filtered under vacuum through a pad of Celite, and the pad was washed with absolute ethanol (ca. 75 mL) and dichloromethane (ca. 75 mL). The crude reaction mixture was evaporated to dryness *in vacuo* and co-evaporated with anhydrous pyridine (3 × 10 mL). The white solid **2** was dried *in vacuo* (14 mg, 94%): t_R = 4.25 min (HPLC using method C); ^{1}H NMR (250.13 MHz, DMSO-d_6): δ 1.20–1.40 (m, 8H), 1.59 (m, 2H), 2.06–2.11 (m, 1H), 2.55–2.70 (m, 1H), 3.71 (s, 2H), 3.98 (s, 1H), 4.46 (d, J = 5.37 Hz, 1H), 6.37 (dd, J = 5.81 Hz, J = 9.27 Hz, 1H), 6.51 (s, 2H. Exchanges rapidly with D_2O), 7.00 (t, J = 5.30 Hz, 1H. Rapidly exchanges with D_2O), 7.96 (s, 1H); ^{13}C NMR (62.9 MHz, DMSO-d_6): δ 25.98, 26.26, 28.7, 33.1, 37.65, 41.38, 42.10, 61.49, 71.35, 82.90, 87.4, 116.98, 148.36, 149.27, 151.08, 152.22. FABMS (*m / z*): $[M + H]^+$ calcd for $C_{16}H_{27}N_7O_3$, 366.22; found, 366.24.

Formation of the NQ–2′-Deoxyadenosine conjugate (1). In order to prevent the invaluable **2** from deteriorating,[117] the compound was not isolated, but directly used after the co-evaporation with pyridine. A five-fold scale-up of the above procedure afforded **2** was produced according to the above procedure (assuming 100% conversion: 73 mg). To a solution of a compound **2** (73 mg, 0.2 mmol) in anhydrous DMF, compound **3**[69] (75 mg, 0.2 mmol) was added at RT.

After 50 min, the reaction was stopped. The solvent was removed *in vacuo* and the crude reaction mixture was adsorbed onto silica gel. The pad of silica was subjected to column chromatography (solvent B), which afforded in a bright-yellow amorphous solid (70 mg, 62%): ^{1}H NMR (DMSO-d_6): δ 1.22–1.39 (overlapping resonances, 7H), 1.51–1.56 (m, 2H), 1.96 (dd, J = 5.77, 12.73 Hz, 1H), 2.21 (s, 3H), 2.36 (t, J = 6.7 Hz, 2H), 2.62–2.69 (m, 1H), 3.63 (bs, 2H), 3.88 bs, 1H. Exchanges with D_2O), 4.39 (bs, 1H. Exchanges with D_2O), 5.72 (t, J = 4.83 Hz, 1H. Slowly exchanges with D_2O), 6.34 (dd, J = 5.83 Hz, J = 9.28 Hz, 1H), 6.44 (bs, 2H. Exchanges with D_2O), 6.92 (t, J = 5.28 Hz, 1H. Slow exchange with D_2O), 7.79–7.84 (m, 2H), 7.87 (s, 1H), 7.97–8.01 (m, 2H). Other protons are obscured after irradiation of the HOD peak. ESIMS: Calcd for $C_{30}H_{37}N_7O_6S$, (623.25); found $[M + H]^+$ 624.3.

Preparation of 11-Aminoundecanol (11). To a solution of 11-aminoundecanoic acid, (20.0 g, 0.10 mol) in anhydrous tetrahydrofuran (40 mL) was added boron trifluoride etherate (12.2 mL, 0.10 mol) under argon at room temperature. The reaction mixture was then heated to reflux before adding 10 M borane·methyl sulfide (10.9 mL, 0.11 mol) dropwise over 30 min. The reaction mixture was allowed to reflux for 20 h, at the end of which time it was cooled to 0 °C and quenched with methanol (20 mL). The clear solution was then evaporated to dryness under high vacuum to yield a white foam that was then refluxed in a 6 M sodium hydroxide solution for 4 h, during which time the

suspension dissolved on heating. Potassium carbonate was then added to saturation, and the solution was cooled (0 °C), filtered through a sintered glass funnel, and washed with water to remove excess potassium carbonate. The white solid remaining was dissolved in chloroform and washed with water (100 mL) and brine (3 × 100 mL). The organic layers were combined, dried (Na_2SO_4), and evaporated to dryness to afford a white solid (18.2 g, 98%): mp 76–79 °C (lit.[73] 71–73 °C; methanol–water); ^{1}H NMR (250 MHz, $CDCl_3$): δ 3.62 (2 H, t, *J* = 6.6 Hz, CH_2-NH_2), 2.68 (2 H, t, *J* = 6.7, CH_2-OH), 1.55–1.28 (21 H, M, -CH_2, -OH, NH_2); ^{13}C NMR (62.9 MHz, $CDCl_3$): δ 62.83, 42.24, 33.82, 32.84, 29.55, 29.47, 26.86, 25.75. Anal. Calcd for $C_{11}H_{25}NO$: C, 70.53; H, 13.45; N, 7.48. Found: C, 70.51; H, 13.41; N, 7.43.

Preparation of 11-(*N*-Benzyloxycarbonylamino)undecanol (12). To a stirred solution of **11** (16.0 g, 0.09 mol) in chloroform (125 mL) was added 4 M sodium hydroxide (125 mL). The resulting two-phase mixture was then cooled to 0 °C, and benzyl chloroformate (16 mL, 0.11 mol) and 4 N sodium hydroxide (20 mL) were added alternatively in portions over 40 min, all the while maintaining the temperature at 0 °C. After the addition, the reaction mixture was warmed to room temperature and stirred for 12 h. The mixture was then separated, and the aqueous phase was extracted with chloroform (4 × 75 mL). The combined organic layers were then washed with brine, dried (Na_2SO_4), and evaporated to dryness. The resulting white solid was subjected to flash column

chromatography (solvent A). The resulting white amorphous product was crystallized from ethyl acetate–hexanes to yield a white solid (10.38 g, 38%): mp 71–73 °C; ^{1}H NMR (250 MHz, $CDCl_3$): δ 7.35 (5 H, M, Ar-**H**), 5.09 (2 H, s, CH_2-Ar), 4.74 (1 H, br s, **NH**), 3.64 (2 H, t, *J* = 6.53, CH_2-OH), 3.18 (2 H, q, *J* = 6.5, *J* = 6.6, CH_2-NH), 1.54 (4 H, M, -OH, -CH_2), 1.27 (15 H, s, -CH_2). Anal. Calcd for $C_{19}H_{31}NO_2$: C, 70.99; H, 9.72; N, 4.36. Found C, 70.79; H, 9.81; N, 4.30

Preparation of 11-(*N*-Benyloxycarbonylamino)-1(-*O*-methylsufonyl) undecanol (13). To a cooled solution of **12** (11.8 g, 0.04 mol) in anhydrous dichloromethane (100 mL) was added triethylamine (25.5 mL, 0.18 mol). After 10 min of stirring, methanesulfonyl chloride (3.7 mL, 0.05 mol) was added dropwise over 20 min, under argon, and the temperature was maintained at 0 °C. The reaction mixture was allowed to warm to room temperature and stir for 12 h. The reaction mixture was then poured onto water (100 mL) and extracted with ethyl acetate (3 × 50 mL). The organic layer was then dried ($MgSO_4$) and evaporated to dryness. The resulting creamy white solid was passed through a silica gel column, by elution with solvent system G. On collecting the fractions containing product, there were still traces of impurity. The solid was then triturated in hexanes and dried overnight in a vacuum oven to afford a white solid (9.93 g, 68%): mp 70–73 °C; ^{1}H NMR (250 MHz, $CDCl_3$): δ 7.73 (5 H, s, Ar-**H**), 5.09 (2 H, s, Ar-CH_2), 4.73 (1 H, br s, **NH**), 4.22 (2 H, t, *J* = 6.5, S-OCH_2), 3.18 (2 H, q, *J* = 6.5, *J* = 6.4, NH-CH_2), 3.00 (3 H, s, CH_3), 1.75 (2 H, p, *J* = 6.6, *J* = 6.8,

O-CH_2CH_2), 1.49–1.27 (16 H, M, CH_2); ^{13}C NMR (62.9 MHz, $CDCl_3$): δ 156.36, 136.67, 128.47, 128.04, 70.13, 66.54, 41.09, 37.34, 29.94, 29.38, 29.32, 29.17, 29.09, 28.94, 26.66, 25.36. Anal. Calcd for $C_{20}H_{33}NO_5S$: C, 60.12; H, 8.32; N,3.51; S, 8.03. Found: C, 60.12; H, 8.39; N, 3.52; S, 8.08.

Preparation of 1-Azido-11-(*N*-benzyloxycarbonylamino)undecane (14). To a cooled solution of **13** (9.93 g, 0.025 mol) in dry DMF (90 mL) was added lithium azide (3.0 g, 0.062 mol). The reaction mixture was then allowed to warm to room temperature and stir for 10 h. The solution was then evaporated to dryness, and the resulting residue was dissolved in an ethyl acetate (200 mL) and water (75 mL). The aqueous layer was extracted with ethyl acetate (3 × 50 mL), and the combined organic extracts were dried ($MgSO_4$) and evaporated to dryness. The resulting yellow oil became a solid when dried *in vacuo*. The water was then removed by lyophilization to yield a white solid (8.29 g, 96%): mp 34–37 °C; ^1H NMR (250 MHz, $CDCl_3$): δ 7.35 (5 H, s, Ar-H), 5.09 (2 H, s, Ar-CH_2), 4.74 (1 H, br s, NH), 3.21 (4 H, M, CH_2N_3 and CH_2NH), 1.59 (2 H, t, J = 7.2, CH_2), 1.54–1.27 (16 H, M,CH_2); IR (KBr), Polystyrene standard ν_{max} 3350 cm^{-1} (NH), 3050 cm^{-1} (Ar), 2925 cm^{-1} (Aliphatic), 2125 cm^{-1}, (N_3), 1680 cm^{-1} (C=O). Anal. Calcd for $C_{19}H_{30}N_4O_2$: C, 65.87; H, 8.73; N, 16.17. Found: C, 66.96; H, 8.78; N, 16.07.

Preparation of 11-(*N*-Benzyloxycarbonylamino)undecylamine (15). To platinum(IV) oxide (9.7 mg, 0.043 mmol) was added absolute ethanol (5 mL).

To this suspension was added a solution of **14** (298 mg, 0.86 mmol) in absolute ethanol (5 mL). The reaction mixture was then carefully evacuated, and hydrogen was added and maintained at atmospheric pressure via a balloon. The mixture was then stirred for 12 h before filtering through Celite and evaporating to dryness. The resulting solid was then placed on a freeze dryer overnight (261 mg, 95%): ^{1}H NMR (250 MHz, $CDCl_3$): δ 7.35 (5 H, s, Ar-**H**), 5.09 (2 H, s, Ar-CH_2), 4.74 (1 H, br s, CO-**NH**), 3.18 (2 H, q, *J* = 6.7, *J* = 6.6, CONH-CH_2), 2.67 (2 H, t, *J* = 6.8, CH_2-NH_2), 1.46 (4 H, M, NH_2 and CH_2), 1.26 (16 H, s, CH_2).

D. Synthesis of 2′-*O*-Modified Nucleosides (Second-generation Electroactive Conjugates)[24]

The phosphoramidite **29** and the modified 2′-*O*-modified nucleosides (**24** and **30**) were prepared by Isis Pharmaceuticals, Inc., Carlsbad, CA.

Preparation of *S*-(2-Methyl-1,4-naphthoquinon-3-yl)-β-mercaptopropionic Acid Pentafluorophenyl Ester (23). To a solution of the *S*-(2-methyl-1,4-naphthoquinonyl-3)-β-mercaptopropionic acid (**22**)[116] (5 g, 18.1 mmol) in dichloromethane (40 mL) at 0 °C was added DCC (4.1 g, 19.9 mmol) and pentafluorophenol (3.7 g, 19.9 mmol, Fluka Chemical Co.). The suspension was allowed to warm up to room temperature overnight. The crude reaction

mixture was adsorbed onto silica gel and submitted to column chromatography (dichloromethane); compound **23** was obtained as an orange solid (6.9 g, 87%): ^{1}H NMR (250.13 MHz, $CDCl_3$): δ 2.34 (s, 3H), 3.12 (t, *J* = 6.8 Hz, 2H), 3.56 (t, *J* = 6.8 Hz, 2H), 7.68–7.73 (m, 2H), 8.01–8.08 (m, 2H); ^{13}C NMR (62.9 MHz, $CDCl_3$): δ 28.56, 28.56, 34.85, 126.51, 126.67, 131.86, 132.59, 133.34, 133.68, 144.93, 147.54, 167.51, 181.08, 181.83. Higher-order resonances associated with the pentafluoro moiety were observed between δ 120 and 150.

2′-*O*-[6-[2-Oxo-*S*-(2-Methyl-1,4-naphthoquinon-3-yl)-β-mercaptopropionyl]hexyl]-5′-*O*-(4,4′-dimethoxytrityl)thymidine (25). To a solution of **23** (1.0 g, 2.3 mmol) in dichloromethane (10 mL) at 0 °C was added triethylamine (0.32 mL, 2.3 mmol). Compound **24**[118,96] (1.0 g, 2.0 mmol) was then added. After 30 min, significant detritylation of the conjugate **25**—formation of the free nucleoside **26**—was observed; thus the reaction was stopped. The crude reaction mixture was then adsorbed onto silica gel and subjected to flash chromatography (dichloromethane → solvent E → solvent M), which afforded a bright-orange, glassy material **25** (1.1 g, 60%): ^{1}H NMR ($CDCl_3$): δ 1.39 (bm, 8H), 1.47 (m, 2H), 1.58–1.64 (m, 3H), 2.35 (s, 3H), 2.59 (t, *J* = 7.20 Hz, 2H), 2.80 (d, *J* = 7.2 Hz, 1H), 3.23 (m, 2H), 3.41–3.46 (m, 3H), 3.53–3.67 (m, 2H), 3.79 (bs, 6H), 3.98 (dd, *J* = 3.60 Hz, *J* = 5.6 Hz, 1H), 5.97 (overlapping resonances, 2H), 6.83 (d, *J* = 8.80 Hz, 4H), 7.28–7.31 (m, 8H), 7.40 (d, *J* = 7.20 Hz, 2H), 7.63 (d, *J* = 0.80 Hz, 1H), 7.66–7.71 (m, 2H), 8.06–8.09 (m, 2H), 8.56 (s, 1H); ^{13}C NMR

($CDCl_3$): δ 11.68, 13.99, 15.21, 22.52, 25.33, 26.25, 29.16, 30.09, 31.45, 37.36, 39.28, 53.35, 55.11, 62.20, 69.08, 70.72, 81.97, 83.53, 86.79, 87.14, 111.06, 113.18, 126.40, 126.67, 127.03, 127.88, 128.07, 130.01, 131.86, 132.68, 133.26, 135.17, 135.29, 144.24, 146.24, 147.14, 150.43, 158.61, 164.03, 170.56, 181.20, 182.02. Anal. Calcd for $C_{51}H_{55}N_3O_{11}S{\cdot}0.25H_2O$: C, 65.94; H, 5.99; N, 4.50; S, 3.43. Found: C, 65.95; H, 6.05; N, 4.36; S, 3.27.

2′-*O*-[6-[2-Oxo-*S*-(2-Methyl-1,4-naphthoquinonyl-3)-β-mercaptopropionyl]hexyl]thymidine (26). Compound **25** (0.32 g, 0.37 mmol) was stirred with a 3% (v/v) dichloroacetic acid–dichloromethane (5 mL) for 10 min. The crude reaction mixture was subjected to flash chromatography (dichloromethane → solvent B) to afford a bright-yellow glassy material **26** (198 mg, 87%). Lyophilization with 1,4-dioxane afforded a bright-yellow solid: ^{1}H NMR (250.13 MHz, DMSO-d_6): δ 1.18–1.28 (m, 7H), 1.41–1.43 (m, 2H), 1.75 (s, 3H), 2.22 (s, 3H), 2.36 (t, J = 6.69 Hz, 2H), 2.87 (m, 2H), 3.26–3.67 (overlapping resonances and 1,4-dioxane, 15H), 2.84 (m, 2H), 4.08 (bd, J = 4.85 Hz, 1H), 5.02 (d, J = 5.73 Hz, 1H. Exchanges with D_2O), 5.15 (bs, 1H. Exchanges with D_2O), 5.82 (d, J = 5.25 Hz, 1H), 7.78–7.86 (m, overlaps with resonance due to the presence of residual $CHCl_3$, 4H), 7.95–8.02 (m, 2H), 11.30 (s, 1H. Exchanges with D_2O); ^{13}C NMR (62.9 MHz, DMSO-d_6): δ 12.21, 15.12, 25.04, 26.19, 28.95, 29.05, 29.60, 36.41, 38.13, 60.58, 68.37, 69.58, 79.13, 80.88, 85.05, 85.91, 109.34, 126.02, 126.44, 131.60, 133.72, 133.88, 136.05, 145.46,

147.04, 150.55, 163.68, 169.72, 180.52, 181.76. Anal. Calcd for $C_{30}H_{37}N_3O_9S \cdot 0.9H_2O$: C, 57.02; H, 6.19; N, 6.65; S, 5.07. Found: C, 57.06; H, 5.99; N, 6.50; S, 5.05.

Compatibility Testing of 2′-*O*-[6-[2-Oxo-*S*-(2-Methyl-1,4-naphthoquinon-3-yl)-β-mercaptopropionyl]hexyl]thymidine (26) with Solutions Used in an Automated ODN Synthesizer.[99] (Scheme 8) To three test tubes containing a solution of **26** (5 mg) in methanol, were added (a) detritylation solution (1 mL), (b) oxidation solution (1 mL), and (c) concd ammonia (1 mL). Five min after solutions (a) and (b) were added, the free nucleoside remained intact, i.e., observed as a bright-yellow solution. Addition of concd ammonia resulted in the immediate darkening of the solution and rapid decomposition of the nucleoside.

9,10-Anthraquinone-2-carboxylic Acid Pentafluorophenyl Ester (34). To a solution of the commercially available 9,10-anthraquinone-2-carboxylic acid (2.1 g, 7.9 mmol) in dichloromethane (50 mL) was added DCC (0.67 g, 4.3 mmol) and pentafluorophenol (0.90 g, 4.3 mmol, Fluka Chemical Co.) at 0 °C . The suspension was allowed to warm up to room temperature overnight. The crude reaction mixture was adsorbed onto silica gel and submitted to column chromatography (hexanes) to give compound **34** as a pale-yellow solid (1.25 g, 45%): mp 197–205 °C; R_f = 0.91 (solvent A); ^{1}H NMR ($CDCl_3$): δ 7.88 (m, 2H), 8.37 (m, 2H), 8.50 (d, 1H, J = 8.15 Hz), 8.58 (dd, 1H, J = 1.52 Hz, J = 8.09 Hz),

9.13 (d, 1H, J = 1.33 Hz); ^{19}F NMR ($CDCl_3$): δ -52.35 (d, 2F, J = 18.31 Hz), -57.23 (t, 1F, J = 21.98 Hz), -161.98 (dd, 2F, J = 18.31 Hz, J = 21.98 Hz); ^{13}C NMR ($CDCl_3$ + two drops of DMSO-d_6): δ 127.19, 127.69, 129.34, 131.59, 133.13, 133.72, 134.34, 134.84, 137.01, 160.92, 181.35, 181.68. Higher-order resonances associated with the pentafluoro moiety were observed between δ 120 and 150. Anal. Calcd for $C_{21}H_7F_5O_4$: C, 60.30; H, 1.69. Found: C, 60.23; H, 1.71.

2′-*O*-[6-[2-Oxo-(9,10-anthraquinon-2-yl)amino]hexyl]-5′-*O*-(4,4′-dimethoxytrityl)uridine (35). To a solution of **34** (1.0 g, 2.4 mmol) in dichloromethane (40 mL) at 0 °C was added pyridine (0.19 mL, 2.4 mmol). Compound **30**[118,96] (1.4 g, 2.2 mmol) was then added. After 50 min, the reaction mixture was allowed to warm up to room temperature and stir for a further 3 h. The crude reaction mixture was then adsorbed onto silica gel and subjected to flash chromatography (solvent C), which afforded a pale-yellow, glassy material **35** (1.6 g, 83%): R_f = 0.44 (solvent B) ; ^{1}H NMR (DMSO-d_6): δ 1.34 (bm, 4H), 1.54 (bm, 4H), 3.07–3.50 (bm, 3H. Obscured by the H_2O signal), 3.50–3.67 (overlapping resonances, 3H), 3.71 (s, 6H), 3.98 (bs, 1H), 3.91 (bs, 1H), 4.18 (t, 1H, J = 5.23 Hz), 5.11 (bs, 1H. Exchanges with D_2O), 5.28 (d, 1H, J = 8.04 Hz), 5.81 (d, 1H, J = 3.15 Hz), 6.88 (d, 4H, J = 8.65 Hz), 7.11–7.50 (overlapping resonances, 9H), 7.73 (d, 1H, J = 8.04 Hz), 7.91 (dd, 2H, J = 3.36 Hz, J = 5.21 Hz), 8.04–8.41 (overlapping resonances, 4H), 8.61 (s, 1H), 8.88 (t, 1H, J = 4.80

Hz), 11.35 (bs, 1H, Exchanges with D_2O) ; ^{13}C NMR (DMSO-d_6): δ 26.28, 28.89, 29.04, 54.99, 62.58, 68.47, 69.82, 79.12, 80.91, 82.60, 85.87, 87.14, 101.43, 113.20, 125.42, 126.75, 126.96, 127.68, 127.84, 129.73, 132.73, 132.99, 134.39, 134.56, 135.05, 135.32, 139.50, 140.14, 144.60, 150.25, 158.10, 162.95, 164.44, 182.06. Anal. Calcd for $C_{51}H_{48}N_3O_{11}\cdot 2H_2O$: C, 66.95; H, 5.73; N, 4.59. Found: C, 66.96; H, 5.57; N, 4.44. ESIMS: Calcd for $C_{51}H_{48}N_3O_{11}$ (878.3); found $[M + Na]^+$ 902.1, $[M + K]^+$ 918.0.

2′-*O*-[6-[2-Oxo-(9,10-anthraquinon-2-yl)amino]hexyl]uridine (31). Compound **34** (0.33 g, 0.38 mmol) was stirred with a 3% (v/v) dichloroacetic acid–dichloromethane solution (7 mL) for 10 min. The crude reaction mixture was subjected to flash chromatography (solvent A → ethyl acetate, followed by dichloromethane → E) to afford a pale-yellow amorphous powder **31** (0.13 g, 60%). Lyophilization with 1,4-dioxane afforded an off-white, fluffy solid: R_f = 0.39 (solvent D); ^1H NMR (DMSO-d_6): δ 1.31 (bm, 4H), 1.53 (bm, 4H), 3.40–3.63 (overlapping resonances, 6H), 3.86 (dd, 2H, J = 2.28 Hz, J = 4.56 Hz), 4.06 (dd, 2H, J = 5.28 Hz, J = 5.9 Hz. The signal collapses to a triplet upon the addition of D_2O), 5.02 (d, 1H, J = 5.9 Hz. Exchanges with D_2O), 5.10 (t, 1H, J = 5.14 Hz. Exchanges with D_2O), 5.63 (dd, 1H, J = 2.06 Hz, J = 7.87 Hz), 7.76–8.10 (overlapping resonances, 3H), 8.13–8.43 (overlapping resonances, 4H), 8.64 (bd, 1H, J = 2.54 Hz), 8.90 (t, 1H, J = 5.08 Hz), 11.31 (s, 1H); ^{13}C NMR (DMSO-d_6): δ 25.32, 26.45, 29.07, 29.23, 60.74, 68.59, 69.92, 81.34, 85.31, 86.39,

101.98, 102.05, 125.80, 125.90, 127.02, 127.37, 133.24, 133.30, 139.79, 140.65, 140.77, 163.49, 165.04, 182.46. Anal. Calcd for $C_{30}H_{31}N_3O_9 \cdot 0.5C_4H_8O_2$ (1,4-dioxane): C, 61.83; H, 5.67; N, 6.76. Found: C, 61.87; H, 5.78; N, 6.60.

2′-*O*-[6-[2-Oxo-(9,10-anthraquinon-2-yl)amino]hexyl]-5′-*O*-(4,4′-dimethoxytrityl)uridine 3′-[2-cyanoethylbis(1-methylethyl)phosphoramidite] (29). Compound **35** (1.12 mmol, 0.98 g, dried *in vacuo* for 12 h) was dissolved in dichloromethane (ca. 1 mL) and maintained under a blanket of argon. To the solution was added diisopropylammoniumtetrazolide (1.13 mmol, 2.0 g) and 2-(cyanoethyl)-*N,N,N′,N′*-tetraisopropyl phosphorodiamidite (2.25 mmol, 0.14 g). After stirring overnight, the crude reaction mixture was purified by column chromatography (solvent F), which afforded the phosphoramidite **29** (0.750 g, 64%): R_f = 0.36 (solvent F); ^{31}P NMR ($CDCl_3$) δ 150.89. FABMS: Calcd for $C_{60}H_{66}N_5O_{12}P$ 1079.45; found $[M + H]^+$ 1080.11, $[M + Na]^+$ 1102.23.

E. 2′-*O*-Modified AQ–ODNs 27a–c and 28[118,24]

The work described in Section D.1 was performed by our collaborators at Isis Pharmaceuticals, Inc., Carlsbad, CA. The experiments described in Sections D.3 and D.4 were conducted in the laboratories of Dr. James Q. Chambers, University of Tennessee, Knoxville, TN.

1. Synthesis and Characterization. All of the AQ–ODNs were synthesized (2 μmol scale)—at least two batches were prepared of each modified ODN—using standard instrument chemistry with the exception of the step to incorporate the modified uridine moiety. This was accomplished by coupling the growing oligomer twice per cycle (5 min each cycle) utilizing an acetonitrile solution of phosphoramidite **29** (0.08–0.1 M). At the end of the synthetic sequence, the final DMT group was left intact. After treatment with ammonium hydroxide (28–30%) for ca. 16 h at 55 °C, the CPG was removed by filtration through a Gelman 0.45 μm nylon acrodisc syringe filter (Gelman Sciences, Ann Arbor, MI). The crude ODNs were purified employing reversed-phase HPLC (method A). Final detritylation was accomplished with acetic acid (80%) for ca. 30 min. The trityl residues and excess salt were removed by passing the AQ-ODNs through a column of Sephadex G-25 (Sigma, St. Louis, MO). Analytical details of AQ–ODNs were as follows:

5′-d(AU*G CAT TCT GCC CCC AAG AG)-3′ (27a). Analytical data for **27a**: t_R = 21.77 min (HPLC using method E); t_R = 4.12 min (CGE using method A). ESIMS: Calcd for $C_{213}H_{262}N_{75}O_{121}P_{19}$: *m/z* 6397.4; found: *m/z* 6398.8.

5′-d(ATG CAT TCU* GCC CCC AAG AG)-3′ (27b). Analytical data for **27b**: t_R = 19.97 min (HPLC using method E); t_R = 5.89 min (CGE using method A). ESIMS: Calcd for $C_{213}H_{262}N_{75}O_{121}P_{19}$: *m/z* 6397.4; found: *m/z* 6398.6.

5′-d(AU*G CAT TCU* GCC CCC AAG AG)-3′ (27c). Analytical data for **27c**: t_R = 22.84 min (HPLC using method E); t_R = 8.16 min (CGE using method A). ESIMS: Calcd for $C_{233}H_{279}N_{76}O_{125}P_{19}$: *m/z* 6732.7; found: *m/z* 6732.9.

5′-d(GAU*CT)-3′ (28). Analytical data for **28**: t_R = 34.72 min (HPLC using method E); t_R = 7.98 min (CGE using method A). ^{1}H NMR (D_2O): δ 5.84–5.88 (overlapping resonances, 3H), 5.98 (d, 1H, *J* = 7.55 Hz), 6.13 (d, 1H, *J* = 6.45 Hz), 6.10–6.30 (overlapping resonances, 3H), 7.53 (d, 1H, *J* = 6.59 Hz), 7.74 (s, 1H), 7.80–7.90 (overlapping resonances, 4H), 8.07–8.15 (overlapping resonances, 3H), 8.20 (s, 1H), 8.24 (s, 1H), 8.34 (d, 1H, *J* = 1.78 Hz); ^{31}P NMR (D_2O): δ −0.32, −0.28, −0.11, 0.11; ESIMS: Calcd for $C_{69}H_{80}N_{18}O_{33}P_4$: *m/z* 1813.4; found: *m/z* 1813.2.

2. Determination of the Concentration of the Novel ODNs 27a–c and 28. In order to accurately determine the concentration of the AQ–ODNs **27a–c**, a stock solution of 20–60 ODs of each of the modified oligomer (dependent on the amount available) was prepared in sterile, deionized water (10 mL). The contribution of AQ to the ϵ_{260} for the modified AQ–ODN **27a** was added to ϵ_{260} for 5′-AUG CAT TCT GCC CCC AAG AG-3′, which was calculated by the nearest-neighbor effect.[119] The ϵ_{260} of AQ was determined to be 26 400 M^{-1} cm^{-1} by subtracting the ϵ_{260} of uridine from the ϵ_{260} of monomer **31**. Thus the ϵ_{260} of **27a** was determined to be 214 000 M^{-1} cm^{-1} (260 nm). By measuring the

absorbance at 260 nm, the concentration of the stock solution of **27a** was found to be 2.09×10^{-5} M. Similarly, the concentrations of the stock solutions of **32** (ε_{260} 194 000 M^{-1} cm^{-1}), and **33** (ε_{260} 188 000 M^{-1} cm^{-1}) were determined to be 2.04×10^{-5} M and 2.83×10^{-5} M, respectively.

3. Electrochemical Studies.[24] Cyclic voltammetry (CV) was carried out using aqueous buffers containing NaCl at various concentrations. For the simultaneous electrochemical–hybridization studies, experiments were performed in 0.1 M phosphate buffer (pH ca. 7) containing 0.05 M NaCl and 5 mM EDTA. Before measurements were taken, solutions were purged with purified nitrogen that had been passed through a column containing Mn(II) oxide dispersed on a vermiculite support to remove traces of oxygen.

4. Hybridization Conditions. Hybridization solutions were prepared by mixing equimolar aliquots (ca. 50 μL) of the stock solutions with 2–3 mL of buffer solution. Temperature profiles were obtained by heating the cell to 90°C for 10 min, followed by slow cooling in 1°C increments while measuring the absorbance at 260 nm. Once confirmation of duplex formation was seen, CV was performed on the solution as described above. Initial experiments used either pH 7.15 BR buffer solution containing 0.25 M NaCl and 3.6 mM EDTA or 0.01 M ammonium acetate–0.001 M ammonium chloride buffer. The ammonium acetate buffers

were chosen to mimic the conditions of Bayer et al.,[120] who detected duplexes in solution using electrospray mass spectroscopy (albeit at higher concentrations). The former experiments were performed in 0.1 M phosphate buffer (pH ca. 7) containing 0.05 M NaCl and 5 mM EDTA. In the latter procedure, melting curves were obtained on solutions before exposure to the HMDE conditions, and the voltammetric behavior was compared to that of an identical solution that was not thermally cycled. Spurious voltammetric waves were obtained for solutions of **27a** and **32** that had been exposed to the HMDE conditions before thermal cycling.

V. CONCLUSIONS

- 2′-*O*-modified nucleosides and phosphoramidites thereof are more easily accessible than their C-8 counterparts.

- Programing the modification of the electroactive AQ–oligodeoxynucleotides in any position along its backbone is readily achieved using standard phosphoramidite chemistry.[24]

- Hanging drop mercury electrodes (HDMEs) are unsuitable electrodes as a means of detecting nucleic acid hybridization[121]

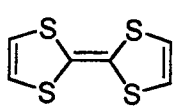
- The series of AQ–oligos produced in collaboration with Isis Pharmaceuticals, Carlsbad, CA are potentially novel electrochemical probes for nucleic acid hybridization.

VI. FURTHER WORK

- Before preparing any novel electroactive second-generation bioconjugates, which bear different EATs to the ones discussed herein, one needs to establish that the integrity of the reporter group will survive the conditions experienced in the synthesis of ODNs (see Scheme 8). If the reporter group is unstable under these conditions, post-derivatization of the ODN with NHS esters of the EAT is a viable alternative.

- Preparation of thiol-modified ODNs that bear the AQ tag: The thiol tether at the 5′-terminus permits modification of gold electrodes.[122]

- Attach a donor molecule, such as tetrathiafulvalene[123] to the backbone of an ODN using the already established



Tetrathiafulvalene (TTF)

methodology by Isis Pharmaceuticals.[94-97,24]

- In order to examine the orientation of the EAT in these modified electroactive ODNs, prepare a series of ODNs with different linker arms of different lengths.

- Attach a donor and acceptor to the backbone of the ODN to study the conductivity of DNA,[124,125] and investigate the utility as a ODN probe for hybridization.

- Explore the use of these 2′-*O*-modified ribonucleosides as substrates in the synthesis of ODNs via the PCR methodology.[126] Naturally, the requisite 5′-*O*-triphosphate would have to be synthesized.

- Preparation of AQ–peptide nucleic acids (PNAs), which are considerably easier to synthesize.[127,128]

REFERENCES AND NOTES

1. Blackburn, G. M.; Gait, M. J. *Nucleic Acids in Chemistry and Biology*; 1st ed.; IRL Press: New York, 1990.

2. Excerpts are from a thesis, which focused on the synthesis of C-8 modified nucleoside that bore a undecylamino tether, produced by Ronnie Palin, which was submitted in part towards a BSc Hons. degree, Nottingham Trent University, Nottingham, UK. **1994**.

3. Excerpts from a thesis, which focused on the synthesis of C-8 modified nucleosides that bore a hexylamino tether, produced by Edward Rippon, which was submitted in part towards a BSc Hons. degree, Nottingham Trent University, Nottingham, UK. **1995**.

4. Khorana, H. G. Total Synthesis of a Gene. *Science* **1979**, *203*, 614–625.

5. Alberts, B.; Bray, D.; Lewis, J.; Raff, M.; Roberts, K.; Watson, J. D. *Molecular Biology of the Cell*; Garland Publishing, Inc.: New York, 1983.

6. Mullis, K. B.; Faloona, F. A. Specific synthesis of DNA in vitro via a polymerase-catalyzed chain reaction. *Methods Enzymol.* **1987**, *155*, 335–350.

7. Panzara, M. A.; Gussoni, E.; Steinman, L.; Oksenberg, J. R. Analysis of the T cell repertoire using the PCR and specific oligonucleotide primers. *BioTechniques* **1992**, *12*, 728–735.

8. Caruthers, M. H.; Barone, A. D.; Beaucage, S. L.; Dodds, D. R.; Fisher, E. F.; McBride, L. J.; Matteucci, M.; Stabinsky, Z.; Tang, J. Y. Chemical synthesis of deoxyoligonucleotides by the phosphoramidite method. *Methods Enzymol.* **1987**, *154*, 287–313.

9. Oksenberg, J. R.; Panzara, M. A.; Steinman, L. *The Polymerase Chain Reaction and the Analysis of the T Cell Repertoire*; R. G. Landes Company: Austin, TX, 1992.

10. Caruthers, M. H.; Beaton, G.; Wu, J. V.; Wiesler, W. Chemical synthesis of deoxyoligonucleotides and deoxyoligonucleotide analogs. *Methods Enzymol.* **1992**, *211*, 3–20.

11. Merrifield, B. Solid phase synthesis [of proteins]. *Biosci. Rep.* **1985**, *5*, 353–376.

12. Merrifield, B. Solid phase synthesis. *Science* **1986**, *232*, 341–347.

13. Merrifield, B. Concept and early development of solid-phase peptide synthesis. *Methods Enzymol.* **1997**, *289*, 3–13.

14. Wetmur, J. G. DNA Probes: Applications of the Principles of Nucleic Acid Hybridization. *Crit. Rev. Biochem. Mol. Biol.* **1991**, *26*, 227–259.

15. Englisch, U.; Gauss, D. H. Chemically Modified Oligonucleotides as Probes and Inhibitors. *Angew. Chem., Int. Ed. Engl.* **1991**, *30*, 613–629, and references therein.

16. de Mesmaeker, A.; Häner, R.; Martin, P.; Moser, H. E. Antisense Oligonucleotides. *Acc. Chem. Res.* **1995**, *28*, 366–374.

17. Isis Pharmaceuticals, Inc., Carlsbad, CA Press Release. http://www.isip.com/press/press98/press0916.htm.

18. Rawls, R. L. Optimistic About Antisense. *Chem. Eng. News* **1997**, *June 2*, 35–39.

19. Kessler, C. *Nonradioactive Labeling and Detection of Biomolecules*; Springer-Verlag: New York, 1992.

20. Sarfati, S. R.; Pochet, S.; Guerreiro, C.; Namane, A.; Huynh Dinh, T.; Igolen, J. Synthesis of fluorescent or biotinylated nucleoside compounds. *Tetrahedron* **1987**, *43*, 3491–3498.

21. Huynh Dinh, T.; Sarfati, S.; Igolen, J.; Guesdon, J. L. Nucleic acid probes containing 2'-deoxyadenosine derivatives. Eur. Pat. Appl. 254646, 1988.

22. Singh, D.; Kumar, V.; Ganesh, K. N. Oligonucleotides, part 5: synthesis and fluorescence studies of DNA oligomers d(AT)5 containing adenines covalently linked at C-8 with dansyl fluorophore. *Nucleic Acids Res.* **1990**, *18*, 3339–3345.

23. Kessler, C.; Hoeltke, H. J.; Seibl, R.; Burg, J.; Muehlegger, K. Nonradioactive labeling and detection of nucleic acids. I. A novel DNA labeling and detection system based on digoxigenin: anti-digoxigenin ELISA principle (digoxigenin system). *Biol. Chem. Hoppe-Seyler* **1990**, *371*, 917–927.

24. Whittemore, N. A.; Mullenix, A. N.; Inamati, G. B.; Manoharan, M.; Cook, P. D.; Tuinman, A. T.; Baker, D. C.; Chambers, J. Q. Synthesis and Electrochemistry of Anthraquinone–Oligodeoxynucleotide Conjugates. *Bioconjugate Chem.* **1999**, *10*, 261–270.

25. Beaucage, S.; Iyer, R. P. The Functionalization of Oligonucleotides via Phopshoramidite Derivatives. *Tetrahedron* **1993**, *49*, 1925–1963.

26. Meinkoth, J.; Wahl, G. Hybrization of Nucleic Acids Immobilized on Solid Supports. *Anal. Biochem.* **1984**, *138*, 267–284.

27. Asseline, U.; Thoung, N. T.; Helene, C. Synthesis and properties of oligonucleotides covalently linked to intercalating agents. *New J. Chem.* **1997**, *21*, 5–17.

28. Thiel, A. J.; Frutos, A. G.; Jordan, C. E.; Corn, R. M.; Smith, L. M. In Situ Surface Plasmon Resonance Imaging Detection of DNA Hybridization to Oligonucleotide Arrays on Gold Surfaces. *Anal. Chem.* **1997**, *69*, 4948–4956.

29. Bard, A. J. New challenges in electrochemistry and electroanalysis. *Pure Appl. Chem.* **1992**, *64*, 185–192.

30. Palecek, E. Modern Polarographic (Voltammetric) Techniques in Biochemistry and Molecular Biology. In *Topics in Bioelectrochemistry and Bioenergetics*; Milazzo, G.; Wiley: New York, 1983; Vol. 5, pp 65–155.

31. Palecek, E. New Trends in Electrochemical Analysis of Nucleic Acids. *Bioelectrochem. Bioenergetics* **1988**, *20*, 179–194.

32. Hall, J. M.; Moore-Smith, J.; Bannister, J. V.; Higgins, I. J. An Electrochemical Method for Detection of Nucleic Acid Hybridisation. *Biochem. Mol. Biol. Int.* **1994**, *32*, 21.

33. Jacobson, K. B.; Arlinghus, H. F.; Schmitt, H. W.; Sachleben, R. A.; Brown, G. M.; Thonnard, N.; Sloop, F. V.; Foote, R. S.; Larimer, F. W.; et al. An Approach to the Use of Stable Isotopes for DNA Sequencing. *Genomics* **1991**, *9*, 51–59.

34. Sloop, F. V.; Brown, G. M.; Sachleben, R. A.; Garrity, M. L.; Elbert, J. E.; Jacobson, K. B. Metalloorganic Labels for DNA Sequencing and Mapping. *New J. Chem.* **1994**, *18*, 317.

35. Takenaka, S.; Uto, Y.; Kondo, H.; Ihara, T.; Takagi, M. Electrochemically Active DNA Probes: Detection of Target DNA Sequences at Femtomole Level by HPLC with Electrochemical Detection. *Anal. Biochem.* **1994**, *218*, 436.

36. Ihara, T.; Maruo, Y.; Takenaka, S.; Takagi, M. Ferrocene-oligonucleotide conjugates for electrochemical probing of DNA. *Nucleic Acids Res.* **1996**, *24*, 4273–4281.

37. Uto, Y.; Kondo, H.; Abe, M.; Suzuki, T.; Takenaka, S. Electrochemical analysis of DNA amplified by the polymerase chain reaction with a ferrocenylated oligonucleotide. *Anal. Biochem.* **1997**, *250*, 122–124.

38. Xu, X.-H.; Bard, A. J. Immobilization and Hybridization of DNA on an Aluminum(III) Alkanebisphosphonate Thin Film with Electrogenerated Chemiluminescent Detection. *J. Am. Chem. Soc.* **1995**, *117*, 2627.

39. Carter, M. T.; Rodriquez, M.; Bard, A. J. Voltammetric Studies of the Interaction of Metal Chelates with DNA. 2. Tris-Chelated Complexes of Cobalt(III) and Iron(II) with 1,10-Phenanthroline and 2,2 -Bipyridine. *J. Am. Chem. Soc.* **1989**, *111*, 8901.

40. Rodriguez, M.; Bard, A. J. Electrochemical Studies of the Interaction of Metal Chelates with DNA. 4. Voltammetric and Electrogenerated Chemiluminescent Studies of the Interaction of Tris(2,2 -bipyridine)osmium(II) with DNA. *Anal. Chem.* **1990**, *62*, 2658.

41. Welch, T. W.; Corbett, A. H.; Thorp, H. H. Electrochemical Determination of Nucleic Acid Diffusion Coefficients through Noncovalent Association of Redox-Active Probes. *J. Phys. Chem.* **1995**, *99*, 11757–11763.

42. Millan, K. M.; Saraullo, A.; Mikkelsen, S. R. Voltammetric DNA Biosensor for Cystic Fibrosis Based on a Modified Carbon Paste Electrode. *Anal. Chem.* **1994**, *66*, 2943.

43. Wang, J.; Rivas, G.; Parrado, C.; Cai, X.; Flair, M. N. Electrochemical biosensor for detecting DNA sequences from the pathogenic protozoan, *Cryptosporidium parvum*. *Talanta* **1997**, *44*, 2003–2010.

44. Wang, J.; Rivas, G.; Cai, X. H.; Dontha, N.; Shiraishi, H.; Luo, D. B.; Valera, F. S. Sequence-specific electrochemical biosensing of *M. tuberculosis* DNA. *Anal. Chim. Acta* **1997**, *337*, 41–48.

45. Zhao, Y.-D.; Pang, D.-W.; Wang, Z.-L.; Cheng, J.-K.; Qi, Y.-P. DNA-modified electrodes. Part 2. Electrochemical characterization of gold electrodes modified with DNA. *J. Electroanal. Chem.* **1997**, *431*, 203–209.

46. Hasshimoto, K.; Ito, K.; Ishimori, Y. Sequence-specific gene detection with a gold electrode modified with DNA probes and an electrochemically active dye. *Anal. Chem.* **1994**, *66*, 3830.

47. Liu, S.; Ye, J.; He, P.; Fang, Y. Voltammetric determination of sequence-specific DNA by electroactive intercalator on graphite electrode. *Anal. Chim. Acta* **1996**, *335*, 239.

48. Kelley, S. O.; Barton, J. K.; Jackson, N. M.; Hill, M. G. Electrochemistry of Methylene Blue Bound to a DNA-Modified Electrode. *Bioconjugate Chem.* **1997**, *8*, 31–37.

49. Palanti, S.; Marrazza, G.; Mascini, M. Electrochemical DNA probes. *Anal. Lett.* **1996**, *29*, 2309–2331.

50. Wang, J.; Rivas, G.; Luo, D.; Cai, X.; Valera, F. S.; Dontha, N. DNA-Modified Electrode for the Detection of Aromatic Amines. *Anal. Chem.* **1996**, *68*, 4365.

51. Johnston, D. H.; Glasgow, K. C.; Thorp, H. H. Electrochemical Measurement of the Solvent Accessibility of Nucleobases Using Electron Transfer between DNA and Metal Complexes. *J. Am. Chem. Soc.* **1995**, *117*, 8933–8938.

52. Johnston, D. H.; Thorp, H. H. Cyclic Voltammetry Studies of Polynucleotide Binding and Oxidation by Metal Complexes: Homogeneous Electron-Transfer Kinetics. *J. Phys. Chem.* **1996**, *100*, 13837–13843.

53. Napier, M. E.; Thorp, H. H. Modification of Electrodes with Dicarboxylate Self-Assembled Monolayers for Attachment and Detection of Nucleic Acids. *Langmuir* **1997**, *13*, 6342.

54. Napier, M. E.; Loomis, C. R.; Sistare, M. F.; Kim, J.; Eckhardt, A. E.; Thorp, H. H. Probing Biomolecule Recognition with Electron Transfer: Electrochemical Sensors for DNA Hybridization. *Bioconjugate Chem.* **1997**, *8*, 906–913.

55. Tohda, K.; Ameniya, S.; Umezawa, Y. Channel Mimetic Sensing Membranes for Nucleotides Based on Multitopic Hydrogen Bonding. *Isr. J. Chem.* **1997**, *37*, 267–275.

56. Korri-Youssoufi, H.; Garnier, F.; Srivastava, P.; Dodillot, P.; Yassar, A. Toward Bioelectronics: Specific DNA Recognition Based on an Oligonucleotide-Functionalized Polypyrrole. *J. Am. Chem. Soc.* **1997**, *119*, 7388–7389.

57. Chambers, J. Q. Electrochemistry of Quinones. In *The Chemistry of the Quinonoid Compounds (Part 2)*; 1st ed.; Patai, S., Ed.; The Chemistry of Functional Groups; John Wiley & Sons: New York, 1974, pp 737–791.

58. Ruth, J. L. Oligodeoxynucleotides with reporter groups attached to the base. In *Oligonucleotides and Analogues*; 1st ed.; Eckstein, F., Ed.; The Practical Approach Series; Oxford University Press: New York, 1991, pp 255–282.

59. Chan, V.; Graves, D.; Mckenzie, S. E. The Biophysics of DNA Hybridization with Immobilized Oligonucleotide Probes. *Biophys. J.* **1995**, *69*, 2243–2255.

60. Roduit, J.-P.; Shaw, J.; Chollet, A.; Chollet, A. Synthesis of Oligodeoxyribonucleotides Containing an Aliphatic Amino Linker Arm at Selected Adenine Bases and Derivatization with Biotin. *Nucleosides Nucleotides* **1987**, *6*, 349–352.

61. Sarfati, S. R.; Namane, A. Synthesis of Fluorosceinylated 2'-Deoxyadenosine. Mono-, Di-, and Triphosphate Derivatives. *Tetrahedron Lett.* **1990**, *31*, 2581–2584.

62. Pieles, U.; Sproat, B. S.; Neuner, P.; Cramer, F. Preparation of a novel psoralen containing deoxyadenosine building block for the facile solid phase synthesis of psoralen-modified oligonucleotides for a sequence specific crosslink to a given target sequence. *Nucleic Acids Res.* **1989**, *22*, 8967–8978.

63. Laayoun, A.; Decout, J.-L.; Lhomme, J. Hydrolysis of 2'-Deoxypurine Nucleosides. The Effect of Substitution at the C-8 Position. *Tetrahedron Lett.* **1994**, *35*, 4989–4990.

64. Laayoun, A.; Decout, J.-L.; Defrancq, E.; Lhomme, J. Hydrolysis of Oligonucleotides Containing 8-Substituted Purine Nucleosides. A New Route for Preparing Abasic Oligodeoxynucleotides. *Tetrahedron Lett.* **1994**, *35*, 4991–4994.

65. Ikehara, M.; Kaneko, M. Studies of Nucleosides and Nucleotides. XLIV. Purine Cyclonuceosides. (2). Synthesis of Cyclonucleosides having 8,3′-*O*- and -*S*-Anhydro Linkage derived from 2′-Deoxyadenosine. *Chem. Pharm. Bull.* **1970**, *18*, 2441–2446.

66. Ikehara, M.; Ohtsuka, E.; Uesugi, S. Studies of Nucleosides and Nucleotides. LVI. A Versatile Method for the Synthesis of 8-Mercaptoadenosine Nucleotides. *Chem. Pharm. Bull.* **1973**, *21*, 444–445.

67. Scriven, E. F.; Turnbull, K. Azides: Their Preparation and Synthetic Uses. *Chem. Rev.* **1988**, *88*, 298–368, and references therein.

68. Greene, T. W.; Wuts, P. G. M. Protection for the amino group. In *Protective Groups in Organic Synthesis*; 2nd ed.; John Wiley & Sons: New York, 1991, pp 309–405.

69. Chatterjee, M.; Rokita, S. E. The Role of a Quinone Methide in the Sequence Specific Alkylation of DNA. *J. Am. Chem. Soc.* **1994**, *116*, 1690–1697.

70. Warren, S. *Organic Synthesis, the Disconnection Approach*; 1st ed.; John Wiley & Sons: New York, 1991.

71. Atwell, G. J.; Denny, W. A. Monoprotection of α,ω-alkanediamines with the *N*-benzyloxycarbonyl group. *Synthesis* **1984**, 1032–1033.

72. Ponpipom, M. M.; Rupprecht, K. M. Methyl β-glycosides of *N*-acetyl-6-*O*-(ω-aminoacyl)muramyl-L-alanyl-D-isoglutamines, and their conjugates with meningococcal group C polysaccharide. *Carbohydr. Res.* **1983**, *113*, 45–56.

73. Dickman, D. A.; Meyers, A. I.; Smith, G. A.; Gawley, R. E. Reduction of α-Amino Acids: L-Valinol. *Org. Synth., Coll. Vol. VII* **1990**, 530–533.

74. For an alternative procedure, see McKay et al. *Can. J. Chem.* **1958**, *147*, 149.

75. McMurry, J. *Organic Chemistry*; 1st ed.; Brooks/Cole Publishing Company: Monterey, CA, 1984.

76. Muramatsu, T.; Egami, F. α-Mannosidase and β-mannosidase from the liver of *Turbo cortunus*. Purification, properties, and application in carbohydrate research. *J. Biochem. (Tokyo)* **1967**, *62*, 700–709.

77. Chipowsky, S.; Lee, Y. C. Synthesis of 1-thioaldosides having an amino group at the aglycon terminal. *Carbohydr. Res.* **1973**, *31*, 339–346.

78. Anteunis, M. J. O.; Becu, C. Chemoselective *N*-acylations of amino alcohols mediated by trimethylsilyl cyanide. *Bull. Soc. Chim. Belg.* **1987**, *96*, 555–556.

79. Fernandez, S.; Menendez, E.; Gotor, V. Oxime esters as acylating agents in the aminolysis reaction. A simple and chemoselective method for the preparation of amides from amino alcohols. *Synthesis* **1991**, 713–716.

80. Lee, H. H.; Palmer, B. D.; Baguley, B. C.; Chin, M.; McFadyen, W. D.; Wickham, G.; Thorsbourne-Palmer, D.; Wakelin, L. P. G.; Denny, W. A. DNA-directed alkylating agents. 5. Acridinecarboxamide derivatives of (1,2-diaminoethane)dichloroplatinum(II). *J. Med. Chem.* **1992**, *35*, 2983–2987.

81. Nicolaou, K. C.; Koide, K.; Bunnage, M. E. Total synthesis of balanol and designed analogs. *Chem.—Eur. J.* **1995**, *1*, 454–466.

82. Shaw, K. J.; Luly, J. R.; Rapoport, H. Routes to mitomycins. Chirospecific synthesis of aziridinomitosenes. *J. Org. Chem.* **1985**, *50*, 4515–4523.

83. Markiewicz, W. T. Tetraisopropyldisiloxane-1,3-diyl, a Group for Simultaneous protection of 3′- and 5′-Hydroxy Functions of Nucleosides. *J. Chem. Res.* **1979**, *1*, 24–25.

84. Markiewicz, W. T.; Padyukova, N. S.; Samek, Z.; Smrt, J. The Reaction of 1,3-Dichloro-1,1,3,3-tetraisopropyldisiloxane with Cytosine Arabinoside and 1-(6-Deoxy-α-L-talofuranosyl)uracil. *Collect. Czech. Chem. Commun.* **1980**, *45*, 1860–1865.

85. Markiewicz, W. T.; Bartoszuk, A. Transformatin of Rings Containing Tetraisopropyldisiloxane-1,3-diyl Group—an Equlibrium Proces Enlarging the Scope of Applications of the Group. *Bull. Pol. Acad. Sci., Chem.* **1984**, *32*, 453–461.

86. Gmeiner, W. H.; Pon, R. T.; Lown, J. W. Synthesis, annealing properties, fluorine-19 NMR characterization, and detection limits of a trifluorothymidine-labeled antisense oligodeoxyribonucleotide 21-mer. *J. Org. Chem.* **1991**, *56*, 3602–3608.

87. Fieser, M. *Fieser and Fieser's Reagents for Organic Synthesis*, John Wiley & Sons, Inc.: New York, 1992; Vol. 16.

88. This experiment was conducted by Kris Scaboo in the laboratories of Prof. James Q. Chambers, Department of Chemistry, University of Tennessee.

89. Whittemore, N. A.; Chambers, J. Q.; Baker, D. C.; Tuinman, A. Synthesis of Novel Phosphoramidites: Precursors for the Construction of Novel Oligodeoxynucleotides Bearing Electrochemically Active Groups. In *Abstracts of Papers,* 212th National Meeting of the American Chemical Society, Orlando, FL, August 25–28, 1996; American Chemical Society: Washington DC, 1996; CARB 012.

90. P. Dan Cook, Isis Pharmaceuticals, Inc., Carlsbad, CA, personal communication.

91. Meyer, R. B., Jr. Incorporation of Modified Bases into Oligonucleotides. In *Protocols for Oligonucleotide Conjugates: Synthesis and Analytical Techniques*; 1st ed.; Agrawal, S., Ed.; Methods in Molecular Biology 26; Humana Press: Totowa: NJ, 1994; Vol. 26, pp 73–91.

92. For details on antisense technology, refer to the extensive review on the subject: ref 16, and references cited therein.

93. Freier, S. M.; Altmann, K.-H. The ups and downs of nucleic acid duplex stability: structure-stability studies on chemically-modified DNA:RNA duplexes. *Nucleic Acids Res.* **1997**, *25*, 4429.

94. Manoharan, M.; Guinosso, C. J.; Cook, P. D. Novel Functionalization of the Sugar Moiety of Nucleic Acids for Multiple Labeling in the Minor Groove. *Tetrahedron Lett.* **1991**, *32*, 7171–7174.

95. Manoharan, M.; Johnson, L. K.; Tivel, K. L.; Springer, R. H.; Cook, P. D. Introduction of a Lipophilic Thioether Tether in the Minor Groove of Nucleic Acids for Antisense Applications. *Bioorg. Med. Chem. Lett.* **1993**, *3*, 2765–2770.

96. Manoharan, M.; Tivel, K. L.; Andrade, L. K.; Cook, P. D. 2′-*O*- and 3′-*O*-Pyrimidine Aminotether-Containing Oligonucleotides: Synthesis and Conjugation Chemistry. *Tetrahedron Lett.* **1995**, *36*, 3647–3650.

97. Manoharan, M.; Tivel, K. L.; Cook, P. D. Lipidic Nucleic Acids. *Tetrahedron Lett.* **1995**, *36*, 3651–3654.

98. The 2′-*O*-modified thymidine bearing a "free" amino group at the end of a hexylamino tether was provided by Isis Pharmaceuticals, Inc., Carlsbad, CA.

99. Atkinson, T.; Smith, M. Solid-Phase Synthesis of Oligodeoxynucleotides by the Phosphite-triester Method. In *Oligonucleotide Synthesis: A Practical Approach*; Gait, M. J., Ed.; IRL Press: Washington, D.C., 1984, pp 35–81.

100. Finley, K. T. The addition and substitution chemistry of quinones. In *The Chemistry of the Quinonoid Compounds (Part 2)*; 1st ed.; Patai, S., Ed.; The Chemistry of Functional Groups; John Wiley & Sons: New York, 1974, pp 877–1144.

101. Wagner, H.-U.; Gompper, R. Quninone methides. In *The Chemistry of the Quinonoid Compounds (Part 2)*; 1st ed.; Patai, S., Ed.; The Chemistry of Functional Groups; John Wiley & Sons: New York, 1974, pp 1145–1178.

102. Mori, K.; Subasinghe, C.; Cohen, J. S. Oligodeoxynucleotide analogs with 5′-linked anthraquinone. *FEBS Lett.* **1989**, *249*, 213–218.

103. Yamana, K.; Nishijima, Y.; Ikeda, T.; Gokota, T.; Ozaki, H.; Nakano, H.; Sangen, O.; Shimidzu, T. Synthesis and Interactive Propeties of an Oligonucleotide with Anthraquinone at the Sugar Fragment. *Bioconjugate Chem.* **1990**, *1*, 319–324.

104. Keller, T. H.; Häner, R. Synthesis and hybridization properties of oligonucleotides containing 2′-O-modified ribonucleotides. *Nucleic Acids Res.* **1993**, *21*, 4499–4505.

105. Deshmukh, H. M.; Joglekar, S. P.; Broom, A. D. Self-Complementary Oligodeoxyribonucleotides Containing 2′-*O*-(Anthraquinone-2-methyl)adenosine. *Bioconjugate Chem.* **1995**, *6*, 578–586.

106. Kang, H.; Rokita, S. E. Site-specific and photo-induced alkylation of DNA by a dimethylanthraquinone–oligodeoxynucleotide conjugate. *Nucleic Acids Res.* **1996**, *24*, 3896–3902.

107. Gasper, S. M.; Schuster, G. B. Intramolecular Photoinduced Electron Transfer to Anthraquinone Linked to Duplex DNA: The Effect of Gaps and Traps on Long-Range Radical Cation Migration. *J. Am. Chem. Soc.* **1997**, *119*, 12762–12771.

108. For a more detailed discussion on the electrochemical behavior of the AQ–conjugates, refer to ref 24.

109. Schaumberg, J. P.; Hokanson, G. C.; French, J. C.; Smal, E.; Baker, D. C. 2'-Chloropentostatin, a New Inhibitor of Adenosine Deaminase. *J. Org. Chem.* **1985**, *50*, 1651–1656.

110. A 0.2% solution of ninhydrin in 95% ethanol was prepared and used as visualization agent.

111. Wagner, G. J.; Chambers, J. Q. Electrochemistry of Covalently Mercurated Uridine Nucleotides. *Langmuir* **1997**, *13*, 3529–3541.

112. Blake, M. R.; Garnett, J. L.; Gregor, I. K.; Bruce, S. Gas phase electron attachment reactions with organometallic compounds; molecular anion formation and negative ion mass spectra of a series of η4-dienetricarbonyliron compounds. *J. Chem. Soc., Chem. Commun.* **1979**, 496–497.

113. Coleman, D. R.; Royer, G. P. New hydrogenation catalyst: palladium-poly(ethylenimine) "ghosts". Applications in peptide synthesis. *J. Org. Chem.* **1980**, *45*, 2268–2269.

114. Ram, S.; Ehrenkaufer, R. E. Ammonium Formate in Organic Synthesis: A Versatile Agent in Catalytic Hydrogen Transfer Reductions. *Synthesis* **1988**, 91–95.

115. Anantharamaiah, G. M.; Sivanandaiah, K. M. Transfer hydrogenation; a convenient method for removal of some commonly used protecting groups in peptide synthesis. *J. Chem. Soc., Perkin Trans. 1* **1977**, 490–491.

116. Hanna, C. *S*-(2-Methyl-1,4-naphthoquinon-3-yl)-β-mercaptopropionic Acid. *J. Am. Chem. Soc.* **1952**, *74*, 2120.

117. This was suggested by the difficulty in isolating pure **10** and **15**.

118. Synthesized by Isis Pharmaceuticals, Carlsbad, CA (collaborators since 1996).

119. Fasman, G. D. *Handbook of Biochemistry and Molecular Biology: Nucleic Acids*; 2nd ed.; CRC Press: Cleveland, OH, 1985; Vol. 1, pp 589.

120. Bayer, E.; Bauer, T.; Schmeer, K.; Bleicher, K.; Maier, M.; Gaus, H.-J. Analysis of Double-Stranded Oligonucleotides by Electrospray Mass Spectrometry. *Anal. Chem.* **1994**, *66*, 3858–3863.

121. For a detailed discussion on the problems associated by using an HDME, refer to ref 24.

122. Kertesz, V.; Mullenix, A. N.; Whittemore, N. A.; Baker, D. C.; Chambers, J. Q. Electrochemical Sensors for Oligodeoxynucleotides With Specific Base Sequences. In *Abstracts of Papers,* 50th Pittsburgh Conference, Orlando, FL, March 7–12, 1999; American Chemical Society: Washington, DC, 1999; PITTCON 082.

123. For a large-scale synthesis of TTF, refer to Moore, A. J.; Bryce, M. R. Tetrathiafulvalene: A Convenient Large-Scale (20 g) Synthesis. *Synthesis* **1997**, 407–409.

124. Barton, J. K. DNA-mediated electron-transfer chemistry. In *Abstracts of Papers,* 216th ACS National Meeting, Boston, MA, August 23–27, 1998; American Chemical Society: Washington, DC, 1998; ORGN 033.

125. Kelley, S. O.; Barton, J. K. Electron Transfer Between Bases in Double Helical DNA. *Science* **1999**, *283*, 375–381.

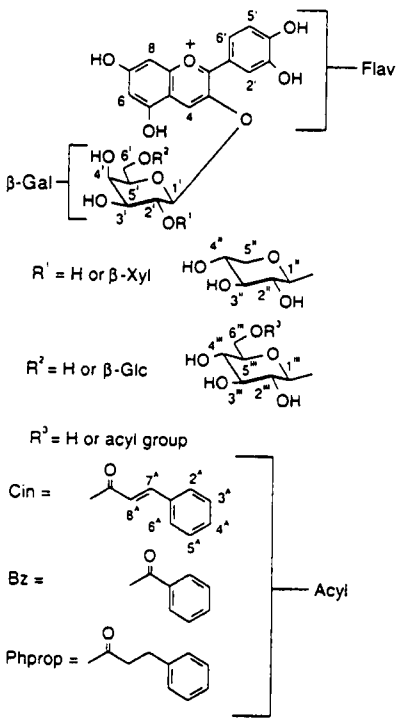
126. Zubritsky, E. Pinning Down PCR. *Anal. Chem.* **1999**, *71*, 191A–195A.

127. Armitage, B.; Ly, D.; Koch, T.; Frydenlund, H.; Ørum, H.; Batz, H. G.; Schuster, G. B. Peptide nucleic acid–DNA duplexes: Long-range hole migration from an internally linked anthraquinone. *Proc. Natl. Acad. Sci. USA* **1997**, *94*, 12320–12325.

128. Armitage, B.; Koch, T.; Frydenlund, H.; Ørum, H.; Batz, H.-G.; Schuster, G. B. Peptide nucleic acid–anthraquinone conjugates: strand invasion and photoinduced cleavage. *Nucleic Acids Res.* **1997**, *25*, 4674–4678.

APPENDICES

APPENDIX A. Miscellaneous Data that Pertains to the Conformational Studies of Monoacylated Anthocyanins



1	R^1 = β-Xyl	R^2 = β-Glc	R^3 = H
2	R^1 = H	R^2 = β-Glc	R^3 = H
3	R^1 = β-Xyl	R^2 = H	
4	R^1 = H	R^2 = H	
5	R^1 = β-Xyl	R^2 = β-Glc	R^3 = 4-OH-3,5-$(OMe)_2$-Cin
6	R^1 = H	R^2 = β-Glc	R^3 = 4-OH-3,5-$(OMe)_2$-Cin
7	R^1 = β-Xyl	R^2 = β-Glc	R^3 = 3,4,5-$(OMe)_3$-Cin
8	R^1 = H	R^2 = β-Glc	R^3 = 3,4,5-$(OMe)_3$-Cin
9	R^1 = β-Xyl	R^2 = β-Glc	R^3 = 4-OH-Cin
10	R^1 = H	R^2 = β-Glc	R^3 = 4-OH-Cin
11	R^1 = β-Xyl	R^2 = β-Glc	R^3 = 4-OMe-Cin
12	R^1 = β-Xyl	R^2 = β-Glc	R^3 = 3-OMe-Cin
13	R^1 = β-Xyl	R^2 = β-Glc	R^3 = 2-OMe-Cin
14	R^1 = β-Xyl	R^2 = β-Glc	R^3 = Cin
15	R^1 = β-Xyl	R^2 = β-Glc	R^3 = 4-F-Cin
16	R^1 = β-Xyl	R^2 = β-Glc	R^3 = 4-Cl-Cin
17	R^1 = β-Xyl	R^2 = β-Glc	R^3 = 4-CF_3-Cin
18	R^1 = β-Xyl	R^2 = β-Glc	R^3 = 4-NO_2-Cin
19	R^1 = β-Xyl	R^2 = β-Glc	R^3 = 4-$(Me_2 N)$-Cin
20	R^1 = β-Xyl	R^2 = β-Glc	R^3 = 3,4,5-$(OMe)_3$-Bz
21	R^1 = β-Xyl	R^2 = β-Glc	R^3 = 4-OH-Bz
22	R^1 = β-Xyl	R^2 = β-Glc	R^3 = 4-Cl-Bz
23	R^1 = β-Xyl	R^2 = β-Glc	R^3 = 4-CF_3-Bz
24	R^1 = β-Xyl	R^2 = β-Glc	R^3 = 4-OH-Phprop

Structure of anthocyanins **1–24** used in ^{1}H NMR and color-stability studies. Reprinted from *Carbohydrate Research*, Vol. 310, Donald K. Dougall, David C. Baker, Elena G. Gakh, Mark A. Redus, and Neil A. Whittemore, Anthocyanins from wild carrot suspension cultures acylated with supplied carboxylic acids, p 178, Copyright (1998), with permission from Elsevier Science.

Table 1
^{1}H NMR data of anthocyanins 1–24[a]

	H	1[b,c]	2	3[d]	4	5[b]	6[b]	7[b]	8[b]	9	10	11
Flav	4	8.981 br s	9.029 br s	8.976 br s	9.027 br s	8.474 d (0.9)	8.605 d (0.9)	8.478 d (0.9)	8.633 br s	8.524 br s	8.702 br s	8.524 br s
	6	6.715 d (2.0)	6.655 br s	6.643 d (1.8)	6.694 d (1.9)	6.684 d (2.0)	6.652 d (2.0)	6.695 d (2.0)	6.634 br s	6.618 br s	6.612 d (2.0)	6.609 d (2.0)
	8	6.964 br d	6.899 br d	6.893 br d	6.887 d (0.8)	6.512 dd (2.0 0.9)	6.536 d (0.9)	6.525 d (0.9)	6.548 br d	6.559 br d	6.593 d (2.0)	6.532 d (2.0)
	2′	8.090 d (2.4)	8.103 d (2.4)	8.065 d (2.4)	8.074 d (2.3)	7.913 d (2.4)	7.916 d (2.3)	7.915 d (2.3)	7.932 d (2.4)	7.934 d (2.3)	7.945 d (2.3)	7.901 d (2.4)
	5′	7.041 d (8.8)	7.018 d (8.7)	7.016 d (8.8)	7.015 d (8.8)	7.022 d (8.8)	7.033 d (8.7)	7.018 d (8.8)	7.028 d (8.8)	7.051 d (8.7)	7.030 d (8.8)	7.046 d (8.7)
	6′	8.292 dd (8.8; 2.4)	8.271 dd (8.7; 2.4)	8.290 dd (8.7; 2.4)	8.259 dd (8.8; 2.4)	8.136 dd (8.8; 2.4)	8.266 dd (8.7; 2.3)	8.186 dd (8.8; 2.3)	8.270 dd (8.8; 2.4)	8.066 dd (8.7; 2.3)	8.241 dd (8.8; 2.3)	8.110 dd (8.7; 2.4)
Gal	1[I]	5.398 d (7.6)	5.217 d (7.7)	5.402 d (7.6)	5.241 d (7.7)	5.256 d (7.3)	5.191 d (7.3)	5.286 d (7.5)	5.218 d (7.5)	5.268 d (7.4)	5.216 d (7.6)	5.260 d (7.4)
	2[I]	4.196 dd (7.6; 9.4)	3.956 dd (7.7; 9.7)	4.213 dd (7.7; 9.3)	3.982 dd (9.6; 7.7)	4.276 dd (9.2; 7.3)	3.994 dd (8.9; 7.3)	4.296 dd (9.3; 7.5)	3.997 dd (8.9; 7.5)	4.218 dd (9.4; 7.4)	3.966 dd (8.6; 7.6)	4.223 dd (9.3; 7.4)
	3[I]	3.919 dd (9.4; 3.3)	3.649 dd (9.7; 3.4)	3.882 dd (9.3; 3.3)	3.650 dd (9.6; 3.4)	4.182 dd (9.2; 3.3)	3.929 dd (8.9; 3.3)	4.184 dd (9.3; 3.4)	3.925 dd (8.9; 3.3)	4.125 dd (9.4; 3.3)	~3.9	4.127 dd (9.3; 3.4)
	4[I]	4.002 d (3.3)	3.966 d (3.4)	3.953 d (3.3)	3.942 d (3.4)	3.944 d (3.3)	3.914 d (3.3)	3.951 d (3.4)	3.909 d (3.3)	3.932 d (3.3)	~3.9	3.930 d (3.4)
	5[I]	4.064 dd (7.3; 4.9)	~3.9	~3.8	~3.7	4.483 dd (9.6; 2.0)	4.427 dd (9.4; 1.5)	4.500 dd (9.2; 1.9)	4.446 dd (9.6; 2.0)	4.427 dd (9.4; 2.0)	~4.4	4.420 dd (9.4; 2.0)
	6[IA]	3.997 dd (4.9; −11.2)	~3.9	~3.8	~3.7	4.215 dd (−13.1; 9.6)	4.224 dd (−12.8; 9.4)	4.222 dd (−13.3; 9.2)	4.229 dd (−13.0; 9.6)	4.195 dd (−13.0; 9.4)	4.184 dd (−12.8; 9.5)	4.192 dd (−12.9; 9.4)
	6[IB]	3.879 dd (7.3; −11.2)	~3.9	~3.8	~3.7	3.747 dd (−13.1; 2.0)	3.734 dd (−12.8; 1.5)	3.758 dd (−13.2; 1.9)	3.732 dd (−13.0; 2.0)	3.742 dd (−13.0; 2.0)	3.743 dd (−13.2; 2.4)	3.744 dd (−12.9; 2.0)
Xyl	1[II]	4.695 d (7.6)	—	4.684 d (7.7)	—	4.829 d (7.8)	—	4.856 d (7.8)	—	4.660 d (7.3)	—	4.694 d (7.4)
	2[II]	3.158 dd (9.0; 7.6)	—	3.135 dd (8.9; 7.7)	—	3.193 dd (9.0; 7.8)	—	3.148 dd (8.9; 7.8)	—	3.240 dd (9.1; 7.4)	—	3.244 dd (9.1; 7.4)
	3[II]	3.296 dd (9.0; 8.8)	—	[e]	—	3.333 dd (9.0; 9.0)	—	3.342 dd (8.9; 8.9)	—	3.298 dd (9.7; 9.1)	—	3.303 dd (9.1; 9.6)
	4[II]	3.392 ddd (10.2; 8.8; 5.3)	—	[e]	—	3.251 ddd (10.9; 9.0; 5.2)	—	3.266 ddd (10.5; 8.9; 4.6)	—	~3.40	—	~3.41
	5[IIA]	3.636 dd (−11.6; 5.3)	—	3.606 dd (−11.6; 5.3)	—	3.610 dd (−11.4; 5.2)	—	3.627 dd (−11.6; 4.6)	—	3.484 dd (−11.2; 5.3)	—	3.521 dd (−11.2; 5.3)
	5[IIB]	3.019 dd (−11.6; 10.2)	—	3.007 dd (−11.3; 10.3)	—	3.121 dd (−11.4; 10.9)	—	3.144 dd (−11.6; 10.5)	—	2.810 dd (−11.2; 10.5)	— dd	2.850 dd (−11.2; 10.8)

Reprinted from *Carbohydrate Research*, Vol. 310, Donald K. Dougall, David C. Baker, Elena G. Gakh, Mark A. Redus, and Neil A. Whittemore, Anthocyanins from wild carrot suspension cultures acylated with supplied carboxylic acids, p 180, Copyright (1998), with permission from Elsevier Science Publishers.

12	13	14	15	16	17	18	19	20	21	22	23	24
8.526 br s	8.603 br s	8.583 br s	8.588 br s	8.515 br s	8.538 d (0.8)	8.554 br s	8.475 d (1.1)	8.447 br s	8.518 br s	8.953 br s	8.500 br s	8.821 br s
6.600 br s	6.552 d (1.9)	6.604 br s	6.587 br s	6.613 br s	6.603 d (2.0)	6.673 d (2.0)	6.622 d (2.0)	6.483 d (2.0)	6.632 d (2.1)	6.551 d (1.7)	6.538 d (2.0)	6.632 d (2.3)
6.483 br d	6.448 d (1.4)	6.497 br d	not seen	6.606 br d	6.514 d (0.8)	6.568 br d	6.521 dd (2.0; 1.1)	6.741 d (1.2)	6.879 br d	6.855 br d	6.818 br d	6.842 br d
7.913 d (2.2)	7.920 d (2.4)	7.915 d (2.4)	7.952 d (2.3)	7.961 d (2.3)	7.951 d (2.4)	7.958 d (2.4)	7.856 d (2.3)	7.973 d (2.3)	8.022 d (2.3)	8.023 d (2.4)	8.018 d (2.4)	8.066 d (2.3)
7.042 d (8.7)	7.037 d (8.8)	7.046 d (8.7)	7.056 d (8.8)	7.062 d (8.7)	7.044 d (8.8)	7.080 d (8.7)	7.026 d (8.7)	7.013 d (8.7)	7.056 d (8.7)	7.038 d (8.7)	7.030 d (8.7)	7.024 d (8.7)
8.095 dd (8.7; 2.2)	8.171 dd (8.6; 2.4)	8.093 dd (8.7; 2.4)	8.114 dd (8.8; 2.3)	8.100 dd (8.7; 2.3)	8.080 dd (8.8; 2.4)	8.116 dd (8.7; 2.4)	8.146 dd (8.7; 2.3)	8.219 dd (8.7; 2.3)	8.230 dd (8.7; 2.3)	8.222 dd (8.7; 2.4)	8.208 dd (8.7; 2.4)	8.257 dd (8.7; 2.3)
5.294 d (7.3)	5.392 d (7.5)	5.304 d (7.4)	5.277 d (7.4)	5.208 d (7.4)	5.254 d (7.4)	5.237 d (7.5)	5.257 d (7.3)	5.388 d (7.5)	5.232 d (7.4)	5.178 d (7.5)	5.190 d (7.4)	5.289 d (7.5)
~4.2	4.240 dd (9.4; 7.3)	4.218 dd (9.4; 7.4)	~4.2	4.221 dd (9.4; 7.4)	4.241 dd (9.4; 7.4)	4.244 dd (9.4; 7.5)	4.232 dd (9.2; 7.3)	~4.2	4.169 dd (9.2; 7.3)	4.182 dd (9.3; 7.5)	4.186 dd (9.3; 7.4)	4.203 dd (9.2; 7.5)
~4.1	4.128 dd (9.2; 3.4)	4.100 dd (9.4; 3.4)	4.091 dd (9.3; 3.3)	4.102 dd (9.4; 3.3)	4.108 dd (9.4; 3.4)	4.091 dd (9.4; 3.4)	4.152 dd (9.2; 3.3)	4.043 dd (9.4; 3.3)	3.983 dd (9.2; 3.4)	3.964 dd (9.4; 3.4)	3.974 dd (9.3; 3.4)	3.912 dd (9.2; 3.3)
3.934 d (3.3)	3.940 d (3.3)	3.935 d (3.4)	3.935 d (3.3)	3.932 d (3.3)	3.943 d (3.3)	3.972 d (3.4)	3.920 d (3.3)	3.917 d (3.3)	3.902 d (3.4)	3.896 d (3.5)	3.902 d (3.4)	3.942 d (3.3)
~4.4	4.490 dd (9.4; 2.2)	~4.4	~4.4	4.368 dd (8.7; 1.1)	4.381 dd (9.5; 2.2)	4.361 dd (9.5; 2.5)	4.410 dd (9.7; 1.9)	~4.2	4.334 dd (9.3; 2.4)	4.282 dd (8.6; 2.4)	4.271 dd (8.8; 2.6)	4.102 dd (7.9; 3.7)
~4.1	4.20 dd (−13.1; 9.3)	~4.1	~4.1	~4.1	4.178 dd (−12.9; 9.5)	4.154 dd (−12.8; 9.1)	4.190 dd (−13.0; 9.7)	4.201 dd (−13.1; 9.2)	4.108 dd (−12.7; 9.3)	4.111 dd (−12.6; 8.8)	4.093 dd (−12.5; 8.8)	3.986 dd (−11.9; 7.9)
~3.7	3.767 dd (−12.0; 1.5)	3.763 dd (−12.9; 2.3)	3.766 dd (−13.1; 3.1)	3.752 dd (−12.9; 2.0)	3.769 dd (−12.9; 2.2)	3.802 dd (−12.8; 2.3)	3.729 dd (−13.0; 1.9)	3.783 dd (−12.9; 2.0)	3.799 dd (−12.7; 2.4)	3.798 dd (−12.5; 2.6)	3.812 dd (−12.5; 2.6)	3.857 dd (−11.9; 3.7)
4.667 d (7.4)	4.731 d (7.4)	4.655 d (7.4)	4.659 d (7.4)	4.656 d (7.4)	4.686 d (7.4)	4.702 d (7.5)	4.755 d (7.3)	4.765 d (7.8)	4.678 d (7.5)	4.657 d (7.5)	4.645 d (7.4)	4.666 d (7.5)
c	c	3.229 dd (9.1; 7.4)	c	3.221 dd (9.1; 7.4)	3.235 dd (9.1; 7.4)	3.219 dd (9.2; 7.5)	3.267 dd (9.2; 7.3)	~3.3	3.198 dd (9.2; 7.5)	3188 dd (9.2; 7.5)	3.200 dd (9.1; 7.4)	3183 dd (9.0; 7.5)
c	c	c	c	c	3.300 dd (9.1; 9.1)	3.317 dd (9.2; 8.9)	3.323 dd (9.2; 9.2)	~3.3	~3.4	~3.4	3.308 dd (9.1; 9.2)	3.282 dd (9.2; 9.0)
c	3.672 dd (9.1 9.1)	3.640 dd (9.1; 9.0)	3.620 dd (9.2; 9.2)	3.631 dd (9.4; 9.0)	~3.38	~3.39	~3.40	~3.4	~3.6	~3.55	~3.40	~3.30
~3.5	3.622 dd (−11.6; 5.2)	~3.5	~3.4	~3.4	3.506 dd (−11.4; 4.9)	3.538 dd (−11.4; 5.2)	3.589 dd (−11.4; 4.3)	~3.6	3.594 dd (−11.6; 5.4)	~3.55	3.540 dd (−11.4; 5.3)	3.582 dd (−11.4; 5.2)
2.812 dd (−10.4; 10.4)	2.932 dd (−10.9; 10.9)	2.811 dd (−11.3; 10.9)	2.825 dd (−11.1; 10.4)	2.824 dd (−10.8; 10.4)	2.856 dd (−11.4; 10.2)	2.860 dd (−11.4; 10.4)	2.922 dd (−11.4; 10.5)	3.049 dd (−11.4; 10.6)	2.837 dd (−11.6; 10.5)	2.841 dd (−11.3; 10.6)	2.833 dd (−11.4; 10.6)	2.967 dd (−11.4; 10.4)

Table 1 contd

	H	1[b,c]	2	3[d]	4	5[b]	6[b]	7[b]	8[b]	9	10	11
Glc	1^{III}	4.267 d (7.7)	4.234 d (7.5)	—	—	4.474 d (7.4)	4.459 d (7.5)	4.478 d (7.5)	4.453 d (7.3)	4.442 d (7.2)	4.409 d (7.3)	4.440 d (7.1)
	2^{III}	3.178 dd (9.3; 7.7)	~3.16	—	—	~3.44	~3.44	~3.44	~3.45	~3.41	~3.41	~3.40
	3^{III}	~3.25	~3.20	—	—	~3.44	~3.44	~3.44	~3.45	~3.43	~3.43	~3.40
	4^{III}	~3.30	~3.20	—	—	3.746 dd (9.5; 9.6)	3.697 dd (9.5; 9.5)	3.747 dd (9.6; 9.4)	3.669 dd (9.4; 9.4)	3.673 dd (9.4; 9.2)	3.618 dd (9.4; 9.3)	3.661 dd (9.4; 9.1)
	5^{III}	~3.30	~3.18	—	—	~3.44	~3.44	~3.44	~3.45	~3.42	~3.42	~3.40
	6^{IIIA}	3.846 dd (−11.7; 1.8)	3.835 dd (−11.7; 2.2)	—	—	5.339 dd (−12.1; 2.8)	5.295 dd (−11.9; 2.8)	5.340 dd (−12.2; 3.0)	5.302 dd (−12.0; 2.8)	5.253 dd (−12.0; 2.7)	5.169 dd (−11.9; 2.6)	5.252 dd (−12.0; 2.7)
	6^{IIIB}	3.633 dd (−11.7; 5.8)	3.503 dd (−11.7; 5.9)	—	—	4.115 dd (−12.2; 1.3)	4.085 dd (−11.9; 1.2)	4.134 dd (−12.2; 1.6)	4.106 dd (−12.0; 1.5)	4.113 dd (−12.0; 1.6)	4.078 dd (−12.0; 2.1)	4.115 dd (−12.0; 1.7)
Acyl	2^{A}	—	—	—	—	6.195 s	6.267 s	6.221 s	6.303 s	6.949 d (8.6)	6.904 d (8.6)	7.046 d (8.7)
	3^{A}	—	—	—	—	—	—	—	—	6.368 d (8.6)	6.356 d (8.6)	6.492 d (8.7)
	4^{A}	—	—	—	—	—	—	—	—	—	—	—
	5^{A}	—	—	—	—	—	—	—	—	6.368 d (8.6)	6.356 d (8.6)	6.492 d (8.7)
	6^{A}	—	—	—	—	6.195 s	6.267 s	6.221 s	6.303 s	6.949 d (8.6)	6.904 d (8.6)	7.046 d (8.7)
	7^{A}	—	—	—	—	7.297 d (15.9)	7.362 d (15.9)	7.310 d (15.9)	7.397 d (16.0)	7.364 d (16.0)	7.406 d (15.9)	7.404 d (16.0)
	8^{A}	—	—	—	—	6.197 d (15.9)	6.137 d (15.9)	6.308 d (15.9)	6.240 d (16.0)	6.130 d (16.0)	6.103 d (16.0)	6.178 d (16.0)
	MeO					3.413 s $3^{A},5^{A}$	3.431 s $3^{A},5^{A}$	3.415 s $3^{A},5^{A}$ 3.823 4^{A}	3.431 s $3^{A},5^{A}$ 3.762 4^{A}			3.787 s 4^{A}

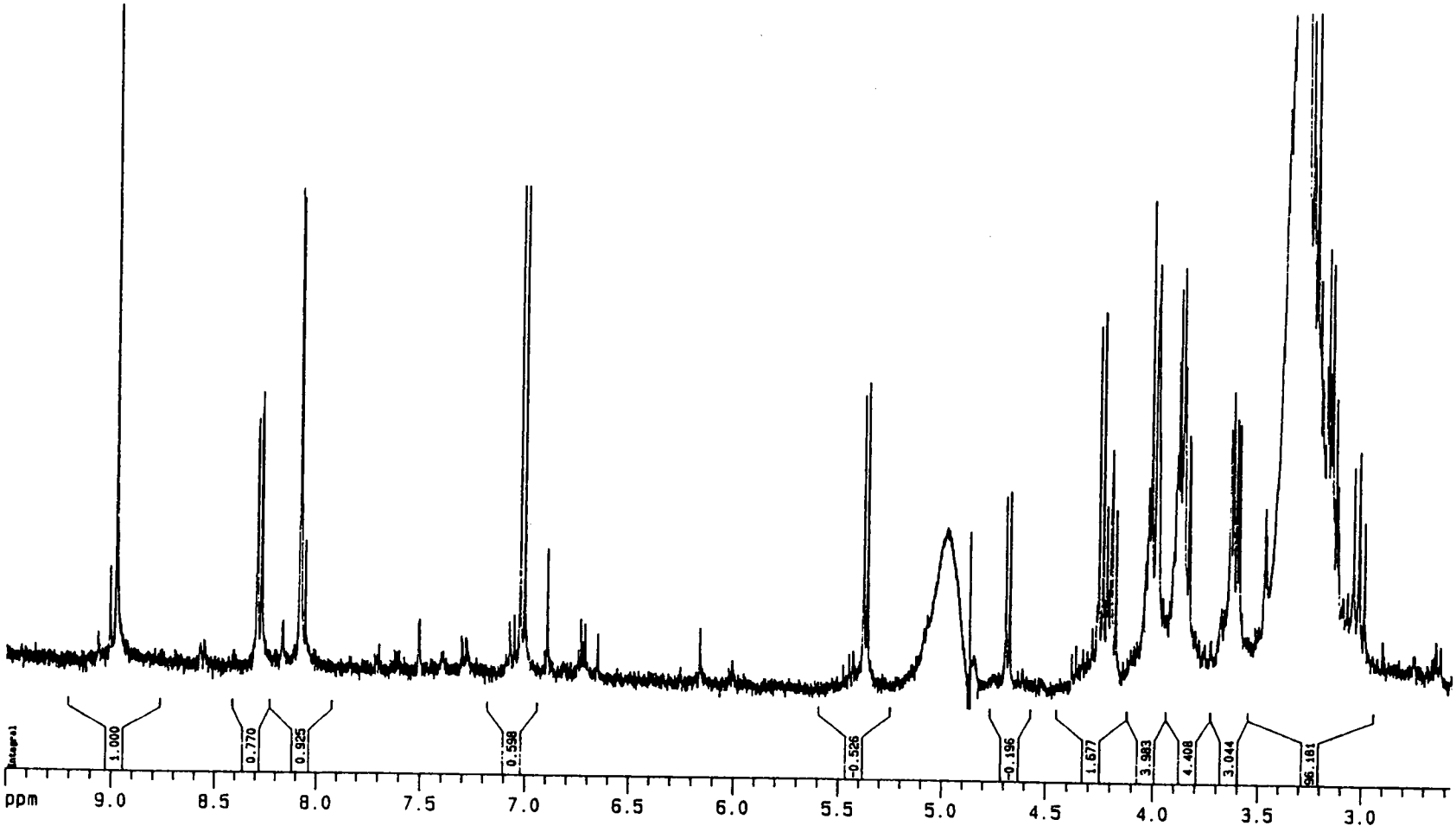
12	13	14	15	16	17	18	19	20	21	22	23	24
4.359 d (7.1)	4.430 d (7.3)	4.422 d (7.6)	4.426 d (7.3)	4.431 d (7.3)	4.434 d (7.4)	4.458 d (7.5)	4.452 d (7.2)	4.452 d (7.4)	4.429 d (7.3)	4.403 d (7.4)	4.644 d (7.4)	4.278 d (7.5)
[c]	[c]	[c]	[c]	[c]	3.354 dd (9.4; 7.4)	~3.37	~3.42	~3.4	~3.40	[c]	3.312 dd (9.2; 7.4)	3.206 dd (9.3; 7.5)
[c]	[c]	3.640 dd (9.1; 9.0)	3.621 dd (9.4; 9.2)	3.631 dd (9.4; 9.0)	3.417 dd (9.8; 9.4)	3.422 dd (8.8; 9.4)	~3.42	~3.4	~3.40	~3.4	~3.40	~3.40
~3.7	~3.6	~3.4	[c]	~3.4	3.630 dd (9.8; 8.8)	3.680 dd (9.8; 8.8)	3.661 dd (9.4; 9.2)	~3.6	3.644 dd (9.6; 9.4)	~3.5	3.589 dd (9.8; 9.6)	~3.30
[c]	[c]	~3.4	~3.4	~3.4	~3.38 ddd (8.8; 2.7; 2.1)	3.490 ddd (9.8; 2.5; 2.6)	~3.42	~3.4	3.495 ddd (9.6; 3.1; 2.2)	3.484 ddd (9.5; 3.0; 3.0)	3.505 ddd (9.8; 3.3; 2.5)	~3.30
5.278 dd (−11.9; 2.6)	5.230 dd (−12.8; 3.1)	5.208 dd (−11.9; 2.7)	5.176 dd (−10.8; 2.6)	5.221 dd (−11.8; 2.6)	5.210 dd (−12.0; 2.5)	5.154 dd (−12.0; 2.5)	5.294 dd (−12.0; 2.8)	5.297 dd (−11.8; 2.3)	5.094 dd (−12.0; 2.2)	5.105 dd (−11.9; 2.3)	5.122 dd (−12.0; 2.5)	4.589 dd (−12.3; 2.0)
~4.2	~4.2	~4.1	~4.1	4.151 dd (−11.8; 1.9)	4.189 dd (−12.0; 2.1)	4.187 dd (−12.0; 2.6)	4.086 dd (−12.0; 1.5)	~4.2	4.250 dd (−12.0; 3.1)	4.282 dd (−12.2; 2.4)	4.383 dd (−12.0; 3.3)	4.083 dd (−12.3; 4.6)
6.99[f] 6.92 6.92 6.81 6.65	7.23[f] 7.13 7.13 6.71 6.59	7.135 d (7.1)	7.207 dd dd (8.6; 5.3)	7.154 d (8.5)	7.378 d (8.2)	7.465 d (8.8)	6.921 d (8.9)	7.109 s	7.759 d (8.8)	7.887dd dd (6.6; 2.0)	8.126 d (8.2)	6.861d d (8.6)
		7.046 d (7.8)	6.776 dd (8.6; 8.7)	6.971 d (8.5)	7.300 d (8.2)	7.870 d (8.8)	6.208 d (8.9)	—	6.405 d (8.8)	7.097dd dd (6.6; 2.0)	7.468 d (8.2)	6.506d d (8.6)
		7.264 dd (7.4; 7.2)	—	—	—	—	—	—	—	—	—	—
		7.046 d (7.8)	6.776 dd dd (8.6; 8.7)	6.971 d (8.5)	7.300 d (8.2)	7.870 d (8.8)	6.208 d (8.9)	—	6.405 d (8.8)	7.097dd dd (6.6; 2.0)	7.468 d (8.2)	6.506d d (8.6)
		7.135 d (7.1)	7.207 dd dd (8.6; 5.3)	7.154 d (8.5)	7.378 d (8.2)	7.465 d (8.8)	6.921 d (8.9)	7.109 s	7.759 d d (8.8)	7.887dd dd (6.6; 2.0)	8.126 d (8.2)	6.681d d (8.6)
7.385 d (16.0)	7.535 d (16.2)	7.450 d (16.1)	7.439 d (16.1)	7.445 d (16.1)	7.532 d (16.1)	7.538 d (16.1)	7.382 d (16.0)	—	—	—	—	~2.74
6.338 d (16.0)	6.521 d (16.2)	6.353 d (16.2)	6.308 d (16.1)	6.371 d (16.1)	6.524 d (16.1)	6.568 d (16.1)	6.046 d (16.0)	—	—	—	—	~2.56
3.602 s 3^	3.593 s 2^							3.623 s 3^,5^ 3.605 s 4^				

[a] Apparent, first-order couplings are indicated (br s, broad singlet; br d, broad doublet; d, doublet; dd, doublet of doublets; ddd doublet of doublets) in parentheses in Hz.
[b] Chemical shift data have been reported. See ref [1].
[c] For a comparison spectrum, see ref [8].
[d] For a comparison spectrum, see ref [10].
[e] Obscured by the MeOH-d_4 signal.
[f] Protons of the acyl moiety could not be assigned.

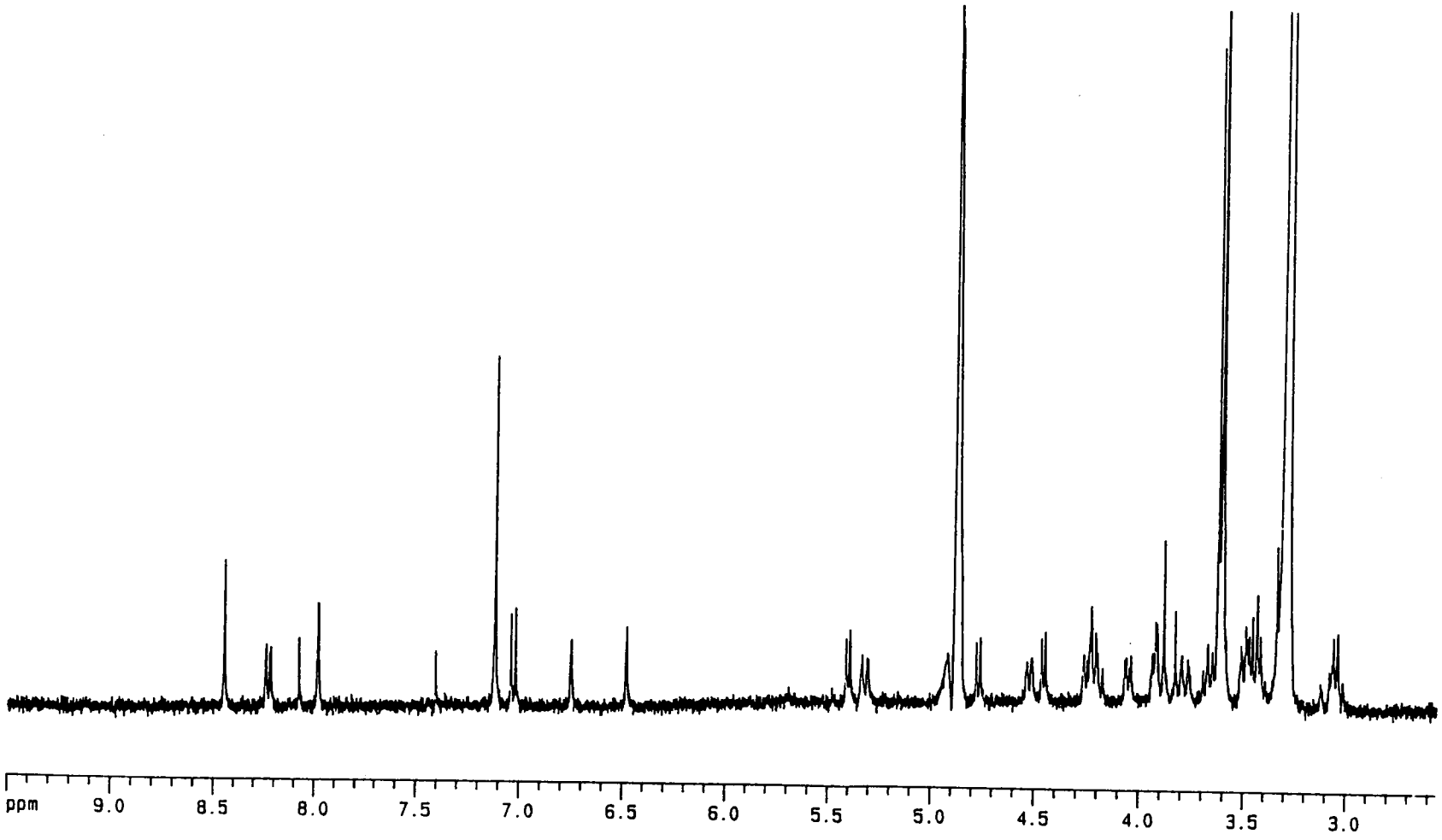
Cpd.[a]	$k_1 \times 10^2$ (sec^{-1})	k_2 ($sec^{-1}.M^{-1}$)	$K_h \times 10^5$ (M)	$K_a \times 10^5$ (M)
1	6 ± 1	139 ± 1	43 ± 6	4.3 ± 0.2
3	8.1 ± 0.3	208 ± 1	39 ± 1	4.2 ± 1.9
5	2.5 ± 0.4	633 ± 52	3.9 ± 0.5	0.9 ± 0.4
6	2.0 ± 0.1	394 ± 20	5.1 ± 0.0	0.35 ± 0.01
7	3.57 ± 0.04	684 ± 42	5.2 ± 0.3	1.65 ± 0.08
8	2.78 ± 0.08	519 ± 20	5.38 ± 0.08	1.6 ± 0.3
9	4.8 ± 0.9	716 ± 56	6.6 ± 0.8	1.6 ± 0.5
11	4.7 ± 0.5	588 ± 17	7.9 ± 0.7	1.2 ± 0.5
12	3.7 ± 0.1	626 ± 12	5.9 ± 0.3	0.19 ± 0.02
13	3.61 ± 0.02	732 ± 18	5.0 ± 0.2	2.02 ± 0.02
14	4.6 ± 0.2	636 ± 8	7.3 ± 0.1	1.6 ± 0.1
15	5.34 ± 0.03	577 ± 1	9.27 ± 0.06	2.6 ± 0.1
16	4.82 ± 0.07	590 ± 9	8.16 ± 0.02	2.0 ± 0.1
17	6.7 ± 0.3	601 ± 106	11 ± 2	2.3 ± 0.4
18	7.88 ± 0.03	409 ± 1	19.25 ± 0.02	2.52 ± 0.01
20	8.7 ± 0.6	586 ± 6	14.9 ± 0.8	1.33 ± 0.03
21	6.9 ± 0.2	629 ± 1	10.9 ± 0.4	2.8 ± 0.3
22	8.1 ± 0.1	515 ± 4	15.8 ± 0.1	2.2 ± 0.2
23	10.8 ± 0.6	455 ± 2	24 ± 1	2.4 ± 0.1
24	6.0 ± 0.2	213 ± 1	28.2 ± 0.9	3.58 ± 0.05

[a] the numbering of the compounds here is identical to that used in Dougall et al., 1998.

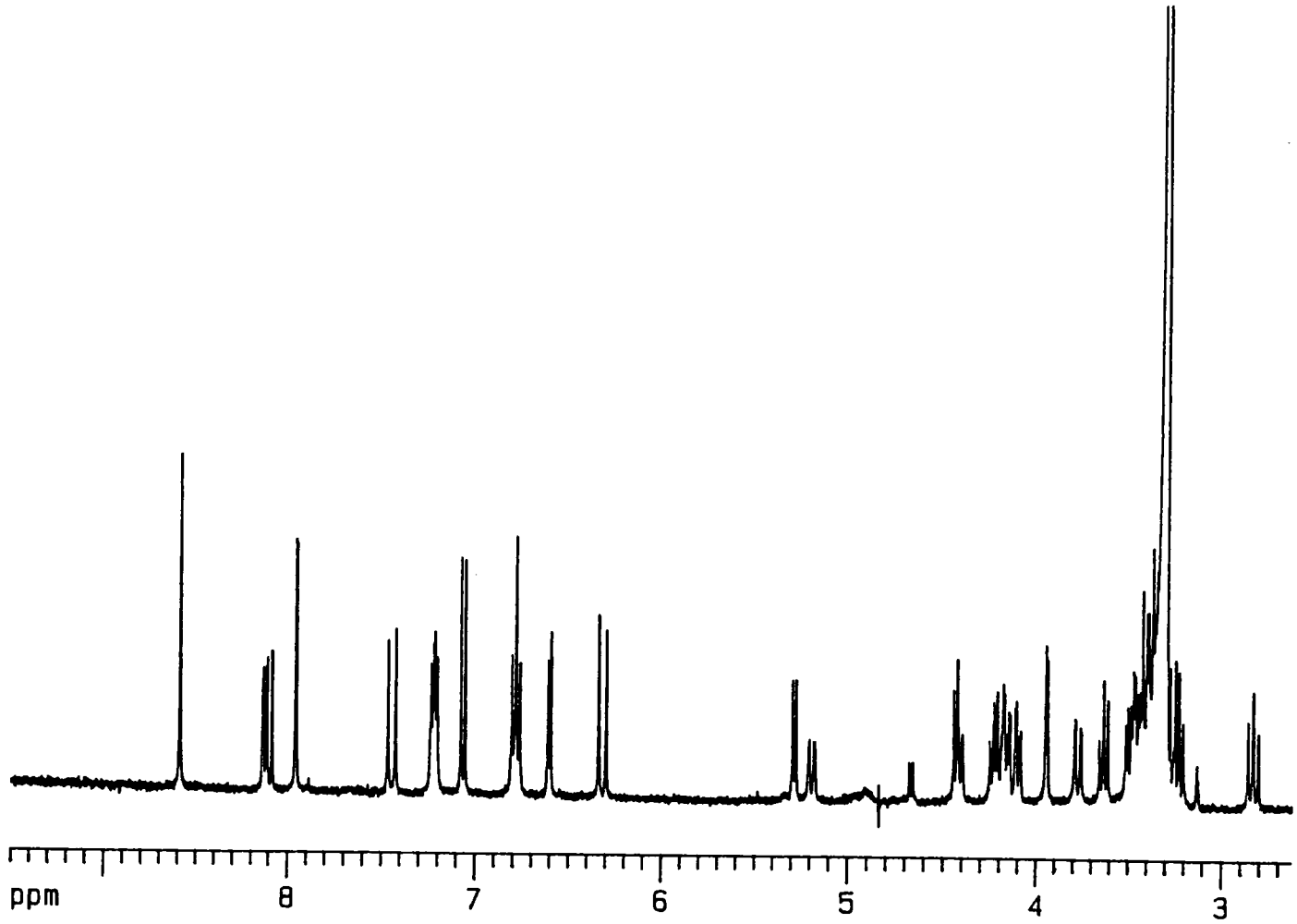
Color-stability data for all 24 anthocyanins (for the structures of these anthocyanins, refer to p 331).



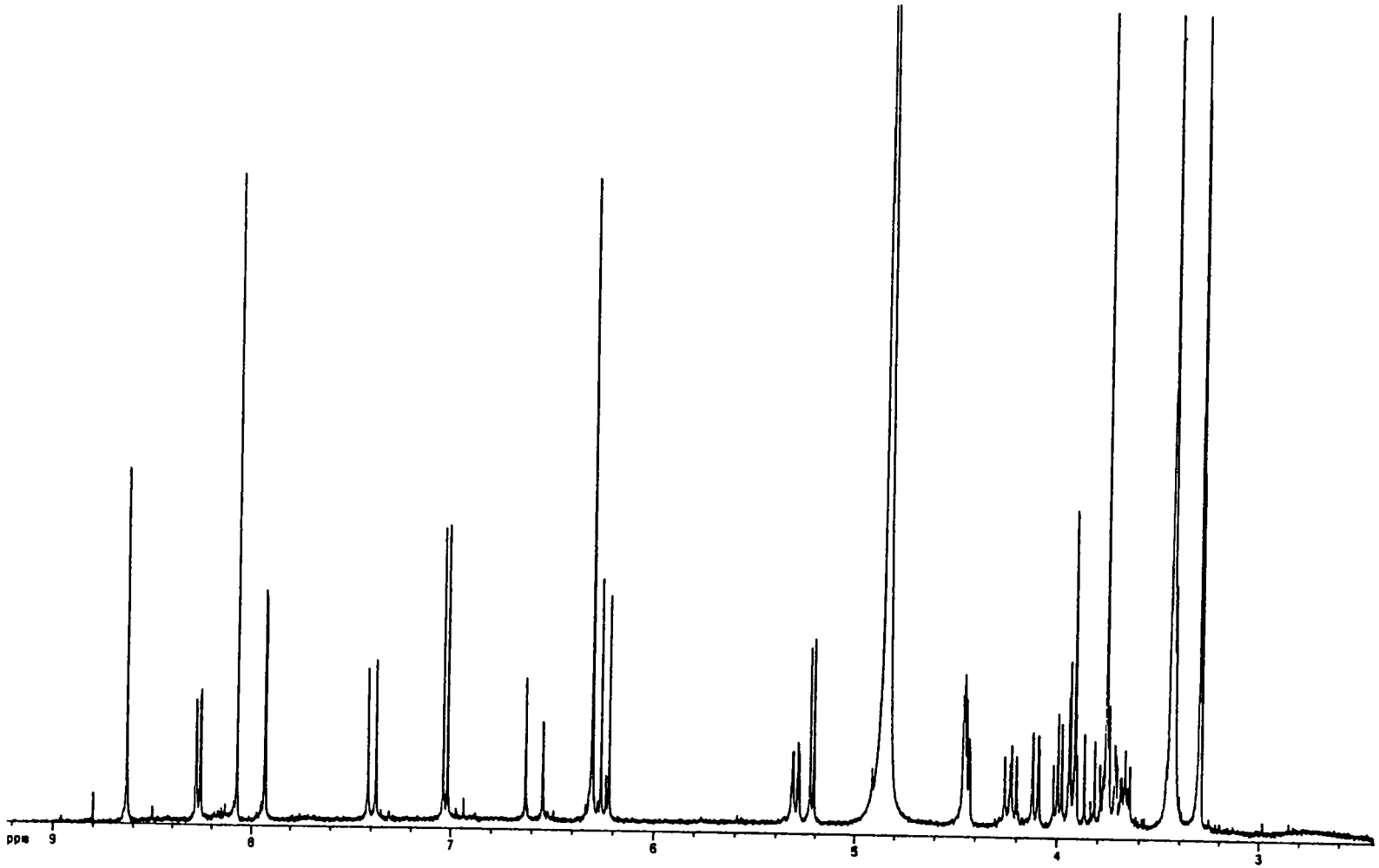
^{1}H NMR spectrum (400.13 MHz, methanol-d_4) of **CyanGXG** at 300 K.



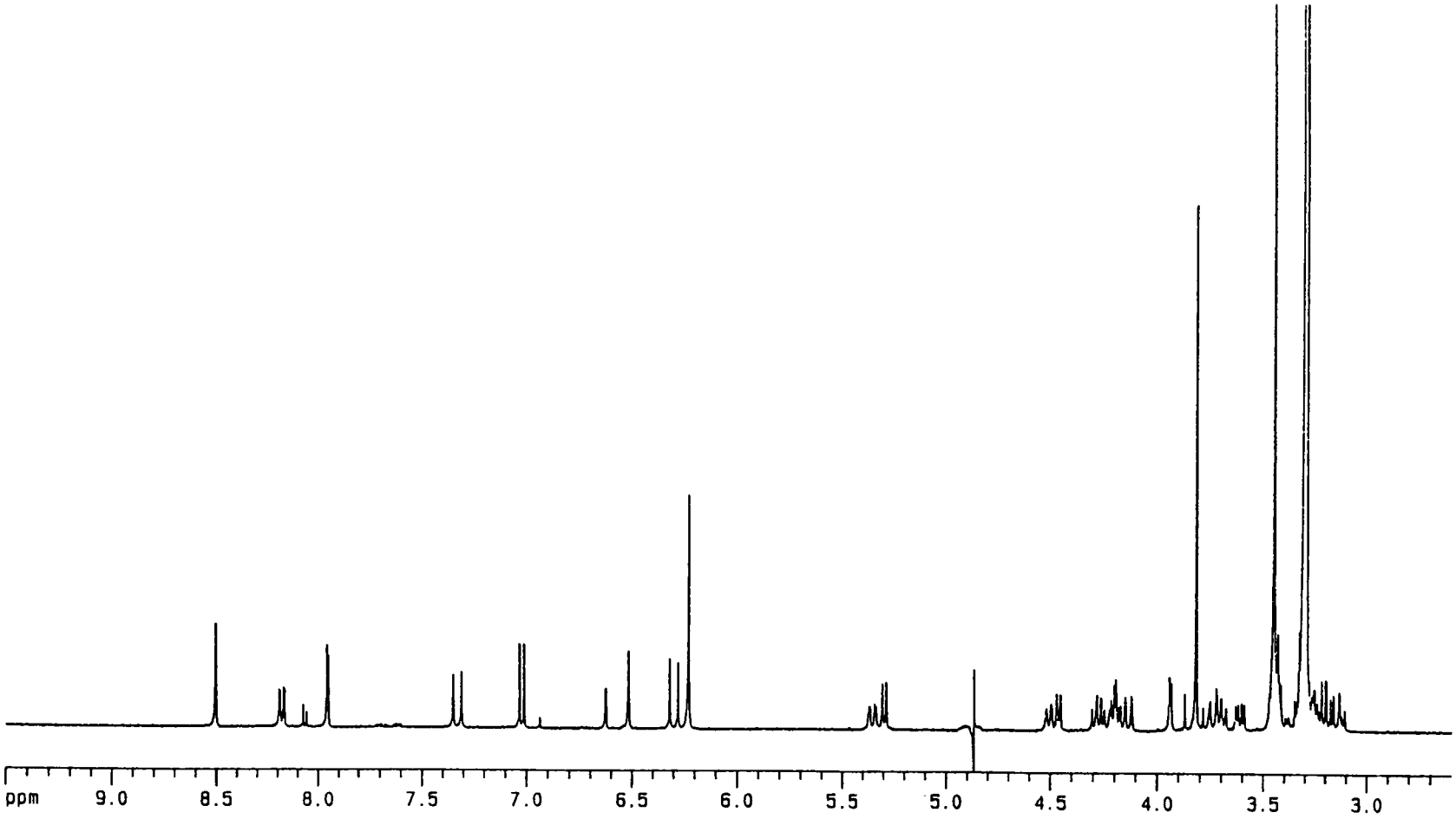
^{1}H NMR spectrum (400.13 MHz, methanol-d_4) of **345-TMBENZ** at 300 K.



^{1}H NMR spectrum (400.13 MHZ, methanol-d_4) of **4-FCIN** at 300 K.



^{1}H NMR spectrum (400.13 MHz, methanol-d_4) of **345-TCIN–X** at 300 K.



^{1}H NMR spectrum (400.13 MHZ, methanol-d_4) of **345-TCIN** at 300 K.

```
!    INPUT FILE FOR DISCOVER GENERATED BY INSIGHT
!
!
      overlap = 0.01
!
      begin simulation
     *    add-automatic bond torsion valence out-of-plane
      reduce
!
      set dielectric  = 32.63
!
!
!
        initialize dynamics at 600 K with a step size of 1.0 femtoseconds
     *  write history file every 1000 steps
        loop=1
100     resume dynamics for 1000 steps
        archive as file number loop
        loop=loop+1
        if loop.le.1000 then 100
        loop=1
200     retrieve file number loop
        minimize using conjugate gradient for 1000000 steps
     *  until the maximum derivative is less than 0.0001000000 kcal/A
        archive as file number loop
        loop=loop+1
        if loop.le.1000 then 200
        end
```

Input file used in the QMD simulation of anthocyanins **CyanGXG**, **345-TMBENZ**, **4-FCIN**, **345-TCIN–X**, **345-TCIN** in methanol (**qmdanthocyanin.inp** in /usr/people/neil on bionmr.bio.utk.edu).

```
!    INPUT FILE FOR DISCOVER GENERATED BY INSIGHT
!
!
      overlap = 0.01
!
      begin simulation
     *    add-automatic bond torsion valence out-of-plane
      reduce
!
      set dielectric  = 80
!
!
!
        initialize dynamics at 600 K with a step size of 1.0 femtoseconds
     *  write history file every 1000 steps
        loop=1
100     resume dynamics for 1000 steps
        archive as file number loop
        loop=loop+1
        if loop.le.1000 then 100
        loop=1
200     retrieve file number loop
        minimize using conjugate gradient for 1000000 steps
     *  until the maximum derivative is less than 0.0001000000 kcal/A
        archive as file number loop
        loop=loop+1
        if loop.le.1000 then 200
        end
```

Input file used in the QMD simulation of anthocyanins **4-FCIN** and **345-TCIN** in water (**qmdanthocyaninwater.inp** in /usr/people/neil on bionmr.bio.utk.edu).

This represents a list of all the anthocyanins (NMR samples) that are in the container in the freezer of **R1**. All samples are marked with the code and experiment #.

Any questions can be directed to Neil Whittemore at University of Colorado, Boulder (For contact information, please refer to Profs. Don Dougall or David C. Baker).

CODE	Expt #	Numbers used are from ref 34
3,4,5-TRIMETHOXYBENZOIC ACID	0	
345TBENZ	1333	20
4DMACIN	1335	19
3MCIN	1347	12
4CCIN	1348	16
4CBENZ	1348	22
4FCIN	1350	15
345TC-X	1354	8
345TC-X	1354	8
345TCIN	1359	7
345TCIN	1359	7
345TCIN DRY DCI	1359	7
345TCIN FROZEN DCI	1359	7
CIN	1360	14
CYANXG	1372	3
CYANGXG	1372	1
4HCIN	1373	9
4HC-X	1373	10
CYANG	1376	4
CYANGG	1377	2
345TBENZ	1389	20
345TBENZ	1402	20

Below are the filenames for select Figs. from Part One: Conformational Studies of Monoacylated Anthocyanins: Factors that Affect Color Stability (these are located in the....**\NAW_dissertation\Part I\Figs** directory).

Fig. 3. . . . . figure1.wpd

Fig. 4. . . . . antho fig4.wpd

Fig. 5. . . . . antho fig5.wpd

Fig. 6. . . . . cyangxg.tif

Fig. 7. . . . . tmbenz.tif

Fig. 8. . . . . fcin.tif

Fig. 9. . . . . tcin.tif

Fig. 10. . . . . tcin_x.tif

Fig. 11. . . . . antho fig6.wpd

Fig. 12. . . . . restraints met CyanGXG.wpd

Fig. 13. . . . . restraints met 345TMBENZ.wpd

Fig. 14. . . . . restraints met 4FCIN.wpd

Fig. 15. . . . . restraints met 345TCIN_X.wpd

Fig. 16. . . . . rests met 345_tcin.wpd

Fig. 17. . . . . anthoflac.pdf

Fig. 18. . . . . anthofld.pdf

Fig. 19. . . . . anthofrac.pdf

File names for select Figs. from Part One: Conformational Studies of Monoacylated Anthocyanins: Factors that Affect Color Stability contd.

Fig. 20. . . . . anthofrb.pdf

Fig. 21. . . . . anthofrd.pdf

Fig. 22. . . . . anthofuac.pdf

Fig. 23. . . . . anthonlac.pdf

Fig. 24. . . . . anthonrac.pdf

Fig. 25. . . . . anthonrd.pdf

Fig. 26. . . . . anthonuac.pdf

Fig. 27. . . . . anthoopface.pdf

Fig. 28. . . . . anthomisc.pdf

Fig. 29. . . . . fcinnrd5ns.jnb

Fig. 30. . . . . fcinflipmeoh.pdf

Fig. 31. . . . . fcinflipmeohmlp.pdf

Fig. 32. . . . . fcinflipmeohmlc.pdf

Fig. 33. . . . . fcinflipmeohmep2.pdf

Fig. 34. . . . . fcinh2oflipstructs.pdf

Fig. 35. . . . . tcinh2oflipstructs.pdf

Fig. 36. . . . . fcinh2ononflipstructs.pdf

Fig. 37. . . . . tcinh2ononflipstructs.pdf

File names for select Figs. from Part One: Conformational Studies of Monoacylated Anthocyanins: Factors that Affect Color Stability contd.

Fig. 38. . . . . fcinnrd1.jnb

Fig. 39 . . . . . fcinfrd1.jnb

Fig. 40. . . . . fcinnrd2.jnb

Fig. 41. . . . . tcinfrd1.jnb

Fig. 42. . . . . tcinfrd2.jnb

Fig. 43. . . . . fcinfliph2ostudy.pdf

Fig. 44. . . . . tcinfliph2ostudy.pdf

Fig. 45. . . . . fcinfliph2omlp.pdf

Fig. 46. . . . . fcinfliph2omep.pdf

Fig. 47. . . . . fcinfliph2omlc.pdf

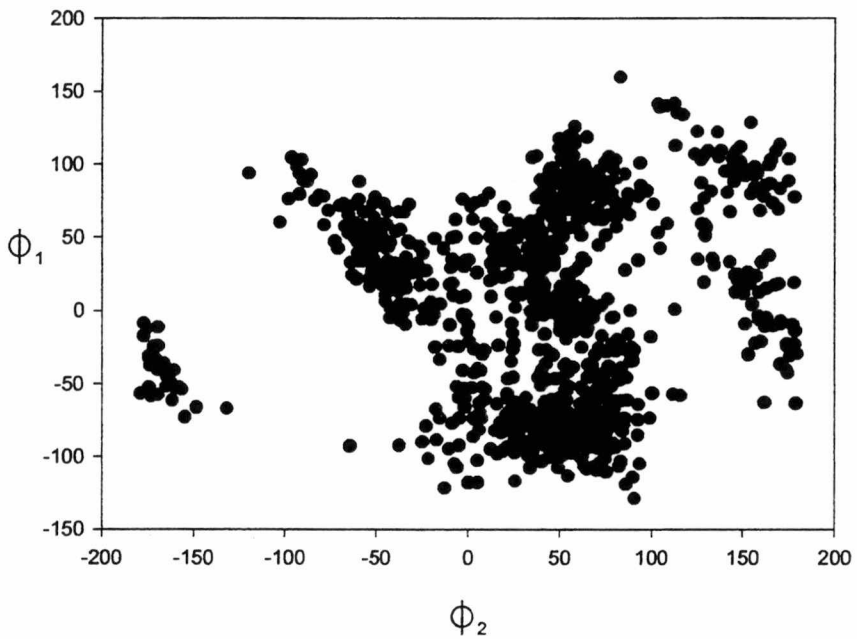
Fig. 48. . . . . tcinfliph2omlp.pdf

Fig. 49. . . . . tcinfliph2omep.pdf

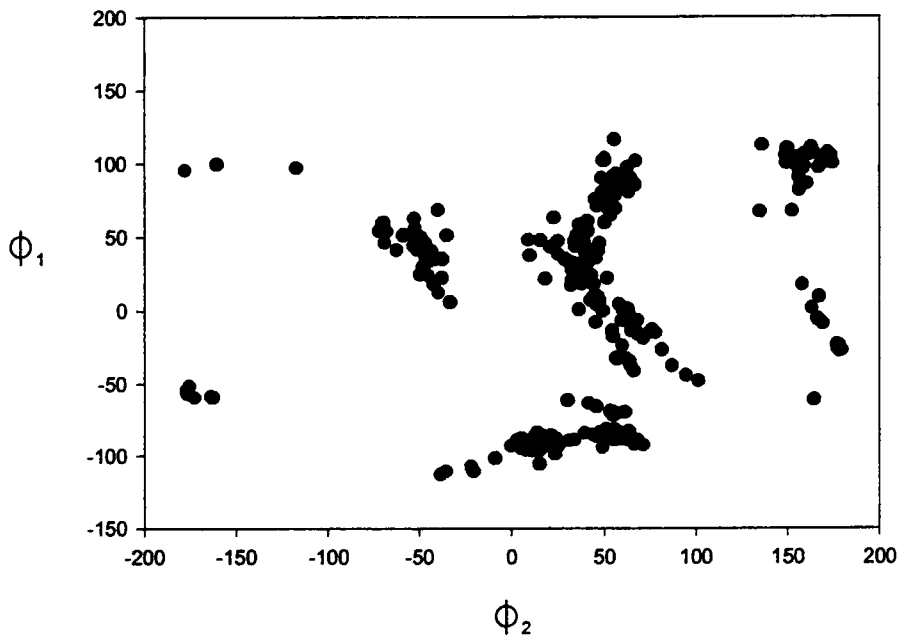
Fig. 50. . . . . tcinfliph2omlc.pdf

Fig. 51. . . . . antho fig51.wpd

Fig. 52. . . . . usda figure 10.wpd

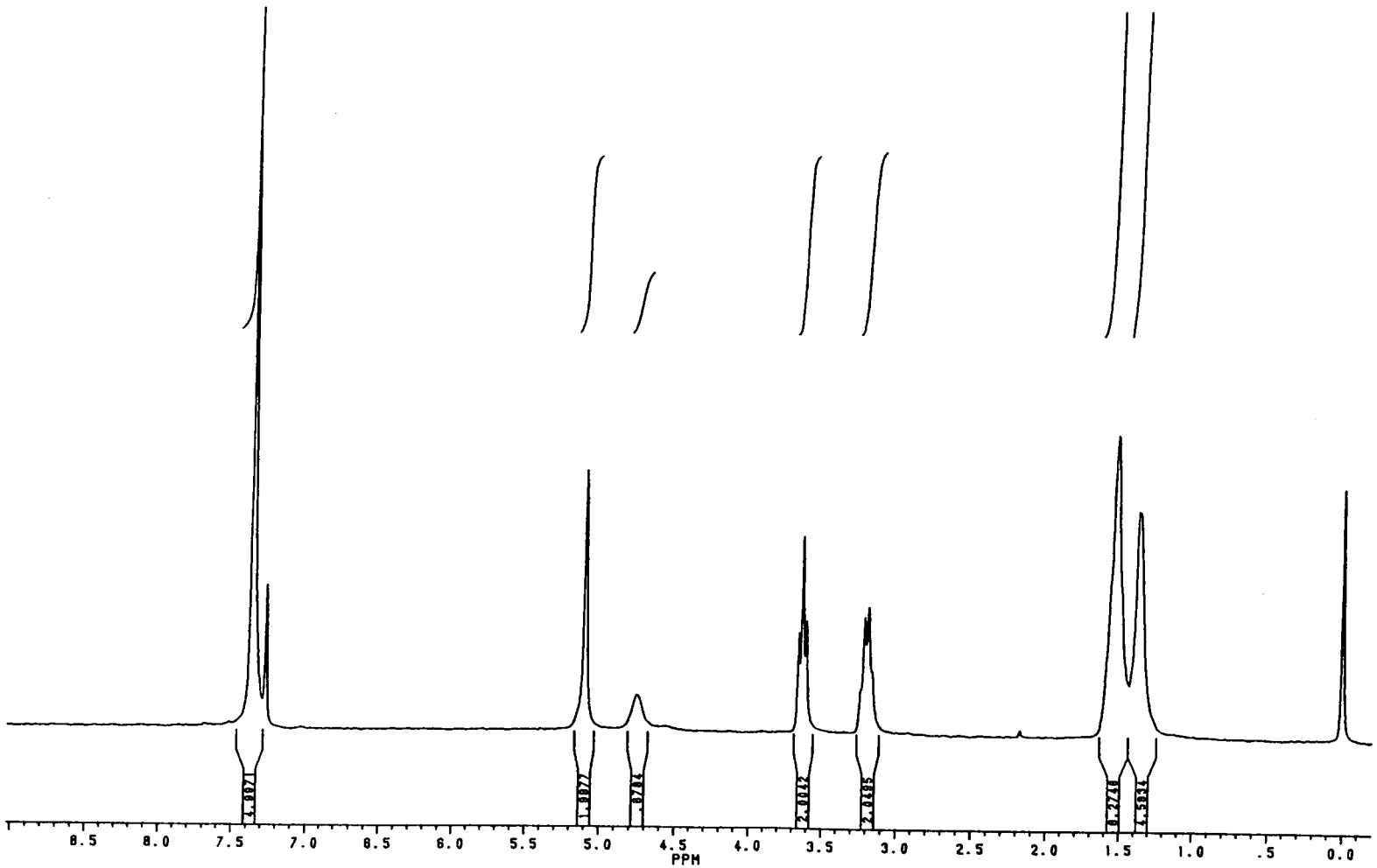


A graph of ϕ_1 *vs* ϕ_2 for the 1000 conformers of **4-FCIN** after the molecular dynamics phase of quenched molecular dynamics in a dielectric continuum of methanol.

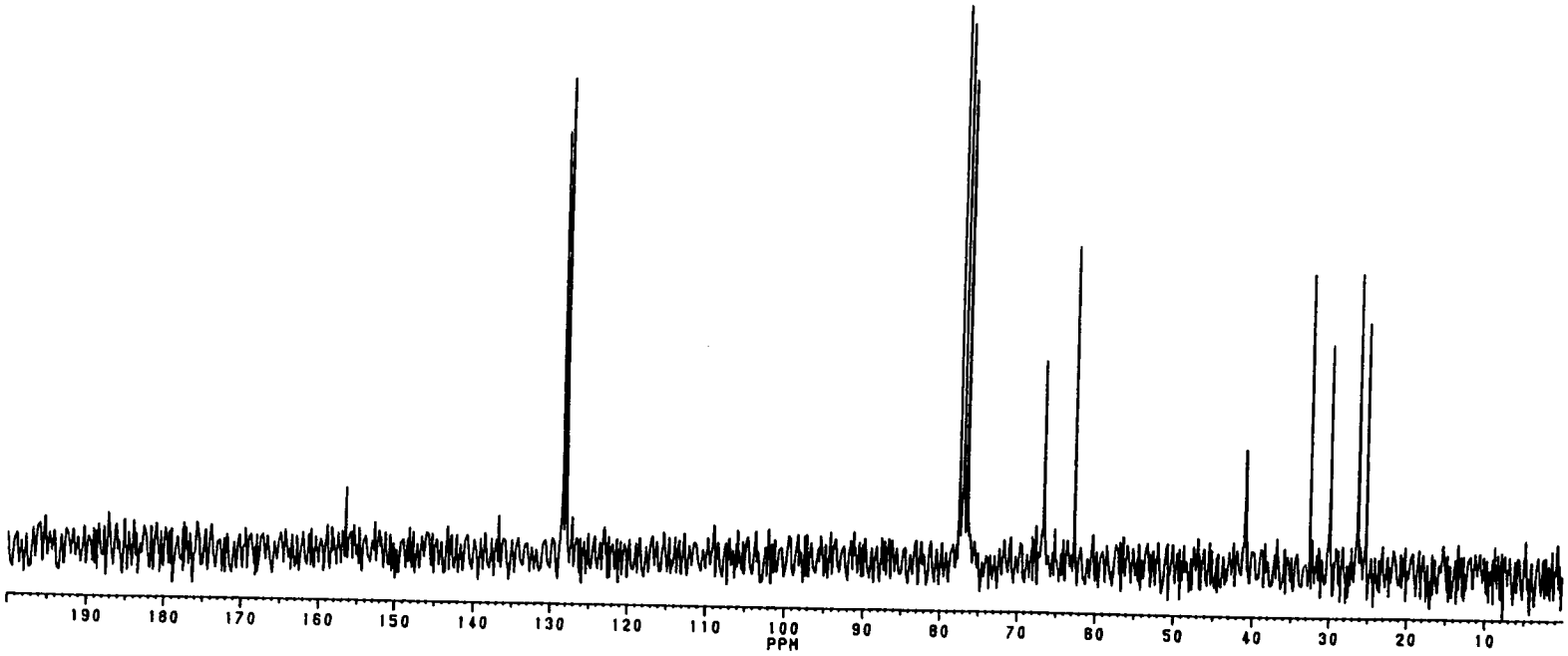


A graph of ϕ_1 *vs* ϕ_2 for anthocyanin **4-FCIN** after the minimization phase of quenched molecular dynamics in a dielectric continuum of methanol.

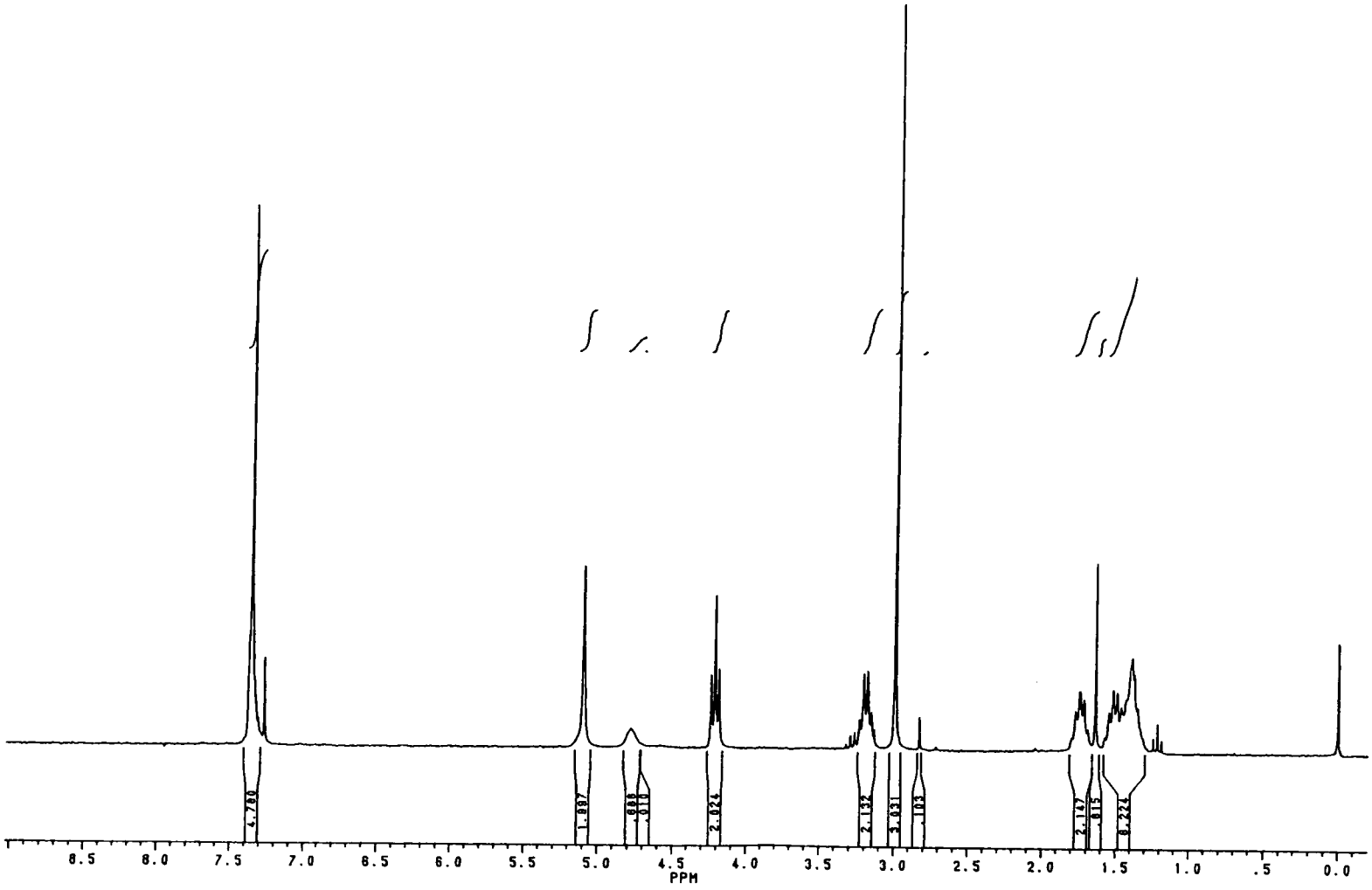
APPENDIX B. ^{1}H and ^{13}C NMR Spectra for Compounds Used to Synthesize C-8-Modified Electroactive Nucleosides



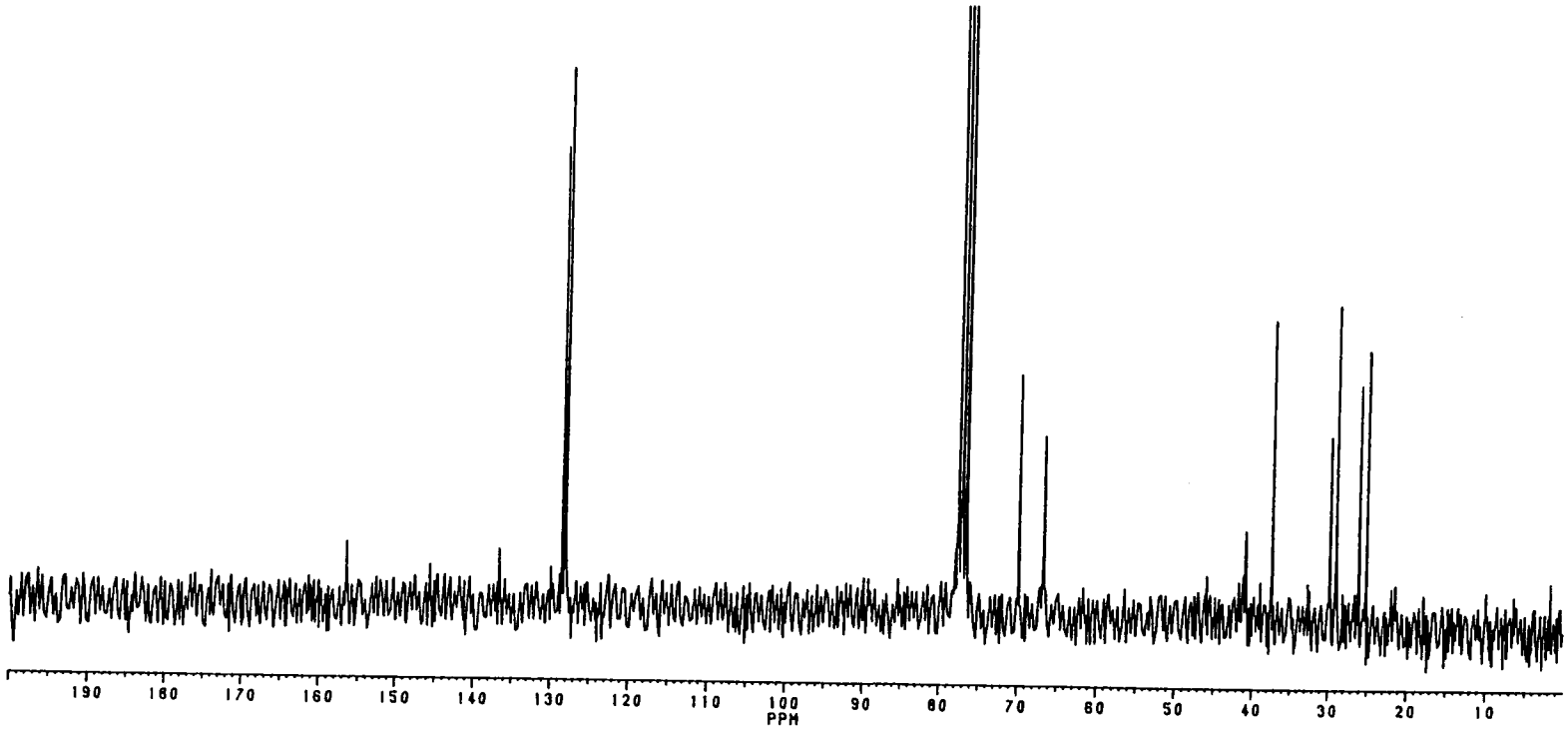
^{1}H NMR spectrum (250 MHz, $CDCl_3$) of 6-(*N*-benzyloxycarbonylamino)hexanol (**7**).



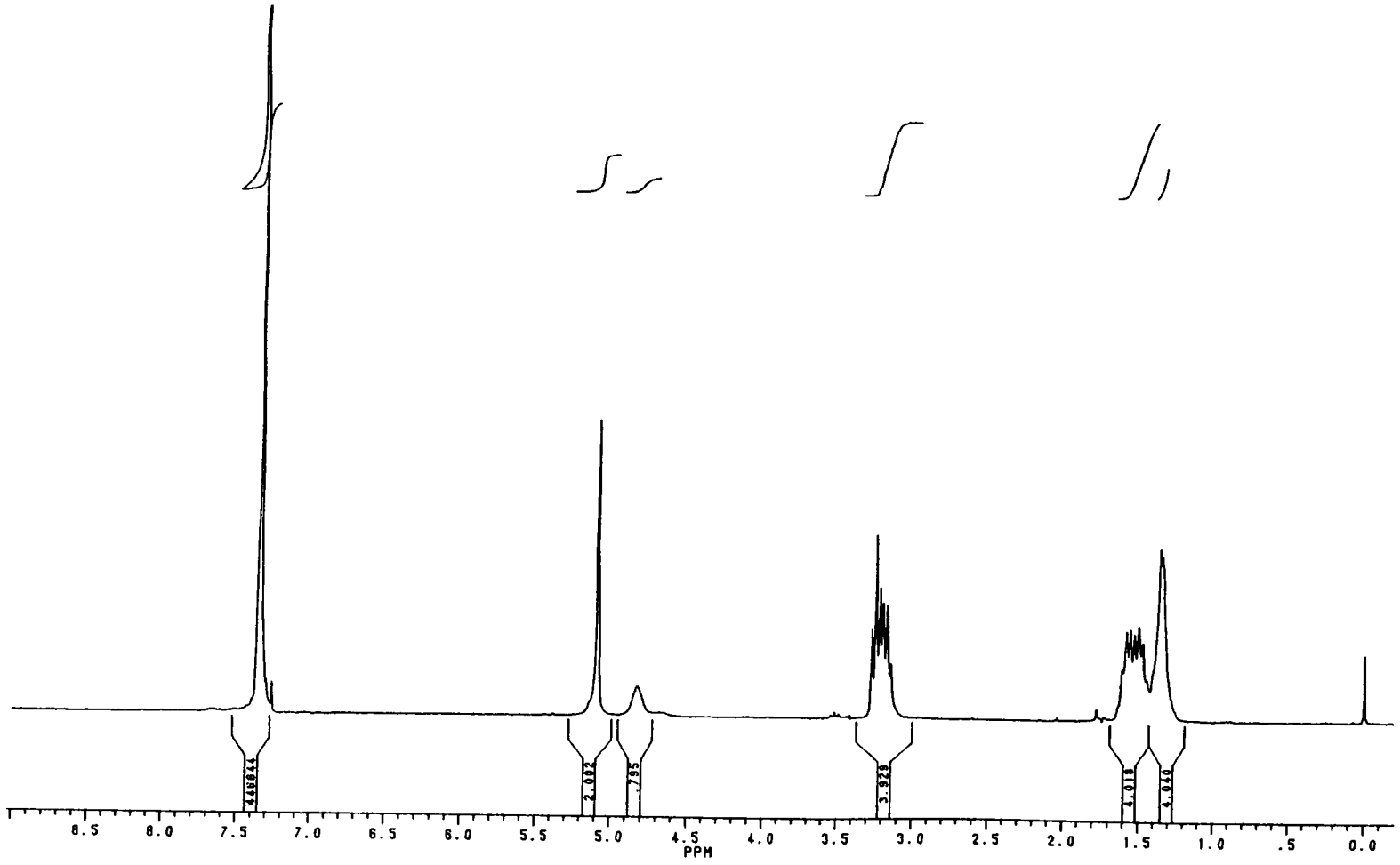
^{13}C NMR spectrum (62.9 MHz, $CDCl_3$) of 6-(*N*-benzyloxycarbonylamino)hexanol (**7**).



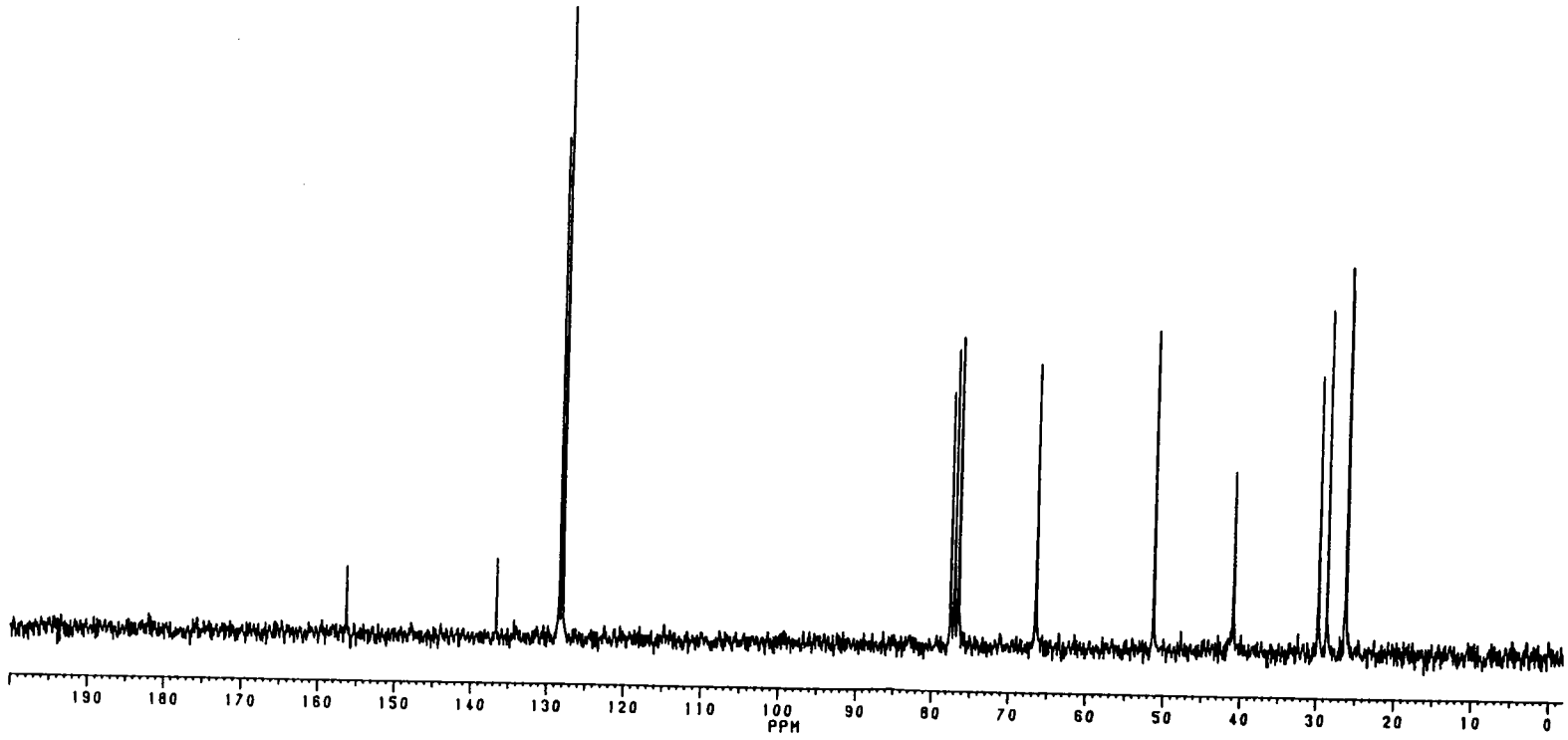
^{1}H NMR spectrum (250 MHz, $CDCl_3$) of 6-(*N*-benzyloxycarbonylamino)-1-*O*-(methylsulfonyl)hexanol (**8**).



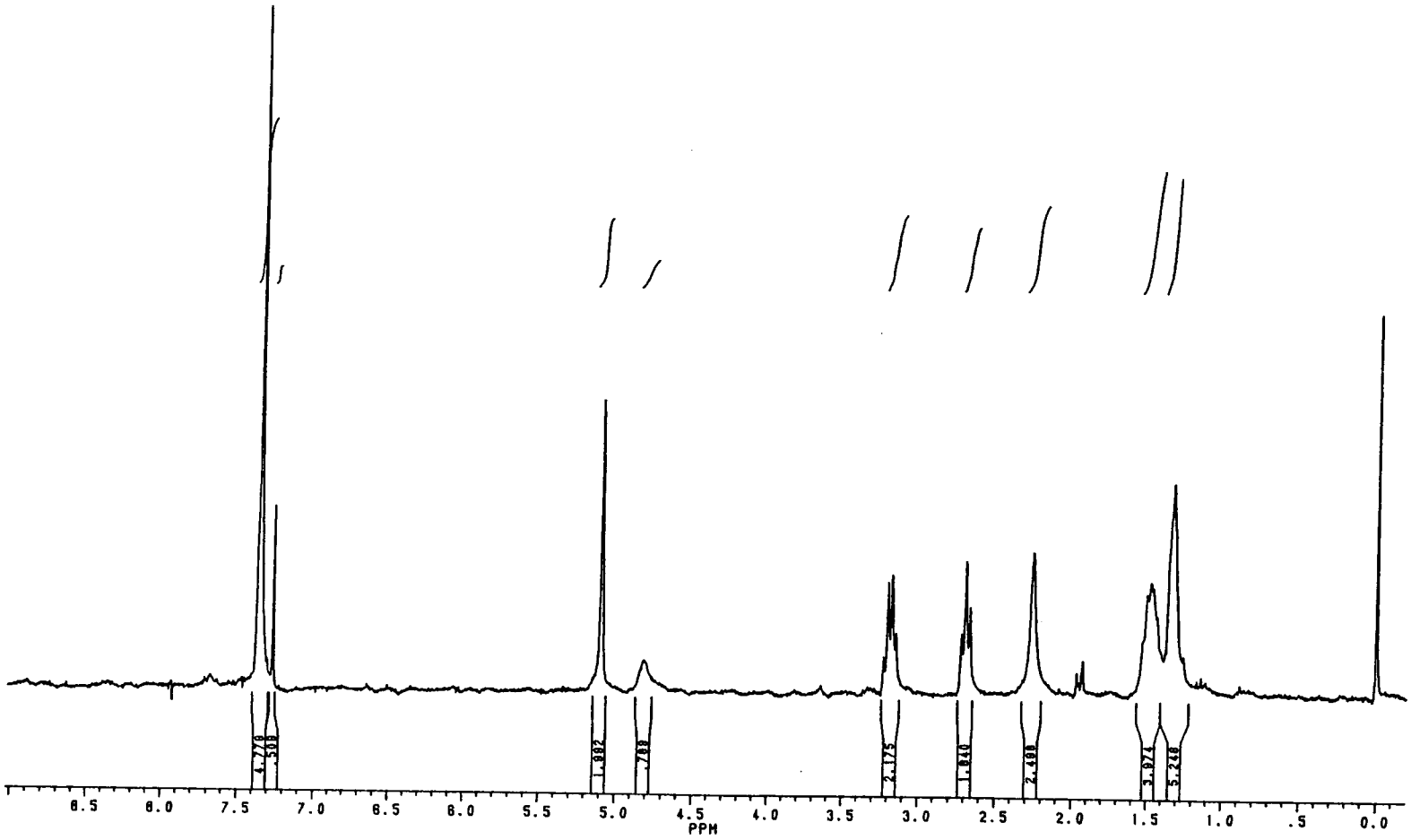
^{13}C NMR spectrum (62.9 MHz, $CDCl_3$) of 6-(*N*-benzyloxycarbonylamino)-1-*O*-(methylsulfonyl)hexanol (**8**).



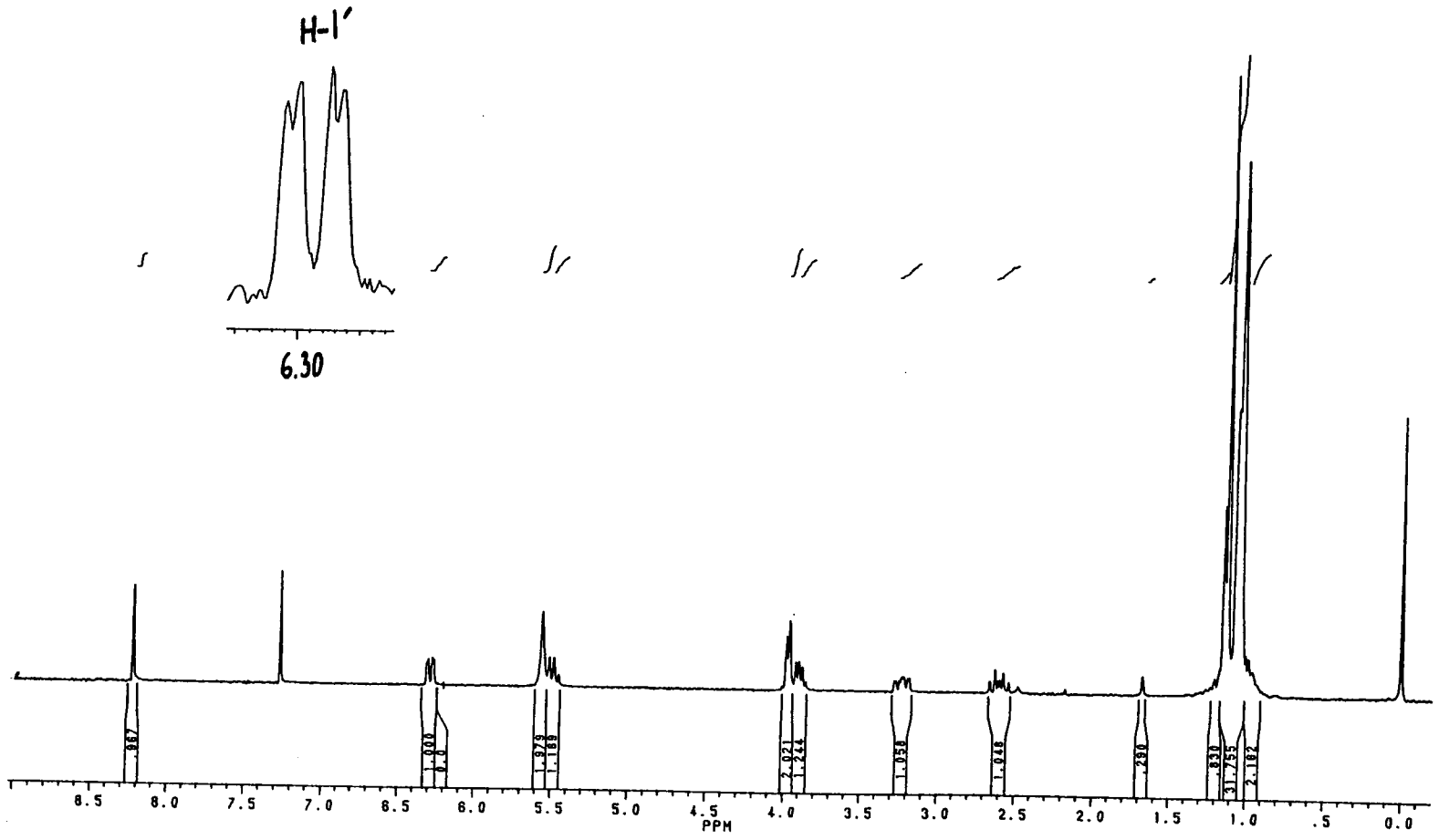
^{1}H NMR spectrum (250 MHz, $CDCl_3$) of 1-azido-6-(*N*-benzyloxycarbonylamino)hexane (**9**).



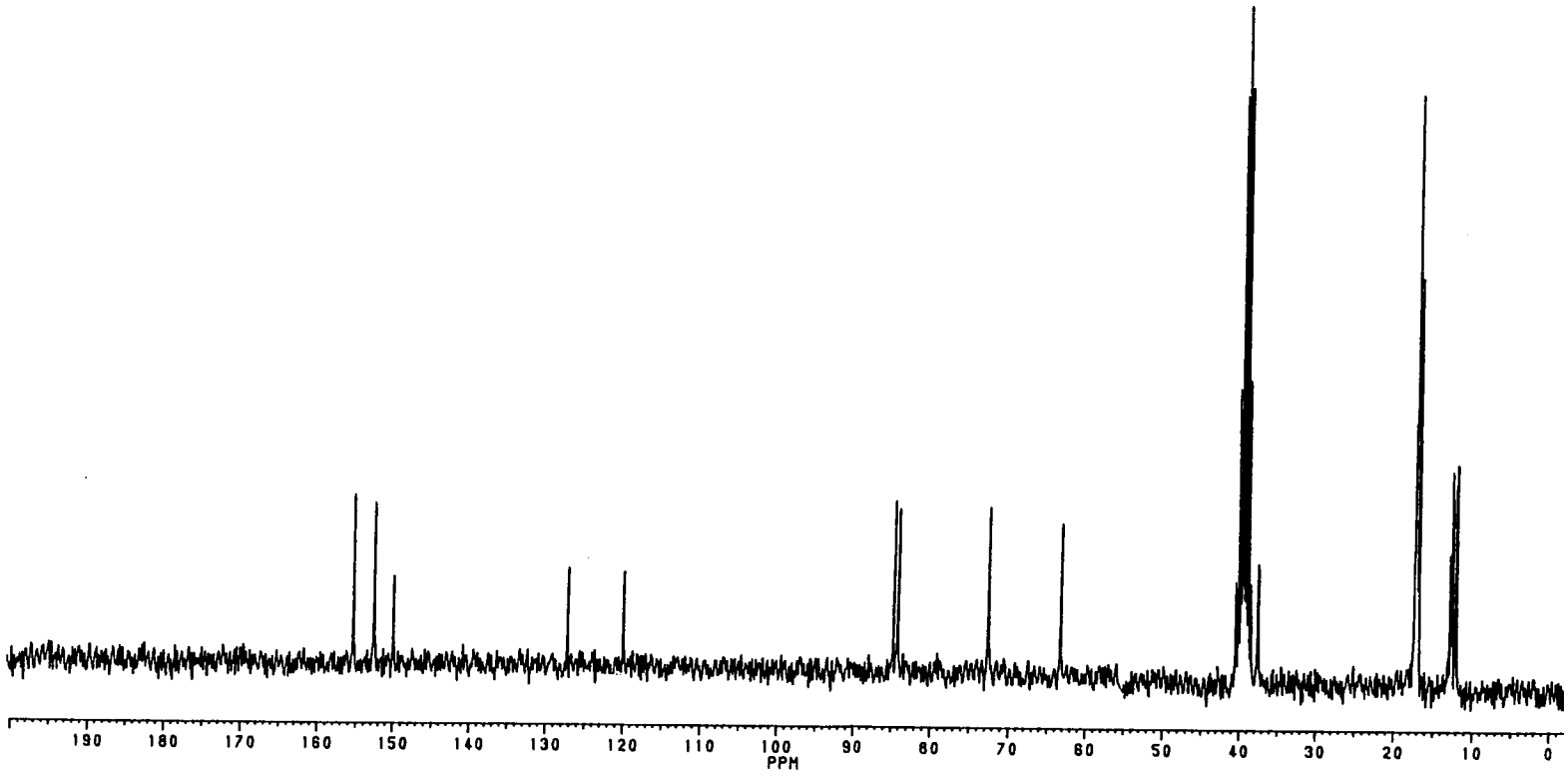
^{13}C NMR spectrum (62.9 MHz, $CDCl_3$) of 1-azido-6-(*N*-benzyloxycarbonylamino)hexane (**9**).



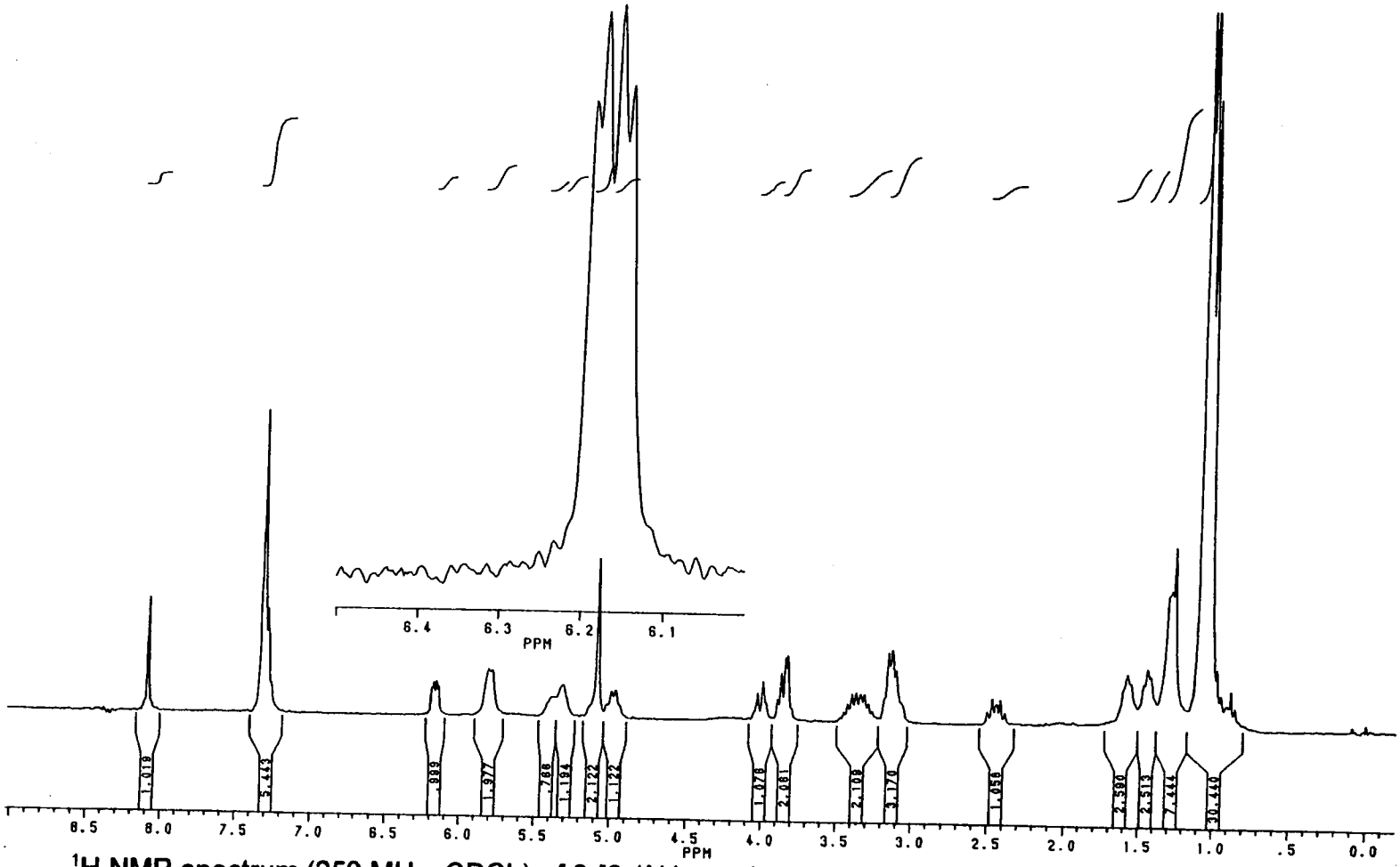
^{1}H NMR spectrum (250 MHz, $CDCl_3$) of 6-(*N*-benzyloxycarbonylamino)hexylamine (**10**).



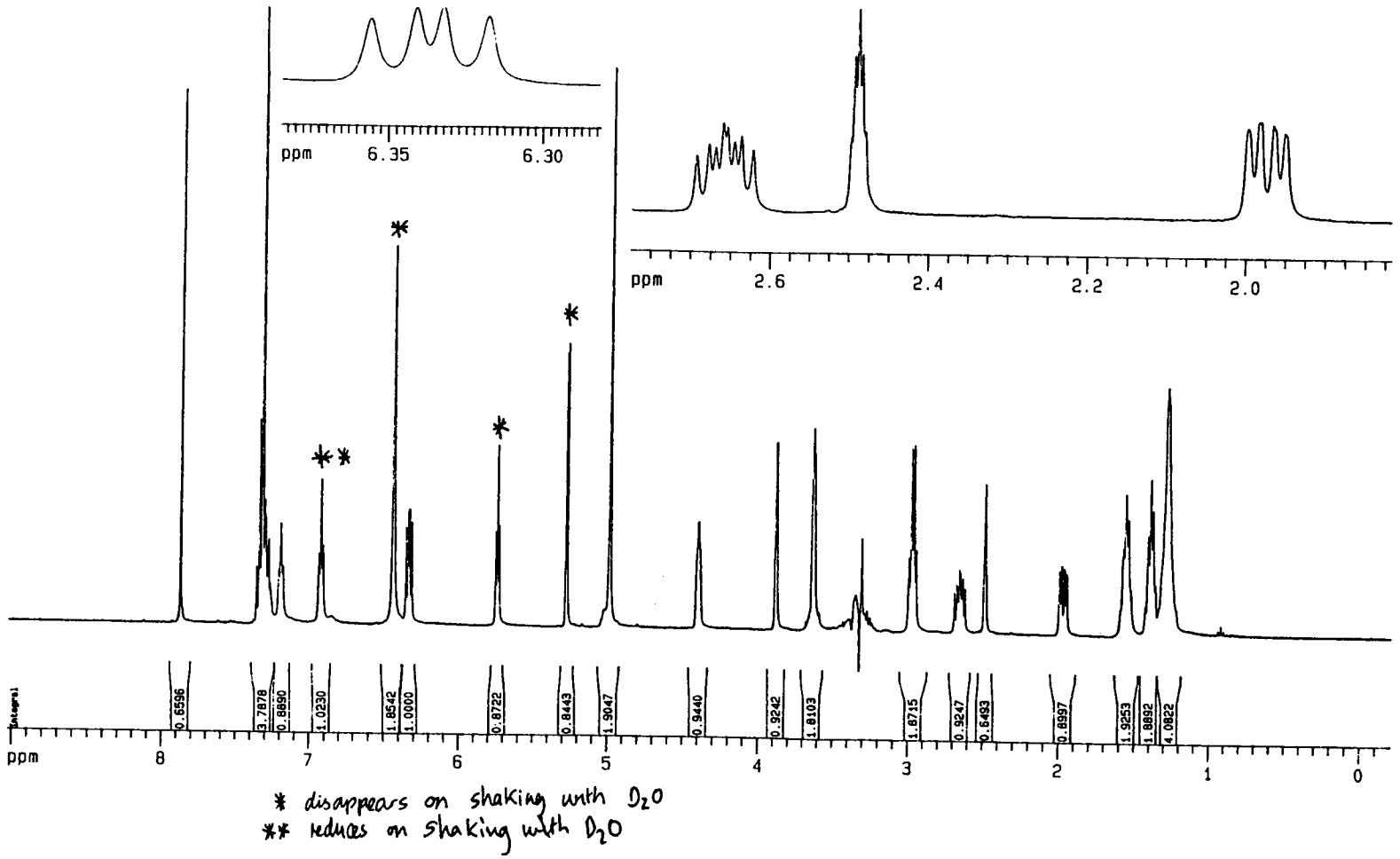
^{1}H NMR spectrum (250 MHz, $CDCl_3$) of 8-bromo-3′,5′-*O*-(1,1,3,3-tetraisopropyldisiloxane-1,3-diyl)-2′-deoxyadenosine (**18**).



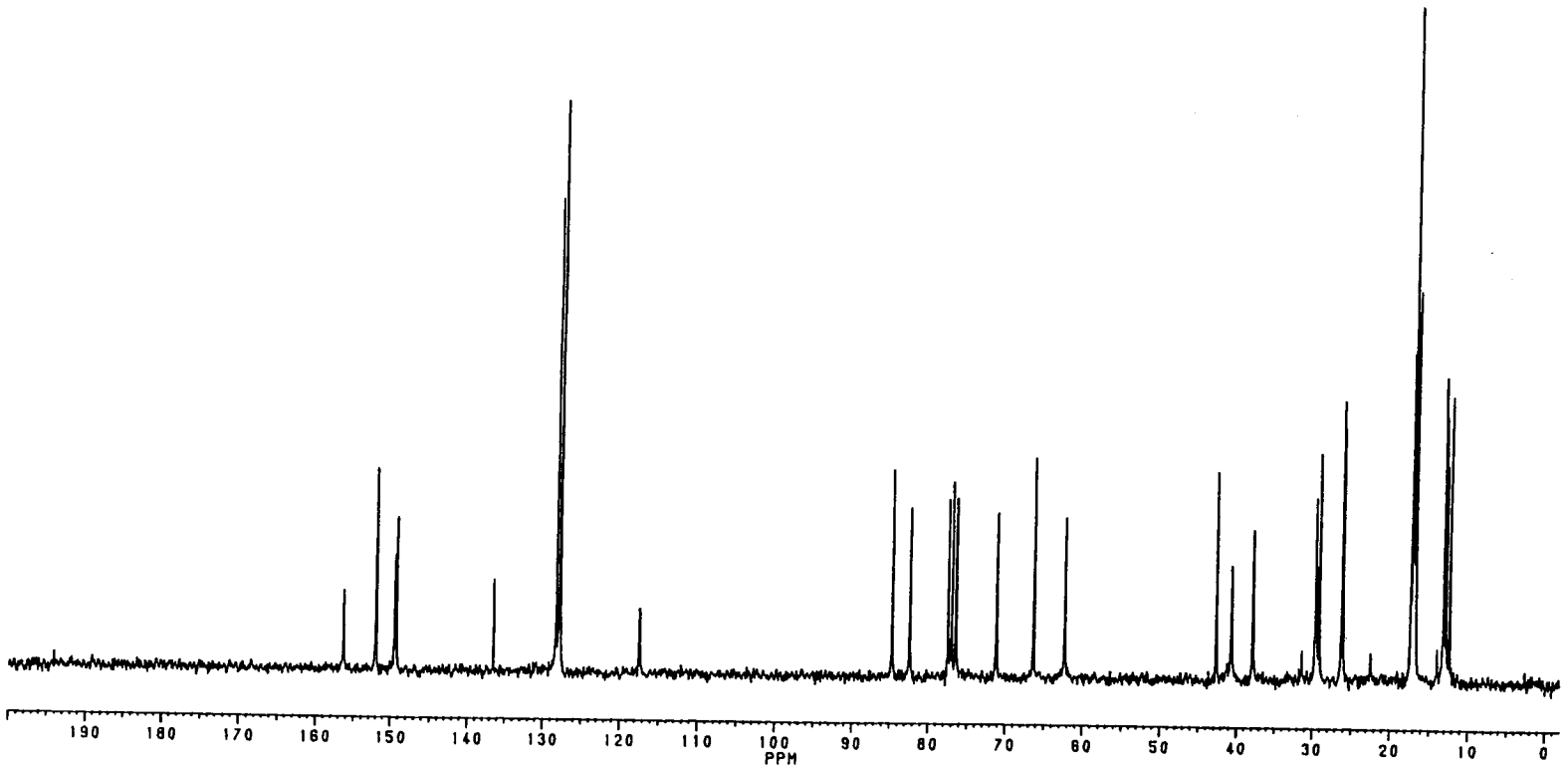
^{13}C NMR spectrum (62.9 MHz, DMSO-d_6) of 8-bromo-3′,5′-*O*-(1,1,3,3-tetraisopropyldisiloxane-1,3-diyl)-2′-deoxyadenosine (**18**).



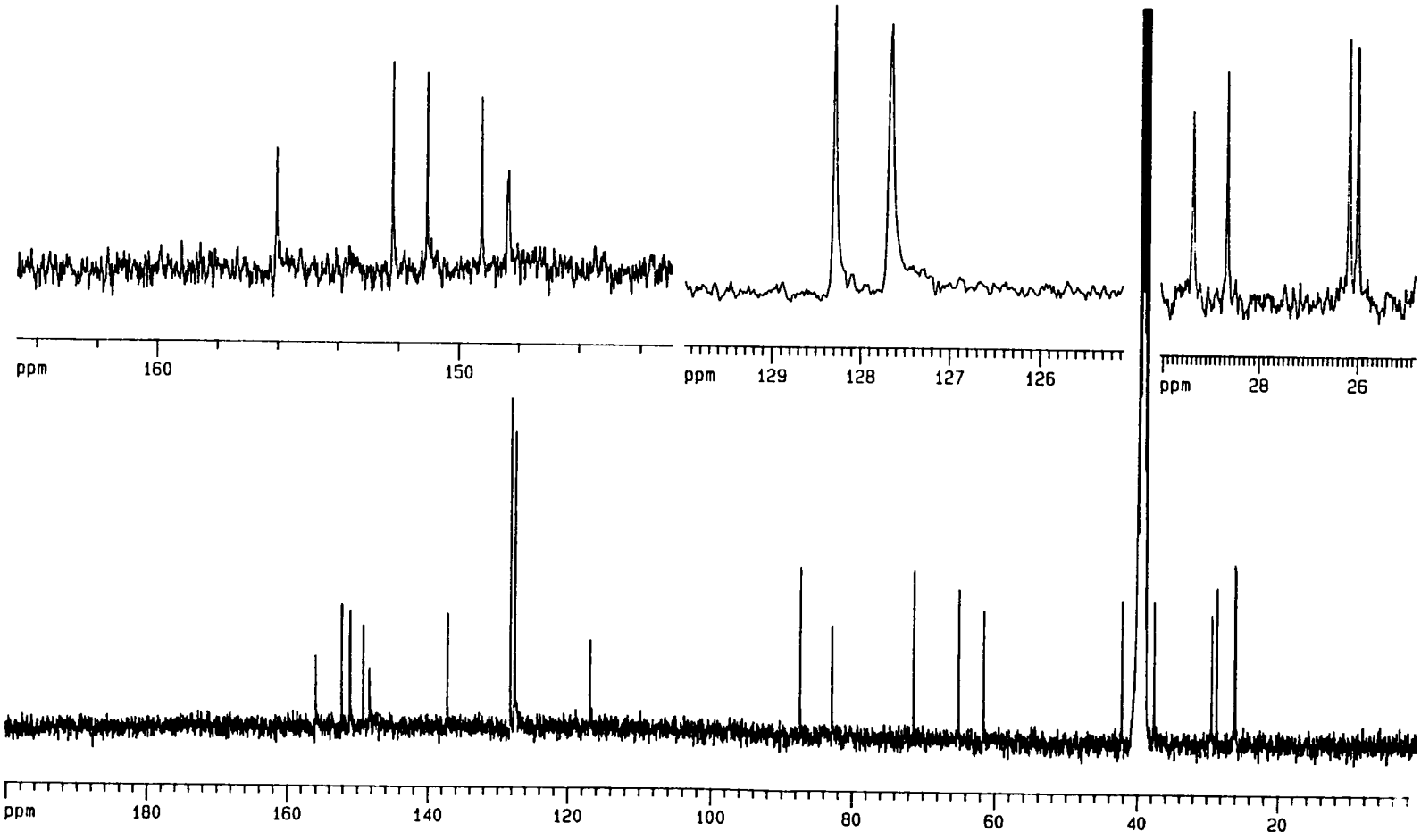
^{1}H NMR spectrum (250 MHz, $CDCl_3$) of 8-[6-(*N*-benzyloxycarbonylamino)hexylamino]-3′,5′-*O*-(1,1,3,3-tetraisopropyldisiloxane-1,3-diyl)-2′-deoxyadenosine (**19**).



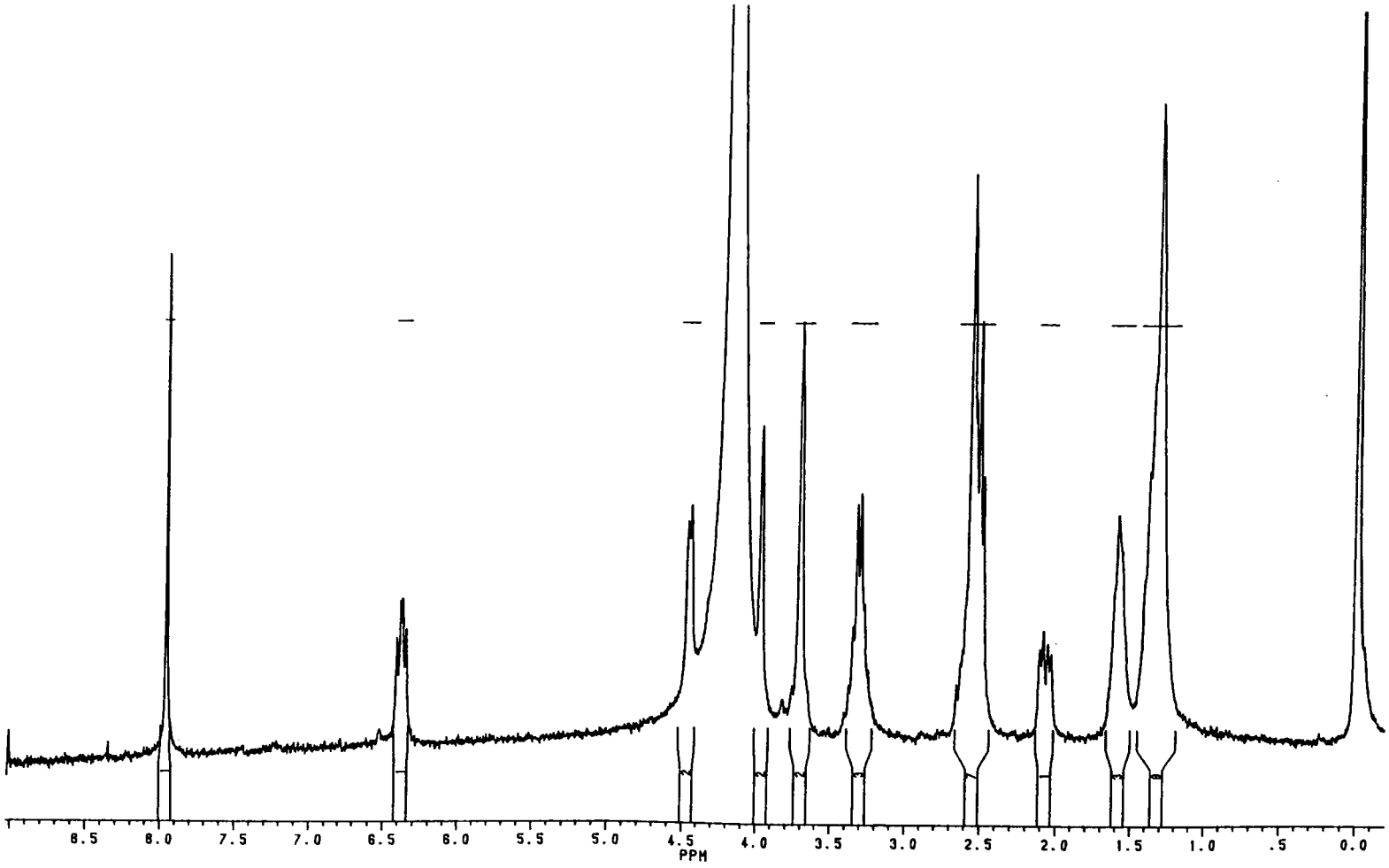
^{1}H NMR spectrum (250 MHz, DMSO-d_6) of 8-[6-(*N*-benzyloxycarbonylamino)hexylamino]-2′-deoxyadenosine (**21**).



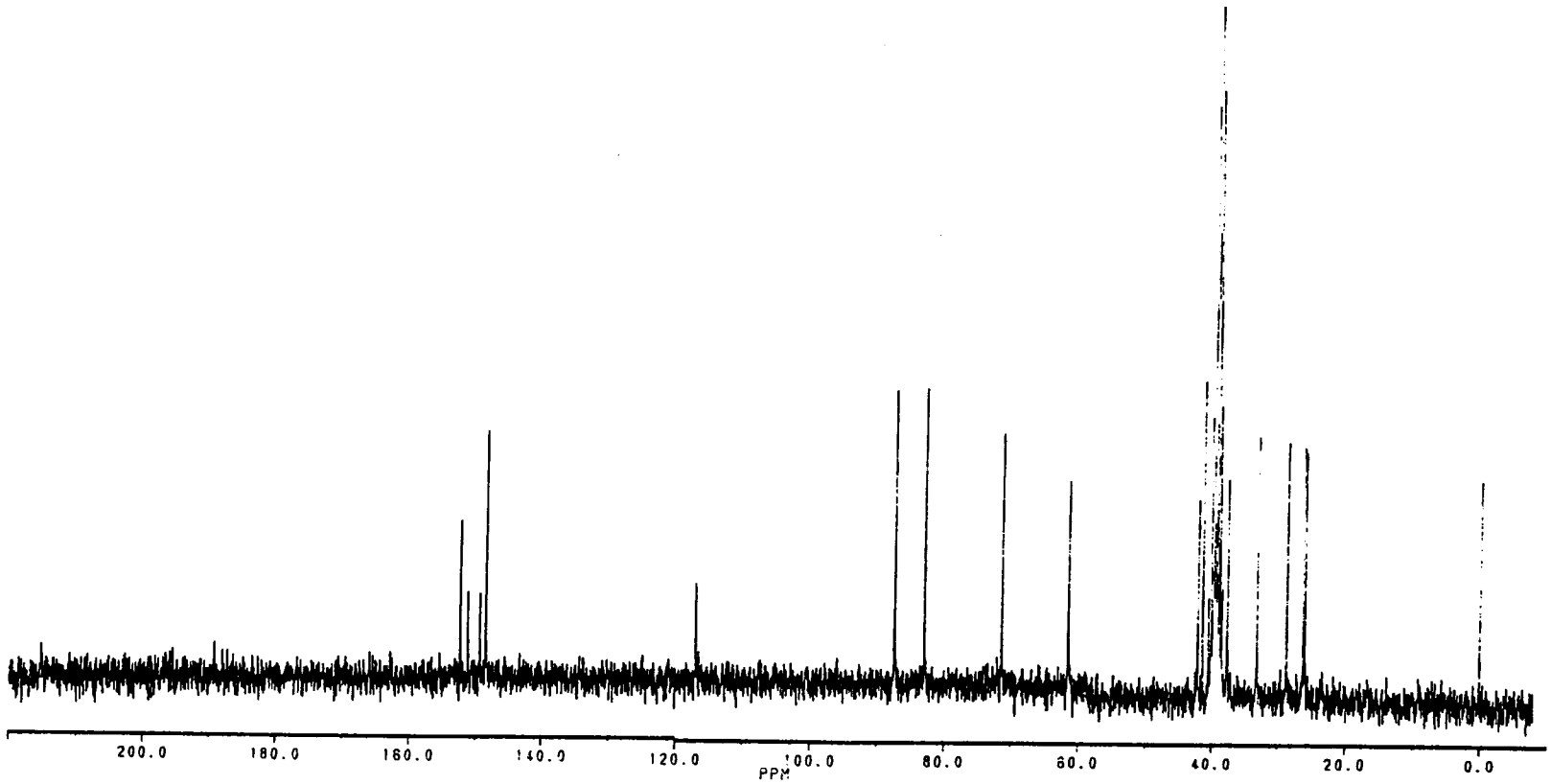
^{13}C NMR spectrum (62.9 MHz, $CDCl_3$) of 8-[6-(*N*-benzyloxycarbonylamino)hexylamino]-3′,5′-*O*-(1,1,3,3-tetraisopropyldisiloxane-1,3-diyl)-2′-deoxyadenosine (**19**).



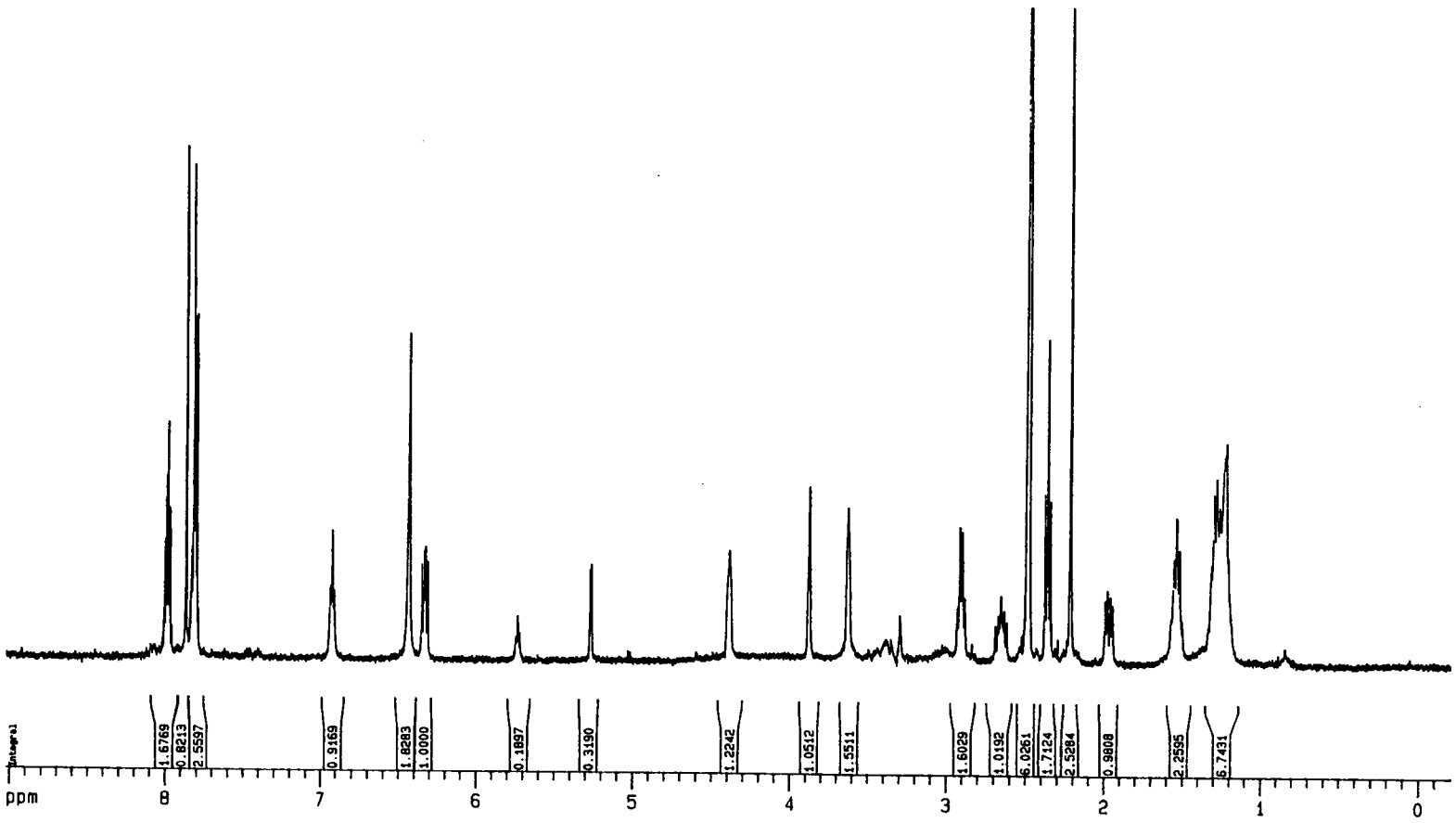
^{13}C NMR spectrum (62.9 MHz, DMSO-d_6) of 8-[6-(*N*-benzyloxycarbonylamino)hexylamino]-2′-deoxyadenosine (**21**).



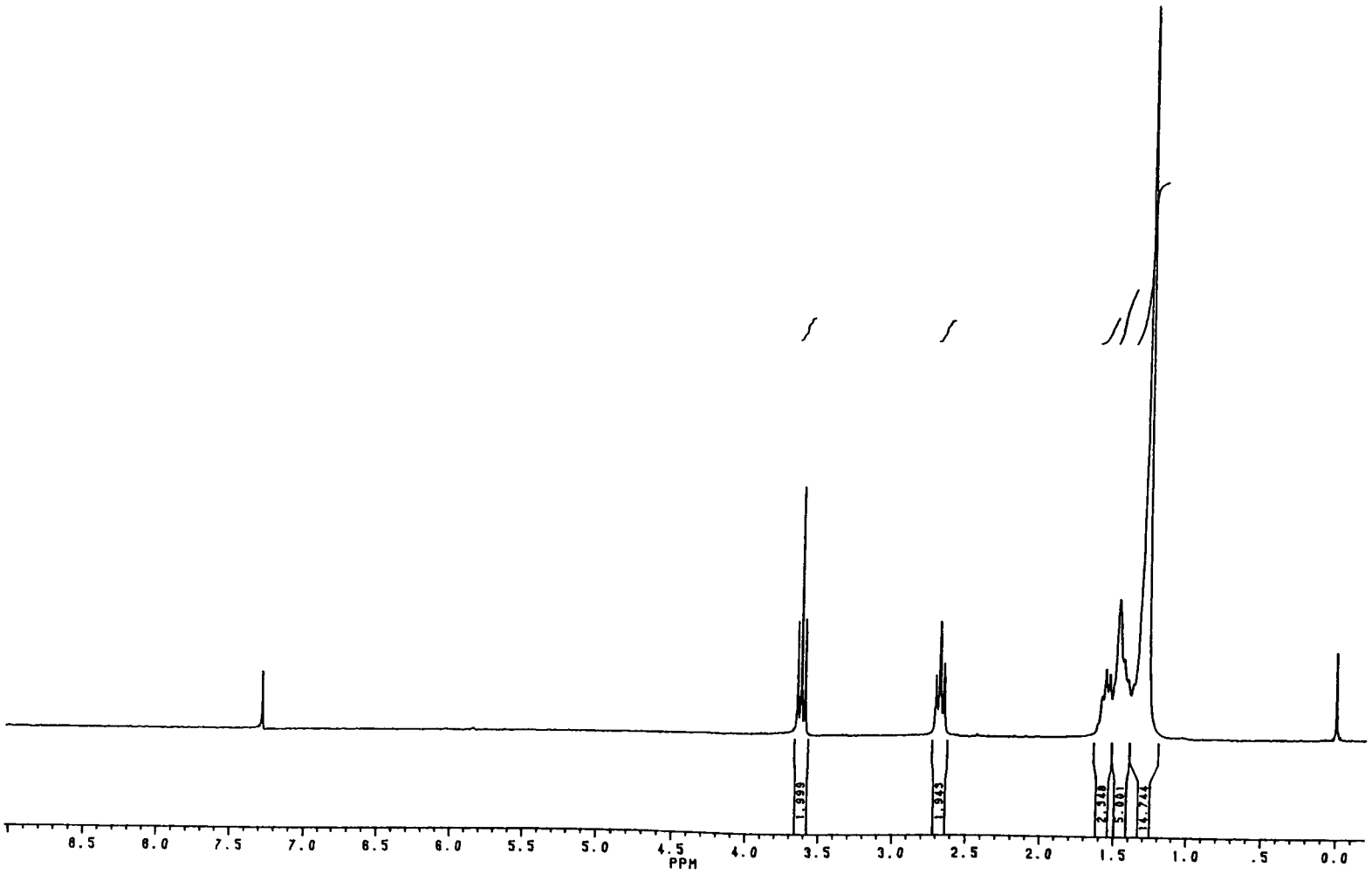
^{1}H NMR spectrum (250 MHz, $CDCl_3$) of 8-(6-hexylamino)-2′-deoxyadenosine (**22**).



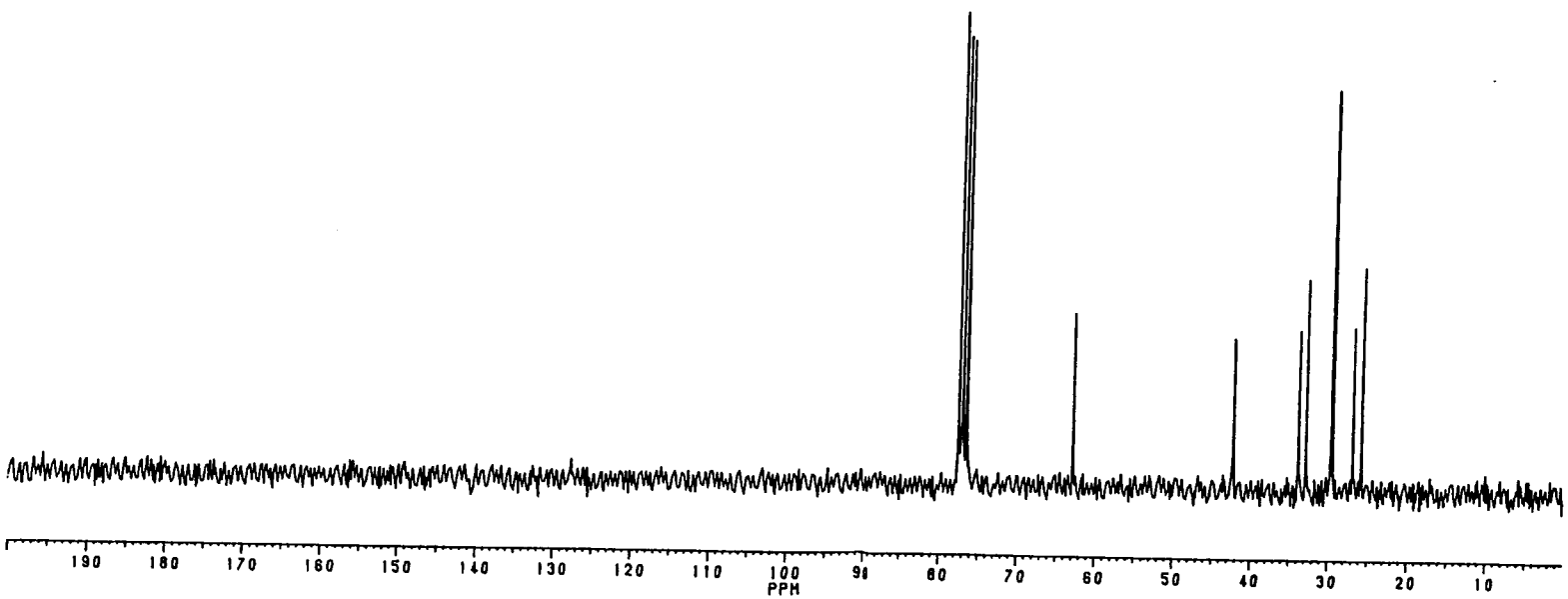
^{13}C NMR spectrum (62.9 MHz, $CDCl_3$) of 8-(6-hexylamino)-2′-deoxyadenosine (**22**).



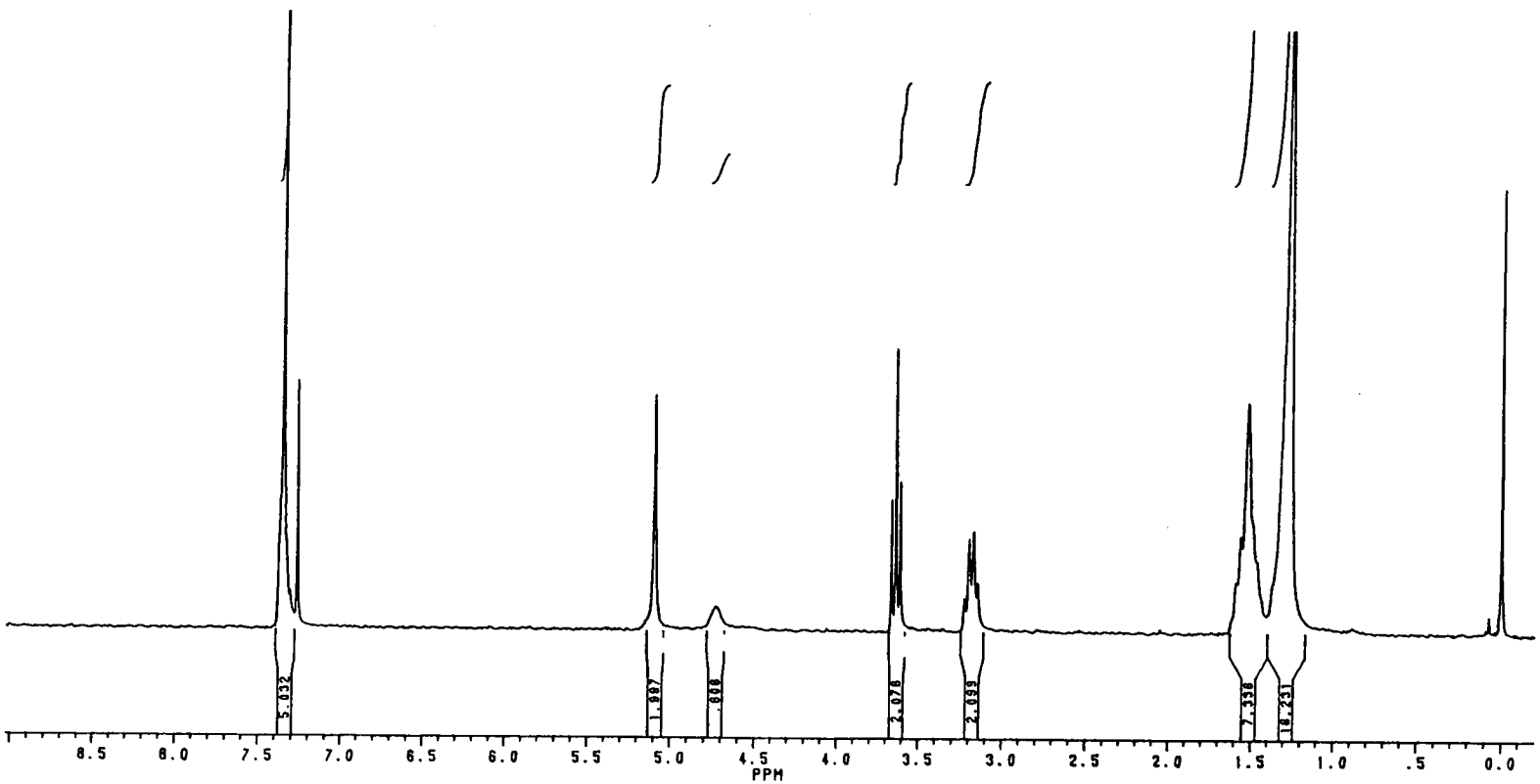
^{1}H NMR spectrum (400.13 MHz, DMSO-d_6) of NQ–2′-Deoxyadenosine conjugate (**1**).



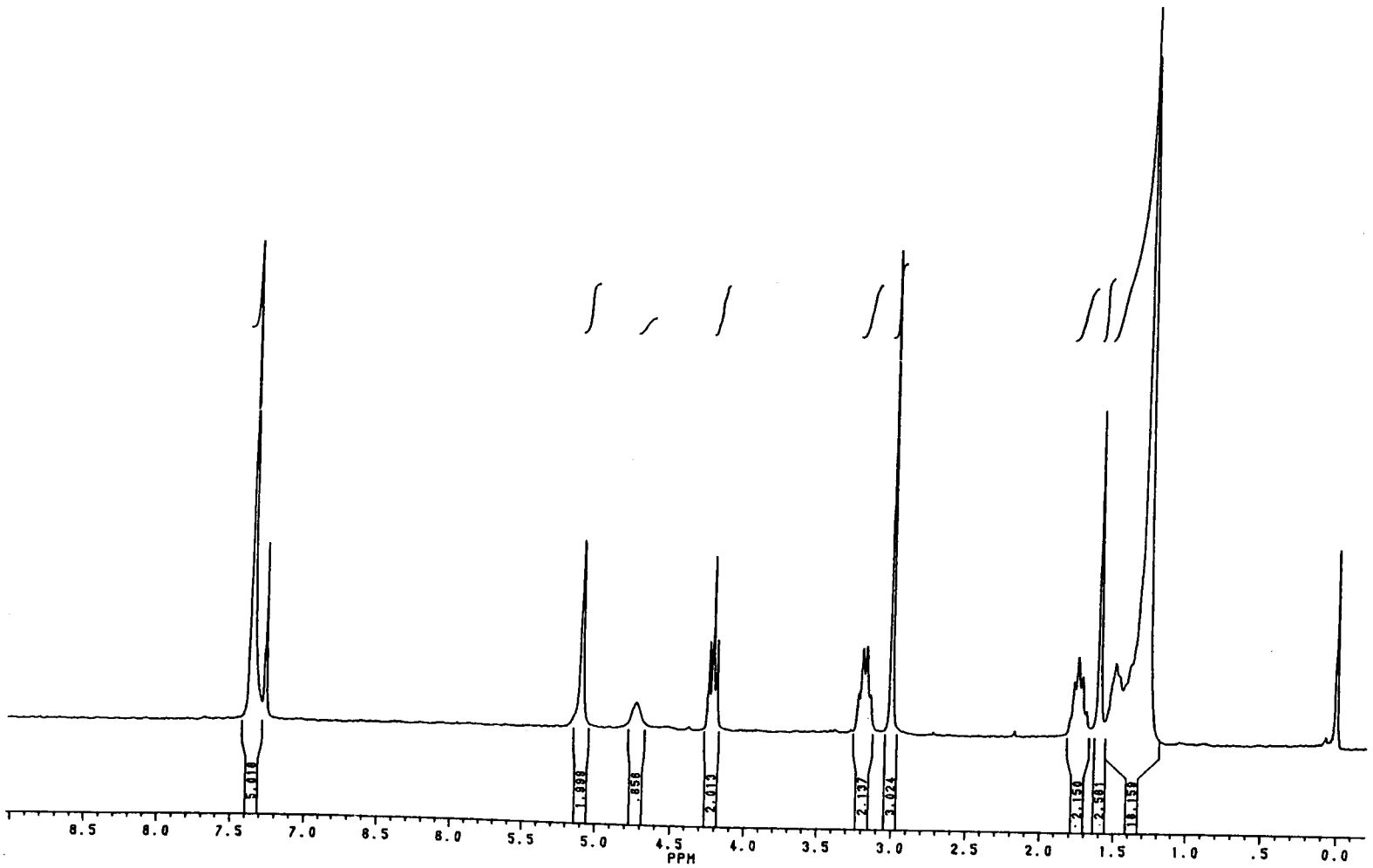
^{1}H NMR spectrum (250.13 MHz, $CDCl_3$) of 11-aminoundecanol (**11**).



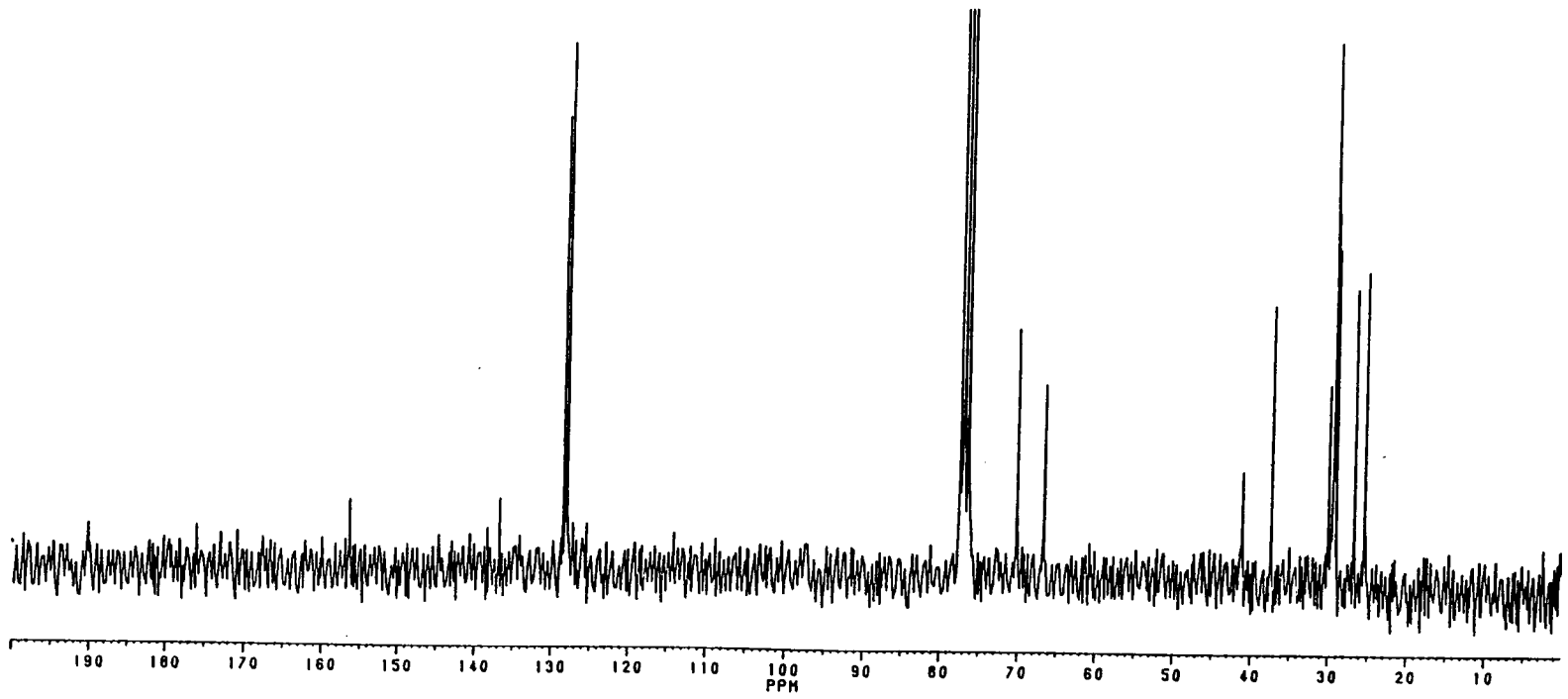
^{13}C NMR spectrum (62.9 MHz, $CDCl_3$) of 11-aminoundecanol (**11**).



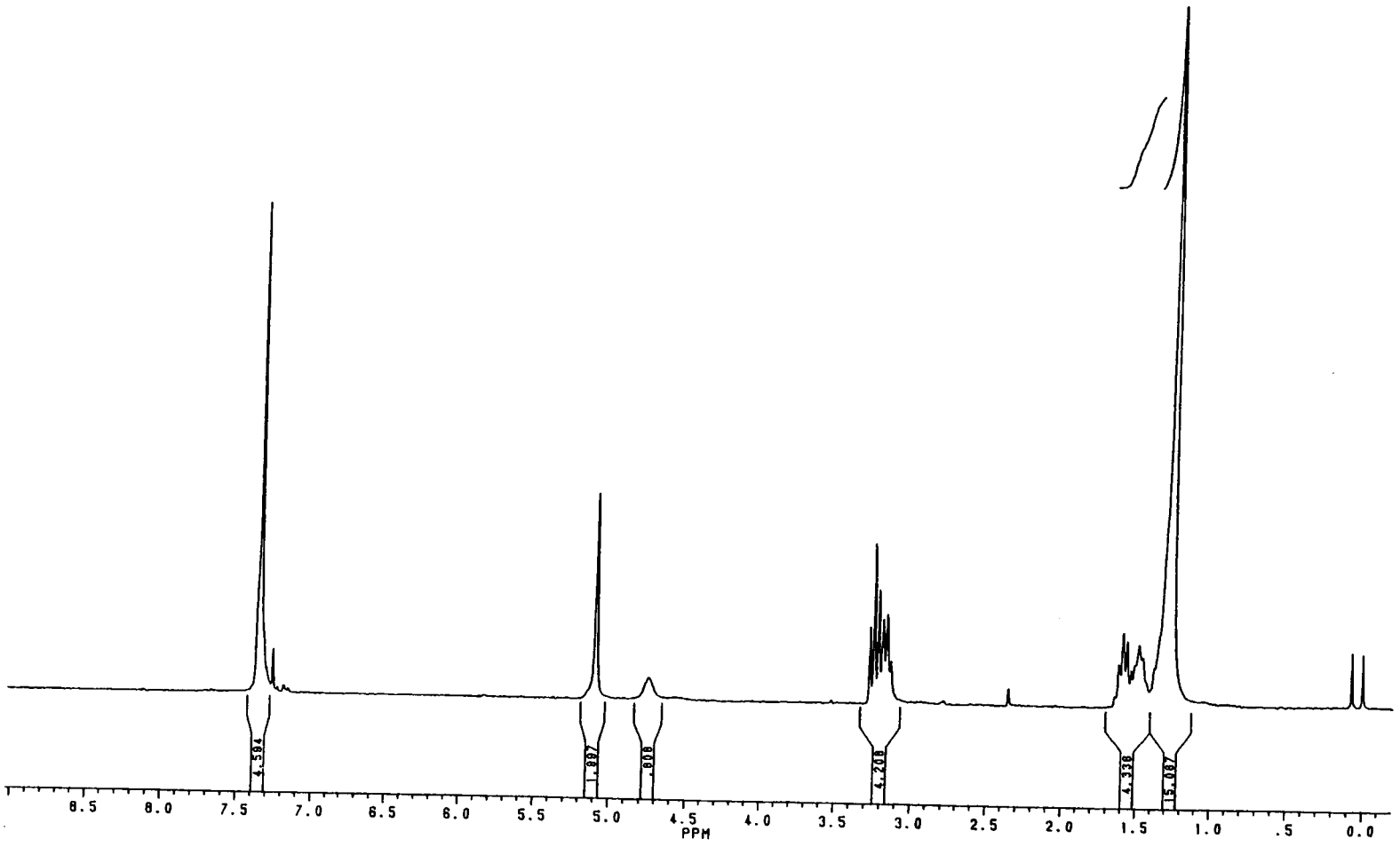
^{1}H NMR spectrum (250 MHz, $CDCl_3$) of 11-(*N*-benzyloxycarbonylamino)undecanol (**12**).



^{1}H NMR spectrum (250.13 MHz, $CDCl_3$) of 11-(*N*-benyloxycarbonylamino)-1-*O*-(methylsufonyl)undecanol (**13**).

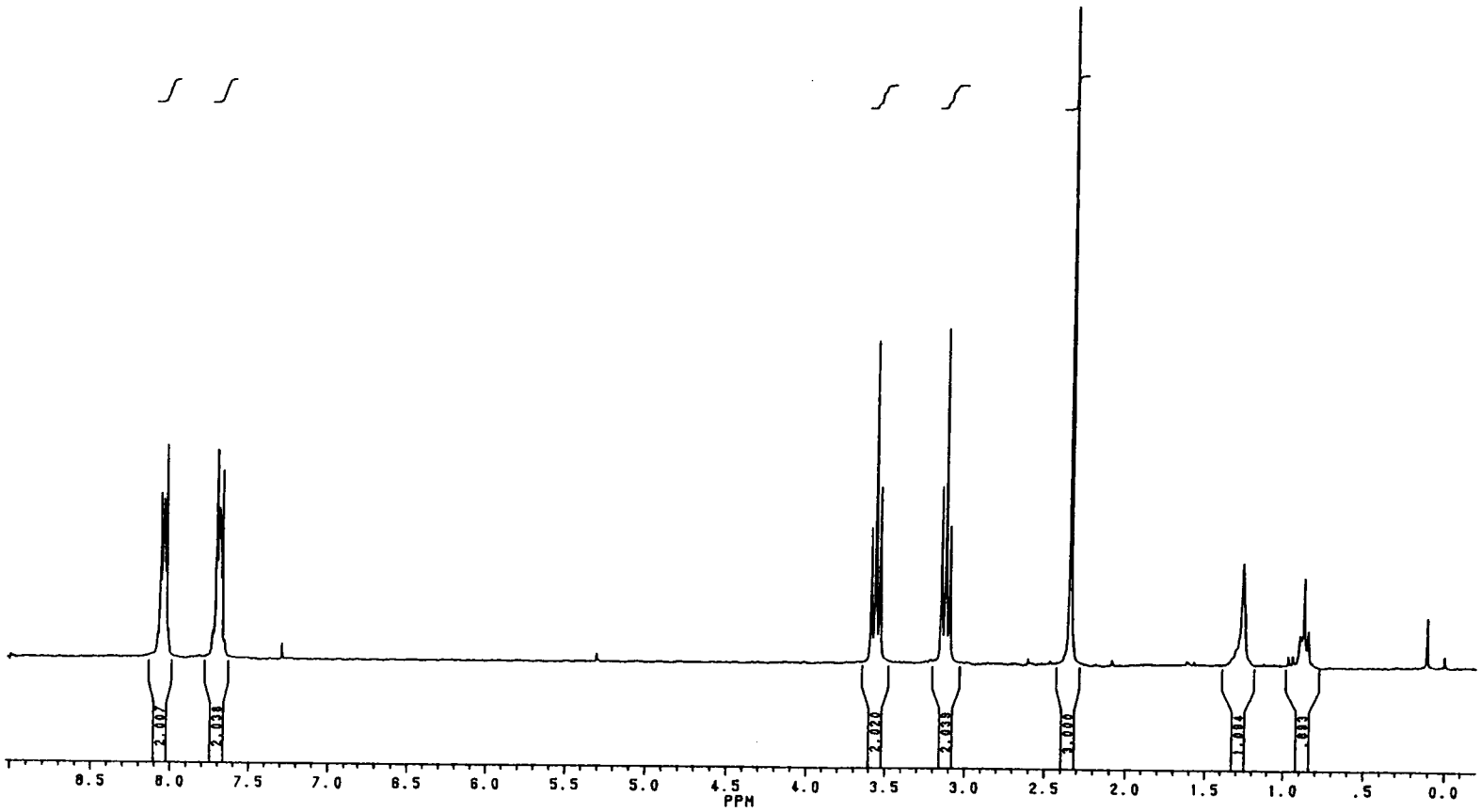


^{13}C NMR spectrum (62.9 MHz, $CDCl_3$) of 11-(*N*-benyloxycarbonylamino)-1-*O*-(methylsufonyl)undecanol (**13**).

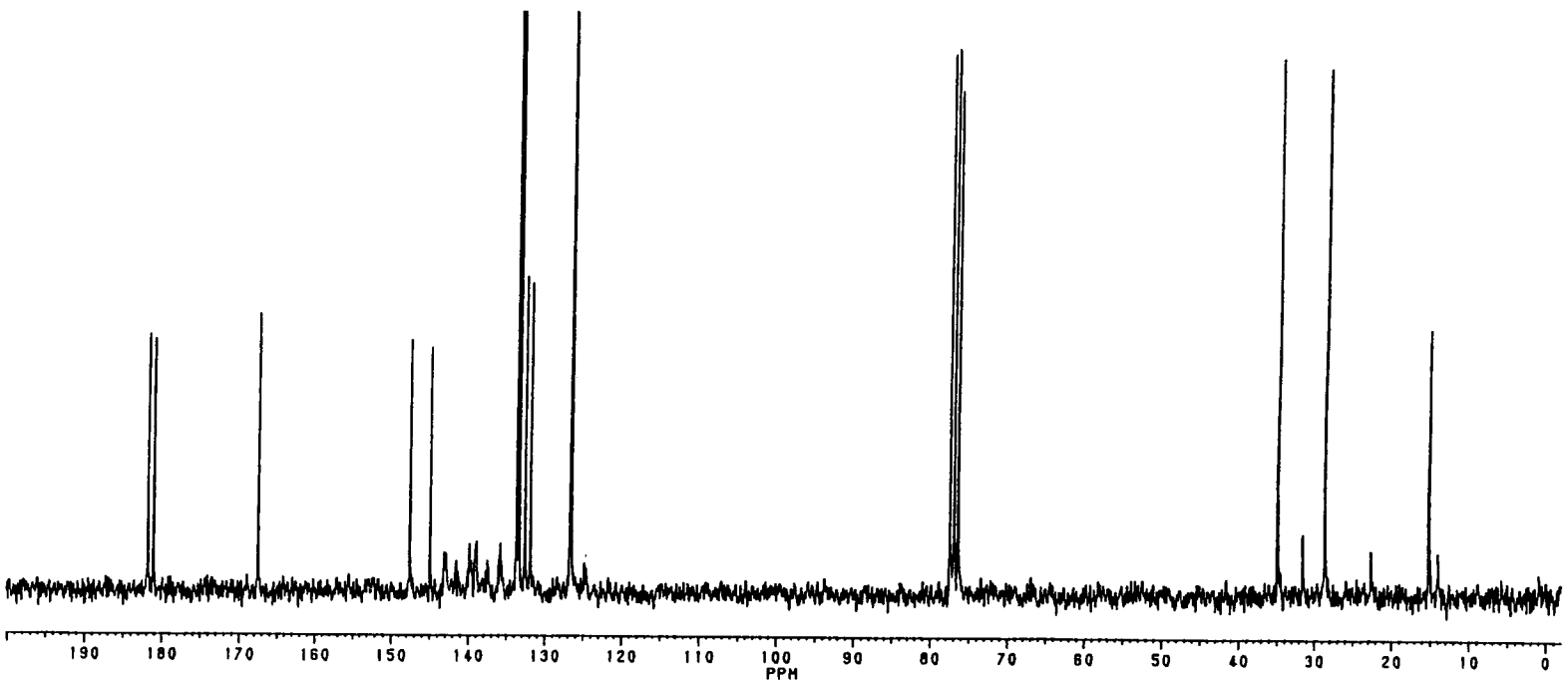


^{1}H NMR spectrum (250.13 MHz, $CDCl_3$) of 1-azido-11-(*N*-benzyloxycarbonylamino)undecane (**14**).

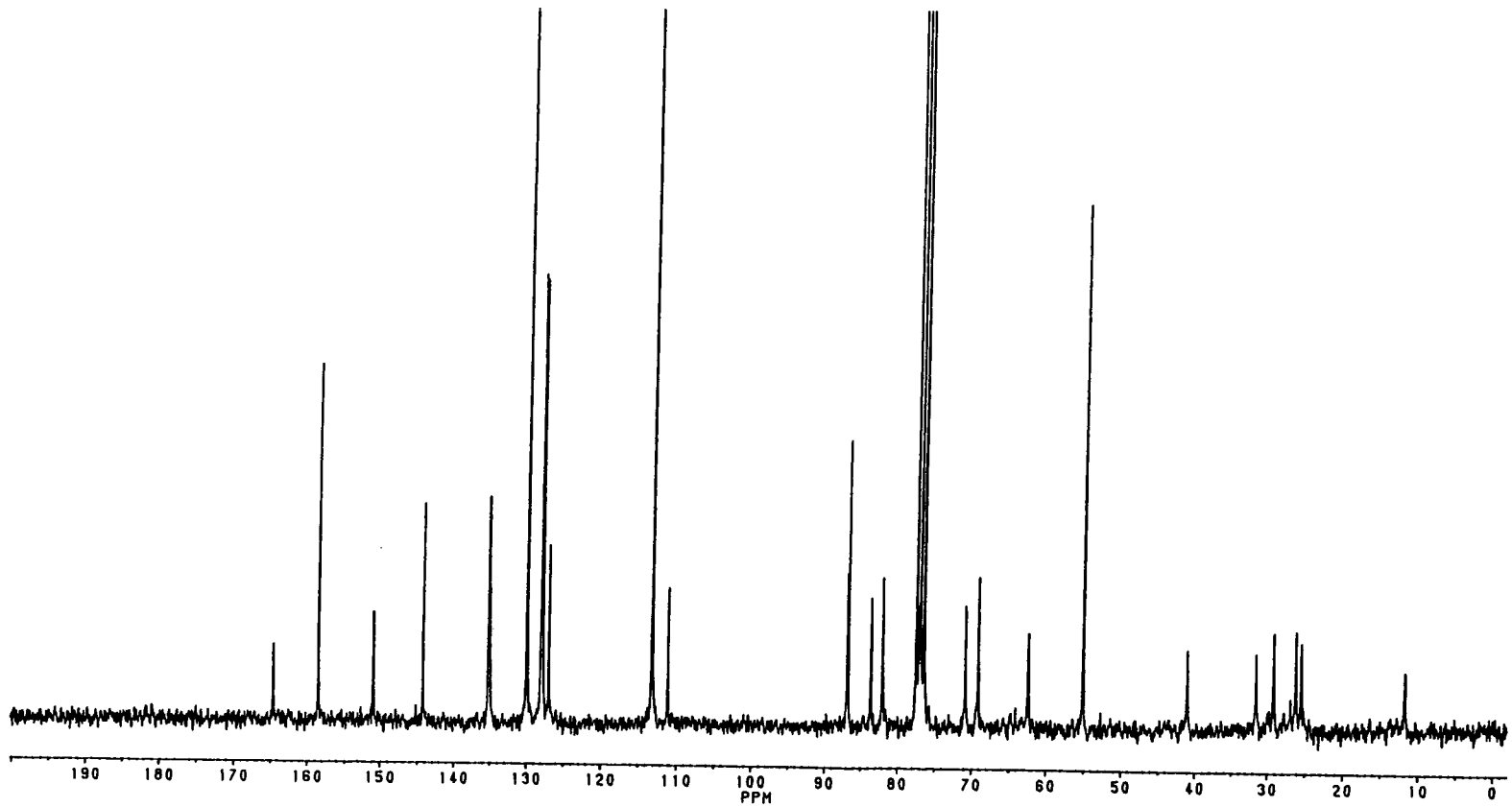
APPENDIX C. ^{1}H and ^{13}C NMR Spectra for Compounds Used to Synthesize 2′-*O*-Modified Electroactive Oligodeoxynucleotides



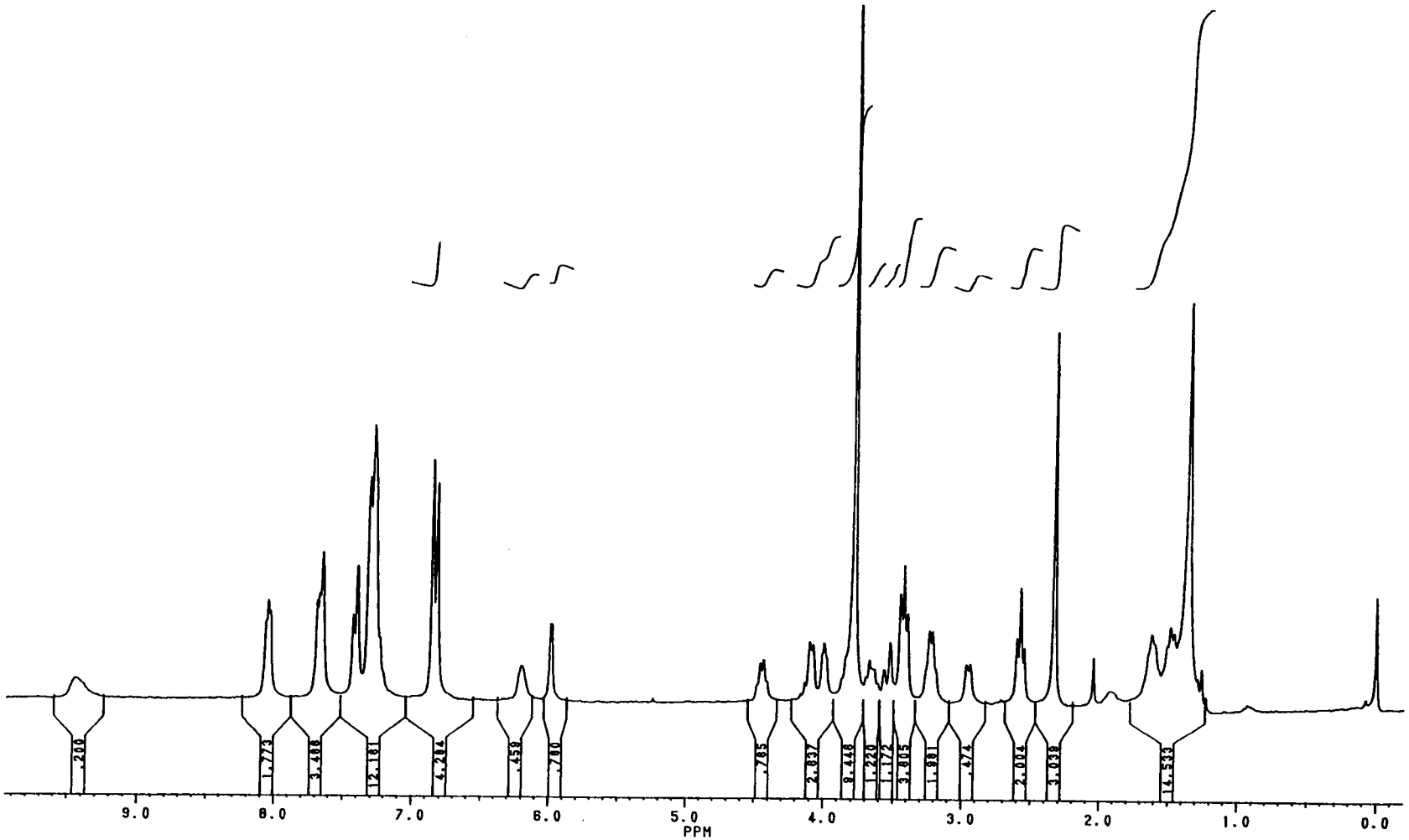
^{1}H NMR spectrum (250 MHz, $CDCl_3$) of *S*-(2-methyl-1,4-naphthoquinon-3-yl)-β-mercaptopropionic acid pentafluorophenyl ester (**23**).



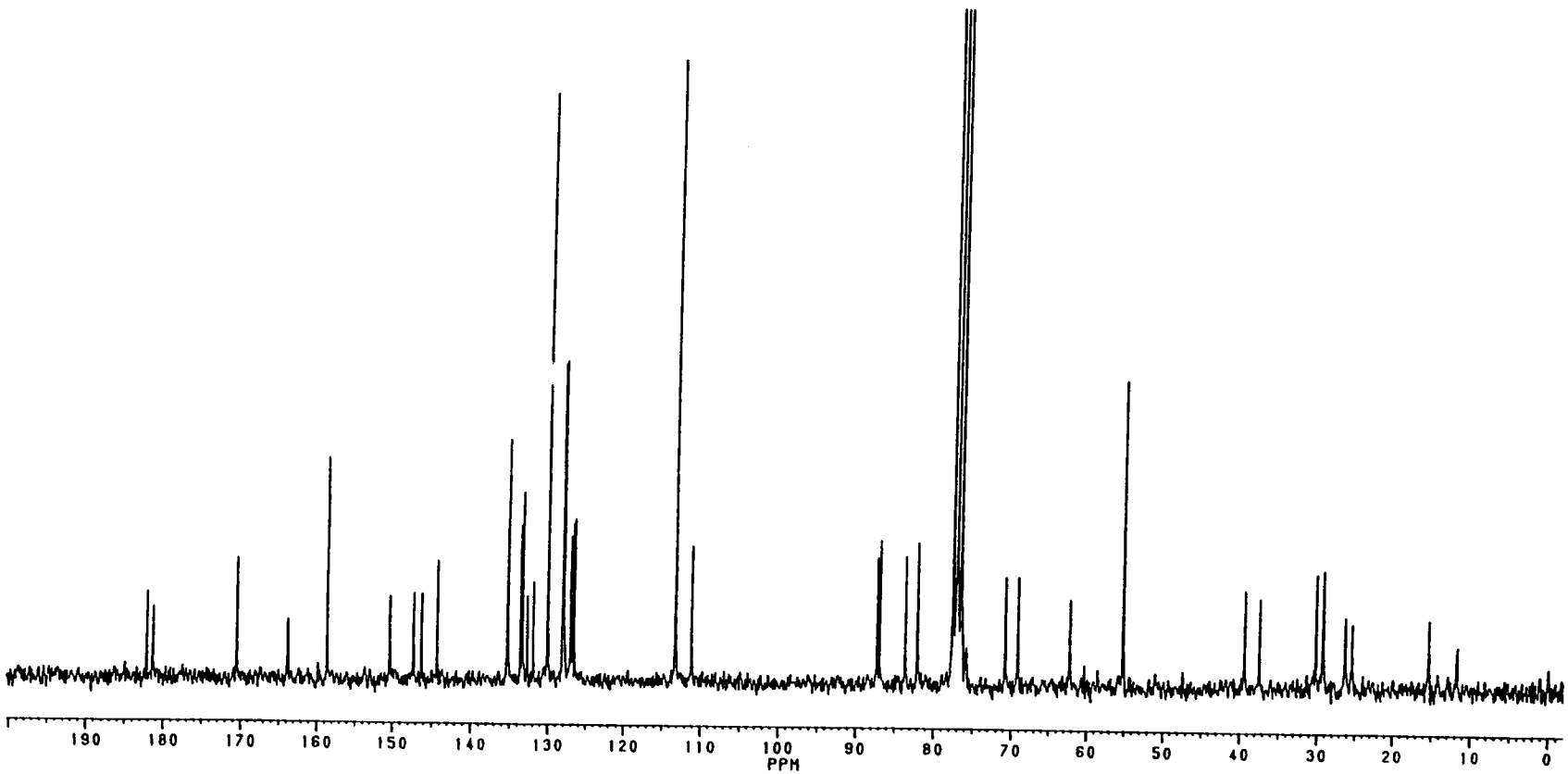
^{13}C NMR spectrum (62.9 MHz, $CDCl_3$) of *S*-(2-methyl-1,4-naphthoquinon-3-yl)-β-mercaptopropionic acid pentafluorophenyl ester (**23**).



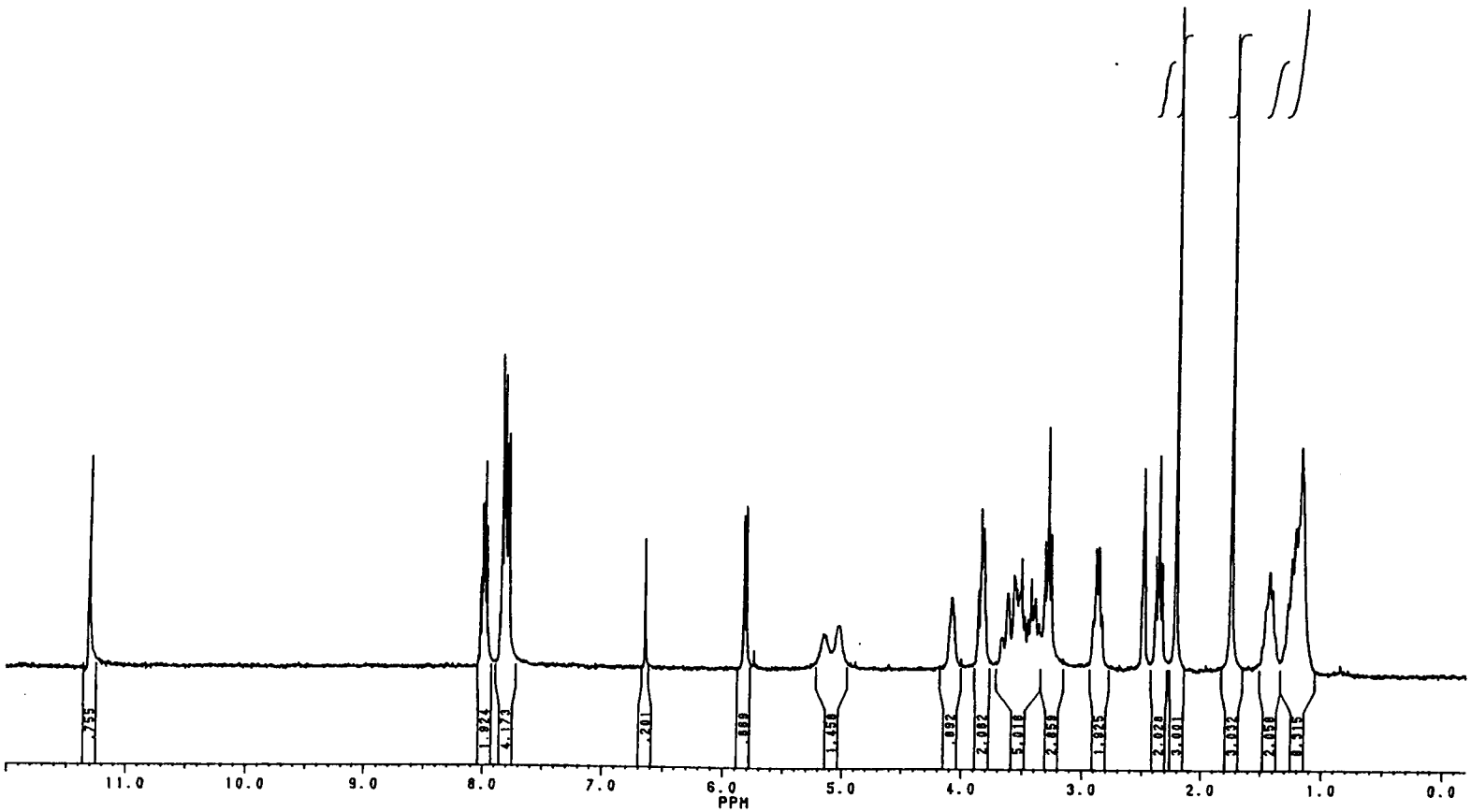
^{13}C NMR spectrum (62.9 MHz, $CDCl_3$) of 2′-*O*-(6-aminohexyl)-5′-*O*-(4,4′-dimethoxytrityl)thymidine (**24**).



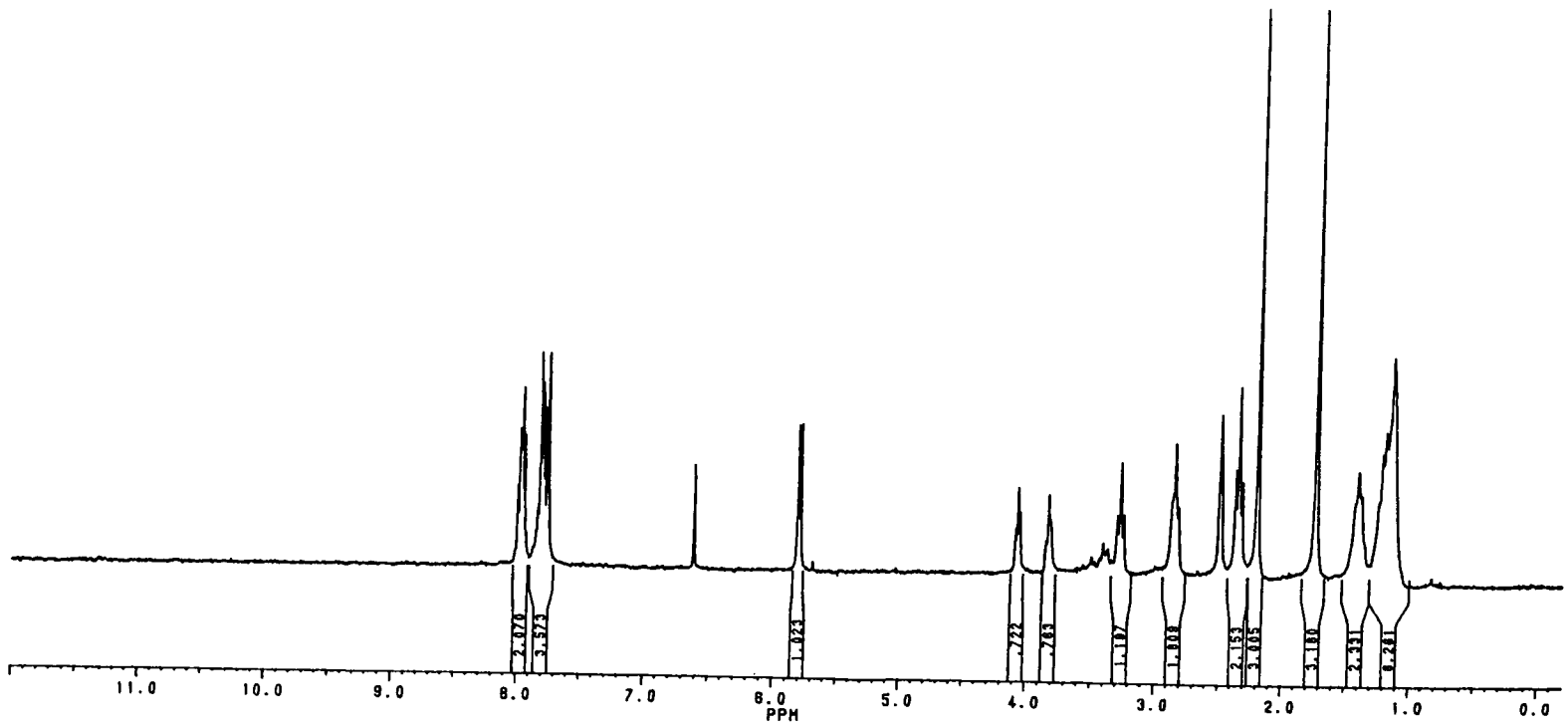
^{1}H NMR spectrum (250 MHz, $CDCl_3$) of 2′-*O*-(6-aminohexyl)-5′-*O*-(4,4′-dimethoxytrityl)thymidine (**24**).



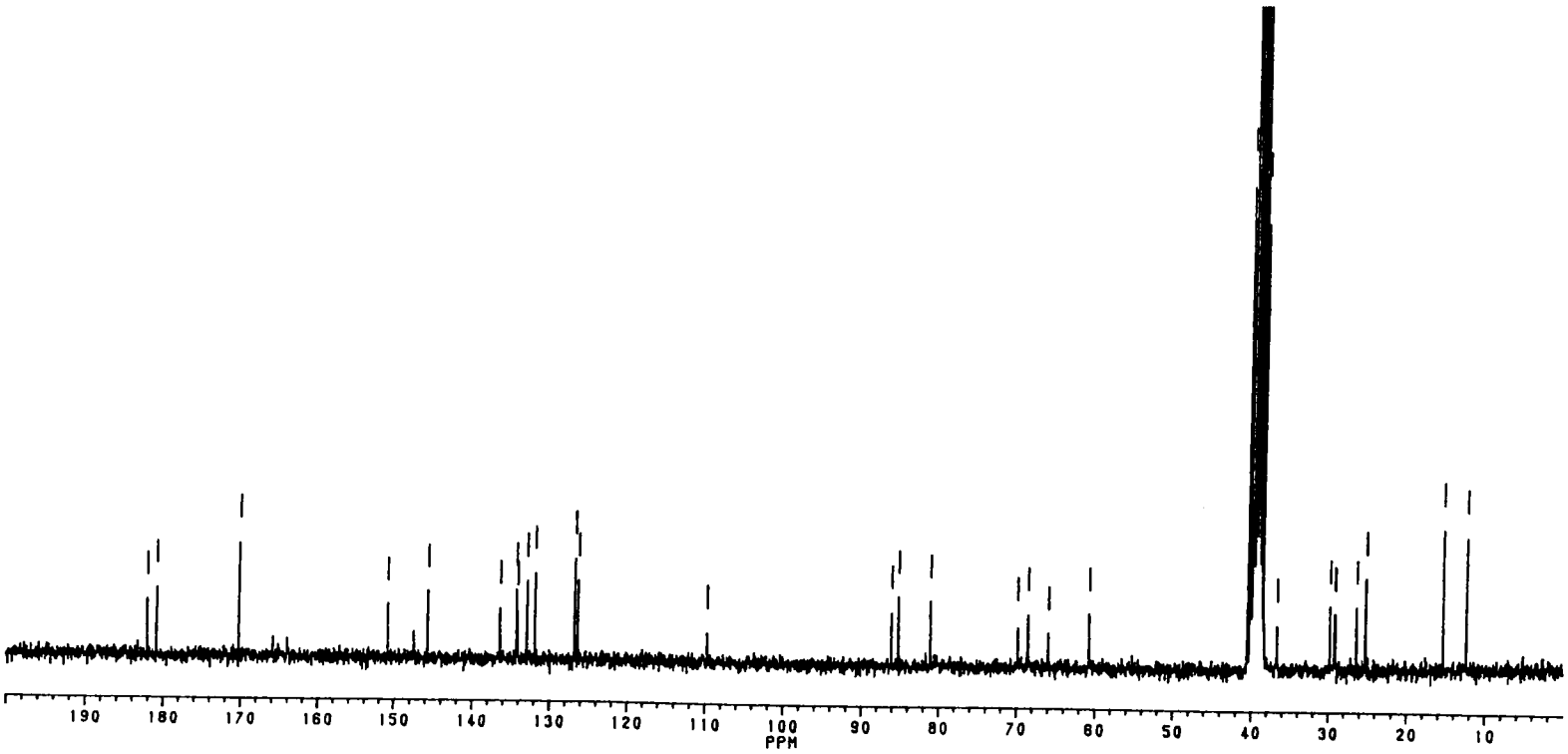
^{13}C NMR spectrum (62.9 MHz, $CDCl_3$) of 2′-*O*-(6-aminohexyl)-5′-*O*-(4,4′-dimethoxytrityl)thymidine (**24**).



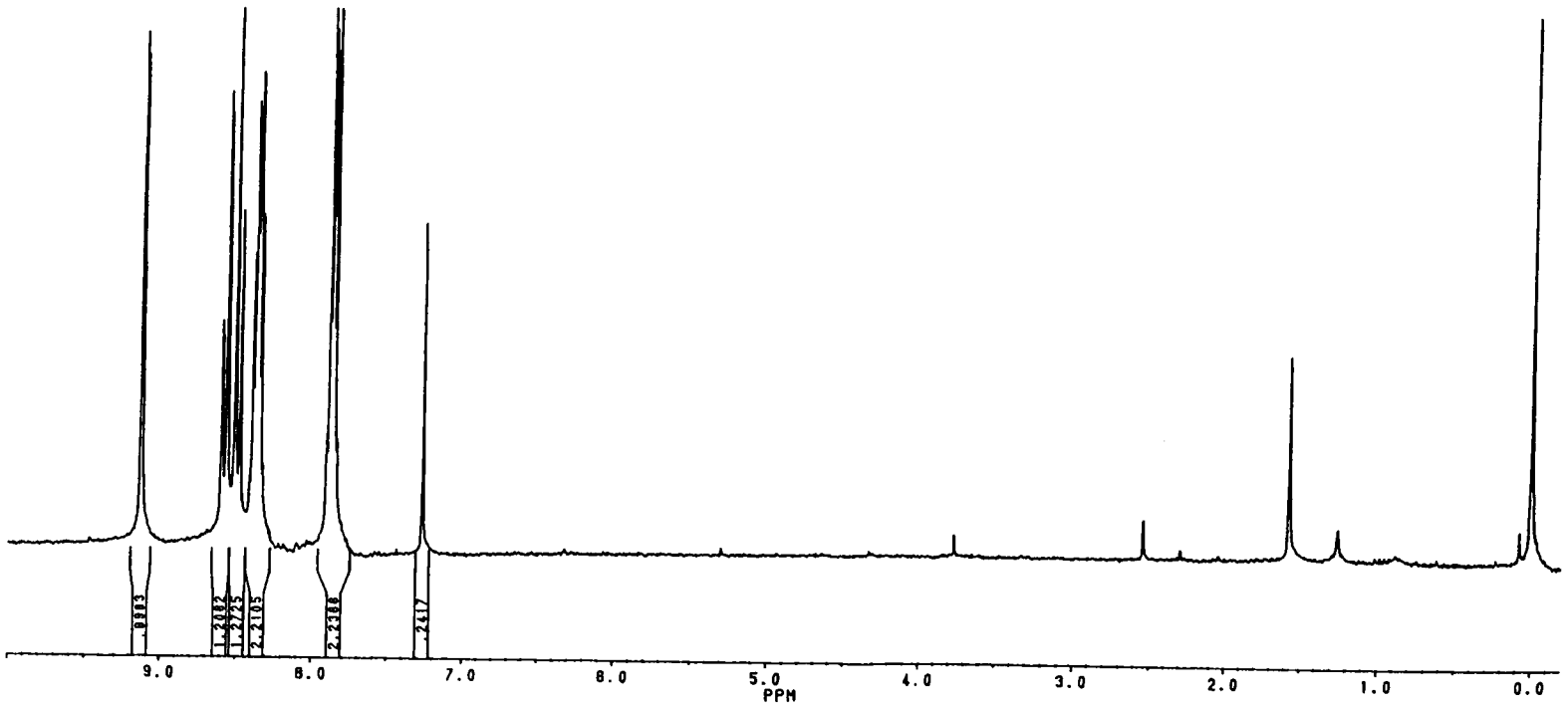
^{1}H NMR spectrum (250 MHz, DMSO-d_6) of 2′-*O*-[6-[2-oxo-*S*-(2-methyl-1,4-naphthoquinon-3-yl)-β-mercaptopropionyl]hexyl]thymidine (**26**).



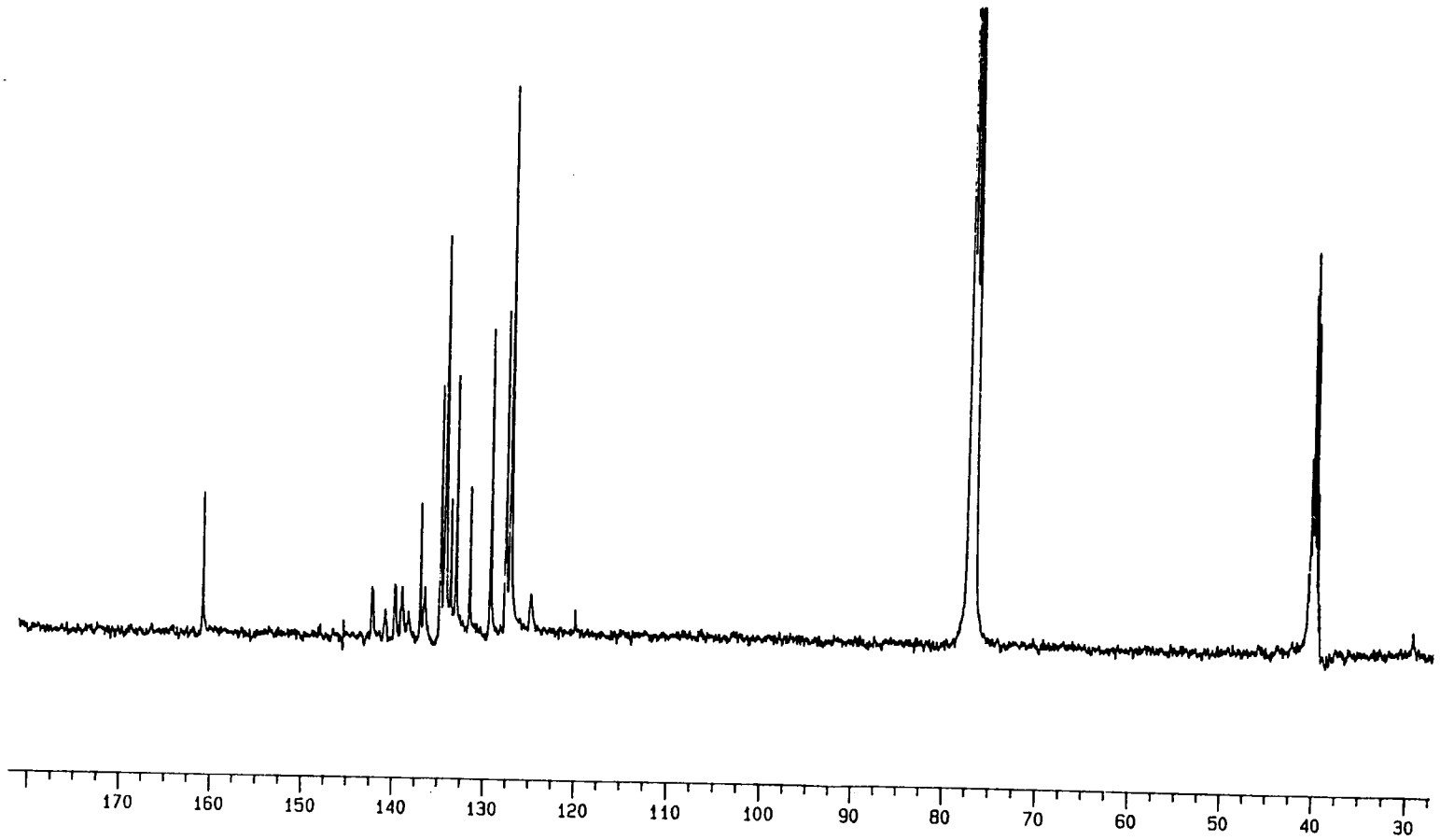
^{1}H NMR spectrum (250 MHz, DMSO-d_6 + D_2O) 2′-*O*-[6-[2-oxo-*S*-(2-methyl-1,4-naphthoquinon-3-yl)-β-mercaptopropionyl]hexyl]thymidine (**26**).



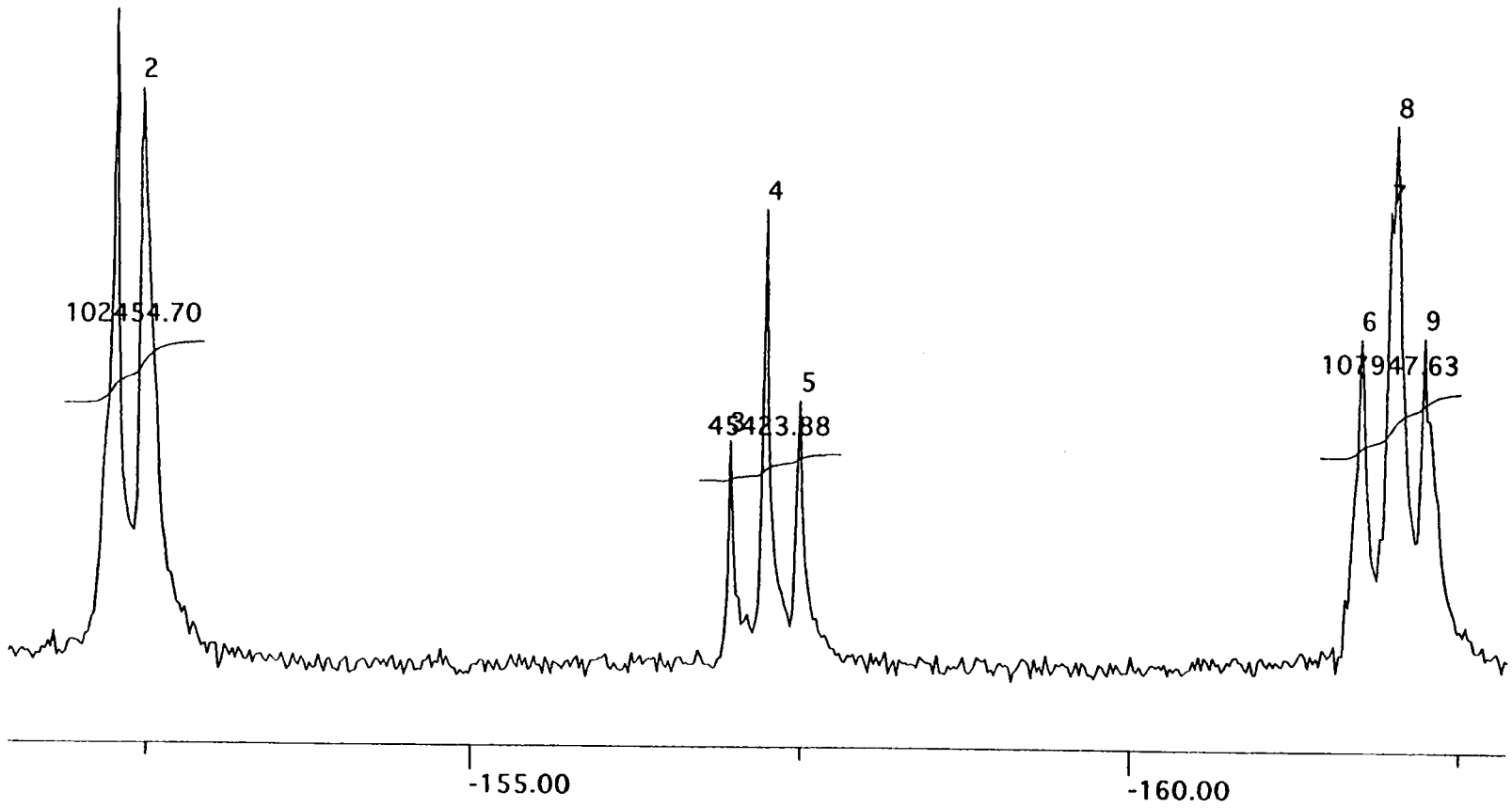
^{13}C NMR spectrum (62.9 MHz, DMSO-d_6)2′-*O*-[6-[2-oxo-*S*-(2-methyl-1,4-naphthoquinon-3-yl)-β-mercaptopropionyl]hexyl]thymidine (**26**).



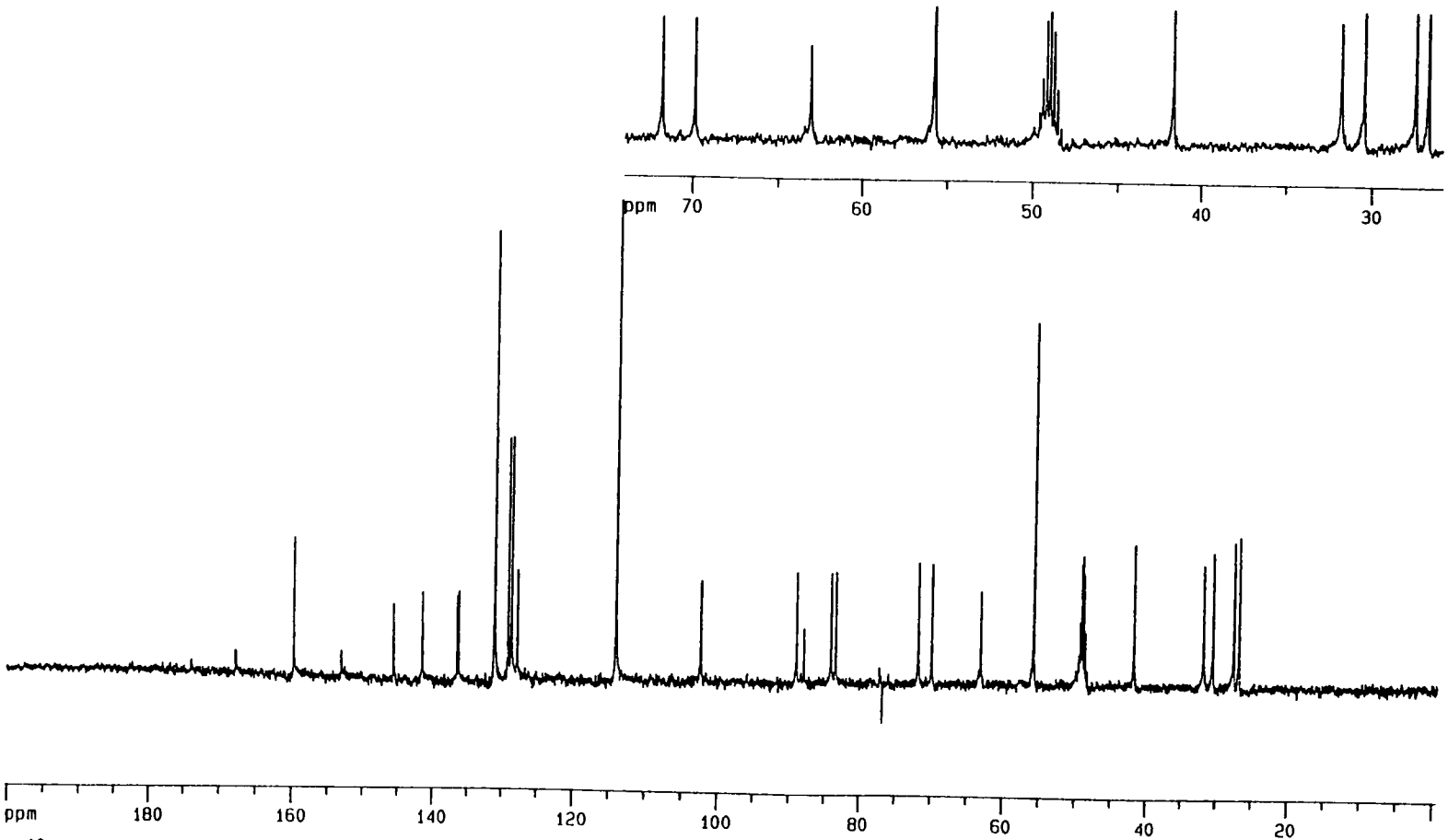
^{1}H NMR spectrum (250 MHz, $CDCl_3$/DMSO-d_6) of 9,10-anthraquinone-2-carboxylic acid pentafluorophenyl ester (**34**).



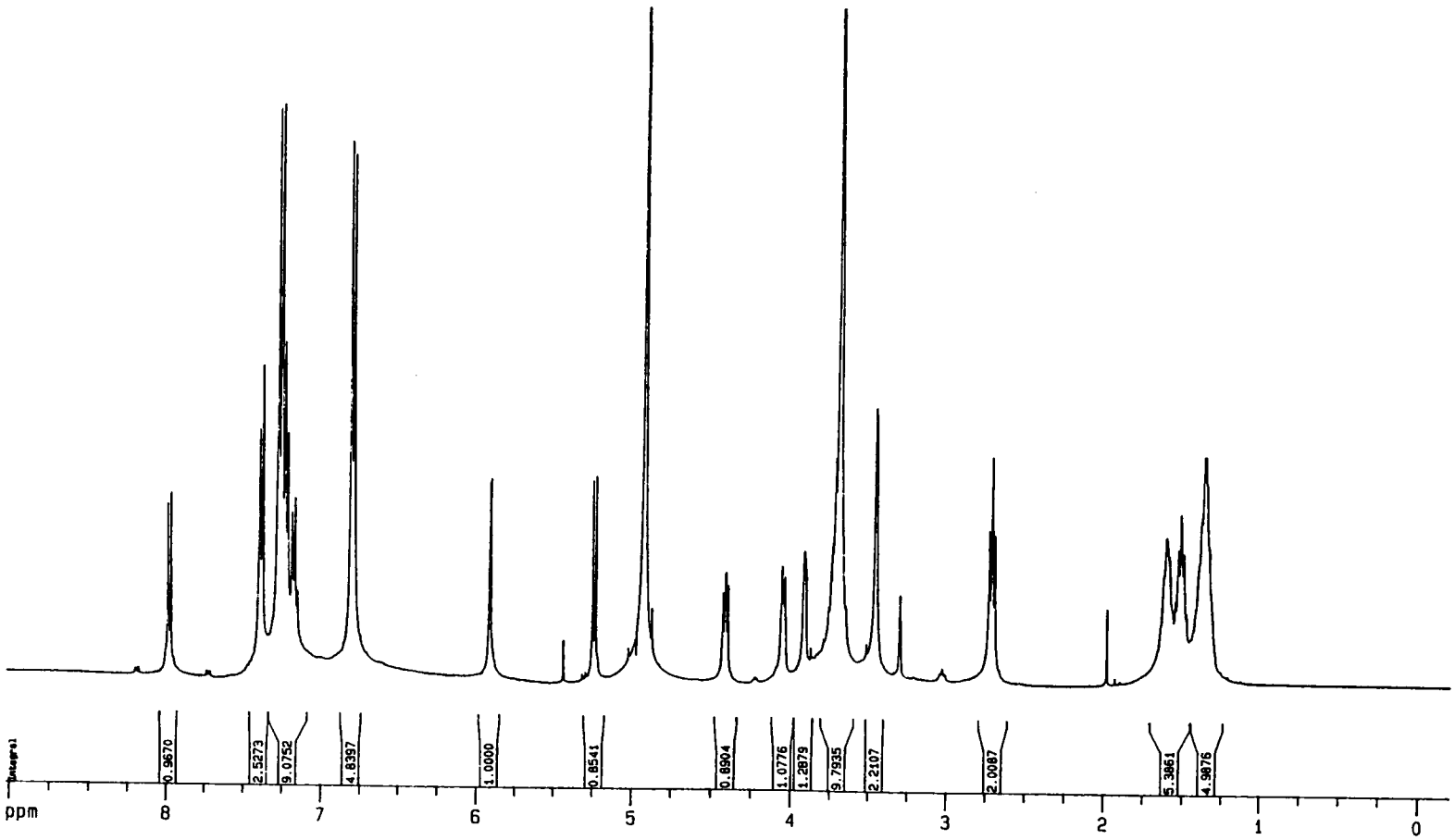
^{13}C NMR spectrum (100.61 MHz, $CDCl_3$/DMSO-d_6) of 9,10-anthraquinone-2-carboxylic acid pentafluorophenyl ester (**34**).



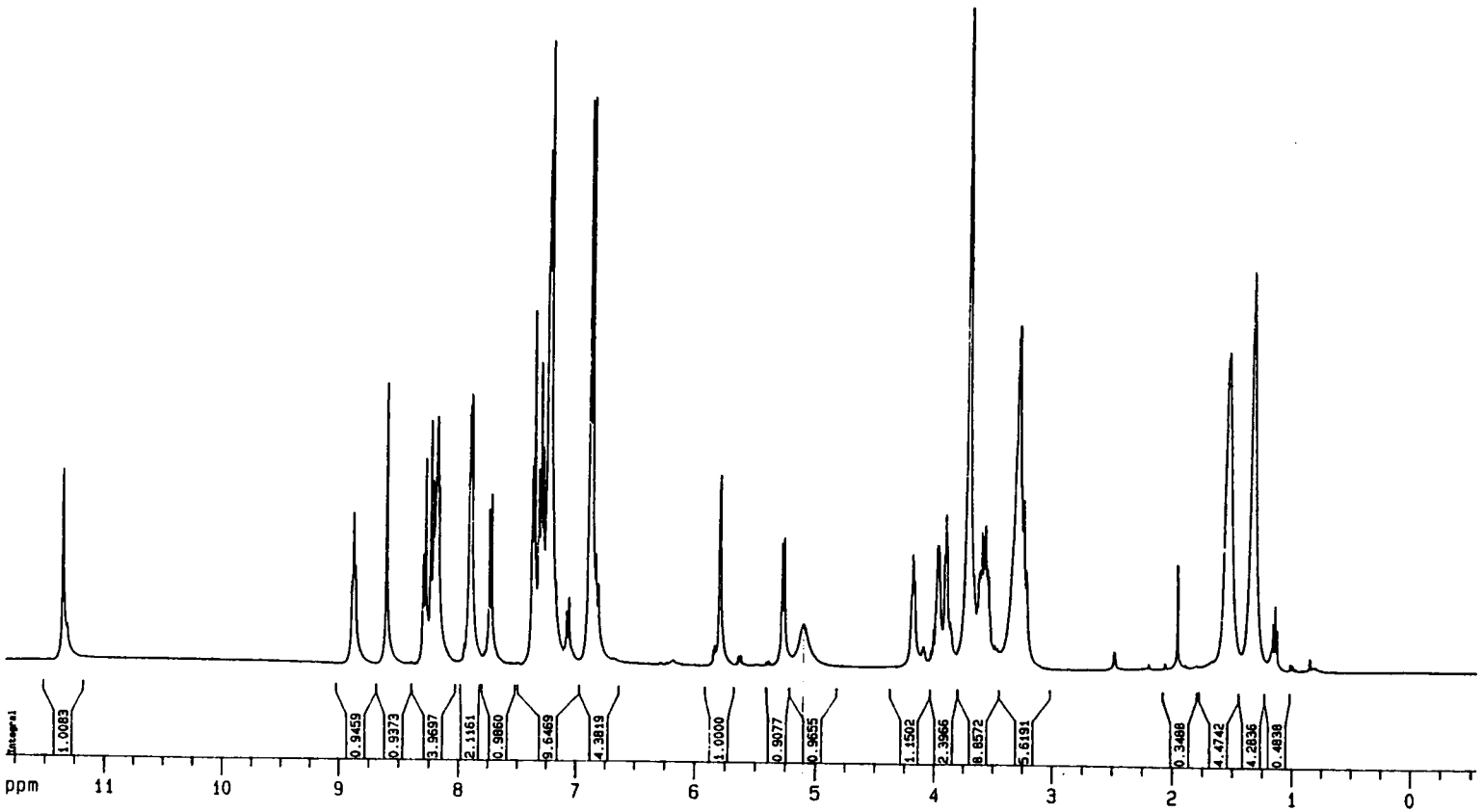
^{19}F NMR spectrum (84.24 MHz, $CDCl_3$/DMSO-d_6) of 9,10-anthraquinone-2-carboxylic acid pentafluorophenyl ester (**34**).



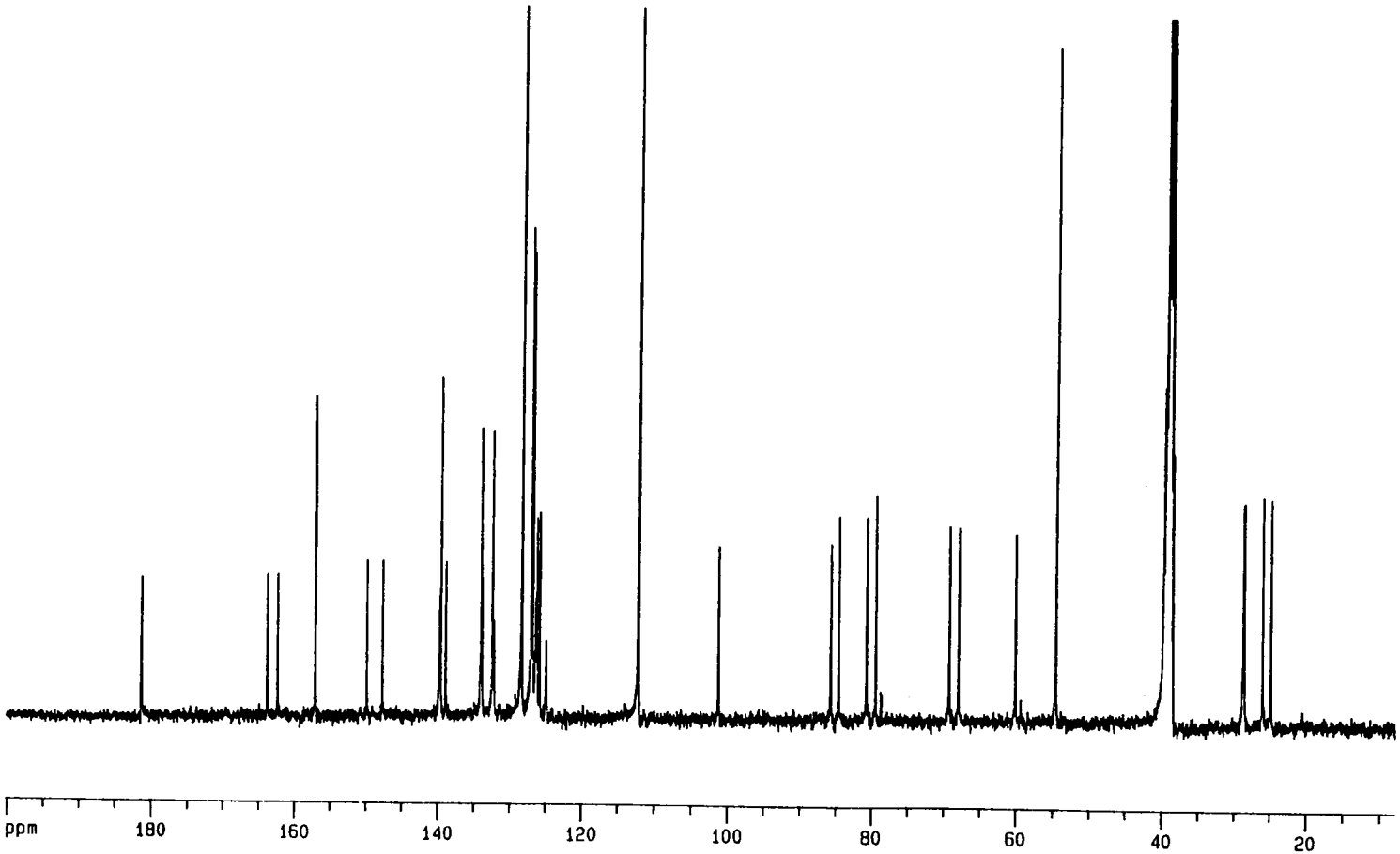
^{13}C NMR spectrum (100.61 MHz, methanol-d_4) of 2′-*O*-(6-aminohexyl)-5′-*O*-(4,4′-dimethoxytrityl)uridine (**30**).



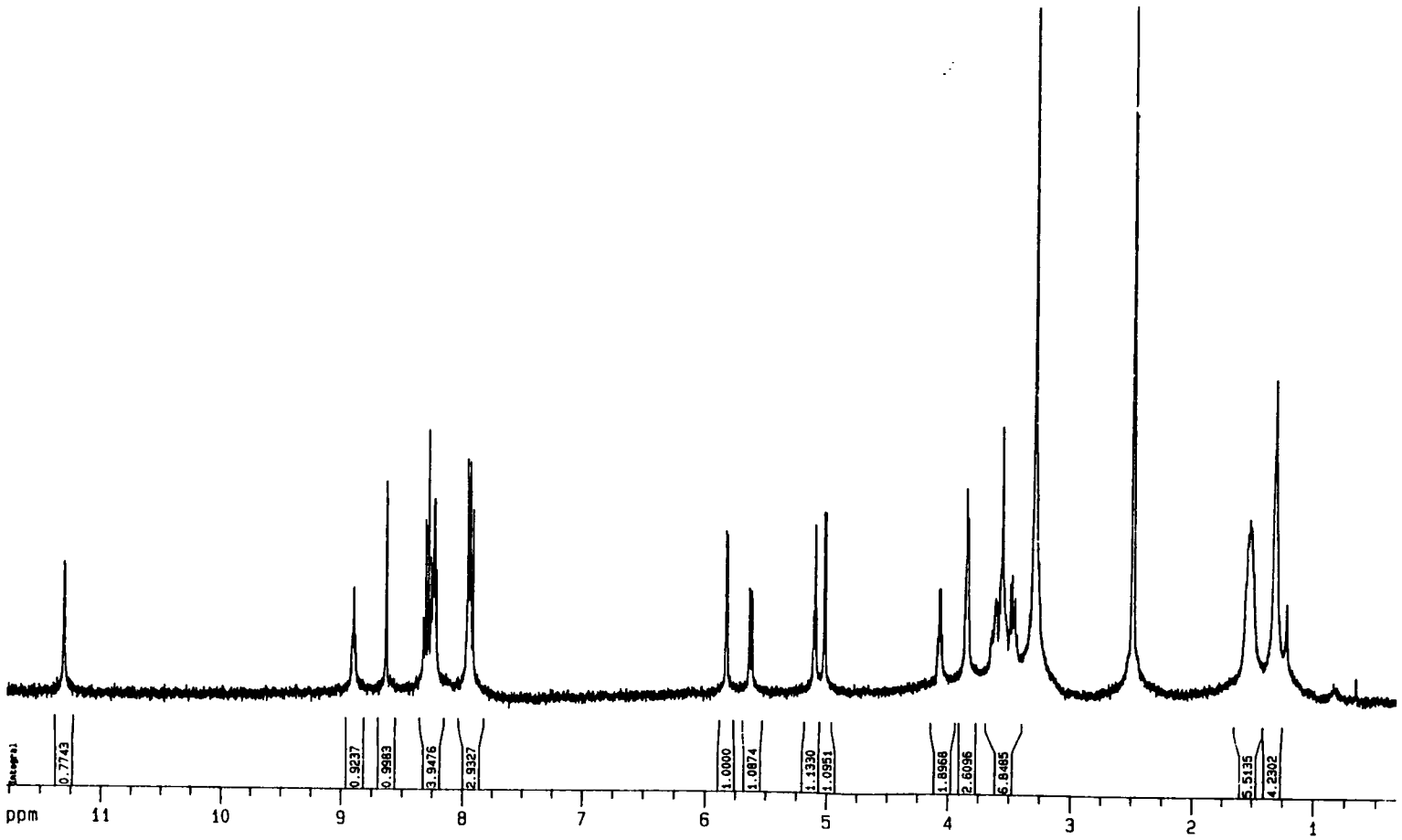
^{1}H NMR spectrum (400.13 MHz, methanol-d_4) of 2′-*O*-(6-aminohexyl)-5′-*O*-(4,4′-dimethoxytrityl)uridine (**30**).



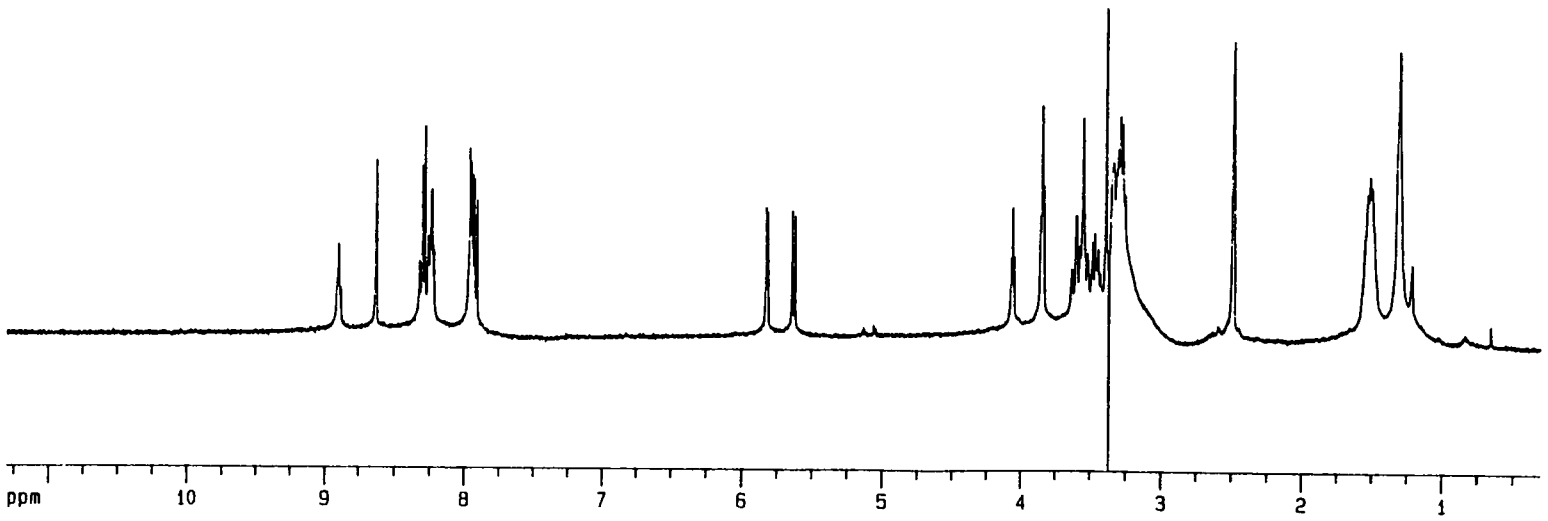
^{1}H NMR spectrum (400.13 MHz, DMSO-d_6) of 2′-*O*-[6-[2-oxo-(9,10-anthraquinon-2-yl)amino]hexyl]-5′-*O*-(4,4′-dimethoxytrityl)uridine (**35**).



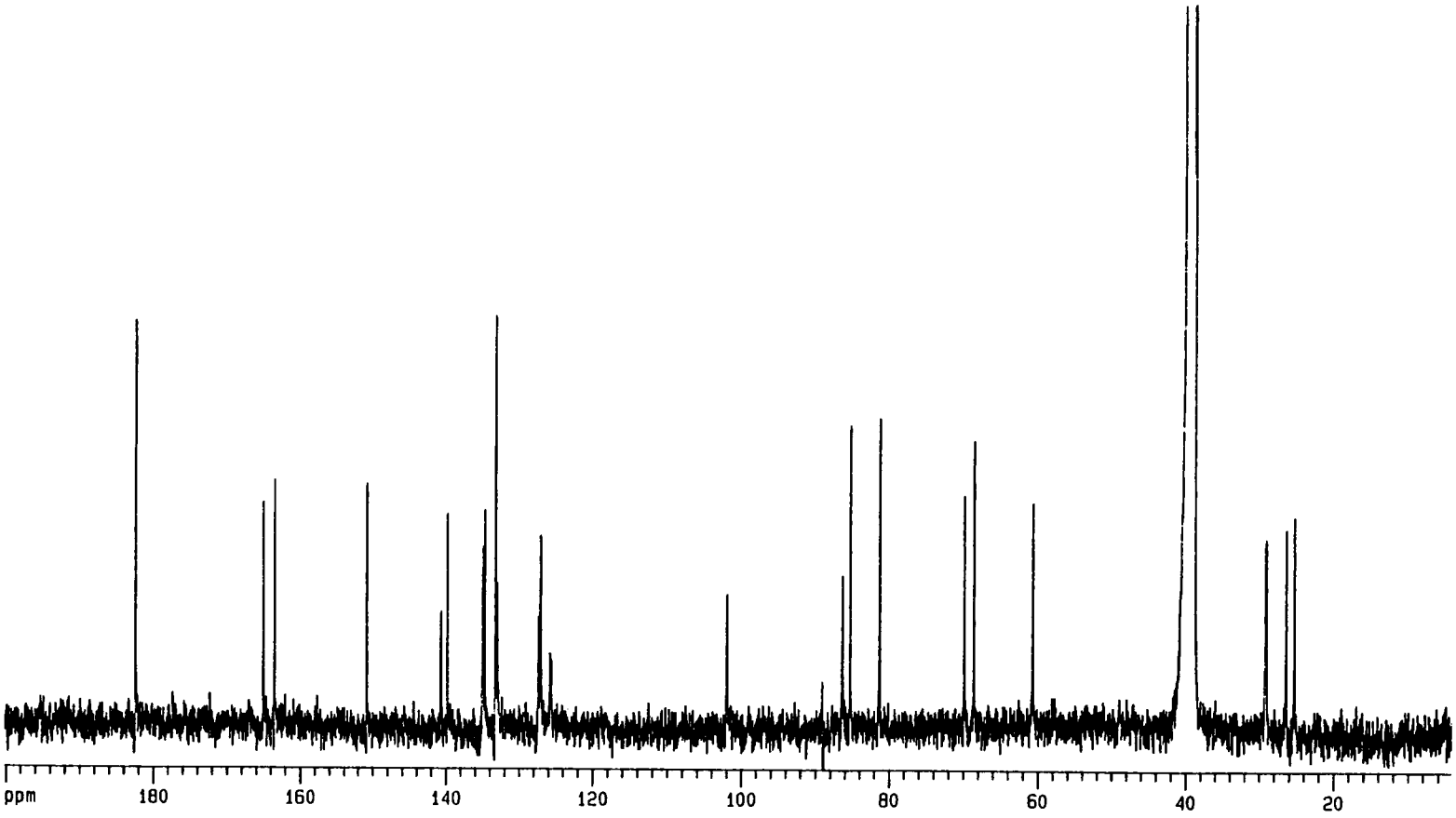
^{13}C NMR spectrum (100.61 MHz, DMSO-d_6) of 2′-*O*-[6-[2-oxo-(9,10-anthraquinon-2-yl)amino]hexyl]-5′-*O*-(4,4′-dimethoxytrityl)uridine (**35**).



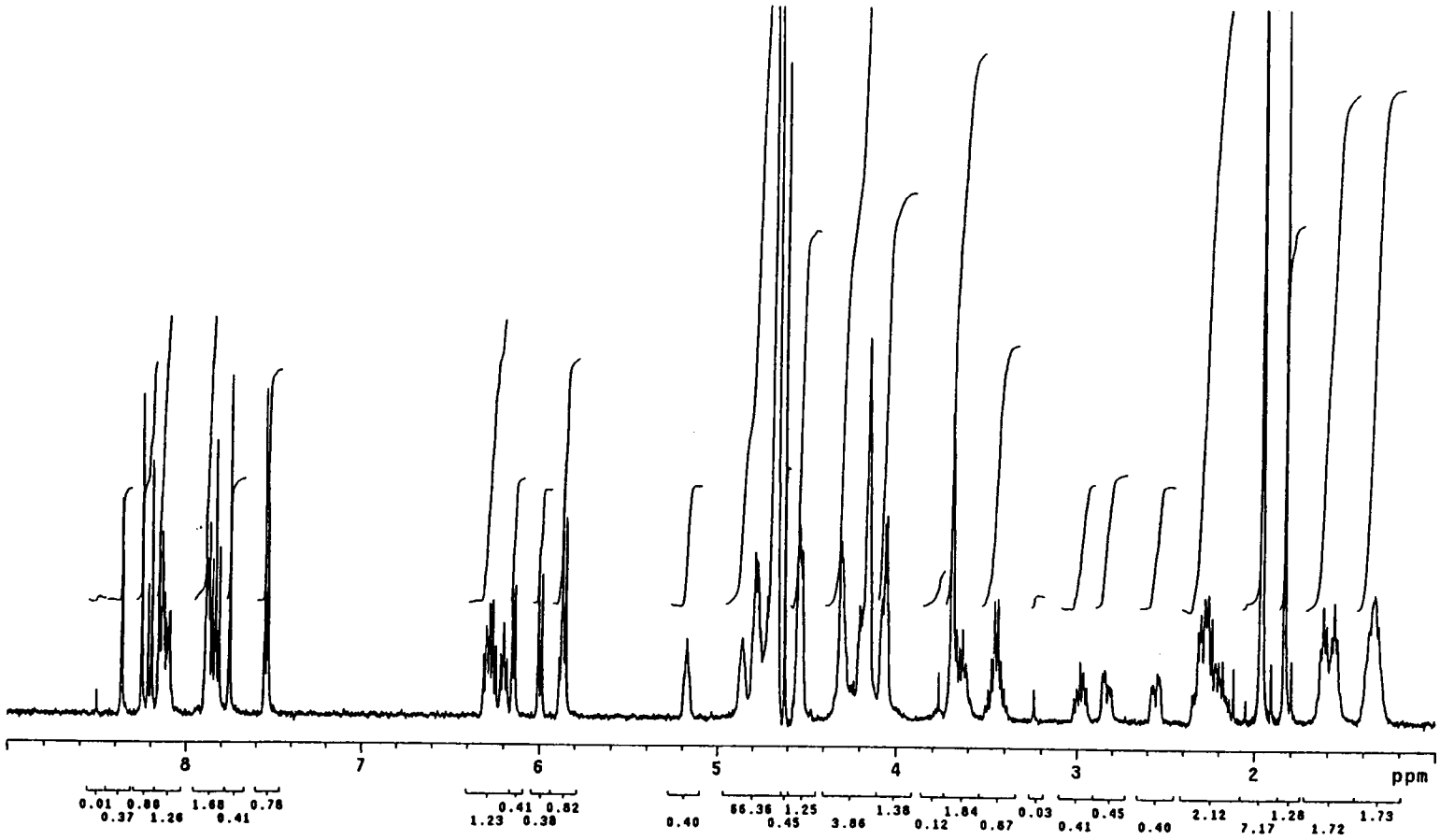
^{1}H NMR spectrum (400.13 MHz, DMSO-d_6) of 2′-*O*-[6-[2-oxo-(9,10-anthraquinon-2-yl)amino]hexyl]uridine (**31**).



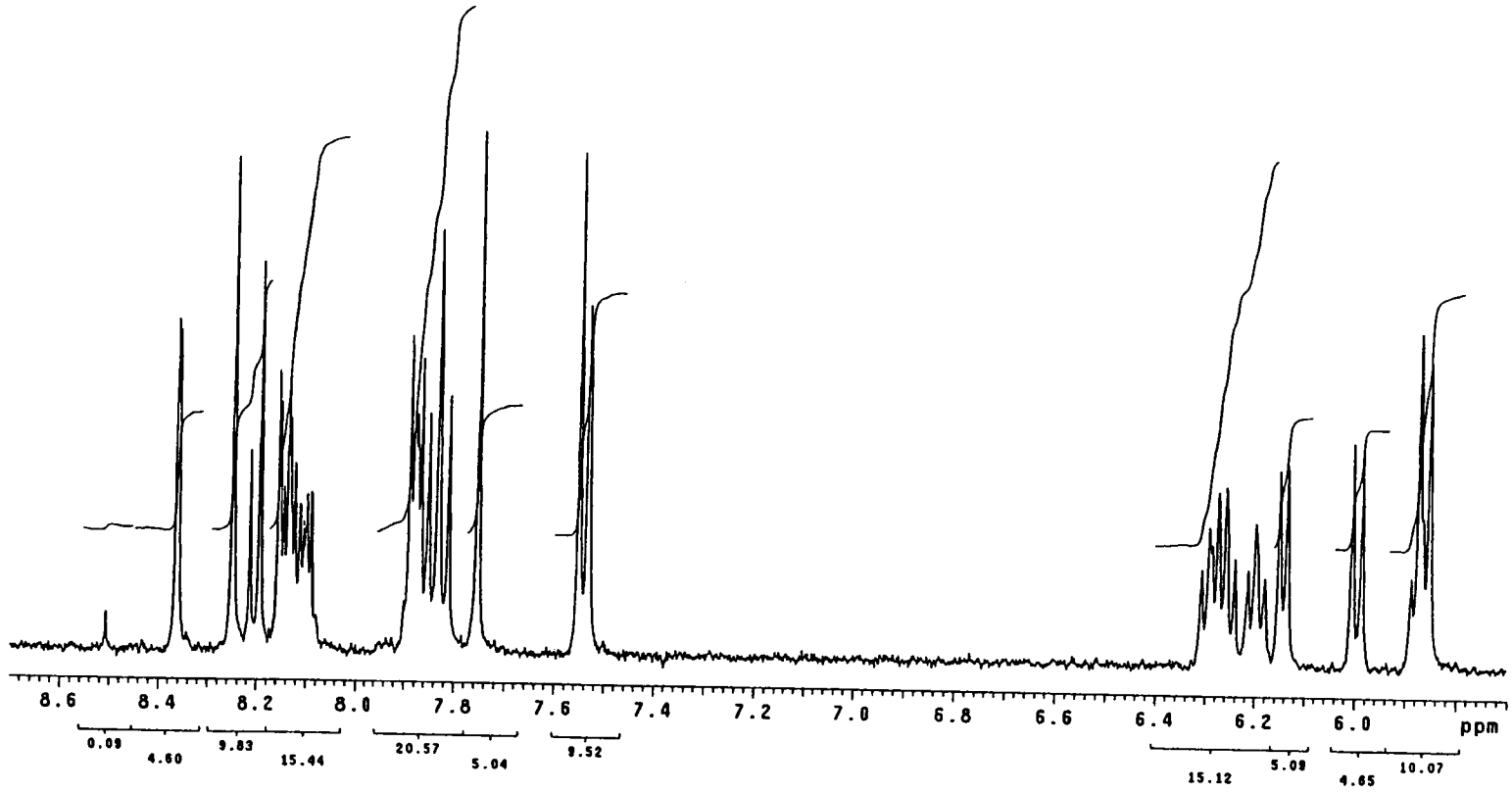
^{1}H NMR spectrum (400.13 MHz, DMSO-d_6 + D_2O) of 2′-*O*-[6-[2-oxo-(9,10-anthraquinon-2-yl)amino]hexyl]uridine (**31**).



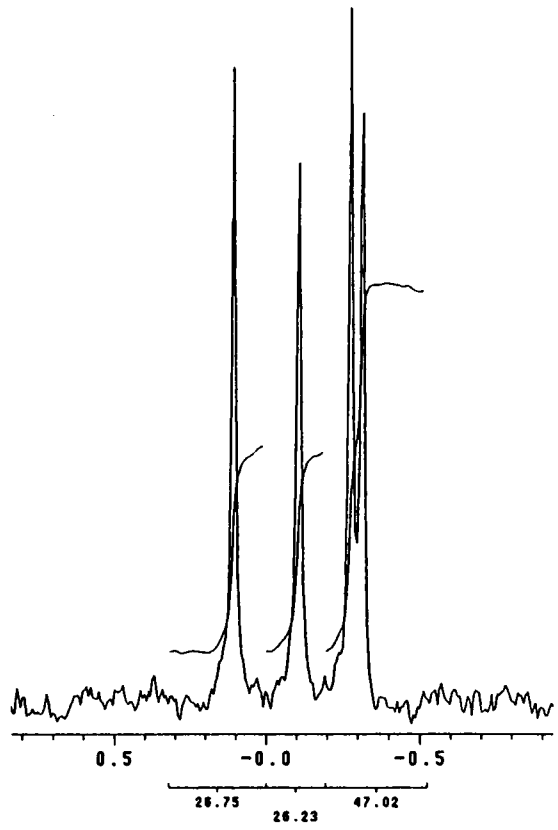
^{13}C NMR spectrum (100.61 MHz, DMSO-d_6) of 2′-*O*-[6-[2-oxo-(9,10-anthraquinon-2-yl)amino]hexyl]uridine (**31**).



^{1}H NMR spectrum (399.94 MHz, D_2O) of the pentamer 5′-d(GAU*CT)-3′ (**28**).



^{1}H NMR spectrum (399.94 MHz, D_2O) of the pentamer 5′-d(GAU*CT)-3′ (**28**).



^{31}P NMR spectrum (161.9 MHz, D_2O) of the pentamer 5′-d(GAU*CT)-3′ (**28**).

VITA

Neil Andrew Whittemore was born in Firs Hospital, Sherwood, Nottingham, England in 1969. He graduated from West Bridgford School, West Bridgford, Nottingham in 1985. After graduation he worked as a Laboratory Technician with Boots MicroCheck—a department within Boots Company, PLC, Nottingham, England. During his employment, he for a degree in Applied Chemistry. He graduated with BSc Hons in Applied Chemistry (upper second class degree) from Nottingham Trent University, Nottingham, England in 1992. In 1993 he left Boots MicroCheck and England to work on his PhD in Chemistry (majoring in Organic Chemistry) in the laboratory of Prof. David C. Baker, University of Tennessee–Knoxville, TN under the joint supervision of Profs. David C. Baker and James Q. Chambers. After obtaining his PhD in May 1999, he will begin as a post-doctoral fellow in the laboratory of Prof. Randall L. Halcomb at the University of Colorado at Boulder.